CNIC-01475
CNDC-0027
INDC(CPR)-050 / L

COMMUNICATION OF NUCLEAR DATA PROGRESS

No .23 (2000)

China Nuclear Data Center

China Nuclear Information Centre

Atomic Energy Press

Beijing, June 2000

EDITORIAL NOTE

This is the 23th issue of *Communication of Nuclear Data Progress* (CNDP), in which the achievements of last year in nuclear data field in China are carried. It includes the measurements of double differential cross section of ^{9}Be at 5.9 and 6.4 MeV and ^{186}W(n,γ) ^{187}W reaction cross section from 0.50 to 1.5 MeV; researches on three body breakup process and energy balance in UNF code, theoretical calculations of n+^{141}Pr, ^{239,240}Pu, P+^{209}Bi reactions; evaluations of n+^{90,91,92,94,96,0}Zr, ^{Nat}Cu, ^{135,136,137,138}Ba neutron data, γ+^{209}Bi photo nuclear reaction data and fission yield from ^{235}U fission; investigation on the systematics of isomatic cross section ratios for neutron-induced reactions around 14 MeV; progress report on prompt γ-ray data evaluation, and a brief report on the test of the fission rate for ^{235}U. Also the activities and cooperation on nuclear data in China are summarized.

The editors hope that our readers and colleagues will not spare their comments in order to improve this publication. If you have any, please contact with us by following address:

Mailing Address: Profs. Liu Tingjin and Zhuang Youxiang
China Nuclear Data Center
China Institute of Atomic Energy
P.O.Box 275 (41), Beijing 102413
People's Republic of China
Telephone: 86-10-69357729 or 69357830
Telex: 222373 IAE CN
Facsimile: 86-10-6935 7008
E-mail: tjliu @ mipsa.ciae.ac.cn or yxzhuang @ mipsa.ciae.ac.cn

EDITORIAL BOARD

CONTENTS

I EXPERIMENTAL MEASUREMENT

Measurement of Double-Differential Neutron Emission Cross Sections of ^{9}Be for 5.9 and 6.4 MeV Neutrons*

Chen Jinxiang, Mao Xiaoyong, Shen Guanren[1)], Li Xia[1)],
Shi Zhaomin, Tang Guoyou, Zhang Guohui, Wang Jianyong
(Institute of Heavy Ion Physics, Peking University, Beijing 100871)
[1)](China Institute of Atomic Energy, P.O. Box 275, Beijing 102413)

Introduction

The double-differential neutron emission cross sections (DDX) for fast neutron induced reactions are great important not only for neutronic designs of fusion and accelerator-based reactors but also for the study of nuclear reaction mechanisms. The DDX data of Be^{9} is of special importance since beryllium nucleus is expected as an effective neutron multiplier and constituent of tritium breeder. Up to now, there are very few experiments for incident energies either lower than 14 MeV or higher than 15 MeV in the previous DDX measurements, most of them are confined to around 14 MeV incident energy. However, even in the case of around 14 MeV, the experimental data, which cover wide range of emission spectrum and are with sufficient energy resolution, are very limited and show disagreement with each other. Furthermore, there is also discrepancy between experimental and evaluated data[1]. In addition, the theoretical calculation could not predict well either the energy spectrum or cross section, because there is no suitable reaction model for the light nucleus with mass number about 10, which is too light for statistical theory and is too heavy for few body problem[2]. More experimental DDX data are very useful for

* The project was funded by the CNDC and National Natural Science Foundation of China under Grant No.19975002.

validation of the models and parameters adopted in the calculations.

In this paper, the measurements of double-differential emission neutron cross sections of beryllium are presented, the measurements were performed for 5.9 and 6.4 MeV incident neutron energy and at 10 angles between 25 and 150 degree. The measured data are compared with other experiments and ENDF/B-6 evaluated data.

1 Experimental Details

The experiments were carried out with the 4.5 MV Van de Graaff accelerator TOF facility in the Institute of Heavy Ion Physics, Peking University. The monoenergetic neutrons with energies of 5.9 and 6.4 MeV were produced via the d+D reaction using a deuterium gas target. The deuteron beam was bunched into pulses of 1.7 ns full width at half maximum (FWHM) by a Klystron bunching system with 3 MHz frequency[3]. The full width at one-hundredth of maximum is 6.3 ns FWHM. The cell of gas target is a tantalum-lined stainless-steel cylinder of 1 cm long and 0.95 cm in diameter, isolated from the vacuum system by a 5.0-μm-thick molybdenum foil and filled to a pressure of 2.8 atm* with 99.9% high purity deuterium. A thin platinum disk was used as beam stop.

The scattering sample was a right cylinder of beryllium metal (3.0 cm in diameter and 4 cm long). The sample was placed at 0° with respect to the deuterium beam about 16.2 cm away from the center of the gas target. Its axis was vertical and perpendicular to the deuterium beam. The distance from the secondary neutron detector to the center of the sample was 376.8 cm. The scattering angle was changed by rotating the neutron detector around the center of sample. A polyethylene sample (2.9 cm in outer diameter, 0.9 cm in inner diameter, 4 cm long) was used to obtain the differential cross section of n-p scattering at a few forward angles between 25 deg and 45 deg.

The secondary neutron detector was an ST–451 liquid scintillator (similar to NE213), 105 mm in diameter and 50 mm thick, coupled to an XP2040 photomultiplier tube[4]. Using a fast/slow timing system for ^{60}Co gamma-gamma coincidence measurements, the time resolution for the detector was 625 ps at

* 1 atm=101325Pa

dynamic range of 70:1[4]. A standard TOF electronics setup was employed for measurements using a timing discriminator and a standard pulse-shape discrimination (PSD) mode based on the zero-crossover technique. Relative detector efficiency was determined by TOF measurement of prompt fission neutron spectrum from a thin ^{252}Cf source,[5] and by Monte Carlo calculations using the code NEFF7 from PTB. The calculated efficiencies are in agreement with the experimental results. The main detector was placed inside a hollow lead cylinder with the wall thickness of 6 cm, which was imbedded in a massive shield[6] containing high-density polyethylene and boron carbonate (8% B_4C) mixture. A double-truncated conical collimator made of copper was inserted into the shield to provide a non-perturbing access channel to the shielded detector for optimum transmission of the neutron flux of interest. The massive shield has a diameter of 1.3 m and length of 2.3 m. A copper shadow bar (80 cm long) was used to shield the direct neutrons from the neutron source. In order to reduce floor –scattered neutrons, the detector was about 1.8 m high from the floor and the gas target was located above a pit of 3.0 m in diameter and 2.0 m in depth, and was about 6.0 m away from the wall.

A Stilbene scintillator (40 mm in diameter and 25 mm thick) coupled to a RCA8575 photomultiplier tube was employed as a monitor to measure the intensity and spectrum of source neutrons by the TOF method, and used for the flux normalization of the measurements at different angles for a certain incident energy. The monitor was also placed in a massive shield made of paraffin+Li_2CO_3, copper and lead, at 90° with respect to the deuteron beam about 356.8 cm away from the center of the gas target.

Owing to the restriction of fixed 3 MHz pulsed beam frequency, and to expect a good energy resolution of the TOF spectrometer, the flight path was taken as 3.768 m and the secondary neutron detector bias was set at 0.85 MeV neutron energy. In the case of 1 cm long gas target, the overall time resolution of the TOF system was 2.0 ns and energy resolution for 6 MeV neutrons was 3.7%.

For data acquisition, TOF and pulse-shape discrimination spectra of the secondary neutron detector and the monitor detector were recorded by using the Canberra 35-plus multi-channels pulse-height analyzer with multi-ADC interface.

The DDX measurements were carried out at 10 lab angles between 25° and 150°. At each scattering angle, sample-in and sample-out measurements were done.

2 Results and Discussion

The measured TOF spectra were corrected for backgrounds, then transformed into the energy spectra with 0.1 MeV energy bin, and also corrected for main detector efficiency. The TOF spectra for gas-out neutron backgrounds were measured in the case of sample in and sample out respectively and discovered that there was no significant structure on the measured spectra in the energy range concerned. For this reason, the corrections were made only for the gas-in and sample-out backgrounds. As for the effects of degraded neutrons via the scattering by the target assembly and shadow bar , it produced negligibly small backgrounds. The corrections for finite sample size effects (flux attenuation and multiple scattering) and for experimental finite geometry of neutron source were performed by Monte Carlo program FAMS[7] calculations. This program simulates neutron scattering processes in the sample, taking into account of the kinematics of neutron scattering and finite geometry. Finally the absolute DDX was determined by using the differential n-p scattering cross section.

The experimental uncertainty was estimated by considering the contributions from counting statistics (2%~10%), detector efficiency (2.2%~4%), absolute normalization (3%~4%) and sample size correction (2%~8%).

In Figs. 1~2, the measured DDXs results for at 5.9 and 6.4 MeV are presented respectively compared with the experimental data by Drake et al. at LANL[8] and Baba et al. at Tohoku[9] as well as ENDF/B-6[10] evaluated data. The uncertainty is only statistical one.

It can be seen from Figs. 1~2 that the general trend of our experimental data, LANL data and Tohoku data is in fair agreement with each other. According to the experimental conditions of LANL and Tohoku, the energy resolution is 3.8% and 5.2% respectively for 6.0 MeV neutrons, ours is somewhat better than LANL's, but is much better than Tohoku's. So in the inelastic-scattering energy region from the low-lying levels in ^{9}Be, there are some differences. (1) The inelastic-scattering from $5/2^{-}$ level (1.68 MeV) was not observed in the experiments of D. M. Drake and M. Baba. The contribution from this level may be submerged in lower energy tail of the elastic scattering peak and the neutrons from (n, 2n) reaction, which is just opened.

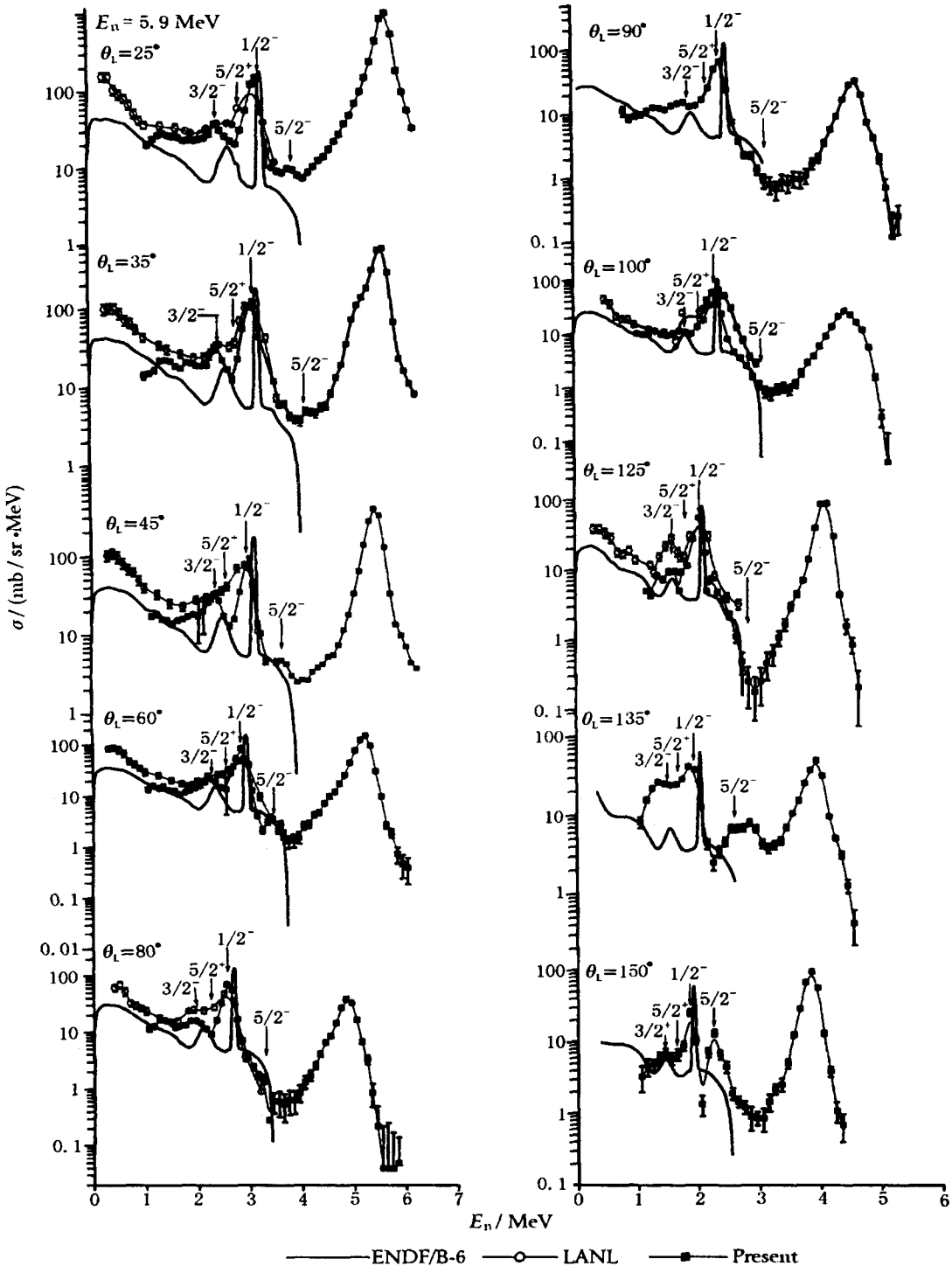

Fig. 1 Double differential cross sections of ^{9}Be at 5.9 MeV

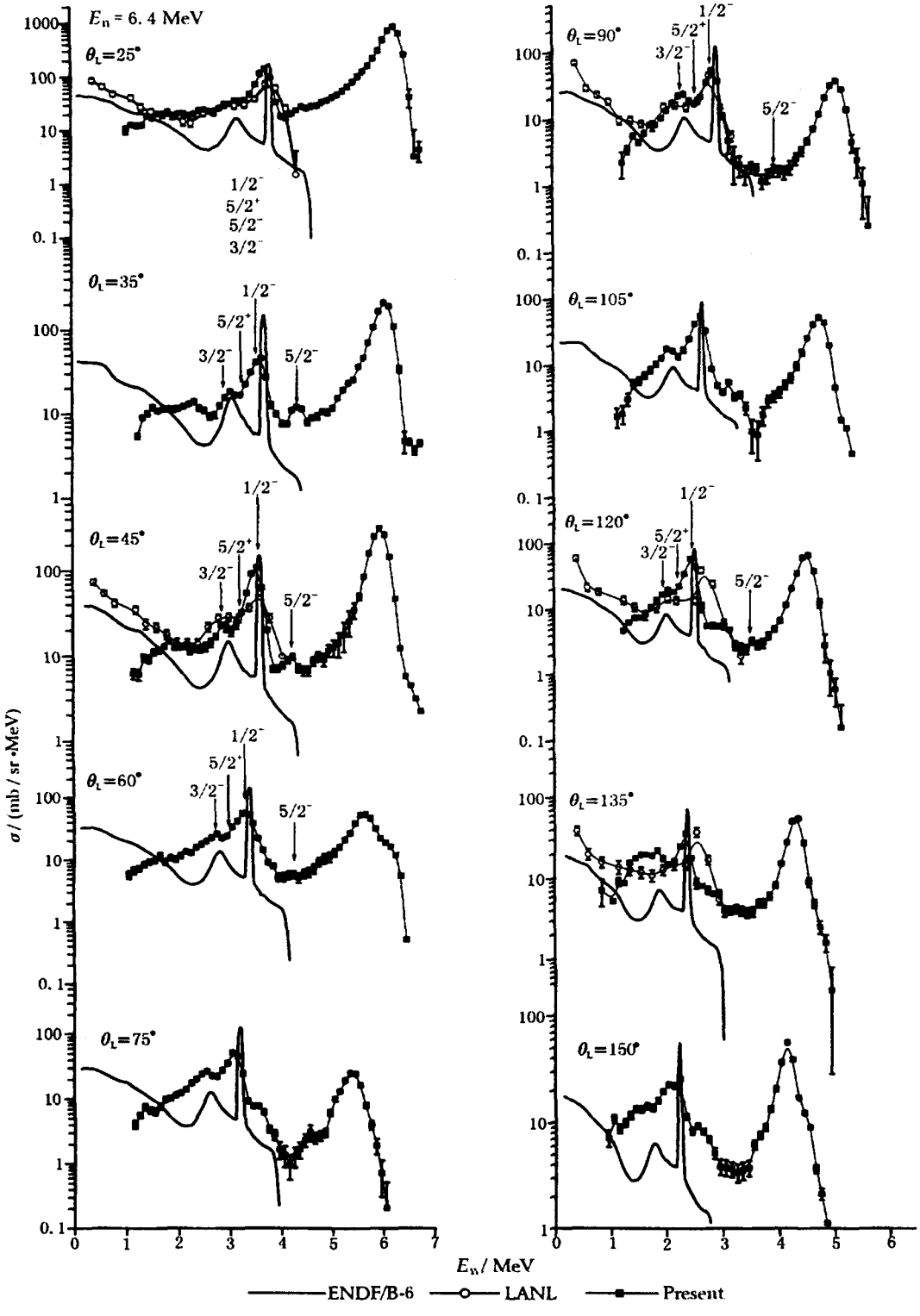

Fig. 2 Double differential cross sections of ^{9}Be at 6.4 MeV

But from Figs. 1~2, it can be seen that there is probably a contribution from this level. (2) In addition to the notable inelastic-scattering from 2.43 MeV level, although the scattering from $5/2^+$ and $3/2^-$ level (2.8 and 3.06 MeV) could not be completely separated with each other, taking into accounts of level width of these levels, it still can be seen that the scattering from $5/2^+$ and $3/2^-$ level exist. This is important for theoretical calculation, because the scattering from 3.06 MeV was neglected in the evaluation[11].

As for lower energy range below 2 MeV, the continuum neutrons come from the multi-particle decay processes reaching to (n, 2n) reaction. The data by Drake et al. are larger than ours. The Ref. 12 pointed out that the experimental data at 14 MeV incident neutron for ^{9}Be by Drake et al. are also larger than that of Baba et al. and Takahashi et al. at lower energy range. According to Zhang's theoretical calculation,[2] the data by Drake et al. are also considered to be larger. Anyway, there exists discrepancy for the ^{9}Be DDX data at low energy region.

The data will be analyzed further.

Acknowledgements

The authors would like to thank the crew of the 4.5 MV Van de Graaff accelerator at Peking University for the accelerator operation.

References

[1] Shen Guangren, Evaluated report on the experimental DDXs of n+^{9}Be reaction below 20 MeV. 1997., Private Communication.

[2] Zhang Jingshang, Han Yinlu, Shen Guangren, et al. INDC(CPR)-047/L (1998)5

[3] Lu Jianqin, Quan Shengwen. Instr. Nucl. Meth. in Phys. Rech. A, 346(1994)31-35.

[4] Chen Jinxiang. Nucl. Elect. and Detect. Technol., 13 120 (1993)

[5] Chen Jinxiang, Shi Zhaomin, Tang Guoyou. Nucl. Elect. Detect. Technol., 13 323 (1993)

[6] Gang Yue, Jinxiang Chen, Med.Phys. 24(6) 852 (1997)

[7] Mao Xiaoyong, Shen Guanren. Development for the Program FAMS and Application. Private Communication.(1998)

[8] D.M. Drake, G.F.Auchampaugh, E.D.Arthur et al. Nucl. Sci. And Engin. 63, 401-412, (1977)

[9] M. Baba, T. Sakase, T. Nishitani, et al. (1978) Proc. Conf. Neutron Phys. Nucl. Data Reaction & Appl. Purposes, U.K.AEA, Harwell. ICPR Neutron 79/9824,p198.

[10] T.D. Beynon and B.S. Sim, Ann. Nucl. Energy 15,27-43 (1988)

[11] M. Baba, JAERI-M 86-029 (1986). p123.

[12] M. Baba. Nucl. Data for Sci. and Technol. (1988 Mito) 210

Measurement of $^{186}W(n,\gamma)^{187}W$ Cross Sections in the Energy Region from 0.50 to 1.50 MeV

Zhang Guohui Shi Zhaomin Liu Guangzhi Tang Guoyou Chen Jinxiang
(Institute of Heavy Ion Physics, Peking University, Beijing 100871)
Lu Hanlin
(China Institute of Atomic Energy, Beijing 102413)

Abstract

On the basis of analyzing previous experimental methods and results, the cross sections of the $^{186}W(n,\gamma)^{187}W$ reaction were measured in the neutron energy range from 0.50 to 1.50 MeV with activation technique. Neutrons were produced through T(p,n) ^{3}He reaction and the cross sections of $^{197}Au(n,\gamma)^{198}Au$ reaction were used to determine neutron fluence. Our experiment shows that without the tungsten resonance absorption foils, the measured cross sections of the $^{186}W(n,\gamma)^{187}W$ reaction by activation method will be larger than the correct ones because of the resonance neutron.

Introduction

Tungsten is one of the structural materials for fusion reactors since it can endure high temperature. The cross sections of the $^{186}W(n,\gamma)^{187}W$ reaction are

important in evaluating the radiation damage of the material. Some experiments were performed to measure the cross sections of $^{186}W(n,\gamma)^{187}W$ reaction[1~13], but there are large discrepancies among them especially in the MeV neutron energy region. Therefor, new experiment is needed to clarify the existing differences.

1 Experiment

The experiments were performed at 4.5 MV Van de Graaff accelerator of the Institute of Heavy Ion Physics, Peking University. The monoenergetic neutron of 0.5, 1.15 and 1.50 MeV was produced via the $T(p,n)^3He$ reaction on a solid T-Ti target of 1.30 mg/cm^2 in thickness. The target was cooled by water during the experiment. The cross sections of the $^{197}Au(n,\gamma)^{198}Au$ reaction were used to determine the neutron fluence.

Natural tungsten disks (the abundance of the ^{186}W is 28.426%) of 19.1 mm in diameter and about 5 g in weight were used. Each tungsten sample was sandwiched between two other tungsten foils (of 19.1 mm in diameter, served as the resonance absorption foils, since the cross section of the $^{186}W(n,\gamma)^{187}W$ reaction is about 50000 b at 18 eV) and then between two gold foils with the diameter of 19.1 mm and weight about 1.0 g. The sample groups were wrapped with cadmium foils 0.5 mm in thickness.

The samples were placed at 0° related to the incident proton beam, and the distance from the sample to the target was about 2.2 cm. The irradiation durations for three samples corresponding to 0.50, 1.15 and 1.50 MeV were about 11, 15 and 23 h, respectively. The incident proton energies were 1.427, 2.025 and 2.378 MeV, respectively. The proton beam current was about 10 μA. The neutron flux was monitored by a BF_3 long counter placed at 0° to the proton beam and at a distance of 3.0 m from the neutron source. The integral count of the long counter per 2 minutes was recorded continuously by a microcomputer multiscalar for calculating the correction factor of the neutron flux fluctuation.

After irradiation, the activities of the residual nuclei ^{187}W β^- and ^{198}Au were measured with an ORTEC HPGe γ-detector (105 cm^3), calibrated by a set of standard γ-sources. The measuring durations for each tungsten and gold sample were

about 30 and 10 minutes to ensure statistics of counts better than 1%. The decay data of the residual nuclei including the half-life, γ-ray energy and γ transition intensity are taken from reference [14] and listed in Table 1.

Table 1 Decay data of the residual nuclei

Nuclei	$T_{1/2}$	E_γ	I_γ
^{187}W	23.72 h	685.73 keV	27.3 %
^{198}Au	2.695 d	411.80 keV	95.57 %

2 Corrections

Two main corrections were made as the following:

2.1 γ-ray Self-absorption in the Sample

The correction factor is given by

$$f_s = \frac{1 - e^{-\mu x}}{\mu x} \tag{1}$$

where μ is the total-mass absorption coefficient in cm^2/g, x is the sample thickness in g/cm^2.

Before the irradiation of the samples, the total-mass absorption coefficient was measured experimentally by means of the γ-ray passing through a series of tungsten or gold samples with different thickness. Because the 661.6 keV γ-ray energy of ^{137}Cs approaches to the 685.73 keV γ-ray energy of ^{187}W, the total-mass absorption coefficient of tungsten sample was measured by using the 661.6 keV γ-ray of ^{137}Cs instead of the 685.73 keV γ-ray of ^{187}W. The values of f_s for our tungsten samples are around 0.920 for the thickness of the samples. Similarly, the total-mass absorption coefficient for the gold sample was measured by using the 411.115 keV γ-ray of ^{152}Eu source instead of the 411.80 keV γ-ray of ^{198}Au and the values of f_s for our gold samples are around 0.986.

2.2 Correction for Sum Peak

Because of the sum peak effect from cascade γ rays, the measured 685.73 keV γ-ray intensity will be a few percent lower than the correct one. So a correction

factor is needed. This correction factor for our measurement is 0.980, according to the decay scheme [14] and the efficiency curve of the HPGe detector.

3 Results

After considering the detector efficiency, γ-intensity, correction factor from the fluctuation of the neutron flux, γ-ray self absorption in the samples and cascade correction, the cross sections of the $^{186}W(n,\gamma)^{187}W$ reaction were calculated using the well known activation formula. The results of present experiment as well as the reference cross sections of the $^{197}Au(n,\gamma)^{198}Au$ reaction are listed in Table 2, and the latter were taken from the ENDF/B-6 library. Calculation shows that the neutron energy spread mainly comes from the thickness of the T-Ti target and the angle subtended by the sample to the target.

Table 2 Measured results and the reference cross section data

E_n / MeV	Cross section / mb	
	$^{186}W(n,\gamma)^{187}W$	$^{197}Au(n,\gamma)^{198}Au$
0.50 ± 0.08	44.5 ± 2.2	132.4 ± 4.6
1.15 ± 0.08	39.6 ± 2.2	75.4 ± 3.4
1.50 ± 0.08	33.4 ± 1.9	67.6 ± 3.0

Table 3 Principal sources of error for the measured cross section

Source of uncertainty	Relative error / %
Reference cross section	3.5~4.5
γ-counting statistics for ^{187}W	1
γ-counting statistics for ^{198}Au	1
γ-detection efficiency for ^{187}W	1.5
γ-detection efficiency for ^{198}Au	1.5
correction of γ self absorption for ^{187}W	1.0
correction of γ self absorption for ^{198}Au	0.5
^{186}W sample weight	0.2
^{197}Au sample weight	0.2
determination of peak area	2.0
Total	5.0~5.7

Principal sources of error and their magnitudes for our measurement are given in Table 3. Errors from the decay scheme were not included.

The results of our and other measurements as well as the data of ENDF/B-6 are plotted in Fig.1, from which the discrepancies can be seen. Among the measurements, two kinds of methods were used. Macklin[4], Bokhovko[3], and Voigner[2] performed their measurements by using time-of-flight method, and all others by using activation method. Our results are in good agreement with those of Macklin, Bokhovko and Voigner. All the measurements carried out by using activation method are in different magnitude larger than the results measured by the time-of-flight method. We think this is due to the effect of the resonace neutrons around 18 eV. For analyzing the effect of resonance neutrons, we performed the cross section measurement of the $^{186}W(n,\gamma)^{187}W$ reaction, with and without the tungsten resonance absorption foils. Our results show that without the resonance absorption foils, the measured value of the cross section are 20% and 14% larger than that with one for 0.50 and 1.15 MeV neutron energies, respectively. Therefore, the correction for the resonance neutron effect should be considered. The ENDF/B-6 data evaluation is also somewhat large in the energy range of E_n<1.2 MeV.

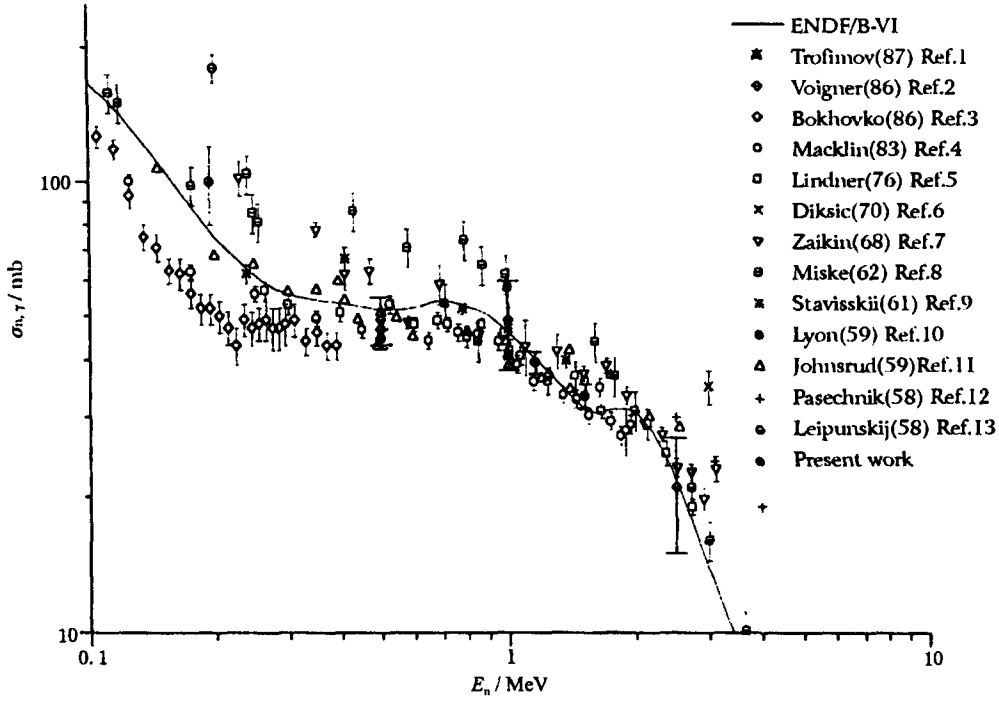

Fig.1 The cross sections of $^{186}W(n,\gamma)$ ^{187}W reaction

The authors appreciate the support from China Nuclear Data Center. They also thank the crew of the 4.5 MV Van de Graaff accelerator at IHIP, Peking University for their kind cooperation.

References

[1] Yu. N. Trofimov et al. Exfor No.41001037

[2] J. Voigner et al. Exfor No.22006021

[3] M. V. Bokhovko et al. Exfor No.40925006

[4] R. L. Macklin et al. Exfor No.10999009

[5] M. Lindner et al. Exfor No.10221044, 10221045, 10221046

[6] M. Diksic et al. Exfor No.30023012

[7] G. G. Zaikin et al. Exfor No.40248004

[8] J. A. Miskel et al. Exfor No.12115005, 12115006

[9] Yu. Ya. Stavisskii et al. Exfor No. 40452005

[10] W. S. Lyon et al. Exfor No. 11407030

[11] A. E. Johnsrud et al. Exfor No. 11675025

[12] M. V. Pasechnik et al. Exfor No. 40336093

[13] A. I. Leipunskij et al. Exfor No. No. 40244080

[14] John Wiley and Sons. Table of Isotopes, 8th edition, 1996

II THEORETICAL CALCULATION

Three Body Breakup Process

Zhang Jingshang
(China Nuclear Data Center, CIAE, Beijing)

Abstract

In the neutron induced reactions of light target nuclei, three body breakup process is an important mechanism. For some cases the compound nucleus or the residual nucleus after particle emission undergo the three body breakup process. In this paper the double differential cross sections of outgoing particles from three body breakup process are given based on Qhlson's formula. The energy balance is discussed.

1 Direct Three Body Breakup Process

In some reaction processes the compound nuclei have direct three body breakup mechanism, like

$$n+^{9}Be \rightarrow ^{10}Be^{*} \rightarrow n+n+^{8}Be$$

and

$$n+^{6}Li \rightarrow ^{7}Li^{*} \rightarrow n+d+\alpha .$$

The three bodied kinetics has been given by Ohlson[1] (1965), the masses of the three outgoing particles are denoted by m_a, m_b, m_c, and $m_a + m_b + m_c = M_1$. All of the nomenclature used in this paper can be found in refs. [2,3]. The triple differential cross section is for the observation of particle a with $(\theta_a, \phi_a, \varepsilon_a)$ simultaneously with particle b with (θ_b, ϕ_b). Regardless the particle b, and integrated over Ω_b, the double differential cross section of the particle a can be obtained analytically with isotropic distribution by

$$\frac{d^2\sigma}{d\varepsilon_a d\Omega_a} = \frac{S(\varepsilon_a)}{4\pi} \tag{1}$$

where the normalized spectrum of the particle a reads

$$S(\varepsilon_a) = \frac{8}{\pi \varepsilon_{a(max)}^2} \sqrt{\varepsilon_a (\varepsilon_{a(max)} - \varepsilon_a)} \tag{2}$$

with $$\varepsilon_{a(min)} = 0, \quad \varepsilon_{a(max)} = \frac{M_1 - m_a}{M_1} Q \tag{3}$$

where Q refers the energy released from the three body breakup process.

For ^{6}He, $Q = E_{k_1} - 0.973$ MeV. The energy carried by the particle a is given by

$$E_a(c) = \int_0^{\varepsilon_{a(max)}} \varepsilon_a S(\varepsilon_a) d\varepsilon_a = \frac{1}{2} \varepsilon_{a(max)} \tag{4}$$

The formula of the particles b or c can be obtained by substituting the subscript a by b or c, respectively. Thus, the energy conservation is satisfied as

$$E_a + E_b + E_c = Q \tag{5}$$

2 Three Body Breakup Process of Residual Nucleus

When the residual nucleus is ^{6}He* in its excited state, like ^{9}Be(n,α)^{6}He*, the three body breakup process of ^{6}He*→n+n+α will be happened. The residual recoil nucleus ^{6}He* has the angular distribution in CMS as

$$\frac{d\sigma}{d\Omega_c^{M_1}} = \sum_l \frac{2l+1}{4\pi} (-1)^l f_l^{m_1}(c) P_l(\cos\theta_c^{M_1}) \tag{6}$$

where M_l is the mass of ^{6}He*. Taking particle a as an example, $S(\varepsilon_a)$ is the normalized spectrum in the residual recoil system, the double differential cross section in CMS can be obtained by averaging over the angular distribution of the residual nucleus. Thus we have

$$\frac{d^2\sigma}{d\varepsilon_c^{m_a} d\Omega_c^{m_a}} = \int \frac{d\sigma}{d\Omega_c^{M_1}} \frac{d^2\sigma}{d\varepsilon_r^{m_a} d\Omega_r^{m_a}} \sqrt{\frac{\varepsilon_c^{m_a}}{\varepsilon_r^{m_a}}} d\Omega_c^{M_1} \tag{7}$$

By multiplying $P_l(\cos\theta_c)$ and integrating over Ω_c, the Legendre coefficient of the particle a in CMS can be given by

$$f_l(\varepsilon_c^{m_a}) = 2\pi \iint \frac{d\sigma}{d\,\Omega_c^{M_1}} \frac{d^2\sigma}{d\varepsilon_r^{m_a} d\,\Omega_r^{m_a}} \sqrt{\frac{\varepsilon_c^{m_a}}{\varepsilon_r^{m_a}}} P_l(\cos\theta_c) d\,\Omega_c^{M_1} d\cos\theta_c \tag{8}$$

let Θ be the angle between $\Omega_c^{M_1}$ and $\Omega_c^{m_a}$, using

$$P_L(\cos\Theta) = \frac{4\pi}{2L+1} \sum_m Y_{Lm}^*(\Theta,\Phi) Y_{Lm}(\Omega_c^{M_1}) \tag{9}$$

carrying out the integration over $d\cos\Theta d\Phi$, one get

$$f_l(\varepsilon_c^{m_a}) = \frac{(-1)^l}{2} f_l^{m_1}(c) \int \sqrt{\frac{\varepsilon_c^{m_a}}{\varepsilon_r^{m_a}}} P_l(\cos\Theta) S(\varepsilon_r^{m_a}) d\,\Theta \tag{10}$$

The relation of $\cos\Theta$ and $\varepsilon_r^{m_a}$ is

$$\cos\Theta = \frac{\varepsilon_c^{m_a} + \frac{m_a}{M_1} E^c(M_1) - \varepsilon_r^{m_a}}{2\sqrt{\frac{m_a}{M_1} E^c(M_1)\varepsilon_c^{m_a}}} \tag{11}$$

Replacing Θ in Eq.10 by $\varepsilon_r^{m_a}$ and denoting

$$\beta = \sqrt{\frac{m_a}{M_1} E^c(M_1)} \tag{12}$$

we have $$f_l(\varepsilon_c^{m_a}) = \frac{(-1)^l}{4\beta} f_l^{m_1}(c) \int_a^b \frac{S(\varepsilon_r^{m_a})}{\sqrt{\varepsilon_r^{m_a}}} P_l\left(\frac{\varepsilon_c^{m_a} + \beta^2 - \varepsilon_r^{m_a}}{2\beta\sqrt{\varepsilon_c^{m_a}}}\right) d\varepsilon_r^{m_a} \tag{13}$$

where the upper and lower integrating limits are given by

$$a = \max\{\varepsilon_{r,\min}^{m_a}, (\sqrt{\varepsilon_c^{m_a}} - \beta)^2\} \qquad b = \min\{\varepsilon_{r,\max}^{m_a}, (\sqrt{\varepsilon_c^{m_a}} - \beta)^2\} \tag{14}$$

The energy region of the particle a in CMS is given by

$$\varepsilon_{c,\max}^{m_a} = (\beta + \sqrt{\varepsilon_{r,\max}^{m_a}})^2 \tag{15}$$

$$\varepsilon_{c,\min}^{m_a} = \begin{cases} \left(\beta - \sqrt{\varepsilon_{r,\max}^{m_a}}\right)^2 & \text{if } \sqrt{\varepsilon_{r,\max}^{m_a}} < \beta \\ 0 & \text{if } \sqrt{\varepsilon_{r,\min}^{m_a}} < \beta < \sqrt{\varepsilon_{r,\max}^{m_a}} \\ (\sqrt{\varepsilon_{r,\min}^{m_a}} - \beta)^2 & \text{if } \beta < \sqrt{\varepsilon_{r,\min}^{m_a}} \end{cases} \tag{16}$$

It is easy to prove that the spectrum $f_0(\varepsilon_c^{m_a})$ of the particle a in CMS is normalized by carrying out the integration

$$\int_{\varepsilon_{c,\min}^{m_a}}^{\varepsilon_{c,\max}^{m_a}} f_0(\varepsilon_c^{m_a})\mathrm{d}\varepsilon_c^{m_a} = \frac{1}{4\beta}\int_0^{\varepsilon_r^{m_a}} \mathrm{d}\varepsilon_r^{m_a} \frac{S(\varepsilon_r^{m_a})}{\sqrt{\varepsilon_r^{m_a}}} \int_{(\sqrt{\varepsilon_r^{m_a}}-\beta)^2}^{(\sqrt{\varepsilon_r^{m_a}}+\beta)^2} \mathrm{d}\varepsilon_c^{m_a} = \int_0^{\varepsilon_{r,\max}^{m_a}} \mathrm{d}\varepsilon_r^{m_a} S(\varepsilon_r^{m_a}) = 1$$

In this case the energy carried by the particle a is

$$E_a^c = \int_0^{\varepsilon_{a(\max)}} f_0(\varepsilon_c)\varepsilon_c \mathrm{d}\varepsilon_c = \frac{1}{2}\varepsilon_{a(\max)} + \frac{m_1}{M_1}E^c(M_1) \tag{17}$$

where $E^c(M_1) = \frac{m_1}{M_c}(E^* - B_1 - E_{k_1})$ stands for the energy carried by the residual nucleus $^6He^*$ after the first particle emission. In laboratory system the energies carried by the three particles becomes into

$$E^l(m_a) = \frac{m_n m_a}{M_T^2}E_n + E^c(m_a) - 2\frac{m_a}{M_c}\sqrt{\frac{m_n}{M_1}E_n E^c(M_1)f_1^{m_1}(c)} \tag{18}$$

$$E^l(m_b) = \frac{m_n m_b}{M_T^2}E_n + E^c(m_b) - 2\frac{m_b}{M_c}\sqrt{\frac{m_n}{M_1}E_n E^c(M_1)f_1^{m_1}(c)} \tag{19}$$

$$E^l(m_c) = \frac{m_n m_c}{M_T^2}E_n + E^c(m_c) - 2\frac{m_c}{M_c}\sqrt{\frac{m_n}{M_1}E_n E^c(M_1)f_1^{m_1}(c)} \tag{20}$$

The total released energy reads

$$E^l(m_a) + E^l(m_b) + E^l(m_c) + E^l(m_1) = E_n + B_n - B_1 + Q \tag{21}$$

where the energy carried by the first emitted particle is

$$E^l(m_1) = \frac{m_1 m_n}{M_c^2}E_n + \frac{M_1}{M_c}(E^* - B_1 - E_{k_1}) + \frac{M_1}{M_c}\sqrt{\frac{m_n}{M_1}E_n E^c(M_1)f_1^{m_1}(c)} \tag{22}$$

Thus, it is easy to see that the energy balance is held.

References

[1] G. G. Ohlson. Nucl. Instrm. Meth. 200 361 (1965)

[2] J. S. Zhang. CNDP 21 5 (1998)

[3] J. Z. Zhang. Nucl. Sci. Eng. 133 218 (1999)

Energy Balance in UNF Code

Zhang Jingshang
(China Nuclear Data Center, CIAE, Beijing)

Introduction

The energy balance for whole reaction processes must be taken into account to set up neutron data file. For each reaction channel with the Q value, the released total energy includes the energies of the outgoing particles E_p, the energy of the recoil nucleus E_R, and the gamma decay energy E_γ. The energy balance needs

$$E_R+E_p+E_\gamma=E_n+Q \tag{1}$$

where E_n stands for the incident neutron energy in LS. Since the charged particles have strong stopping power, it is easy to be detained in nuclear material and transformed the kinetic energy into heat, which is called reaction heat. Information on the energy of charged particles produced in the nuclear reactions is needed in several applications. For example, the kerma factor (Kinetic Energy Released from Material) is of specific interest regarding the heat produced in fusion reactors as well as regarding the calculation of radiation dose in radiobiology. If the recoil nucleus is assumed static in CMS after the first particle emission, in this way the energy balance can not be held. This paper will give the formulation of the energy balance of the secondary particle emissions, which is used in the UNF code.

All of the nomenclature used in this paper can be found in Ref. [1, 2]. The particle emissions have three cases: (1) from continuum states to continuum states, (2) from continuum states to discrete levels, (3) form levels to levels, of which the formulation is given in ref. [3]. Beside the laboratory system (LS) and the center of mass system (CMS), the recoil nucleus system (RNS) is also needed, which are labeled by subscripts l,c,r, respectively. At low incident energies (<20 MeV) the isotropic distribution is used for the secondary particle emissions in CMS [1]. In this case the double differential cross sections of the secondary particle emissions can be easily obtained.

1 Double Differential Cross Sections from Continuum State to Continuum State

Based on the relation of the double differential cross sections between CMS and RNS

$$\frac{\mathrm{d}^2\sigma}{\mathrm{d}\varepsilon_c \mathrm{d}\Omega_c}\mathrm{d}\varepsilon_c \mathrm{d}\Omega_c = \frac{\mathrm{d}^2\sigma}{\mathrm{d}\varepsilon_r \mathrm{d}\Omega_r}\mathrm{d}\varepsilon_r \mathrm{d}\Omega_r \tag{2}$$

the Jacobian is given by

$$\mathrm{d}\varepsilon_r \mathrm{d}\Omega_r = \sqrt{\frac{\varepsilon_c}{\varepsilon_r}}\mathrm{d}\varepsilon_c \mathrm{d}\Omega_c \tag{3}$$

The normalized double differential cross section reads

$$\frac{\mathrm{d}^2\sigma}{\mathrm{d}\varepsilon \mathrm{d}\Omega} = \sum_l \frac{2l+1}{4\pi} f_l(\varepsilon)\mathrm{P}_l(\cos\theta) \tag{4}$$

where $\mathrm{P}_l(\cos\theta)$ refers to the Legendre polynomial. Averaged by the double differential cross section of the residual nucleus after the first particle emission, the double differential cross section of the second particle emission can be obtained by

$$\begin{aligned}\frac{\mathrm{d}^2\sigma}{\mathrm{d}\varepsilon_c^{m_2}\mathrm{d}\Omega_c^{m_2}} &= \iint \frac{\mathrm{d}^2\sigma}{\mathrm{d}E_c^{M_1}\mathrm{d}\Omega_c^{M_1}} \frac{\mathrm{d}^2\sigma}{\mathrm{d}\varepsilon_r^{m_1}\mathrm{d}\Omega_r^{m_1}} \sqrt{\frac{\varepsilon_c^{m_1}}{\varepsilon_r^{m_1}}}\mathrm{d}\varepsilon_c^{M_1}\mathrm{d}\Omega_c^{M_1} \\ &= \sum_l \frac{2l+1}{4\pi} f_l(\varepsilon_c^{m_2})\mathrm{P}_l(\cos\theta_c^{m_2})\end{aligned} \tag{5}$$

where

$$\frac{\mathrm{d}^2\sigma}{\mathrm{d}E_c^{M_1}\mathrm{d}\Omega_c^{M_1}} = \sum_l \frac{2l+1}{4\pi} f_l(E_c^{M_1})\mathrm{P}_l(\cos\theta_c^{M_1}) \tag{6}$$

The isotropic distribution of the second particle emission reads

$$\frac{\mathrm{d}^2\sigma}{\mathrm{d}\varepsilon_r^{m_2}\mathrm{d}\Omega_r^{m_2}} = \frac{1}{4\pi}\frac{\mathrm{d}\sigma}{\mathrm{d}\varepsilon_r^{m_2}} \tag{7}$$

In terms of the orthogonal property of the Legendre polynomial, one get the Legendre coefficient

$$f_l(\varepsilon_c^{m_1}) = \frac{1}{2}\iiint \frac{\mathrm{d}^2\sigma}{\mathrm{d}E_c^{M_1}\mathrm{d}\Omega_c^{M_1}} \frac{\mathrm{d}\sigma}{\mathrm{d}\varepsilon_r^{m_2}} \sqrt{\frac{E_c^{M_1}}{\varepsilon_r^{m_2}}}\mathrm{P}_l(\cos\theta_c^{M_1})\mathrm{d}E_c^{M_1}\mathrm{d}\Omega_c^{M_1}\mathrm{d}\varepsilon_r^{m_2} \tag{8}$$

Denoting Θ as the angle between $\Omega_c^{M_1}$ and $\Omega_c^{m_2}$, using the relation

$$P_L(\cos\Theta)=\frac{4\pi}{2L+1}\sum_m Y^*_{Lm}(\Theta,\Phi)Y_{Lm}(\Omega_c^{M_1}) \tag{9}$$

and integrating over d cosΘdΦ, we have

$$f_l(\varepsilon_c^{m_1})=\frac{1}{2}\int\int f_l(E_c^{M_1})\frac{d\sigma}{d\varepsilon_r^{m_2}}\sqrt{\frac{\varepsilon_c^{m_1}}{\varepsilon_r^{m_1}}}P_l(\cos\Theta)dE_c^{M_1}d\cos\Theta \tag{10}$$

From the energy relation

$$\varepsilon_r^{m_2}=\varepsilon_c^{m_2}+\frac{m_2}{M_1}E_c^{M_1}-2\sqrt{\frac{m_2}{M_1}E_c^{M_1}\varepsilon_c^{m_2}}\cos\Theta \tag{11}$$

and substituting cosΘ in Eq.(10) by $\varepsilon_r^{m_2}$, then Eq.(10) changes into the following form

$$f_l(\varepsilon_c^{m_2})=\frac{1}{4}\sqrt{\frac{M_1}{m_2}}\int_A^B dE_c^{M_1}\frac{f_l(E_c^{M_1})}{\sqrt{E_c^{M_1}}}\int_a^b\frac{d\varepsilon_r^{m_2}}{\sqrt{\varepsilon_r^{m_2}}}\frac{d\sigma}{d\varepsilon_r^{m_2}}P_l\left(\frac{\varepsilon_c^{m_2}+\frac{m_2}{M_1}E_c^{M_1}-\varepsilon_r^{m_2}}{2\sqrt{\frac{m_2}{M_1}E_c^{M_1}\varepsilon_c^{m_2}}}\right) \tag{12}$$

For a given value of $\varepsilon_c^{m_2}$ the integration limits are given by

$$\begin{aligned}a&=\max\left\{\varepsilon_{r,\min}^{m_2},\left(\sqrt{\varepsilon_c^{m_2}}-\sqrt{\frac{m_2}{M_1}E_c^{M_1}}\right)^2\right\}\\ b&=\min\left\{\varepsilon_{r,\min}^{m_2},\left(\sqrt{\varepsilon_c^{m_2}}+\sqrt{\frac{m_2}{M_1}E_c^{M_1}}\right)^2\right\}\end{aligned} \tag{13}$$

The energy region of the second particle emission is obtained by

$$\varepsilon_{c,\max}^{m_2}=\left(\sqrt{\frac{m_2}{M_1}E_{c,\max}^{M_1}}+\sqrt{\varepsilon_{r,\max}^{m_2}}\right)^2 \tag{14}$$

$$\varepsilon_{c,\min}^{m_2}=\begin{cases}\left(\sqrt{\varepsilon_{r,\max}^{m_2}}-\sqrt{\frac{m_2}{M_1}E_{c,\min}^{m_2}}\right)^2 & \text{if } \varepsilon_{r,\max}^{m_2}<\frac{m_2}{M_1}E_{c,\min}^{M_1}\\ 0 & \text{othewise}\\ \left(\sqrt{\varepsilon_{r,\min}^{m_2}}-\sqrt{\frac{m_2}{M_1}E_{c,\max}^{m_1}}\right)^2 & \text{if } \frac{m_2}{M_1}E_{c,\max}^{M_1}<\varepsilon_{r,\min}^{m_2}\end{cases} \tag{15}$$

When $f_0(E_c^{M_1})$ is normalized, by means of exchanging the integration order one can prove that $f_0(\varepsilon_c^{m_2})$ is also normalized. It is easy to see that the scope of the outgoing energy spectrum is broaded if the recoil effect is taken into account. The lighter of the nucleus, the stronger of recoil effect and the broadening effect even more obviously.

When the value of $\varepsilon_c^{m_2}$ is given, and $\varepsilon_{c,\min}^{m_2} \le \varepsilon_c^{m_2} \le \varepsilon_{c,\max}^{m_2}$, the integration area of $E_c^{M_1}$ is given as follows

$$A=\begin{cases}\left(\sqrt{\varepsilon_{r,\min}^{m_2}}-\sqrt{\dfrac{m_2}{M_1}E_{2,\max}^{c}}\right)^2 & \text{if } \dfrac{m_2}{M_1}E_{2,\max}^{c}<\varepsilon_{2,\min}^{r}\\ 0 & \text{othewise}\\ \left(\sqrt{\dfrac{m_2}{M_1}E_{c,\min}^{m_1}}-\sqrt{\varepsilon_{r,\max}^{m_2}}\right)^2 & \text{if } \varepsilon_{r,\max}^{m_2}<\dfrac{m_2}{M_1}E_{c,\min}^{M_1}\end{cases}$$

$$B=\min\left\{E_{c,\max}^{M_1},\frac{M_1}{m_2}\left(\sqrt{\varepsilon_c^{m_2}}+\sqrt{\varepsilon_{r,\max}^{m_2}}\right)\right\} \tag{16}$$

The double differential cross section and the energy region of the recoil residual nucleus after the second particle emission can be obtained by replacing m_2 and $\varepsilon_r^{m_2}$ with M_2 and $E_r^{M_2}$, respectively.

2 Double Differential Cross Sections from Continuum State to Discrete levels

When the residual nucleus is in the discrete level states, the double differential cross section has different expression since $\varepsilon_r^{m_2}$ is a single value. In this case

$$\frac{d^2\sigma}{d\varepsilon_r^{m_2}d\Omega_r^{m_2}}=\frac{1}{4}\delta(\varepsilon_r^{m_2}-\varepsilon_{r,k}^{m_2}) \tag{17}$$

where

$$\varepsilon_{r,k}^{m_2}(E_c^{M_1})=\frac{M_2}{M_1}(E^*-B_1-B_2-E_k-\frac{M_c}{m_1}E_c^{M_1}) \tag{18}$$

and E_k refers to the energy of the residual nucleus in its k level. The Legendre

coefficient in Eq.(12) becomes into the form

$$f_l(\varepsilon_c^{m_2})_k = \frac{1}{4}\sqrt{\frac{M_1}{m_2}}\int_A^B \frac{f_l(E_c^{M_1})}{\sqrt{\varepsilon_{r,k}^{m_2}}\sqrt{E_c^{M_1}}} P_l(\cos\Theta)\mathrm{d}E_c^{M_1} \tag{19}$$

with

$$\cos\Theta = \frac{\frac{m_2}{M_1}E_c^{M_1} + \varepsilon_c^{m_2} - \varepsilon_{r,k}^{m_2}}{2\sqrt{\frac{m_2}{M_1}E_c^{M_1}\varepsilon_c^{m_2}}} \tag{20}$$

The maximum energy of the second emitted particle $\varepsilon_{c,max}^{m_2}$ corresponds to the opposite direction of the first outgoing particle. The $\varepsilon_{r,k}^{m_2}$ is the function of $E_c^{M_1}$, ei.

$$\varepsilon_{c,,max}^{m_2}(E_c^{M_1}) = \left(\sqrt{\frac{m_2}{M_1}E_c^{M_1}} + \sqrt{\varepsilon_{r,k}^{m_2}}\right)^2$$

The minimum value is given by

$$E_c^{M_1} = \frac{\frac{m_1}{M_c}E_k'}{1+\frac{M_c}{m_1}\frac{M_2}{m_2}}$$

with $$E_k' = E^* - B_1 - B_2 - E_k$$

There are three cases for the minimum values

$$\varepsilon_{c,min}^{m_2} = \begin{cases} \left(\sqrt{\frac{m_2}{M_1}E_{c,min}^{M_1}} - \sqrt{\varepsilon_{r,k}^{m_2}}\right)^2 & \text{if } \varepsilon_{r,k}^{m_2} \le \frac{m_2}{M_1}E_{c,min}^{M_1} \\ 0 & \text{if } \frac{m_2}{M_1}E_{c,min}^{M_1} < \varepsilon_{r,k}^{m_2} < \frac{m_2}{M_1}E_{c,max}^{M_1} \\ \left(\sqrt{\varepsilon_{r,k}^{m_2}} - \sqrt{\frac{m_2}{M_1}E_{c,max}^{M_1}}\right)^2 & \text{if } \frac{m_2}{M_1}E_{c,max}^{M_1} \le \varepsilon_{r,k}^{m_2} \end{cases} \tag{21}$$

For a given value of $\varepsilon_c^{m_2}$, from the condition of $-1 \le \cos\Theta \le 1$, one can get the integration area of $E_c^{M_1}$ as follows

$$A=\max\left\{E_{\mathrm{c,min}}^{M_1},\frac{1}{R^2}\left(\sqrt{U}-\sqrt{\frac{m_2}{M_1}\varepsilon_{\mathrm{c}}^{m_2}}\right)^2\right\}$$
$$B=\min\left\{E_{\mathrm{c,max}}^{M_1},\frac{1}{R^2}\left(\sqrt{U}+\sqrt{\frac{m_2}{M_1}\varepsilon_{\mathrm{c}}^{m_2}}\right)^2\right\} \tag{22}$$

where $R=\frac{m_2}{M_1}+\frac{M_2}{M_1}\frac{M_{\mathrm{c}}}{m_1}$; $U=\frac{M_2}{M_1}(RE_k'-\frac{M_{\mathrm{c}}}{m_1}\varepsilon_{\mathrm{c}}^{m_2})$. If $E_{\mathrm{c}}^{M_1}$ has its integration area ($A<B$), then we have the low integration limitation of $\varepsilon_{\mathrm{c}}^{m_2}$

$$\varepsilon_{\mathrm{c,min}}^{m_2}=\left(\sqrt{\frac{M_2}{M_1}(E_k'-\frac{M_c}{m_1}E_{\mathrm{c,max}}^{M_1})}-\sqrt{\frac{m_2}{M_1}E_{\mathrm{c,max}}^{M_1}}\right)^2 \tag{23}$$

The expression of the double differential cross section of the residual nucleus can be obtained by replacing m_2 and $\varepsilon_{\mathrm{r}}^{m_2}$ with M_2, and $E_{\mathrm{r}}^{m_2}$ in Eq. (19), respectively.

3 The Energy Balance

Using the formula

$$E_1=\frac{m}{2}\int v_l^2\frac{\mathrm{d}^2\sigma}{\mathrm{d}E_{\mathrm{c}}^{M_1}\mathrm{d}\,\Omega_{\mathrm{c}}^{M_1}}\mathrm{d}E_{\mathrm{c}}^{M_1}\mathrm{d}\,\Omega_{\mathrm{c}}^{M_1} \tag{24}$$

when the final state is in the continuum state, all of the released energies can be given by

$$\varepsilon_1^{m_1}=\int\left\{\left(\frac{m_{\mathrm{n}}m_1}{M_{\mathrm{c}}^2}E_{\mathrm{n}}+\varepsilon_{\mathrm{c}}^{m_1}\right)f_0(\varepsilon_{\mathrm{c}}^{m_1})+2\frac{\sqrt{m_{\mathrm{n}}m_1}}{M_{\mathrm{c}}}\sqrt{E_{\mathrm{n}}\varepsilon_{\mathrm{c}}^{m_1}}f_1(\varepsilon_{\mathrm{c}}^{m_1})\right\}\mathrm{d}\varepsilon_{\mathrm{c}}^{m_1} \tag{25}$$

$$E_1^{M_1}=\int\left\{\left(\frac{m_1M_1}{M_{\mathrm{c}}^2}E_{\mathrm{n}}+\frac{m_1}{M_1}\varepsilon_{\mathrm{c}}^{m_1}\right)f_0(\varepsilon_{\mathrm{c}}^{m_1})-2\frac{\sqrt{m_{\mathrm{n}}m_1}}{M_{\mathrm{c}}}\sqrt{E_{\mathrm{n}}\varepsilon_{\mathrm{c}}^{m_1}}f_1(\varepsilon_{\mathrm{c}}^{m_1})\right\}\mathrm{d}\varepsilon_{\mathrm{c}}^{m_1} \tag{26}$$

The residual energy is $E=E^*-B_1-\varepsilon_{\mathrm{c}}^{m_1}-E_{\mathrm{c}}^{M_1}$. for a given normalized spectrum the released γ energy is given by

$$\varepsilon_{\mathrm{c}}^{\mathrm{r}}=E^*-B_1-\left(1+\frac{m_1}{M_1}\right)\int\varepsilon_{\mathrm{c}}^{m_1}(\mathrm{c})f_0(\varepsilon_{\mathrm{c}}^{m_1})\mathrm{d}\varepsilon_{\mathrm{c}}^{m_1} \tag{27}$$

Thus, the total released energy E_c^T is given by the summation over eqs.25 through (27)

$$E_c^T = \varepsilon_1^{m_1} + E_1^{M_1} + \varepsilon_c^r = E_n + Q \tag{28}$$

From the aforementioned formulation, one can see that the quantity of the Legendre expansion coefficient with l=1 ($f_1^{m_1}$ >0) caused by the forward emission in the pre-equilibrium process increases the energy of the first emitted particle in the laboratory system, while the recoil effect reduce the energy of the second particle emitted from the recoil residual nuclei. Meanwhile the shape of $f_0(\varepsilon_c^{m_1})$ can also influence the energy distributions of the emitted particle, the residual nucleus and γ energy. The harder of the emitted spectrum, the more energy carried by the emitted particle, therefore the energies released by the residual nucleus and γ emissions are reduced. But in equilibrium emission process, either isotropic approximation or the Hauser-Feshbach theory, the partial wave with l=1 of the Legendre expansion is zero, only the energy distributions for all of kinds of the emitted particles are influenced by the shapes of the emitted first particle.

For the case of the secondary particle emissions, if the final state of the residual nucleus is in the continuum state, the energy carried by the first emitted particle in LS is given by

$$\varepsilon_{k_1}^{m_1}(\mathrm{l}) = \frac{m_n m_1}{M_c^2} E_n + \varepsilon_{k_1}^{m_1}(\mathrm{c}) + 2\frac{\sqrt{m_n m_1}}{M_c}\sqrt{E_n \varepsilon_{k_1}^{m_1}(\mathrm{c})} f_1(\varepsilon_{k_1}^{m_1}(\mathrm{c})) \tag{29}$$

where $$\varepsilon_{k_1}^{m_1}(\mathrm{c}) = \frac{M_1}{M_c}(E^* - B_1 - E_{k_1})$$

The energies of the second emitted particle and its residual nucleus in LS can be obtained by

$$\varepsilon_1^{m_2} = \int\left\{\left(\frac{m_n m_2}{M_c^2} E_n + \varepsilon_c^{m_2}\right) f_0(\varepsilon_c^{m_2}) + 2\frac{\sqrt{m_n m_2}}{M_c}\sqrt{E_n \varepsilon_c^{m_2}} f_1(\varepsilon_c^{m_2})\right\} \mathrm{d}\varepsilon_c^{m_2} \tag{30}$$

$$E_1^{M_2} = \int\left\{\left(\frac{m_n M_2}{M_c^2} E_n + E_c^{M_2}\right) f_0(\varepsilon_c^{M_2}) + 2\frac{\sqrt{m_n M_2}}{M_c}\sqrt{E_n E_c^{M_2}} f_1(E_c^{M_2})\right\} \mathrm{d}E_c^{M_2} \tag{31}$$

Substituting the expressions of $f_l(\varepsilon_c^{m_2})$ and $f_l(E_c^{M_2})$ for the l=1 partial wave into Eq. (30) and Eq. (31), and by using exchanging the integration order the energies released by the second emitted particle and its residual nucleus can be obtained by

$$\begin{aligned}\varepsilon_1^{m_2} = &\frac{m_n m_2}{M_c^2}E_n + \int\frac{d\sigma}{dE_c^{M_1}}E_c^{M_1}dE_c^{M_1} + \frac{m_1 m_2}{M_1^2}\int f_0(\varepsilon_c^{m_1})\varepsilon_c^{m_1}d\varepsilon_c^{m_1} \\ &-2\frac{\sqrt{m_n m_1}}{M_c}\frac{m_2}{M_1}\sqrt{E_n}\int f_1(\varepsilon_c^{m_1})\sqrt{\varepsilon_c^{m_1}}d\varepsilon_c^{m_1}\end{aligned} \tag{32}$$

$$\begin{aligned}E_1^{M_2} = &\frac{m_n M_2}{M_c^2}E_n + \frac{m_2}{M_2}\int\frac{d\sigma}{dE_c^{M_1}}E_c^{M_1}dE_c^{M_1} + \frac{m_1 M_2}{M_1^2}\int f_0(\varepsilon_c^{m_1})\varepsilon_c^{m_1}d\varepsilon_c^{m_1} \\ &-2\frac{\sqrt{m_n m_1}}{M_c}\frac{M_2}{M_1}\sqrt{E_n}\int f_1(\varepsilon_c^{m_1})\sqrt{\varepsilon_c^{m_1}}d\varepsilon_c^{m_1}\end{aligned} \tag{33}$$

The γ de-excitement energy is obtained by

$$\begin{aligned}\varepsilon_c^r &= \int\frac{d^2\sigma}{d\varepsilon_c^{m_1}d\Omega_c^{m_1}}\left[E^* - B_1 - B_2 - \left(1+\frac{m_1}{M_2}\right)\varepsilon_c^{m_1} - \left(1+\frac{m_2}{M_1}\right)E_c^{M_1}\right]d\varepsilon_c^{m_1}dE_c^{M_1}d\Omega_c^{m_1} \\ &= E^* - B_1 - B_2 - \left(1+\frac{m_1}{M_1}\right)\int\varepsilon_c^{m_1}f_0(\varepsilon_c^{m_1})d\varepsilon_c^{m} - \left(1+\frac{m_2}{M_2}\right)\int E_c^{M_1}\frac{d\sigma}{dE_c^{M_1}}dE_c^{M_1}\end{aligned} \tag{34}$$

Thus, the total released energy is

$$E_1^T = \varepsilon_1^{m_1} + \varepsilon_1^{m_2} + E_1^{M_2} + \varepsilon_c^r = E_n + Q \tag{35}$$

When the final state is in a discrete level state, with analogy procedure all of the released energies can be obtained. If the residual nucleus is in E_{k_2} level, the energy carried by the second emitted particle is obtained by

$$\begin{aligned}\varepsilon_k^{m_2}(1) = &\frac{m_n m_2}{M_c^2}E_n + \frac{M_2}{M_1}(E^* - B_1 - B_2 - E_{k_2}) - \left(\frac{M_2 M_c}{M_1^2} - \frac{m_1 m_2}{M_1^2}\right)\int f_0(\varepsilon_c^{m_1})\varepsilon_c^{m_1}d\varepsilon_c^{m_1} \\ &-2\frac{\sqrt{m_n m_1}}{M_c}\sqrt{E_n}\frac{m_2}{M_1}\int f_1(\varepsilon_c^{m_1})\sqrt{\varepsilon_c^{m_1}}d\varepsilon_c^{m_1}\end{aligned} \tag{36}$$

$$\begin{aligned}E_k^{M_2}(1) = &\frac{m_n M_2}{M_c^2}E_n + \frac{m_2}{M_1}(E^* - B_1 - B_2 - E_{k_2}) - \left(\frac{m_2 M_c}{M_1^2} - \frac{m_1 M_2}{M_1^2}\right)\int f_0(\varepsilon_c^{m_1})\varepsilon_c^{m_1}d\varepsilon_c^{m_1} \\ &-2\frac{\sqrt{m_n m_1}}{M_c}\sqrt{E_n}\frac{M_2}{M_1}\int f_1(\varepsilon_c^{m_1})\sqrt{\varepsilon_c^{m_1}}d\varepsilon_c^{m_1}\end{aligned} \tag{37}$$

in this case the γ de-excitement energy is $\varepsilon_k^{\gamma} = E_{k_2}$, the total released energy is given by

$$E_k^{\mathrm{T}} = \varepsilon_k^{m_1}(\mathrm{l}) + \varepsilon_k^{m_2}(\mathrm{l}) + E_k^{M_2}(\mathrm{l}) + \varepsilon_k^{\mathrm{r}} = E_{\mathrm{n}} + Q \tag{38}$$

the energy balance is held.

From the aforementioned formulation, when the recoil effect is taken into account strictly, the energy balance can be given in the analytical form. All of the recoil effect caused the energy spectra broaden.

Reference

[1] J. S. Zhang et al. Nucl. Sci. Eng. 133, p218 (1999)

[2] J. S. Zhang et al. Commu. Nucl. Data Prog. 20, p7 (1998)

[3] J. S. Zhang. Commu. Nucl. Data Prog. 22, p1 (1999)

CN0101645

Calculations of the Gamma Energy Spectra from Neutron Radiative Capture Reactions for ^{197}Au

Liu Jianfeng Zhao Weijuan

(Department of Physics, Zhengzhou University, 450052)

Abstract

The aim of this paper is to theoretically explain the abnormal protuberances near and above 5.5 MeV in the gamma spectra of the (n,γ) reactions of the nuclei within the nuclear mass regions from 110 to 140 and from 180 to 210, respectively.

Supposing that in the primary and cascade gamma de-excitation processes of the compound nucleus, in addition to the giant dipole resonance model, there exist the de-excitation processes of the excited states of ^{6}He, ^{6}Li, ^{6}Be, ^{7}Li and ^{7}Be particle cliques, for which the gamma-ray strength function was developed. The (n,γ) reaction cross sections and the gamma energy spectra at the neutron incident energies from 0.01 MeV to 3 MeV for ^{197}Au were calculated and the results are in better coincidence with the experimental data. Especially for the gamma energy spectra, the abnormal protuberances near and above 5.5 MeV were reproduced very well.

Introduction

A large number of experimental data[1] indicate that in the nuclear mass regions from 110 to 140 and from 180 to 210, there exist abnormal protuberances near and above 5.5 MeV in the gamma energy spectra of the neutron radiative captures, and the locations of these abnormal protuberances do not change basically at least below 4 MeV of the neutron incident energies. Their strengths do not change basically as well. These abnormal protuberances can not be explained in terms of the non-statistical effects[2~6] of the radiative captures since the energies of the separated spectrum lines corresponding to the non-statistical effects are changed with the changes of the incident neutron energies. The general approach for calculating the (n,γ) reaction cross sections and gamma energy spectra in the compound nucleus statistical theory is the form of the gamma-ray strength function. If the calculations of the gamma-ray strength function adopt the general used giant dipole resonance model, the compound nucleus statistical theory can not explain the abnomal protuberance around 5.5 MeV. A point of view for this abnormal phenomenon coming from the results of the decouplings of the partial E1strength in terms of the giant dipole resonance states was once proposed[7], but up to now the quantitative calculation results which can be compared with the experiments have not been found yet. Because the compound nucleus is a very complex configuration, there exist a large number of de-excitation pattens. In this paper, we suppose that in the primary and cascade gamma de-excitation processes of the compound nucleus, there exist the

de-excitation processes of the excited states of ^{6}He ^{6}Li ^{6}Be ^{7}Li and ^{7}Be particle cliques, combining the de-excitation patterns described by means of the giant dipole resonance model. The gamma-ray strength function of these processes was constructed. The (n,γ) reaction cross sections and the gamma energy spectra in the neutron incident energy region from 0.01 MeV to 3 MeV for ^{197}Au were calculated and the results are in better agreement with the experimental data. Especially for the gamma energy spectra, the abnormal protuberances near and above 5.5 MeV were reproduced very well. This so-called abnormal phenomenon was explained successfully.

1 The Calculation Formulas

The (n,γ) reaction cross sections and gamma energy spectra are calculated by solving the integral equations which describing the cascade gamma de-excitation processes. Its advantage is that the physical presentation is clear and the influences of the (n, γn') processes on the (n, γ) reaction cross sections are deducted.

Suppose that E_m represents the excitation energy of the compound nucleus, the region from E_m to E_c is the continuous one, where E_c is its inferior limit, below E_c there are N discrete energy levels denoted from the ground state by (E_1,J_1,π_1), (E_2,J_2,π_2), ... , (E_N,J_N,π_N), respectively. The continuous region is described by means of the energy level density $\rho(E,J,\pi)$, and $\sigma_c(E,J,\pi)$ is defined as the total excitation cross section in a unit energy interval with energy E, spin J and parity π in the whole gamma deexcitation process, $\sigma_{c0}(E,J,\pi)$ is its initial value, i.e. the contributions coming from the primary gamma transitions from the compound nucleus, σ_i is the total exitation cross section of i_{th} discrete energy level in the whole process and σ_{i0} is its initial value, it is also the contribution coming from the primary gamma transitions of the compound nucleus. Then the processes of the cascade gamma de-excitation of the compound nucleus satisfy the following integral equations:

$$\sigma_c(E,J,\pi)=\sigma_{c0}(E,J,\pi)+\int_{E}^{E_m}\sum_{J'\pi'}\sigma_c(E',J',\pi')\frac{T_\gamma^{E'J'\pi',EJ\pi}}{T^{E',J',\pi'}}\rho(E,J,\pi)\mathrm{d}E' \tag{1}$$

$$\sigma_i=\sigma_{i0}+\sum_{j=i+1}^{N}\sigma_j\frac{T_\gamma^{j}}{T^{j}}S^{ji}+\int_{E_c}^{E_m}\sum_{J'\pi'}\sigma_c(E',J',\pi')\frac{T_\gamma^{E'J'\pi',E_iJ_i\pi_i}}{T^{E',J',\pi'}}\mathrm{d}E' \tag{2}$$

the gamma energy spectra are:

$$\frac{d\sigma^{\gamma}}{dE_{\gamma}}=\sum_{i=1}^{N}\sum_{j=i+1}^{N}\sigma_{j}\frac{T_{\gamma}^{j}}{T^{j}}S^{ji}\,\delta(E_{\gamma}+E_{i}-E_{j})+\sum_{i=1}^{N}\sum_{J'\pi'}\sigma_{c}(E_{i}+E_{\gamma},J'\pi')\cdot$$

$$\frac{T_{\gamma}^{E_{i}+E_{\gamma}J'\pi'}}{T^{E_{i}+E_{\gamma}J'\pi'}}+\int_{E_{c}+E_{\gamma}}^{E_{m}}\sum_{J\pi J'\pi'}\sigma_{c}(E',J',\pi')\frac{T_{\gamma}^{E'J'\pi',E'-E_{\gamma}J\pi}}{T^{E',J',\pi'}}dE' \tag{3}$$

the gamma production cross section is:

$$\sigma^{\gamma}=\int_{0}^{E_{m}}\frac{d\sigma^{\gamma}}{dE_{\gamma}}dE_{\gamma} \tag{4}$$

but the (n,γ) reaction cross section is:

$$\sigma_{\gamma}=\sigma_{1} \tag{5}$$

σ_{i0} and $\sigma_{c0}(E,J,\pi)$ in equations (1) and (2) are calculated in terms of the absorption cross sections of the compound nucleus:

$$\sigma_{i0}=\sum_{J\pi}\sigma_{a}^{J\pi}\frac{T_{\gamma}^{E_{m}J\pi,E_{i}J_{i}\pi_{i}}}{T^{E_{m}J\pi}} \tag{6}$$

$$\sigma_{c0}(E,J,\pi)=\sum_{J'\pi'}\sigma_{a}^{J'\pi'}\frac{T_{\gamma}^{E_{m}J'\pi',EJ\pi}}{T^{E_{m}J'\pi'}}\rho(E,J,\pi) \tag{7}$$

where $\sigma_{a}^{J\pi}$ is absorption cross section of the compound nucleus state with energy E_{m} , spin J, and parity π. S^{ji} is the gamma transition branching ratio among the discrete levels. T_{γ}^{j} and T^{j} are the gamma transmission coefficient and the total transmission coefficient of j-th discrete energy level respectively. $T^{EJ\pi}$ is the total transmission coefficient of the energy level with energy E_{1}, spin J and parity π. $T_{\gamma}^{E'J'\pi',EJ\pi}$ is the gamma transmission coefficient from the energy level (E, J, π) to the energy level (E′, J′, π′), its relation to the gamma-ray strength function is:

$$T_{\gamma}^{E'J'\pi',EJ\pi}=2\pi(E'-E)^{3}f_{\gamma}^{E'J'\pi',EJ\pi} \tag{8}$$

where only the electric dipole transition is considered. If the giant dipole resonance model is adopted only, then:

$$f_{\gamma}^{E'J'\pi',EJ\pi}=\frac{1}{6\pi^{2}h^{2}c^{2}}H(J',J;\pi',\pi)\sum_{g=1}^{2}\frac{\sigma_{g}(E'-E)\Gamma_{g}^{2}}{[E_{g}^{2}(E'-E)^{2}]^{2}+(E'-E)^{2}\Gamma_{g}^{2}} \tag{9}$$

where σ_{g}, Γ_{g} and E_{g} are the cross section, width and energy of the giant dipole resonance peek respectively. H(J',J; $\pi'\pi$) represents the conservation of the angular

momentum and the parity:

$$H(J',J;\pi'\pi)=\begin{cases}1 \text{ if } |J'-1|\le J\le J'+1 \text{ and } \pi'.\pi=-1\\ 0 \text{ else}\end{cases}$$

As supposed above in this paper, besides the giant dipole resonance model, there exist the de-excitation processes of excited states of ^{6}He, ^{6}Li, ^{6}Be, ^{7}Li and ^{7}Be particle cliques. Based on the saturation nature of the nuclear force, we further suppose that the differences of the excited energies and decay widths of the energy levels of these particle cliques in the compound nucleus to those when these particles exist alone are small. But we also consider the residual interactions between the particle cliques and other nucleons in the compound nucleus. Therefore the contribution of the de-excitations of these particle cliques to the gamma-ray strength function can be expressed as the similar form to the giant dipole resonance model:

$$f_{\gamma}^{E'J'\pi',EJ\pi}=\frac{\alpha}{6\pi^2h^2c^2}H(J',J;\pi',\pi)\sum_{g=1}^{2}\frac{\sigma_g(E'-E)\Gamma_g^2}{[E_g^2(E'-E)^2]^2+(E'-E)^2\Gamma_g^2}$$
$$+\frac{1}{6\pi^2h^2c^2}H(J',J;\pi',\pi)\sum_{p=1}^{M}\frac{\beta_{\mathrm{p}}(E'-E)\Gamma_g^2}{[E_{\mathrm{p}}^2(E'-E)^2]^2+(E'-E)^2\Gamma_{\mathrm{p}}^2} \qquad (10)$$

where the first item represents the giant dipole resonance model, α represents the de-excitation probability in terms of the giant dipole resonances. The second one is the contribution of the excited state de-excitations of the 5 particle cliques mentioned above. Where β_{p} has the same dimension as $\alpha\cdot\sigma_g$ and represents the deexcitation probability of some excited state of some particle clique. E_{p} is the excited state energy and Γ_{p} is its decay width, they all adopt the experimental values of the excited state energies and decay widths of these particles.

2 Numerical Calculations

Using the above formulas, the numerical calculations of the (n,γ) reaction cross sections and gamma energy spectra for ^{197}Au have been done in the energy region from 0.01 to 3 MeV. In the calculations the universal optical potential[8] has been used to calculate the transmission coefficients and scattering wave functions of the neutrons. Gilbert-Cameron[9] formulas have been used to calculate the energy level

densities. The giant dipole resonance parameters were taken from reference [10]. the excited state energies and decay width of ^{6}He, ^{6}Li, ^{6}Be as well as ^{7}Li and ^{7}Be were taken from reference [11]. the discrete energy level data and the gamma decay branching ratios were taken from references [12,13].

In the calculations the optical potential parameters and the energy level density parameters of the residual nucleus are adjusted firstly by the calculations of the total cross sections and the elastic and inelastic scattering cross sections. Then by adjusting the energy level density parameters of the compound nucleus and α as well as β_p in the formula (10) to make the calculated results of the (n,γ) reaction cross sections and the gamma energy spectra coincide with the experiments as well as possible. The gamma-ray strength function in the formula (9) has also been used to calculate the (n, γ) reaction cross sections and gamma energy spectra in order to compare the calculation results obtained by using two kinds of the gamma-ray strength functions.

Table 1 shows the energy level density parameters and the giant dipole resonance parameters adopted in the calculations as well as the values of α in formula (10). Table 2 shows the experimental values of the excited state energies and the decay widths of ^{6}He, ^{6}Li, ^{6}Be as well as ^{7}Li and ^{7}Be and the values of β_p in formula (10).

Table 1 The energy level density parameters and the giant dipole resonance parameters

	energy level density parameters					giant dipole resonance parameters			
	E_x/ MeV	T/ MeV	E_0/ MeV	$P(Z)+P(N)$/ MeV	a/ MeV^{-1}	σ_g/ b	Γ_g/ MeV	E_g/ MeV	α
^{197}Au	4.18142	0.50500	-0.55000	0.92000	19.41000	0.56901	4.50000	13.69754	
^{198}Au	4.08758	0.59500	-1.75000	0.23000	17.90000	0.51191	4.50000	13.69159	0.29675

Table 2 The experimental data of E_p and Γ_p and the values of β_p

	E_p /MeV	Γ_p /MeV	β_p/b		E_p /MeV	Γ_p /MeV	β_p/b
^{6}He	1.80	0.113	0.0001	^{6}Be	1.67	1.16	0.0002
^{6}Li	4.31	1.700	0.00005	^{7}Li	6.68	0.80	0.0100
	5.37	0.540	0.0059		7.46	0.10	0.0150
	5.65	1.500	0.0209		9.85	1.80	0.0100
^{7}Be	6.73	1.200	0.0150				
	7.21	0.500	0.0400				

Fig. 1 shows the calculation results of the (n,γ) reaction cross sections and their comparisons with the experimental data. Where the solid line represents the calculated results when the gamma-ray strength function is calculated in terms of formula (10). The dotted line represents the calculated results when the gamma-ray strength function is calculated in terms of formula (9), i.e., the giant dipole resonance model. In order to see clearly the difference between them, the calculated results below 8 MeV are given. The experimental data were taken from EXFOR. Fig. 2 and Fig. 3 show the calculation results of the gamma energy spectra and their comparisons with the experimental values when the neutron incident energies are 1.25 MeV and 2.25 MeV respectively. The meaning of the solid line and the dotted line is the same as in Fig. 1. The experimental values were taken from ORNL. From Fig. 1 it can be seen that the calculated results by using the formula (10) are better than by using the formula (9). Fig. 2 and Fig. 3 show clearly that adopting the gamma-ray strength function (10) the calculated results of the gamma energy spectra can reproduce the abnormal protuberances near and above 5.5 MeV very well.

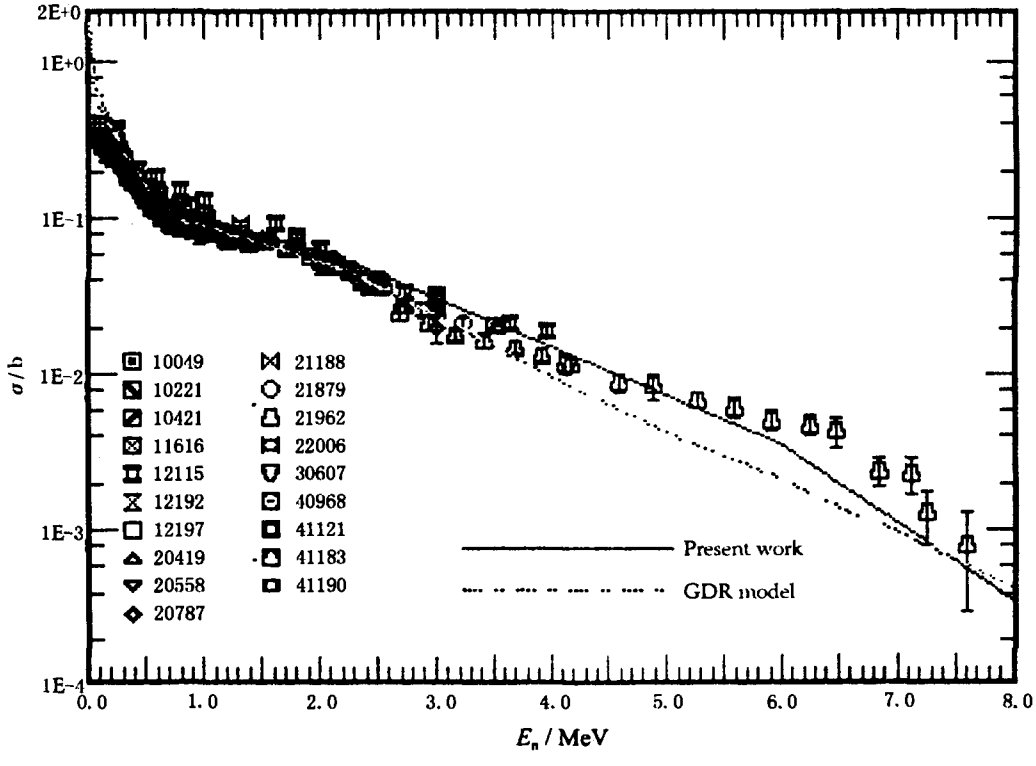

Fig. 1 Calculated ^{197}Au(n,γ) cross section

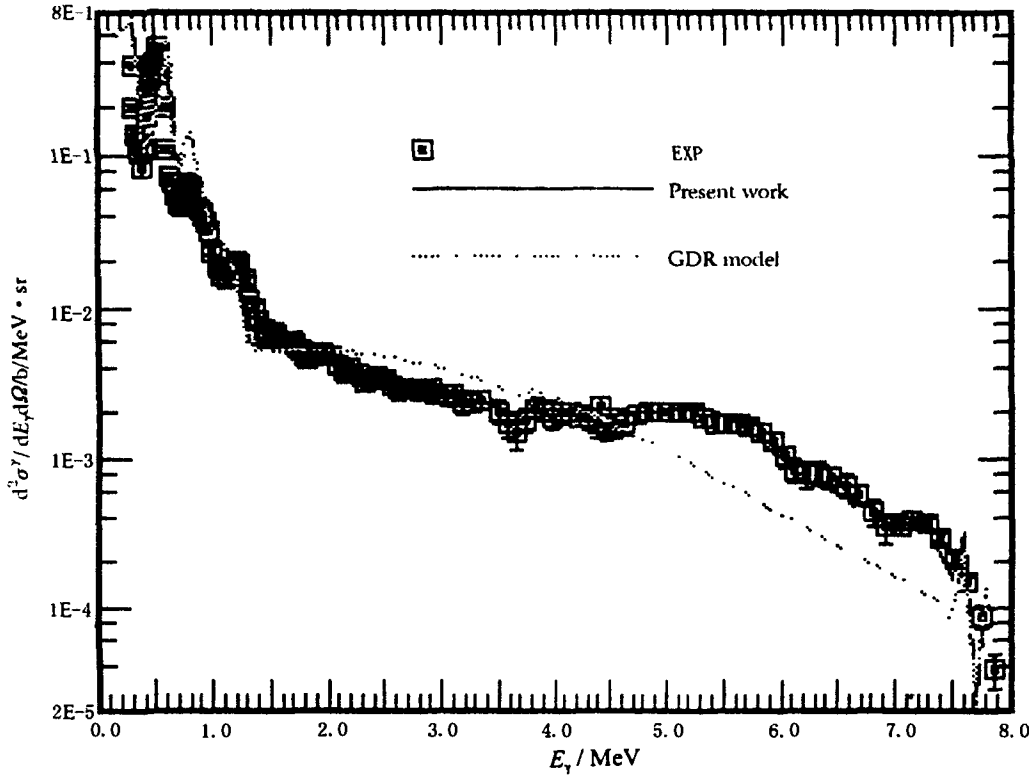

Fig. 2 Calculated γ-spectrum from ^{197}Au(n,γ) reaction at E_n=1.25 MeV

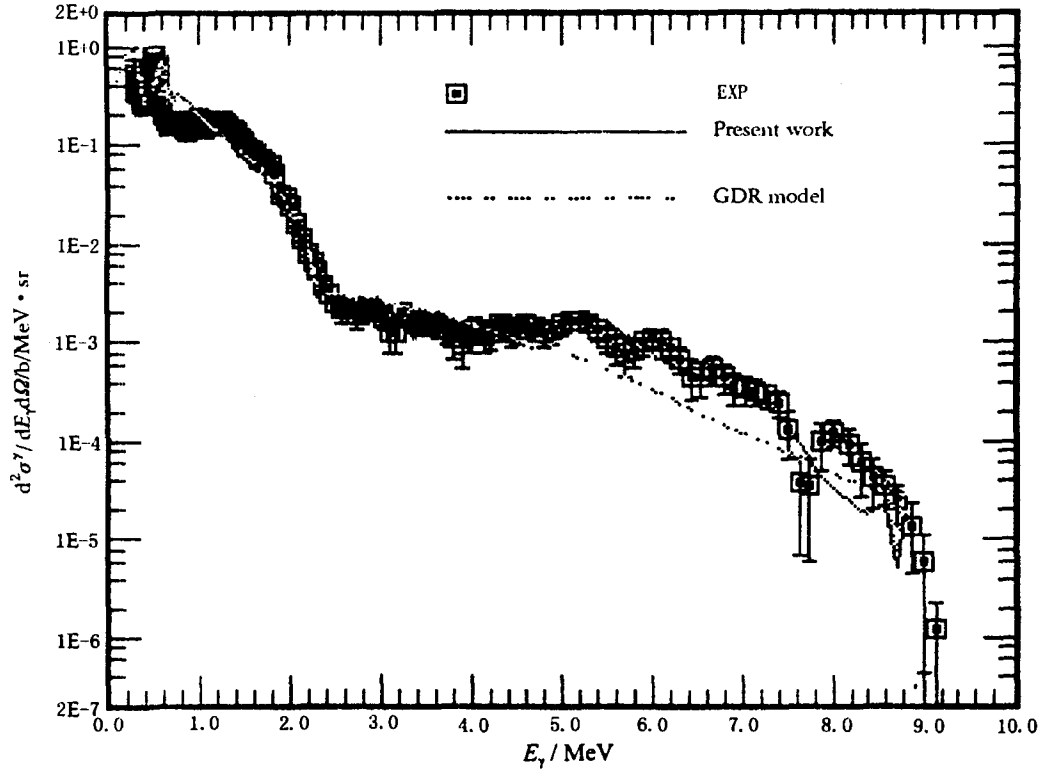

Fig. 3 Calculated γ-spectrum from ^{197}Au(n,γ) reaction at E_n=2.25 MeV

3 Conclusion

From the calculated results one can give the following conclusions:

(1) In order to explain the abnormal protuberances near and above 5.5 MeV of the gamma energy spectra in the (n,γ) reactions for the nuclei in the nuclear mass regions from 110 to 140 and from 180 to 210, we suppose that in the primary and cascade gamma de-excitation processes of the compound nucleus, besides the giant dipole resonance model, there exist the de-excitation processes of the excited states of ^{6}He, ^{6}Li, ^{6}Be, ^{7}Li and ^{7}Be particle cliques. For which the gamma-ray strength function was constructed. The calculated results of the (n,γ) reactions for ^{197}Au show that the experiments could be explained by this supposition very well. The evidence has been obtained for the reasonableness of this supposition.

(2) The form of the gamma-ray strength function is important for the compound nucleus statistical theory. The work of this paper shows that when the gamma-ray strength function is selected reasonably, the compound nucleus theory can completely reproduce the abnormal protuberances near and above 5.5 MeV of the gamma spectra.

References

[1] Ding Dazhao. Progress in Neutron Radiative Capture Study (in Chinese). Nuclear Physics (Material Compilation of the conference in 1978). Atomic Energy Press, 1979. 292-306

[2] Allen B J et al. Advances in Nucl. Phys., 1978, 10:129

[3] Raman S et al. Phys. Rev., 1985, C32:18

[4] Huo Yukun et al. Nucl. Phys., 1983, A406:1

[5] Liu Jianfeng et al. High Energy Phys. and Nucl. Phys. (in Chinese), 1983, 3:355

[6] Lane A M, Lynn J E. Nucl. Phys., 1959, 11:646

[7] Lane A M. Nucl. Phys., 1971, 63:171

[8] Becchetti F D et al. Phys. Rev., 1969, 182:1190

[9] Gilbert A, Cameron A G W. Can. J. Phys., 1965, 43:1446

[10] Dietrich S S et al. Atomic Data and Nuclear Data Tables, 1988, 38:199

[11] Ajzenberg-selove F. Nucl. Phys., 1984, A413:1

[12] Harmatz B. Nuclear Data Sheets, 1981, 34:105

[13] Auble R L. Nuclear Data Sheets, 1983, 40:301

Calculations of Complete Neutron Data of n+^{239}Pu Reaction in the Energy Region up to 20 MeV

Shen Qingbiao Cai Chonghai* Yu Baosheng
(China Nuclear Data Center, CIAE, Beijing)
* (Department of Physics, Nankai University, Tianjin)

Abstract

A complete set neutron cross sections, elastic scattering angular distributions, double differential cross sections, γ production data as well as the charged particle emission cross sections of n+^{239}Pu reaction in the energy region up to 20 MeV were calculated. Pretty good theoretical results in agreement with the experimental data were obtained and they are comparable with those given by ENDFB-6 and JENDL-3 libraries.

A complete set neutron data of n+^{239}Pu reaction plays important role for the design of all thermal and fast reactor systems. The further improvement to them is necessary obviously.

There are quite a lot experimental data for σ_{tot}, $\sigma_{n,F}$, elastic scattering angular distributions and some experimental data for $\sigma_{n,\gamma}$, $\sigma_{n,inl}$, $\sigma_{n,2n}$ and neutron emission double differential cross sections.

The code APFO96[1] was used to automatically get the optimal optical potential parameters for neutron channel based on various experimental data. The obtained optimal neutron optical potential parameters in energy region up to 20 MeV are as follows:

$$V=50.4623-0.432E_n+0.01523E_n^2-24(N-Z)/A \quad (1)$$

$$W_s=3.7516+0.278E_n-12(N-Z)/A \quad (2)$$

$$W_v=1.5325+0.1909E_n-0.01719E_n^2 \quad (3)$$

$$V_{so}=6.2 \quad (4)$$

$$r_r=1.2557,\quad r_s=1.1890,\quad r_v=1.2326,\quad r_{so}=1.2557 \quad (5)$$

$$a_r=0.6037,\quad a_s=0.8352,\quad a_v=0.2900,\quad a_{so}=0.6037 \quad (6)$$

where E_n is incident neutron energy in laboratory system and Z, N, A are proton, neutron, mass number of the target nucleus.

The coupled channel optical model code ECIS95[2] was used to calculate the direct inelastic scattering cross sections and angular distributions for 7 excited states belong to ground state rotational band ($3/2^+$,$5/2^+$,$7/2^+$,$9/2^+$,$11/2^+$,$13/2^+$,$15/2^+$). The used coupled channel optical model parameters are as follows[3]:

$$V=46.2-0.3E_n \quad (7)$$

$$W_s=3.6+0.4E_n \quad E_n \le 7\ \text{MeV} \quad (8)$$

$$W_s=6.4-0.1(E_n-7) \quad E_n>7\ \text{MeV} \quad (9)$$

$$W_v=-1.2+0.15E_n \quad E_n \ge 8\ \text{MeV} \quad (10)$$

$$V_{so}=6.2 \quad (11)$$

$$r_r=1.26,\quad r_s=1.24,\quad r_v=1.26,\quad r_{so}=1.12 \quad (12)$$

$$a_r=0.615,\quad a_s=0.5,\quad a_v=0.615,\quad a_{so}=0.47 \quad (13)$$

$$\beta_2=0.21,\quad \beta_4=0.065 \quad (14)$$

The main calculation code used for fission nuclei is FUNF[4]. The main statistical theory parameters obtained by code ADFP[5] are as follows:

	(n,γ)	(n,f)	(n,n')	(n,n'f)	(n,2n)	(n,2nf)	(n,3n)
Level density (a):	29.1700	29.1700	29.0505	29.0505	28.7760	28.7760	33.0000
Pair correction (Δ):	1.5176	0.4104	0.2936	0.0219	0.1695	0.1617	-0.2000
Fission barrier (V_f):		6.1166		5.7682		5.7812	
Fission curvature ($\hbar\omega$):		0.3000		0.3412		1.0000	
Saddle level density factor (K_1):		11.926		8.598		1.000	

Exciton model parameter: CK=2700
(n,γ) factor: CE_1=0.2315
Direct (n,γ) factor: DGMA=0.065

The calculated σ_{tot} as well as the experimental data are given in Fig.1, which shows that the calculated values are in good agreement with the experimental data. Fig.2 presents the comparison of the $\sigma_{n,F}$ between the calculated results and the experimental data, which is in agreement with each other. The comparison of $\sigma_{n,\gamma}$ between the calculated values, the values in ENDFB-6 and JENDL-3 libraries, and the experimental data is shown in Fig.3, they are basically in agreement with each other. In high energy region the calculated $\sigma_{n,\gamma}$ are more reasonable since they are more closed to the experimental data of (n,γ) cross sections of other fission nuclei. Figs.4(a)~(c) show the comparisons of the elastic scattering angular distributions between the calculated results and the experimental data for incident energies

1.0~14.1 MeV, respectively. The calculated results for 23 incident energies in the range 0.5~14.1 MeV are in good agreement with each other. Figs.5 and 6 show the comparisons between the calculated values, the values in ENDFB-6 and JENDL-3 libraries, and the experimental data for (n,n') and (n,2n), respectively. They are comparable with each other. Fig.7 shows that the calculated (n,3n) cross sections is comparable with the values in ENDFB-6 and JENDL-3 libraries. Fig.8 shows that the calculated (n,p) cross section is in agreement with the experimental data. Fig.9 presents the calculated inelastic scattering excitation functions of 7 discrete levels (their excited energies are 0.0079, 0.0573, 0.0757, 0.1638, 0.1928, 0.3181, 0.3581 MeV) by statistical theory and coupled channel theory. Fig.10 shows that the calculated inelastic scattering excitation function for continuous state is comparable with the values in ENDFB-6 and JENDL-3 libraries. Figs.11(a)~(c) show the comparisons of neutron emission double differential cross sections for 14.1 MeV incident neutron between the calculated values and the experimental data[6]. From all calculated results for the 11 outgoing angles from 30 to 140 degree one can see that the calculated results are basically in agreement with the experimental data, but in rather low energy region the experimental values are higher than the calculated values, it is necessary to be studied in the future.

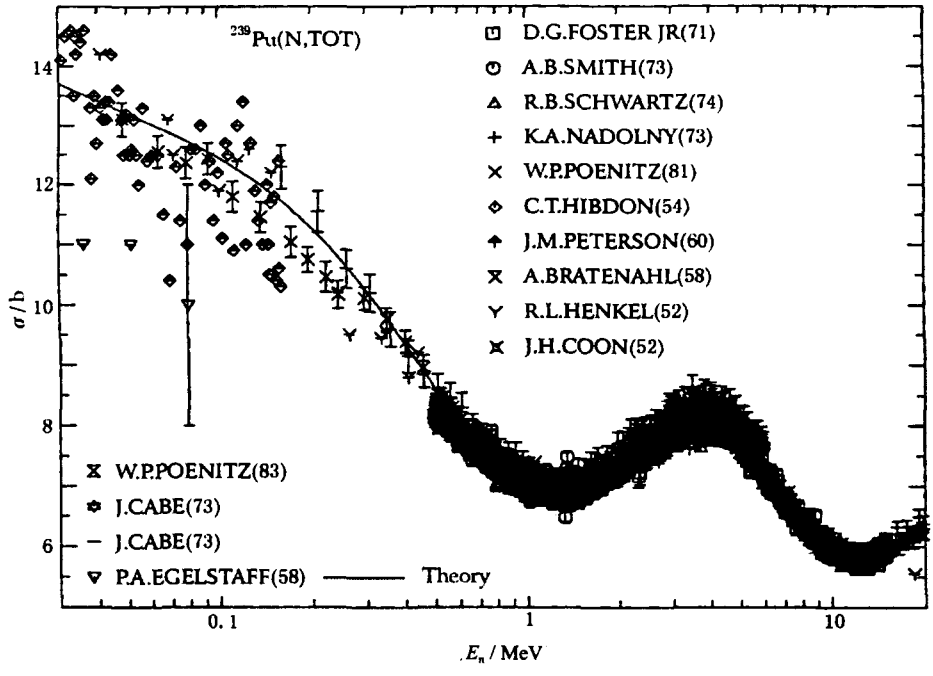

Fig.1 ^{239}Pu total cross sections

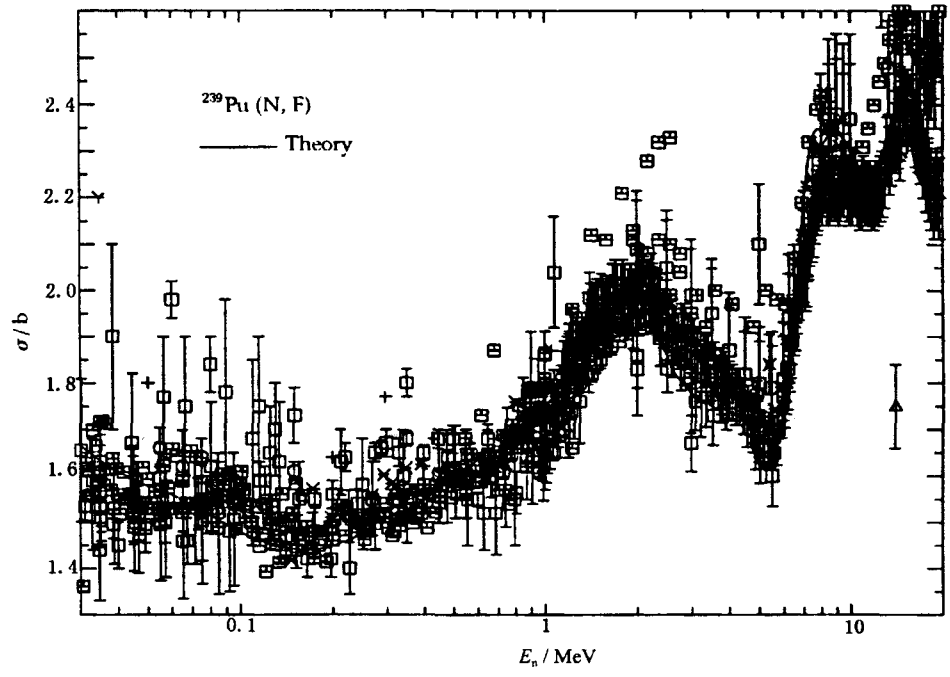

Fig.2 ^{239}Pu fission cross sections

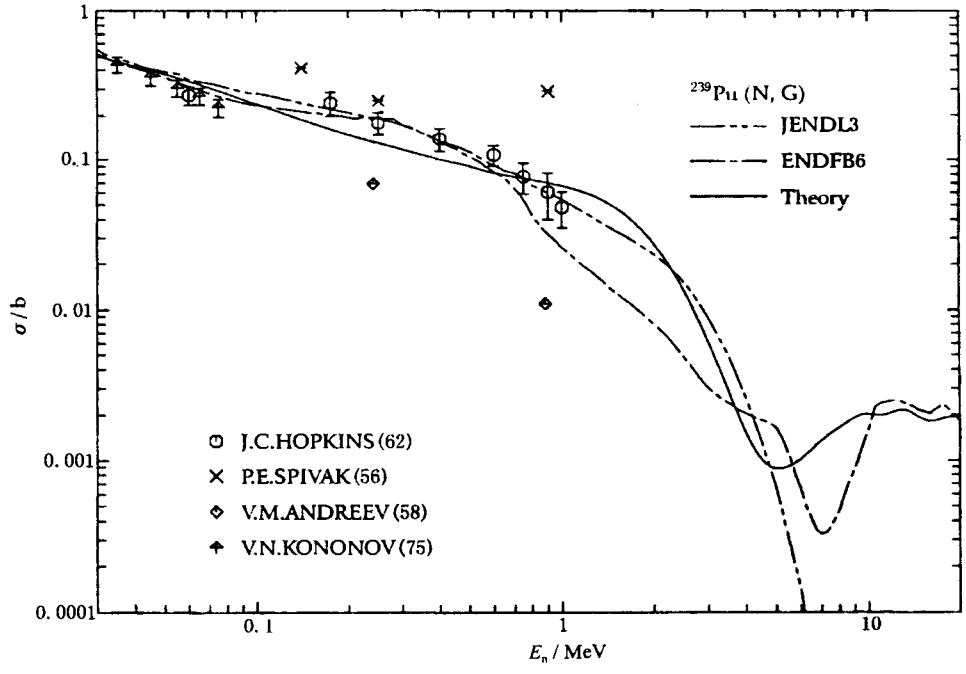

Fig.3 ^{239}Pu (n,γ) cross sections

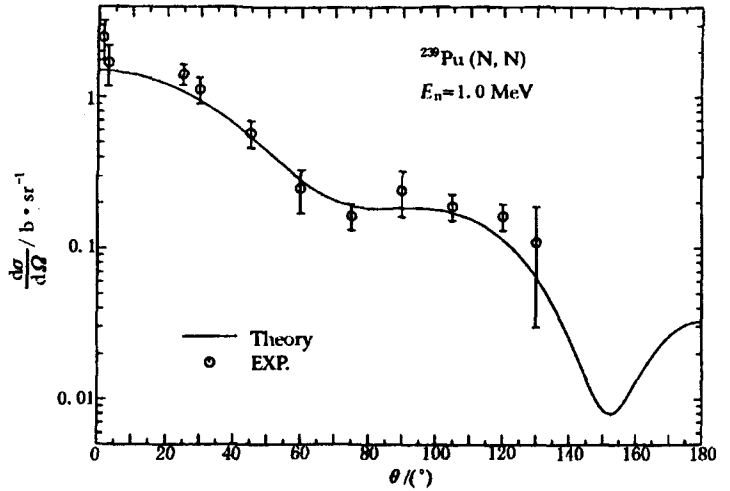

Fig.4(a) ^{239}Pu elastic scattering angular distributions for E_n=1.0 MeV

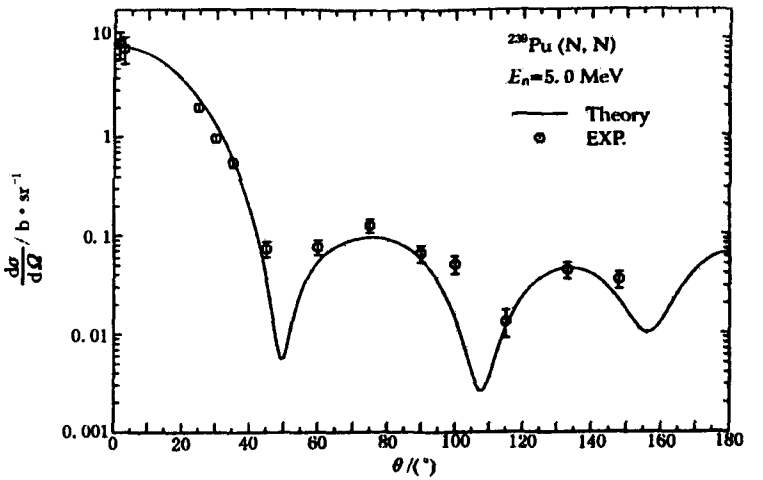

Fig.4(b) ^{239}Pu elastic scattering angular distributions for E_n=5.0 MeV

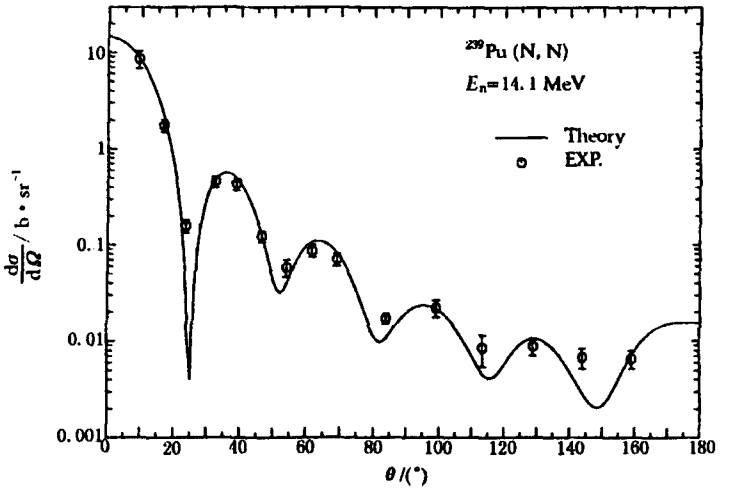

Fig.4(c) ^{239}Pu elastic scattering angular distributions for E_n=14.1 MeV

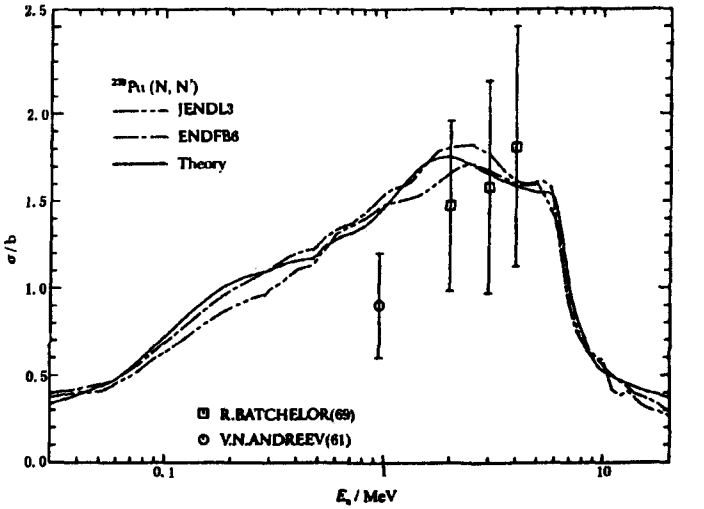

Fig.5 ^{239}Pu (n,inl) cross sections

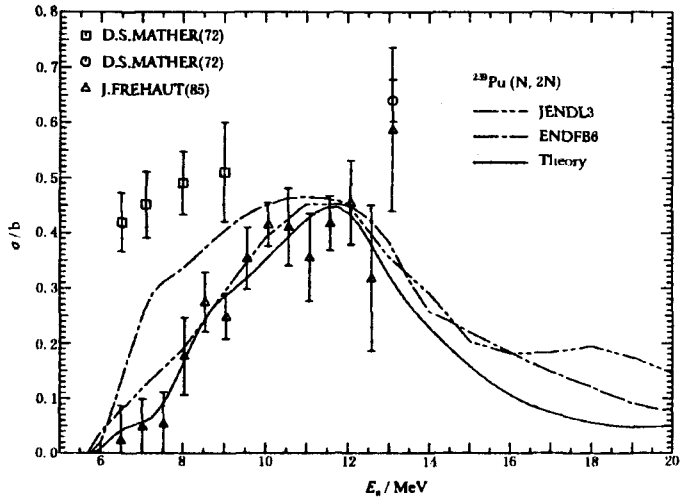

Fig.6 ^{239}Pu (n,2n) cross sections

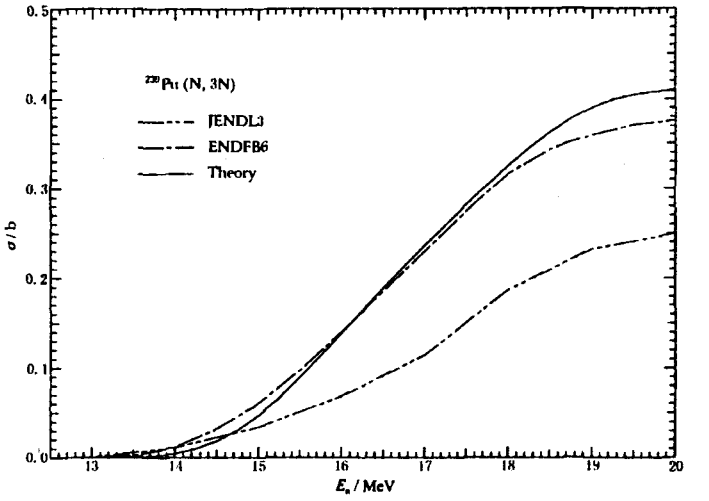

Fig.7 ^{239}Pu (n,3n) cross sections

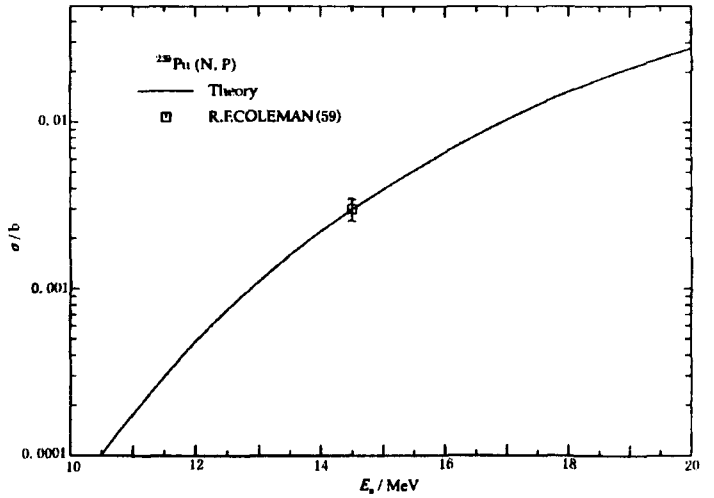

Fig.8 ^{239}Pu (n,p) cross sections

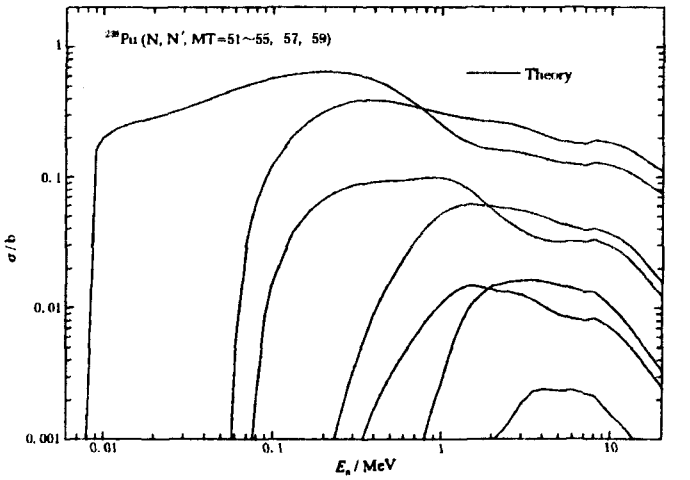

Fig.9 ^{239}Pu discrete level inelastic scattering cross sections

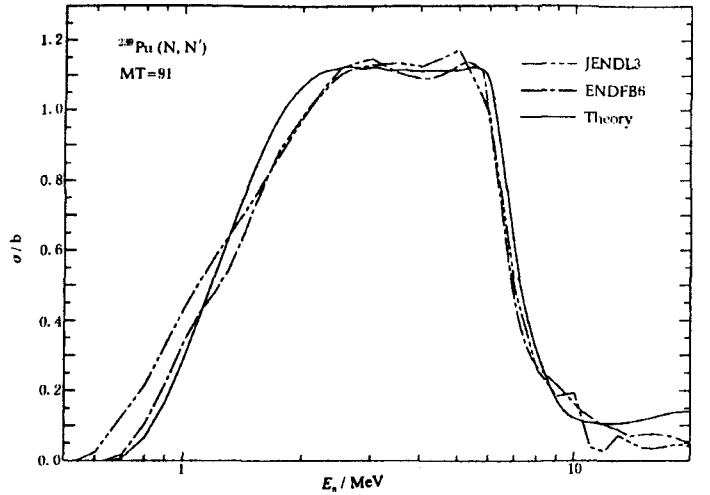

Fig.10 ^{239}Pu continuous state inelastic scattering cross sections

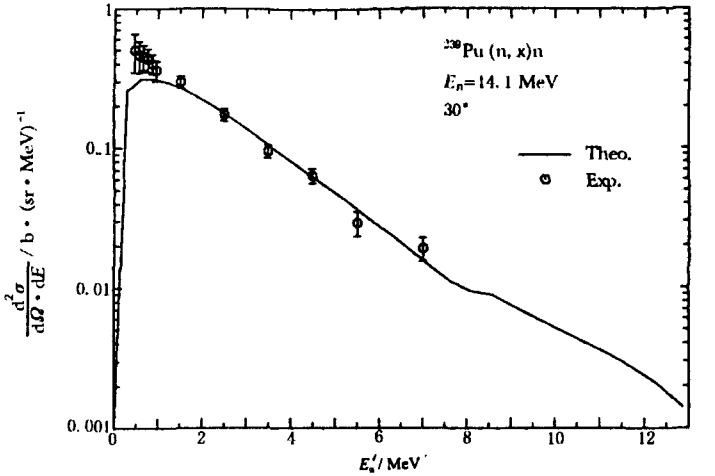

Fig.11(a) ^{239}Pu neutron emission double differential cross sections for 14.1 MeV incident neutron at 30.0 degree

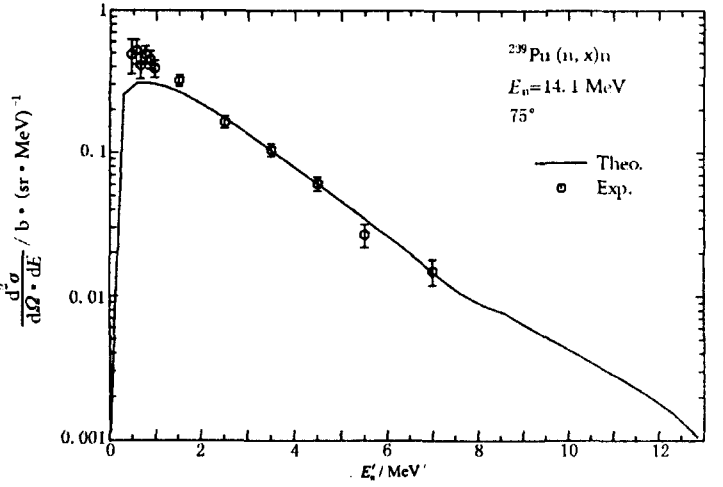

Fig.11(b) The same as Fig.11(a) but for 75.0 degree

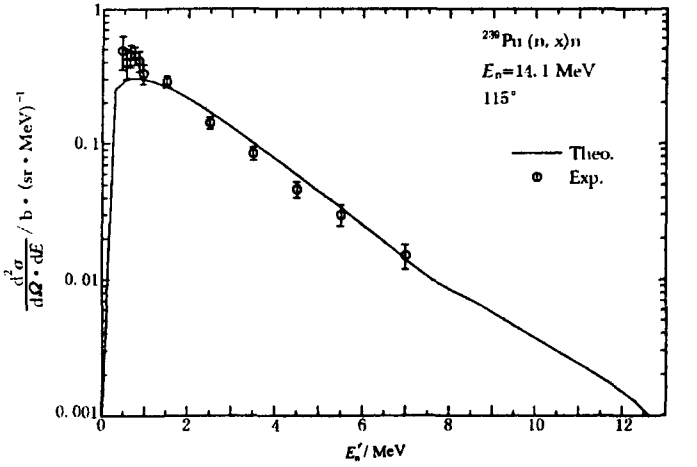

Fig.11(c) The same as Fig.11(a) but for 115 degree

The authors would like to thank Prof. Zhang Jingshang for his helpful discussions.

References

[1] Shen Qingbiao and Cai Chonghai. APFO96, a code for automatically searching for a set of optimal optical potential parameters of fission nucleus (unpublished).

[2] J. Raynal. ECIS95, a code for coupled channel calculation, Notes on ECIS94 – Note CEA-N-2772 (1994).

[3] E.D.Arthur, P.G.Young, D.G.Madland, R.E.MacFarlane. Nucl.Sci.Eng., 88 (1984) 56-70.

[4] Zhang Jingshang. FUNF, a code for comprehensive calculations of fission nucleus based on unified model, CNDC, CIAE (unpublished).

[5] Cai Chonghai, Zhang Jingshang. ADFP, a code for automatically searching for a set of optimal statistical theory parameters of fission nucleus (unpublished).

[6] J.Voignier, G.Clayeux, F.Bertrand. Inelastic Neutron Cross Sections in Several Elements with 14.1 MeV Neutrons, CEA-R-3936, France, 1970.

CN0101647

Calculations of n+^{240}Pu Reaction in the Energy Region up to 20 MeV

Shen Qingbiao Yu Baosheng

(China Nuclear Data Center, CIAE, Beijing)

Cai Chonghai

(Department of Physics, Nankai University, Tianjin)

All reaction cross sections, elastic scattering angular distributions, double differential cross sections, and the γ production data of n+^{240}Pu reaction in the energy region up to 20 MeV were calculated. Pretty good theoretical results in accordance with experimental data were obtained and they are comparable with those given by ENDFB-6 and JENDL-3 libraries.

The isotope ^{240}Pu is a major constituent of many fast breeding reactors. Thus, fast neutron interactions with this isotope are of a consideration in the neutron design of these systems.

There are quite a lot experimental data for σ_{tot}, $\sigma_{n,F}$ and some experimental data for $\sigma_{n,\gamma}$, elastic scattering angular distributions and inelastic scattering cross sections for some discrete levels.

The code APFO96[1] was used to automatically get the optimal optical potential parameters for neutron channel based on various experimental data. The obtained optimal neutron optical potential parameters in energy region up to 20 MeV are as follows:

$$V=49.5758-0.12895\,E_n-0.006311\,E_n^2-24(N-Z)/A \quad (1)$$

$$W_s=4.4975+0.985\,E_n-12(N-Z)/A \quad (2)$$

$$W_v=2.2284+0.1797\,E_n-0.0066\,E_n^2 \quad (3)$$

$$V_{so}=6.2 \quad (4)$$

$$r_r=1.2701,\quad r_s=1.0387,\quad r_v=1.1841,\quad r_{so}=1.2701 \quad (5)$$

$$a_r=0.5658,\quad a_s=0.3100,\quad a_v=0.3000,\quad a_{so}=0.5658 \quad (6)$$

where E_n is incident neutron energy in laboratory system and Z, N, A are proton, neutron, mass number of the target nucleus.

The coupled channel optical model code ECIS95[2] was used to calculated the direct inelastic scattering cross sections and angular distributions for 5 excited states belong to ground state rotational band (2^+,4^+,6^+,8^+,10^+). The used coupled channel optical model parameters are as follows[3]:

$$V=51.32134-0.57\,E_n+0.02\,E_n^2-24(N-Z)/A \quad (7)$$

$$W_s=5.04567+0.4\,E_n+0.001\,E_n^2 \quad (8)$$

$$W_v=0 \quad (9)$$

$$V_{so}=6.0 \quad (10)$$

$$r_r=1.256,\quad r_s=1.26,\quad r_{so}=1.12 \quad (11)$$

$$a_r=0.62,\quad a_s=0.58,\quad a_{so}=0.5 \quad (12)$$

$$\beta_2=0.2,\quad \beta_4=0.07 \quad (13)$$

The main calculation code used for fission nuclei is FUNF[4]. The main

statistical theory parameters obtained by code ADFP[5] are as follows:

	(n,γ)	(n,f)	(n,n')	(n,n'f)	(n,2n)	(n,2nf)	(n,3n)
Level density (a):	27.3392	27.3392	25.9602	25.9602	25.8000	25.8000	28.5935
Pair correction (Δ):	0.5945	-0.0025	0.4746	-0.0410	-0.0483	-0.0051	0.4975
Fission barrier (V_f):		5.8399		6.2300		5.3372	
Fission curvature ($\hbar\omega$):		0.7001		1.0000		0.9900	
Saddle level density factor (K_1):		4.953		3.200		1.000	

Exciton model parameter: CK=400
(n,γ) factor: CE_1=0.3879
Direct (n,γ) factor: DGMA=0.14

The calculated σ_{tot} as well as the experimental data are given in Fig.1, which shows that the calculated values are in good agreement with the experimental data. Figs. 2(a)~(d) show the comparisons of the elastic scattering angular distributions between the calculated results and the experimental data[6] for incident energies 0.4, 0.6, 0.8, 1.2 MeV, respectively. They are basically in agreement with each other. Fig. 3 presents the comparison of the $\sigma_{n,F}$ between the calculated results and the experimental data, the agreement with each other is better. The comparison of $\sigma_{n,\gamma}$ between the calculated values, the values in ENDFB-6 and JENDL-3 libraries, and the experimental data is shown in Fig. 4, they are basically in agreement with each other. In high energy region the calculated $\sigma_{n,\gamma}$ are more reasonable since they are more closed to the experimental data of (n,γ) cross sections of other fission nuclei. Figs.5~7 show the comparisons between our calculated values and the values in ENDFB-6 and JENDL-3 libraries for (n,inl), (n,2n), and the (n,3n), respectively. They are comparable with each other. Fig. 8 shows the calculated inelastic scattering excitation functions of 5 discrete levels (their excited energies are 0.0428, 0.1417, 0.2943, 0.4975, 0.7478 MeV) by statistical theory and coupled channel theory. Fig. 9 is the comparison between the calculated values, the values in ENDFB-6 and JENDL-3 libraries, and the experimental data[6] for inelastic scattering of the first excited state , the agreement with each other is better. Fig.10 shows that the calculated inelastic scattering excitation function for continuous state is comparable with the values in ENDFB-6 and JENDL-3 libraries.

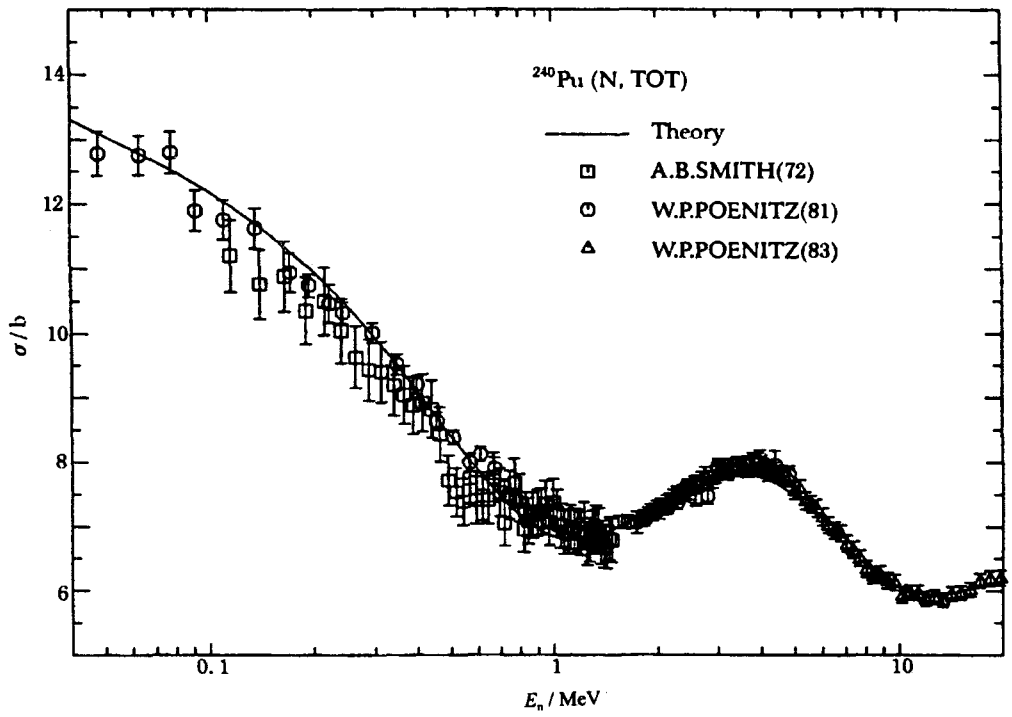

Fig.1 ^{240}Pu total cross sections

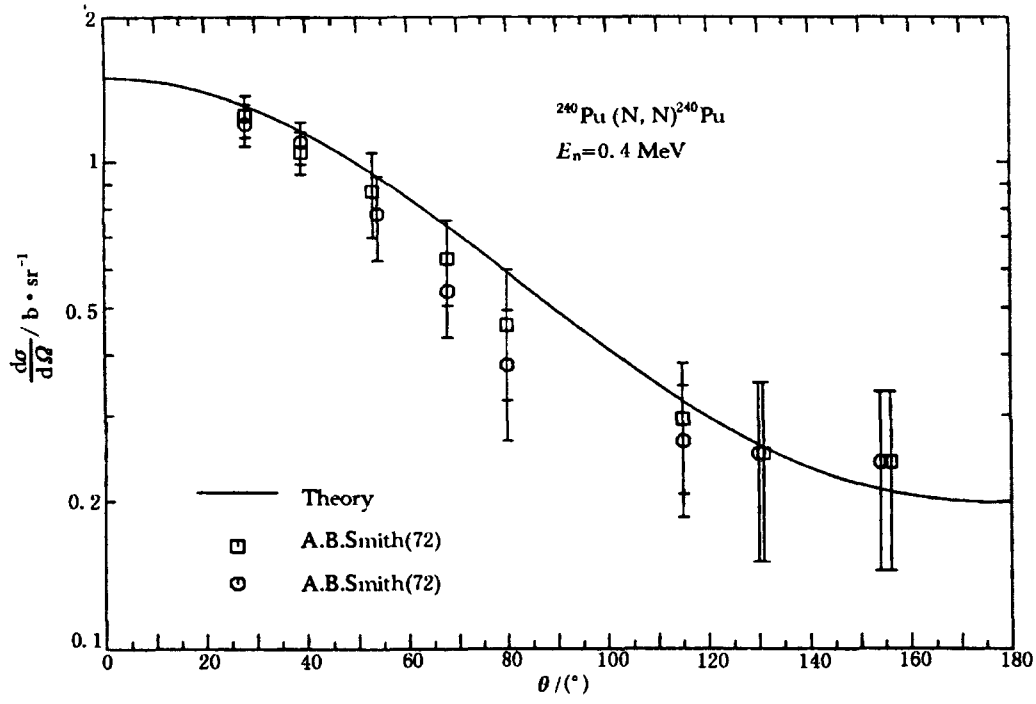

Fig.2(a) ^{240}Pu elastic scattering angular distributions for E_n=0.4 MeV

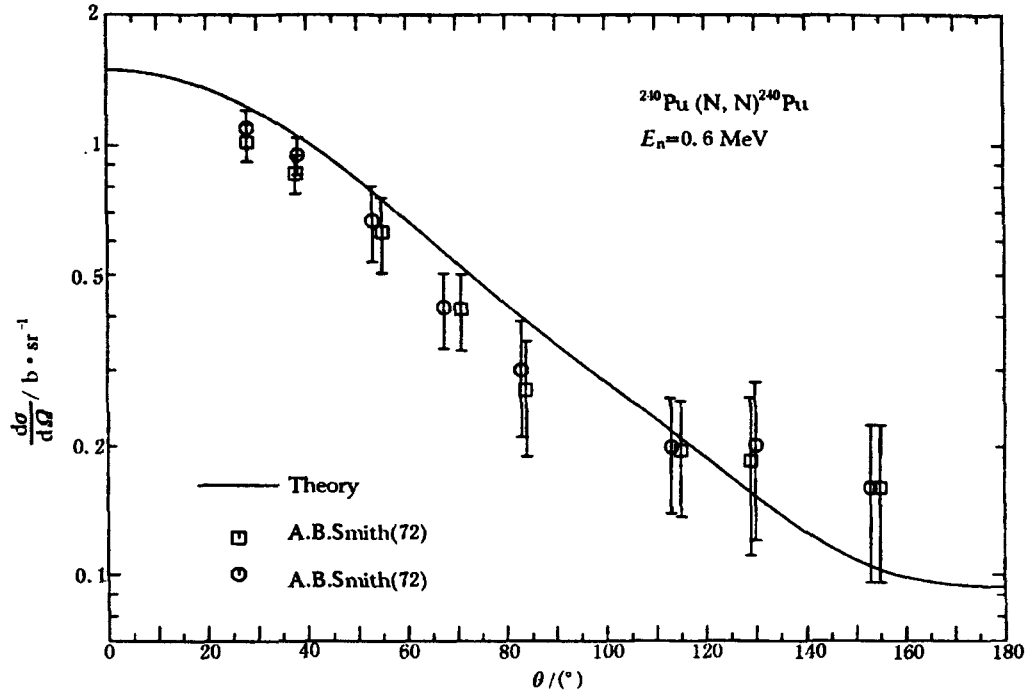

Fig.2(b) ^{240}Pu elastic scattering angular distributions for E_n =0.6 MeV

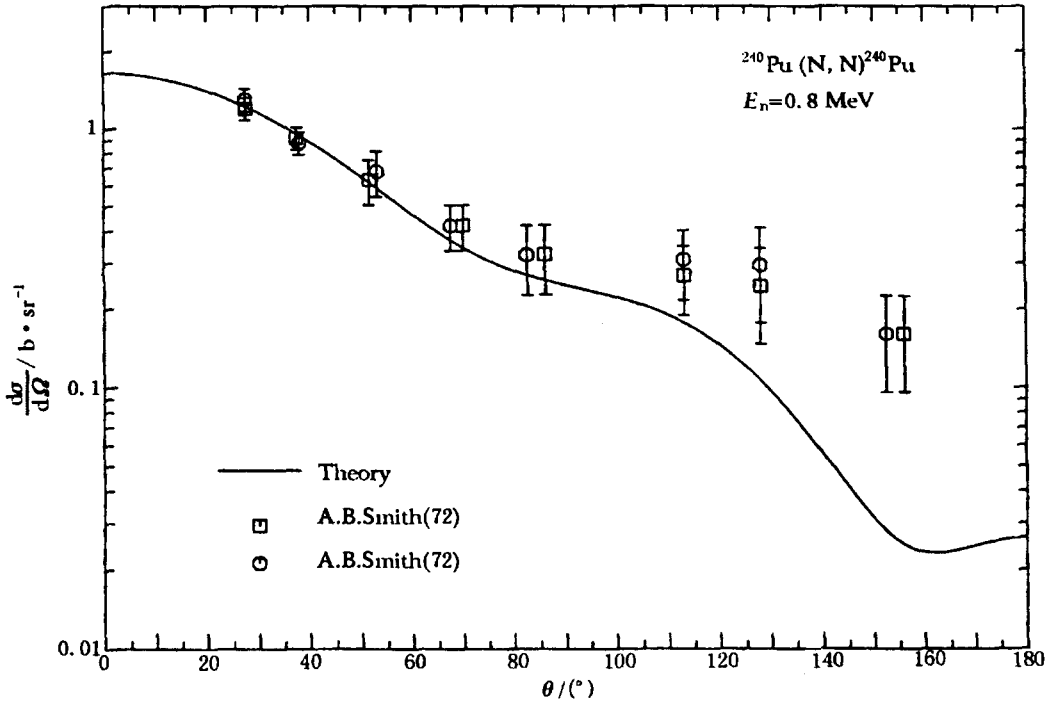

Fig.2(c) ^{240}Pu elastic scattering angular distributions for E_n =0.8 MeV

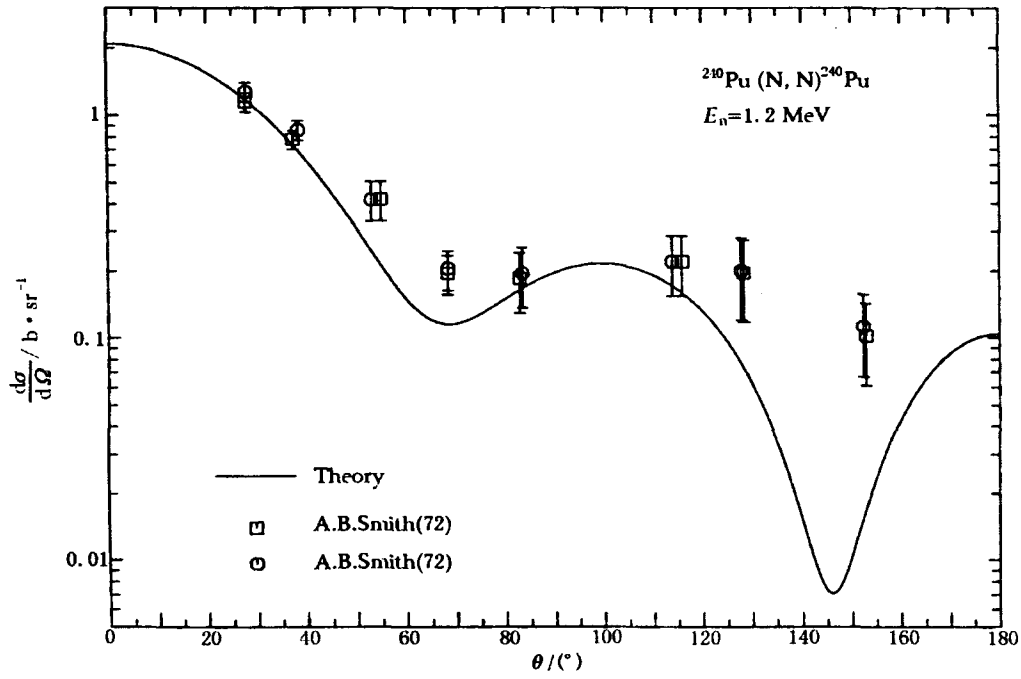

Fig.2(d) ^{240}Pu elastic scattering angular distributions for E_n =1.2 MeV

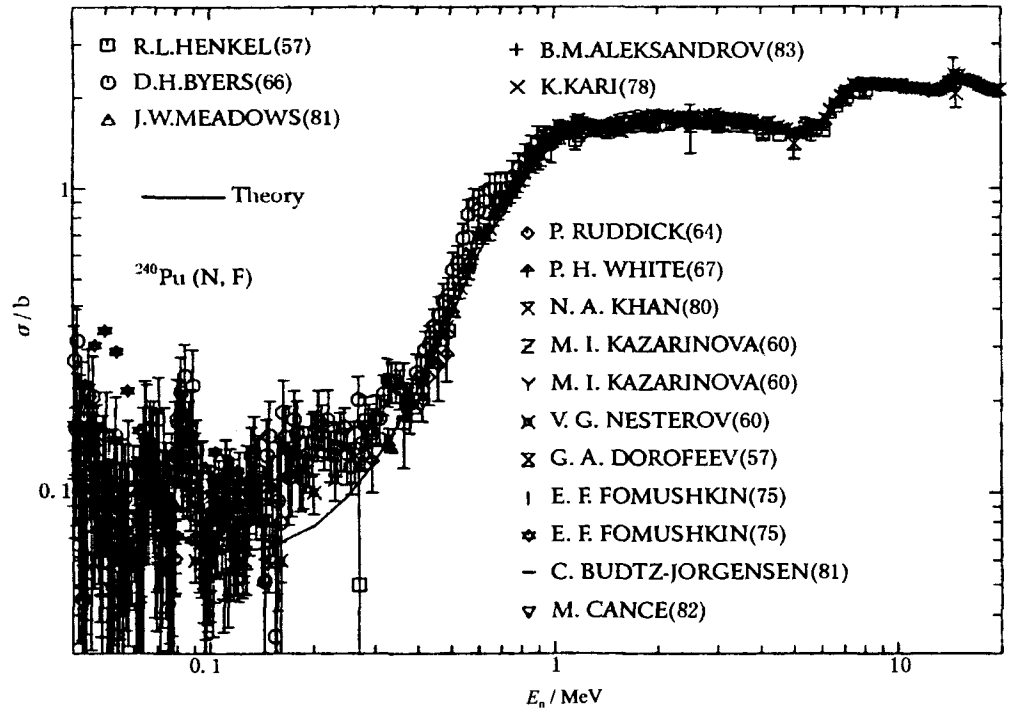

Fig.3 ^{240}Pu fission cross sections

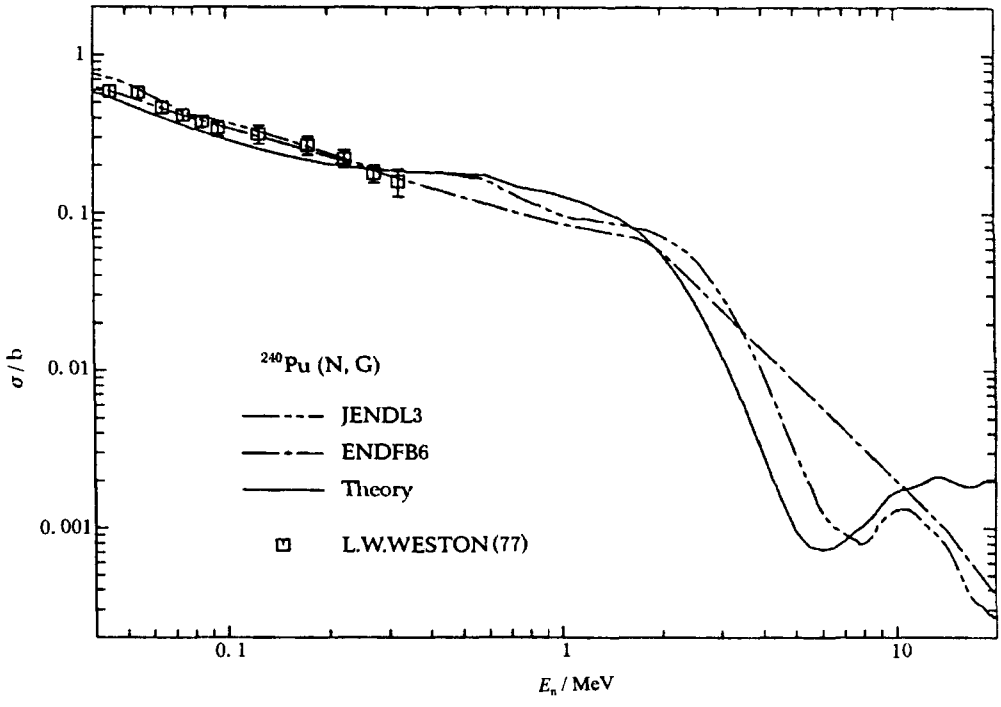

Fig.4 ^{240}Pu (n,γ) cross sections

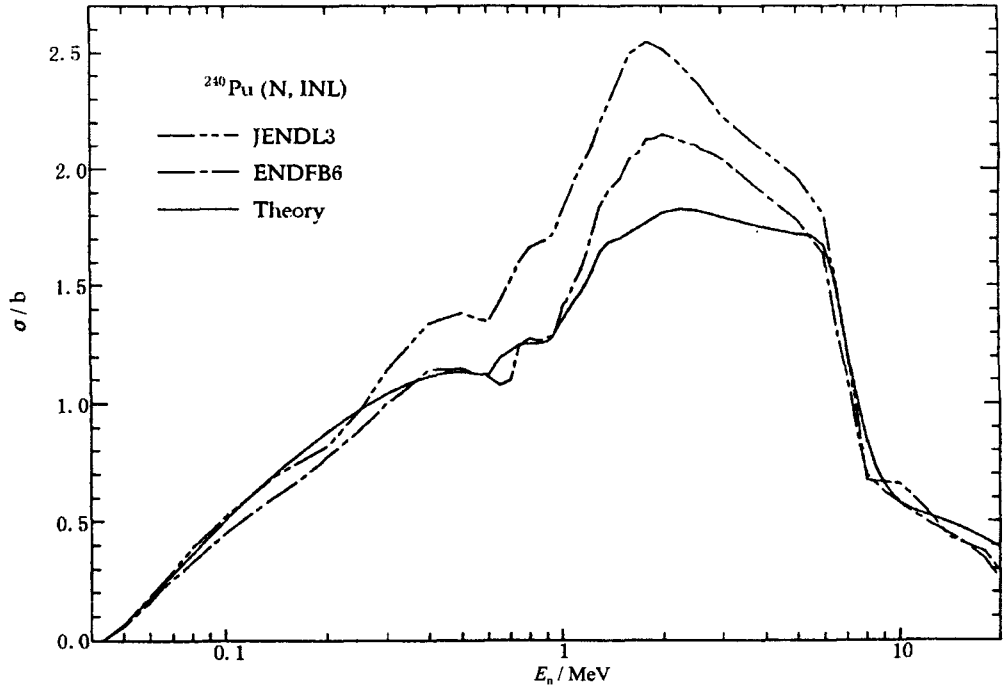

Fig.5 ^{240}Pu (n,inl) cross sections

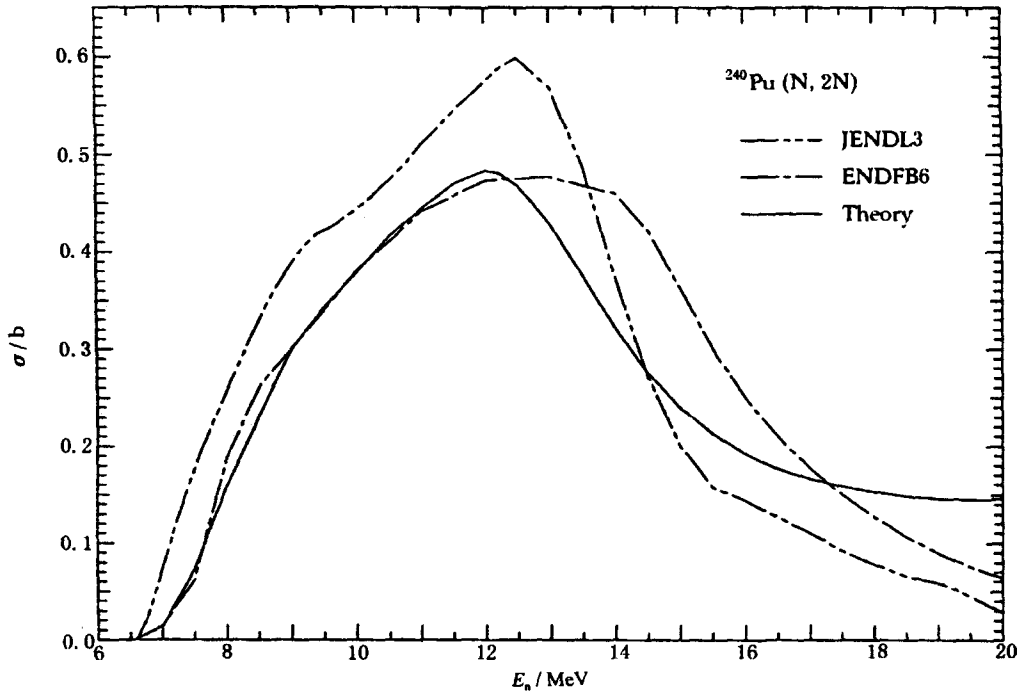

Fig.6 ^{240}Pu (n,2n) cross sections

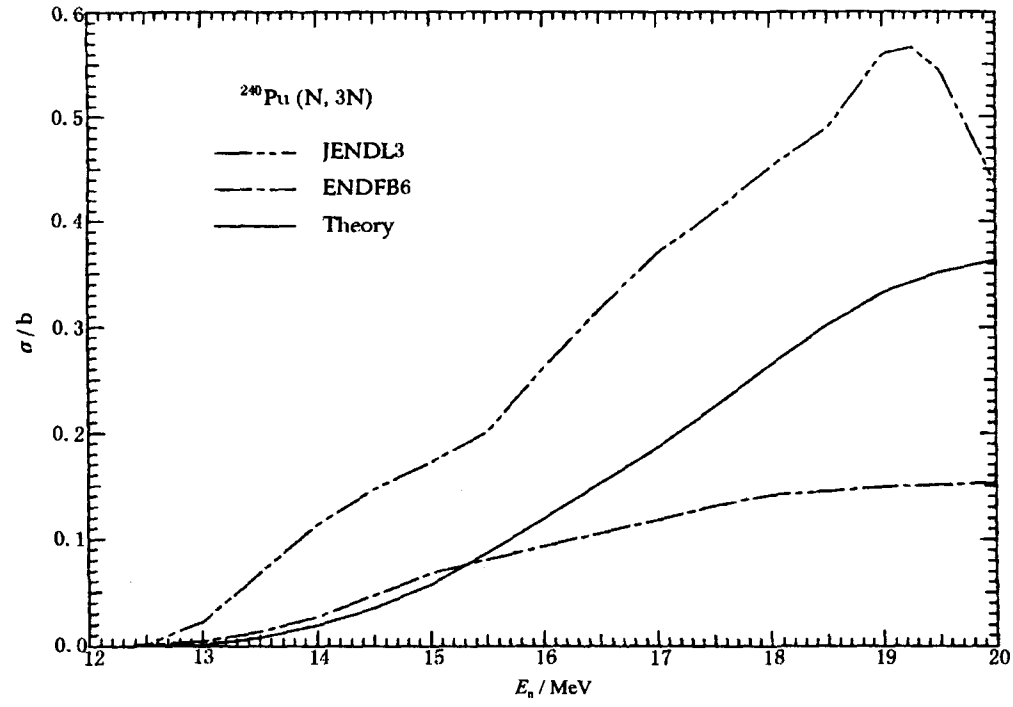

Fig.7 ^{240}Pu (n,3n) cross sections

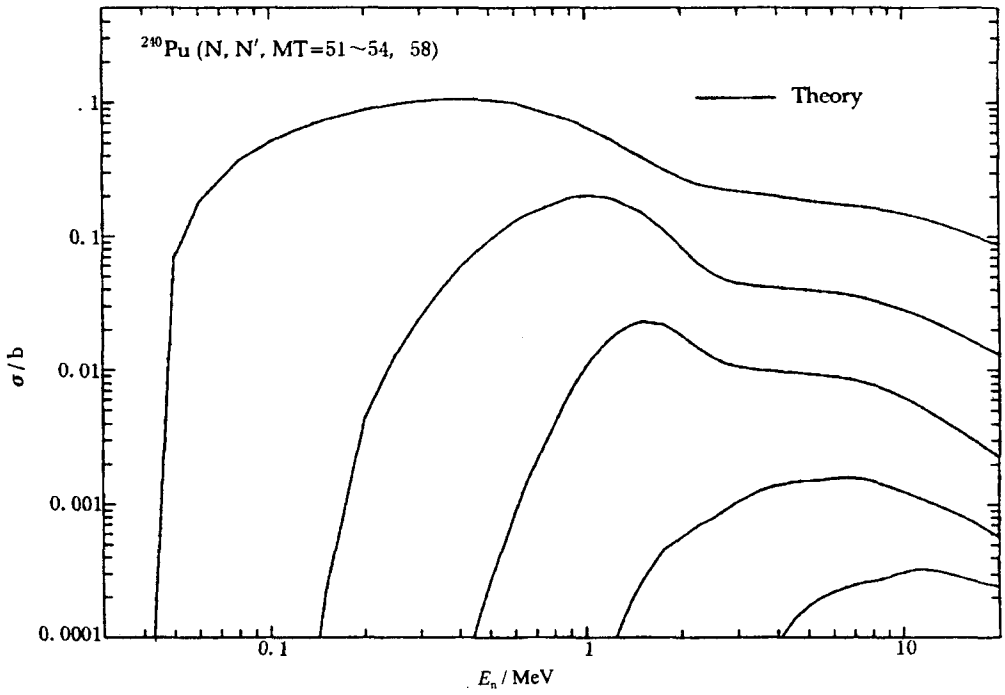

Fig.8 ^{240}Pu discrete level inelastic scattering cross sections

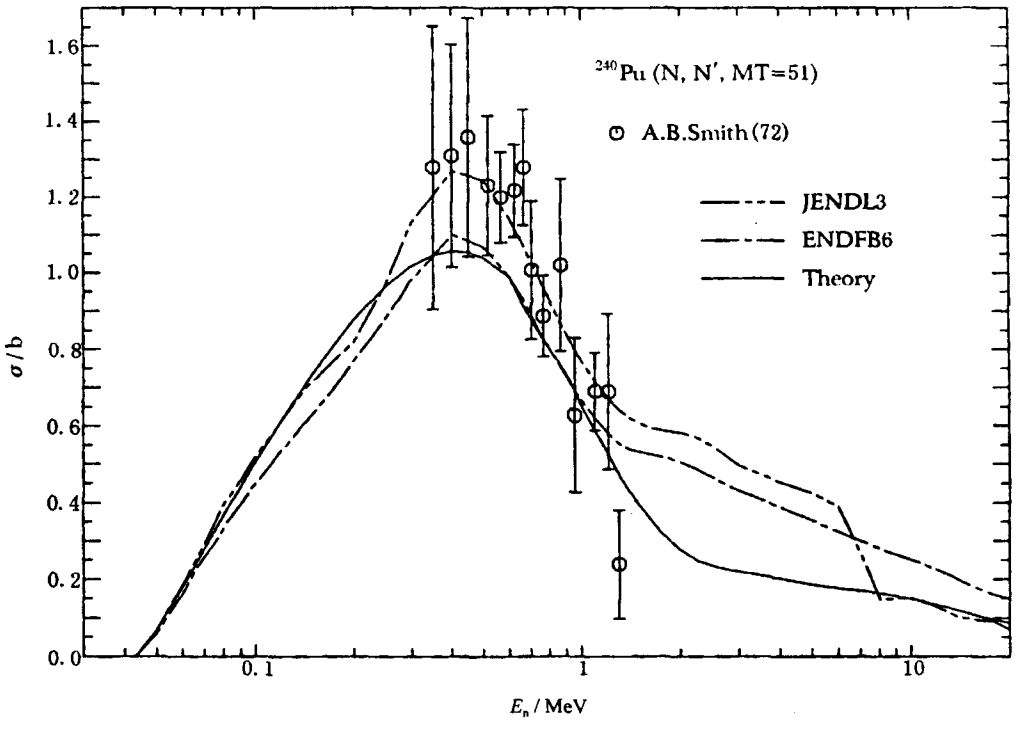

Fig.9 ^{240}Pu first excited state inelastic scattering cross sections

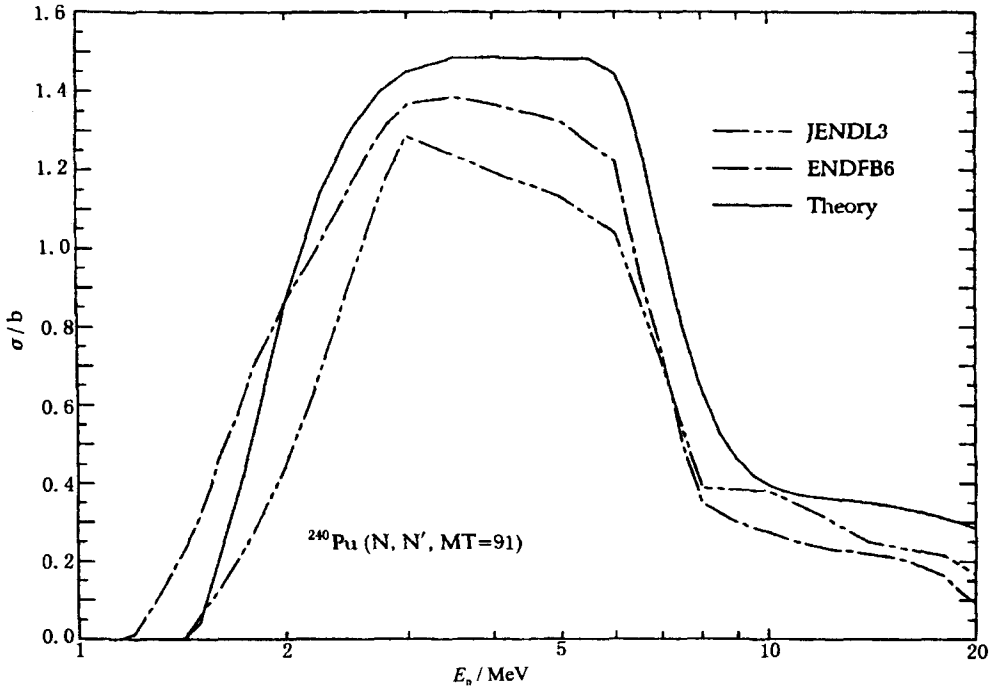

Fig.10 ^{240}Pu continuous state inelastic scattering cross sections

The authors would like to thank Prof. Zhang Jingshang for his helpful discussions.

References

[1] Shen Qingbiao and Cai Chonghai. APFO96, a code for automatically searching for a set of optimal optical potential parameters of fission nucleus (unpublished)

[2] J. Raynal. ECIS95, a code for coupled channel calculation, Notes on ECIS94 – Note CEA-N-2772 (1994)

[3] G.Vladuca, A.Tudora, M.Sin. Rom. J. Phys., tome 41, no. 7-8 (1996) 515-526

[4] Zhang Jingshang. FUNF, a code for comprehensive calculations of fission nucleus based on unified model, CNDC, CIAE (unpublished)

[5] Cai Chonghai, Zhang Jingshang. ADFP, a code for automatically searching for a set of optimal statistical theory parameters of fission nucleus (unpublished)

[6] A.B. Smith, P. Lambropoulos, J.F.Whalen. Fast Neutron Total and Scattering Cross Sections of Plutonium-240. Nucl. Sci. Eng., 47 (1972)19-28

Calculations of n+^{141}Pr Reaction in Energy Region up to 20 MeV

Shen Qingbiao
(China Nuclear Data Center, CIAE, Beijing)

A set of neutron optical potential parameters for ^{141}Pr in energy region up to 20 MeV is obtained based on concerned experimental data. Various cross sections, secondary neutron spectra, and elastic scattering angular distributions of n+^{141}Pr reaction are calculated. The calculated results are in good agreement with the experimental data.

^{141}Pr is one of the important fission product nuclei. The evaluated neutron nuclear data of ^{141}Pr are useful in the design of the nuclear engineering. There are sufficient experimental data of total, (n,γ), and (n,2n) cross sections and there are few experimental data of elastic scattering, (n,3n), (n,p), (n,α), and (n,t) cross sections for n+^{141}Pr reaction in the energy region up to 20 MeV. All the experimental data are taken from EXFOR library.

Firstly, the code APMN[1] is used for automatically searching the optimal optical potential parameters for neutron channel based on various neutron experimental data of ^{141}Pr. The obtained optimal neutron optical potential parameters in the energy region up to 20 MeV are as follows:

$$V=55.0870-0.85838\,E_n+0.040285\,E_n^2-23.9839(N-Z)/A-0.007876Z/A^{1/3} \quad (1)$$

$$W_s=\max\{0,\ 4.9731+0.74982\,E_n-12.6599(N-Z)/A\}, \quad (2)$$

$$W_v=\max\{0,\ -0.049723+0.7305\,E_n-0.18053\,E_n^2\}, \quad (3)$$

$$V_{so}=6.2, \quad (4)$$

$$r_r=1.19157,\ r_s=1.32534,\ r_v=1.89773,\ r_{so}=1.19157, \quad (5)$$

$$a_r=0.74345,\ a_s=0.41047,\ a_v=0.89661,\ a_{so}=0.74345, \quad (6)$$

where E_n is the incident neutron energy and Z, N, A are the number of proton, neutron and mass of the target nucleus, respectively.

Then the code DWUCK4[2] is used to calculate the direct inelastic scattering cross sections and angular distributions of 5 levels for ^{141}Pr. The main code SUNF[3] is used to calculate the various reaction data. In the calculations the Gilbert-Cameron level density formula[4] is applied. Through changing some parameters of level density and charged particle optical potential and taking the exciton model constant K as 1900 MeV^3, the calculated various cross sections are in good agreement with the experimental data.

Fig. 1 shows the comparison of neutron total cross sections between the calculated values and the experimental data in the energy region up to 20 MeV for n+^{141}Pr reaction. The theoretical values are in good agreement with the experimental data. Fig. 2 shows that the calculated (n,γ) cross sections are basically in agreement with the experimental data. Fig. 3 shows the neutron elastic scattering cross sections. After considering and comparing the total and inelastic scattering cross sections it seems that the elastic scattering experimental data above 1 MeV are too high so that the calculated values are reasonable. The calculated neutron inelastic scattering cross sections of ^{141}Pr are shown in Fig. 4. Fig. 5 gives the comparison of the calculated and experimental (n,2n) cross sections of ^{141}Pr. They are in good agreement with each other. The comparisons of the calculated and experimental (n,3n), (n,p), (n,α), and (n,t) cross sections of ^{141}Pr are given in Figs. (6)~(9), respectively. The calculated results are all in good agreement with the experimental data. Fig. 10 shows the relations of the calculated various cross sections with energy are reasonable. Fig. 11 shows that the calculated excitation function of the third excited state (E_x=1.1268 MeV) is in good agreement with the experimental data. The calculated total, (n,n'), and (n,2n) neutron emission spectra at 8, 14, 20 MeV are given in Fig. 12 (a)~(c), respectively, and they are of reasonable shapes in physics. Fig. 13 (a) and (b) show the comparison of the calculated and experimental elastic scattering angular distributions at 11 incident energies. The calculated results are also in good agreement with the experimental data.

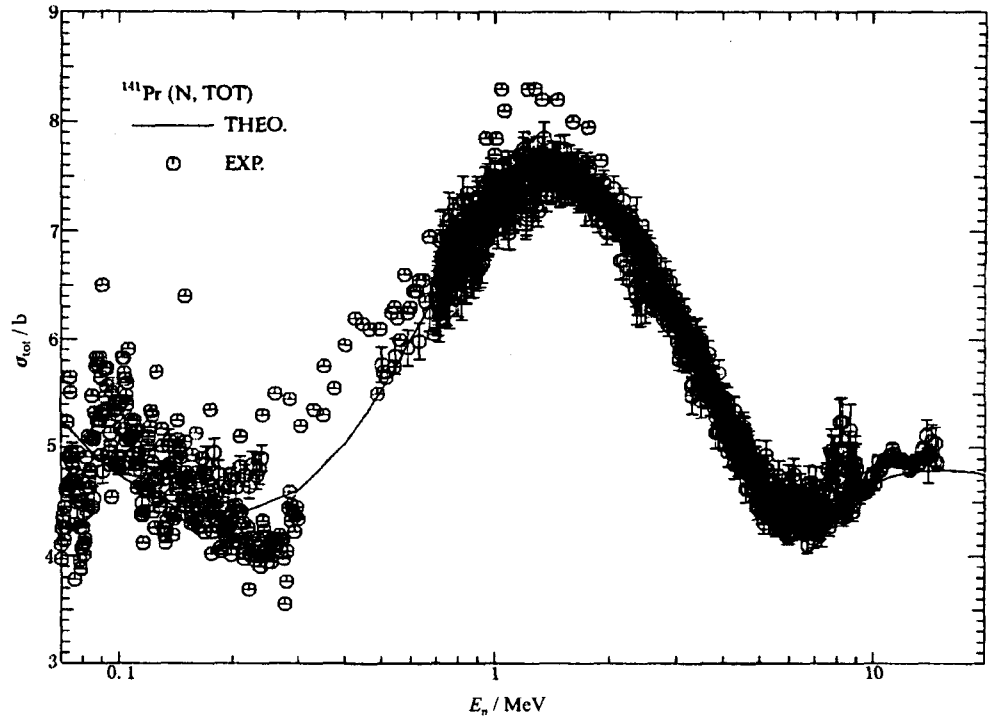

Fig.1 Comparison of neutron total cross sections of ^{141}Pr between the calculated values and the experimental data

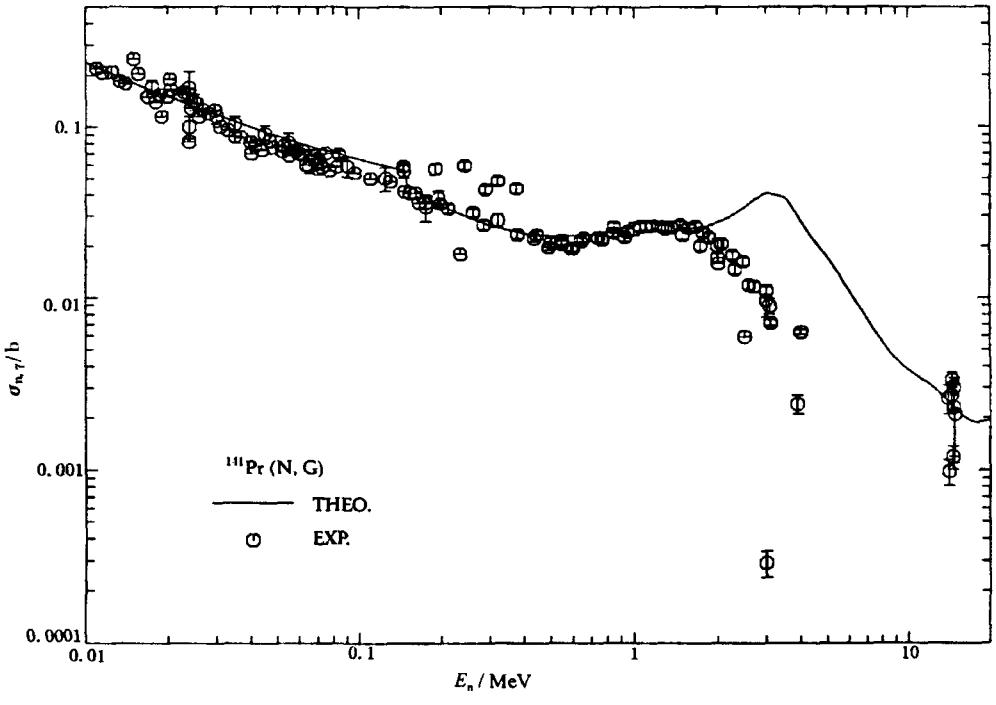

Fig.2 Comparison of (n,γ) cross sections of ^{141}Pr between the calculated values and the experimental data

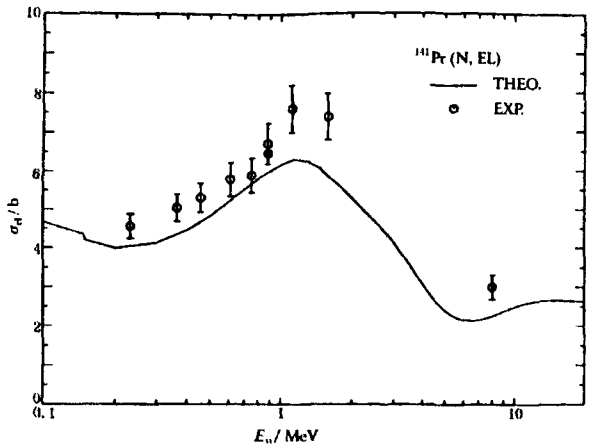

Fig.3 Comparison of neutron elastic scattering cross sections of ^{141}Pr between the calculated values and the experimental data

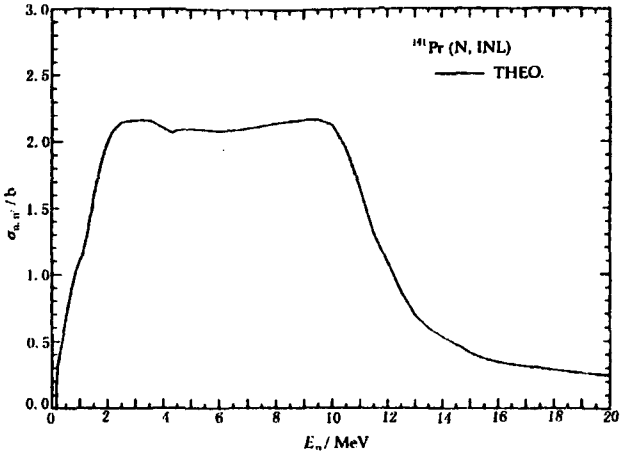

Fig.4 Calculated neutron inelastic scattering cross sections of ^{141}Pr

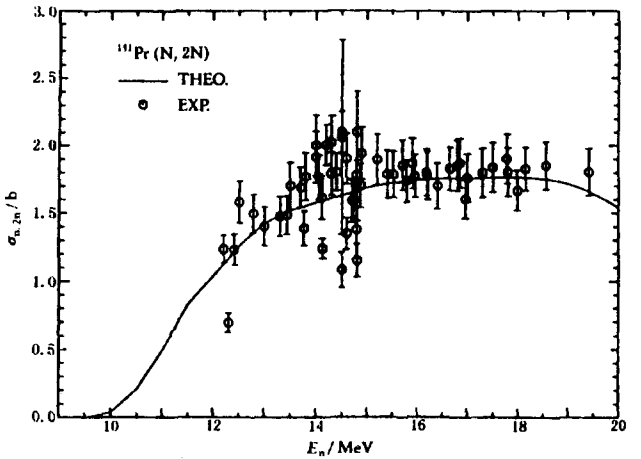

Fig.5 Comparison of (n,2n) cross sections of ^{141}Pr between the calculated values and the experimental data

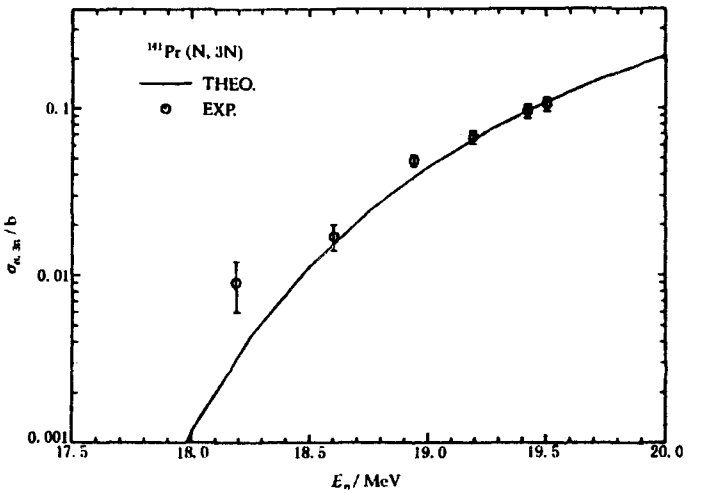

Fig.6 Comparison of (n,3n) cross sections of ^{141}Pr between the calculated values and the experimental data

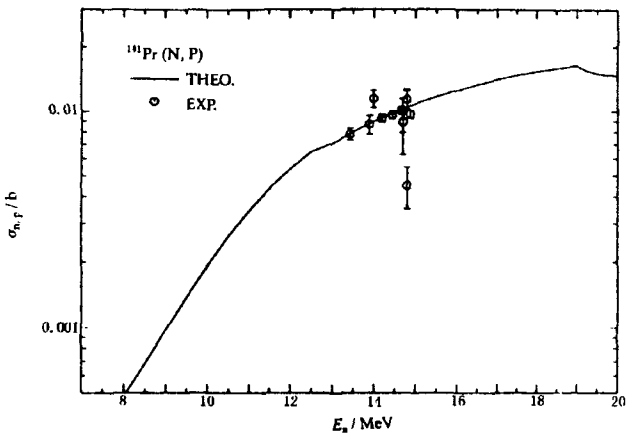

Fig.7 Comparison of (n,p) cross sections of ^{141}Pr between the calculated values and the experimental data

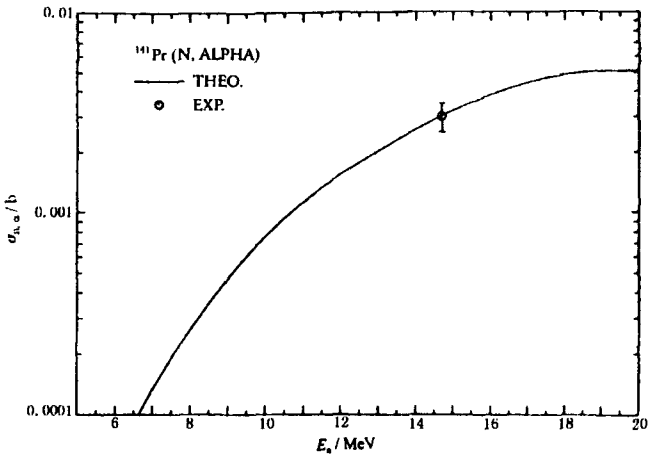

Fig.8 Comparison of (n,α) cross sections of ^{141}Pr between the calculated values and the experimental data

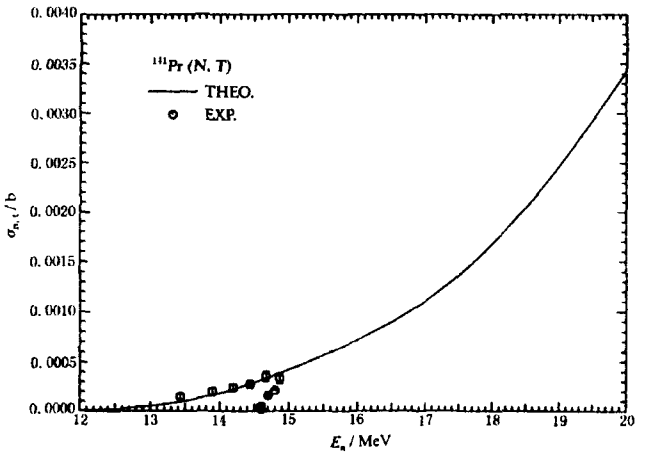

Fig.9 Comparison of (n,t) cross sections of ^{141}Pr between the calculated values and the experimental data

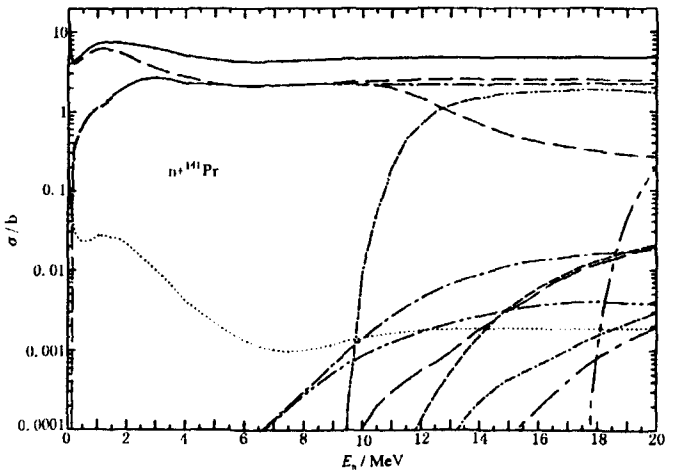

Fig.10 Calculated various cross sections of ^{141}Pr

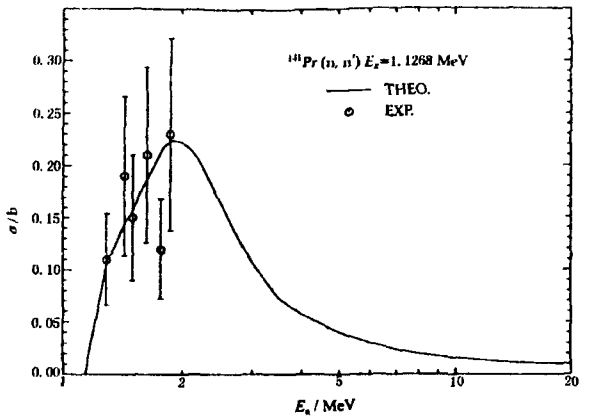

Fig.11 Comparison of the excitation function of the third excited state (E_x=1.1268 MeV) of ^{141}Pr between the calculated values and the experimental data

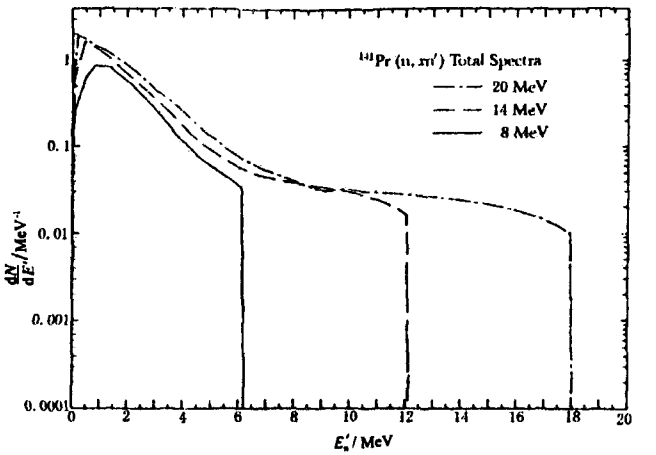

Fig.12(a) Calculated total neutron emission spectra of n+^{141}Pr reaction

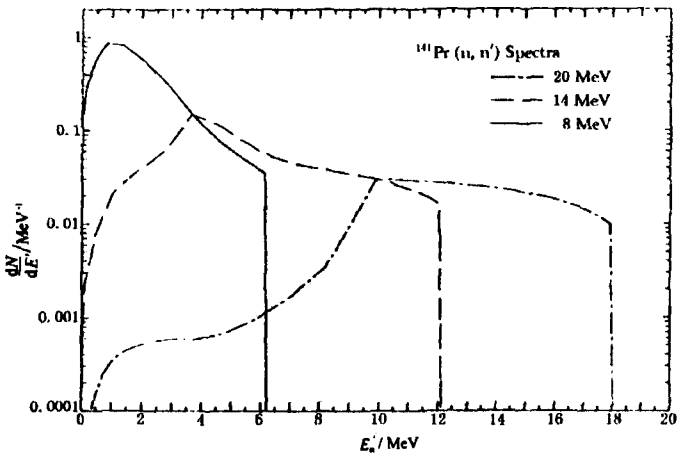

Fig.12(b) Calculated (n,n') neutron emission spectra of n+^{141}Pr reaction

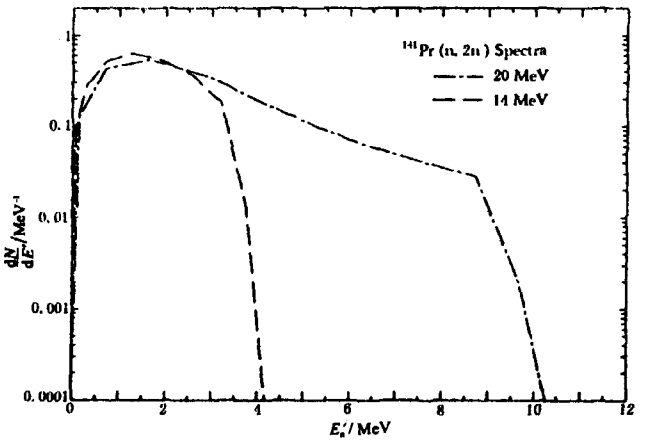

Fig.12(c) Calculated (n,2n) neutron emission spectra of n+^{141}Pr reaction

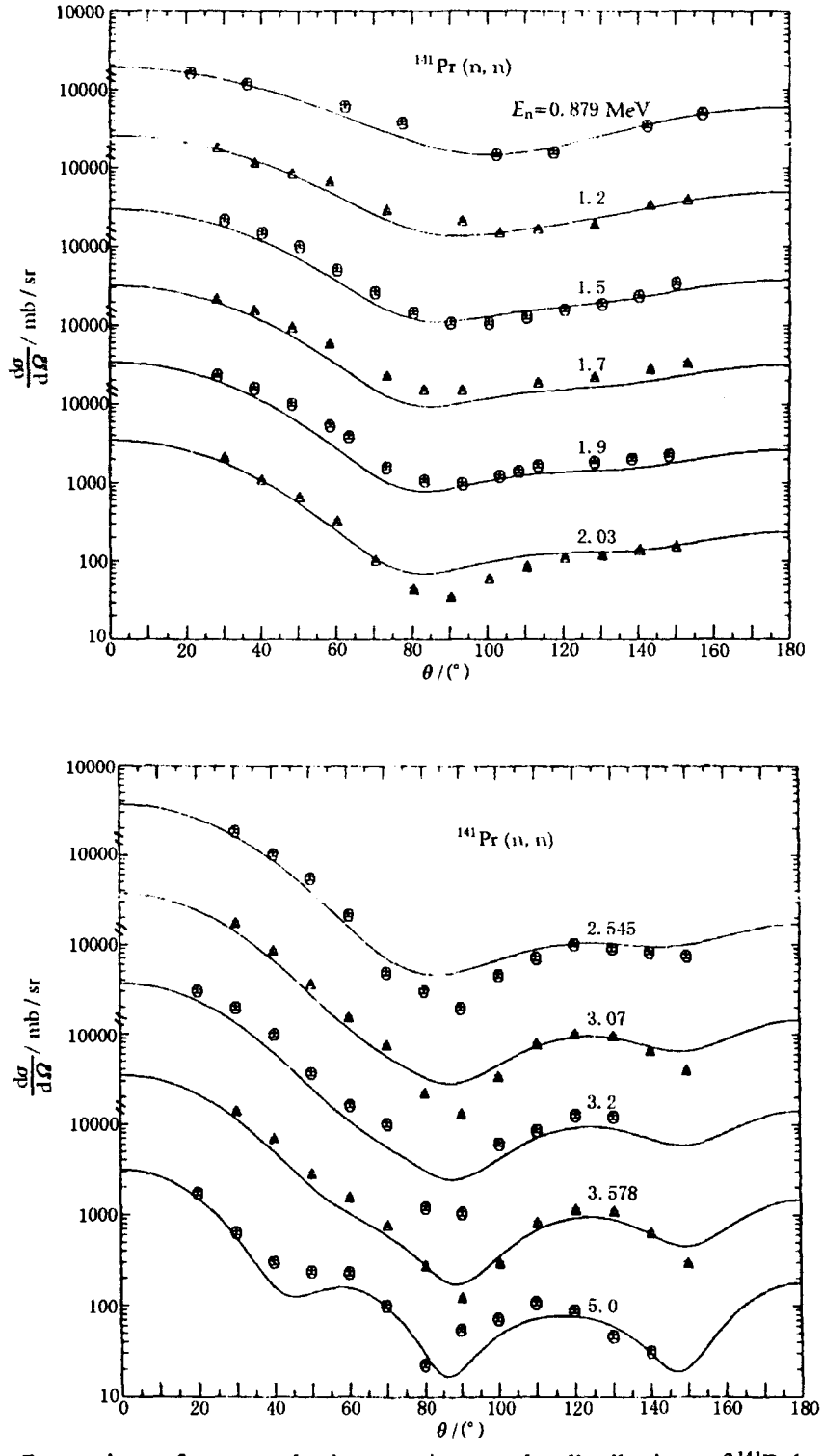

Fig.13 Comparison of neutron elastic scattering angular distributions of ^{141}Pr between the calculated values and the experimental data

References

[1] Q. B. Shen. APMN-a code for automatically searching for a set of optimal optical potential parameters of many nuclei, unpublished.

[2] P. D. Kunz. "Distorted Wave Code DWUCK4", University of Colorado, unpublished.

[3] J. S. Zhang. SUNF - a code for calculations of fission product nuclei based on unified model, CNDC, CIAE, unpublished.

[4] A. Gilbert, C. G. W. Cameron, Can. J. Phys., 43, 1446(1965).

CN0101649

Calculation of Proton Induced Reaction on ^{209}Bi in Energy Region from 7 to 250 MeV

Gao Bo, Shen Qingbiao*, Sun Xiuquan

(Physics Department, North West University, Xian, 710069)

* (CNDC, China Institute of Atomic Energy, P. O. Box 275 (41), Beijing, 102413)

Abstract

Cross sections of p+^{209}Bi reaction are calculated from 7 to 250 MeV based on various nuclear reaction models, i.e., the optical model, evaporation model, exciton model, as well as direct reaction process. The comparison of the calculated results with the experimental data shows that our calculations are quite reasonable. Simultaneously, excitation functions of some long-lived radioactive nuclei and neutron multiplicity are predicted.

Introduction

Accelerator-driven clean nuclear energy system (ADS) research is of interest to many countries. An important part of ADS is the high-intensity neutron source,

which consists of a lead or bismuth target irradiated by proton at medium energies. In this energy region, residual nuclei can be produced through particle emission process and fission process. Some long-lived radioactive nuclei may be produced and cumulated in the target. If their yields are large enough, how to dispose of them must be considered.

Recently, the theoretical calculation of proton reaction cross sections in a lead target with energy $E_p \leq 300$ MeV[1] has been done, and some interesting results have been obtained. Our work analyzes theoretically the experimental data of p+^{209}Bi reaction cross sections in the wide energy region, predicts the long-lived radioactive nuclei produced in the target, and gives the relation of the cross section and projectile proton energy.

1 Theory Models and Calculation Parameters

1.1 Proton Optical Potential Parameters

Based on the experimental data of p+^{209}Bi elastic-scattering angular distributions at energies of 65 MeV[2], 156 MeV[3], 340 MeV[4] and the reaction cross sections of p + ^{208}Pb[5], a set of optimum proton potential parameters in the region of $E_p \leq 350$ MeV is obtained by using APMN code as follows:

$$V = 42.31863 - 0.16493E_p + 0.00011929E_p^2 + 24.0(N\text{-}Z)/A + 0.4(Z/A^{1/3})$$

$$W_s = \max\{0, 3.22095 + 0.014476E_p + 12.0(N\text{-}Z)/A\}$$

$$W_v = \max\{0, 0.456667 - 0.002990E_p - 0.007103E_p^2\}$$

$$U_{so} = 6.2$$

$$r_r = 1.187584, \quad r_s = 1.070189, \quad r_v = 1.297927,$$

$$r_{so} = 1.187584, \quad r_c = 0.932820,$$

$$a_r = 0.764903, \quad a_s = 0.710988, \quad a_v = 0.290000, \quad a_{so} = 0.764903.$$

The neutron and other charged-particle optical potential parameters are chosen properly. The compound-nucleus elastic-scattering contribution is calculated by Hauser-Feshbach theory. The fission cross sections of the p+^{209}Bi reaction were taken from the experimental data[5] and were subtracted from the calculated absorption cross section. The value of the fission cross section of the p+^{209}Bi

reaction at 300 MeV is about 200 mb.

In Fig. 1 the calculated values of the p+^{209}Bi reaction cross sections are compared with the experimental data of the neighbor nucleus p+^{208}Pb[1,6] reaction. In order to get the good agreement with the experimental data of the multiple neutron emission cross sections, let the calculated values of the p+^{209}Bi reaction be lower a little than the experimental values of the neighbor nucleus p+^{209}Bi reaction .

In Fig. 2 the elastic scattering angular distributions for the p+^{209}Bi reaction between the calculated values and the experimental data are compared. The calculated values fit the experimental data very well in the whole $E_p \leq 250$ MeV energy region.

1.2 Direct Inelastic Cross Sections

The direct inelastic cross sections of the p+^{209}Bi reaction are calculated by using the DWUCK code [7] which is based on distorted wave Born approximation theory. The DWUCK code used proton optical potential parameters obtained in Sec.1.A as input data.

1.3 Production Cross Sections of Residual Nuclei

The production cross sections of residual nuclei produced through a multi-particle emission process and neutron multiplicity are calculated using the CCRMN code [8, 9] for the p+^{209}Bi reaction.

This version of the CCRMN code is based on nuclear reaction models, i.e., the optical, evaporation, exciton models, and direct reaction theory. The pre-equilibrium mechanism of gamma-ray emission and the pickup mechanism of cluster formation for composite particle emission are included in the first-, second-, and third-particle emission processes.

In this energy region, CCRMN code includes 16 emission processes. The reaction channels are as follows:

$A+a \rightarrow b_1+B_1^*$,	a=n, p, α, d, t, ^{3}He,	b_1=n, p, α, d, t, ^{3}He, γ
$B_{i-1}^* \rightarrow b_i+B_i^*$,	B_i=n, p, α , d, t, ^{3}He, γ,	i=2, 3, 4
$B_{j-1}^* \rightarrow b_i+B_j^*$,	b_j=n, p, α d, γ,	j=5, 6, 7
$B_{k-1}^* \rightarrow b_k+B_i^*$,	b_k=n, p, α, γ,	k=8, 9, 10
$B_{l-1}^* \rightarrow b_l+B_i^*$,	b_l=n, p, γ,	l=11, 12, 13, 14, 15, 16.

Of course, it is better if the fission process can be included in every reaction

process. Since the experimental values of the fission cross sections of the p+^{209}Bi reaction up to 300 MeV are less than 200 mb, the neutron emission processes are still the main reaction processes in the energy range below 300 MeV. The contribution of the fission process as was considered in this paper as that mentioned above. One can call all the multiple particle emission and the fission processes as spallation reaction in high energy region.

2 Calculation Results and Analysis

Figs. 3, 4 and 5 show the comparisons of the calculated results with the experimental data[10-13] for (p,n), (p,3n), (p,4n) reactions, which are in good agreement with each other.

Fig. 6 shows the dependence of the neutron multiplicity on the proton energy. The calculation values do not include the prompt neutrons in the fission process. In the $E_p \leq 175$ MeV energy region, neutron multiplicity rises quickly with E_p, but in the $E_p \geq 175$ MeV energy region, it rises very slow and smoothly.

Figs. 7 and 8 show the dependence of the cross sections of multiple neutron emission reaction channels on the proton energy in the p+^{209}Bi reaction. Because its compound nucleus ^{210}Po is neutron-rich, the neutron emission channels are the main channels.

Figs. 9 and 10 show the calculated value of production cross sections of the residual nuclei for the p+^{209}Bi reaction at E_p=200 MeV. The calculation values do not include the fission yield.

Fig. 11 shows the production cross-sections of the long-lived radioactive nuclei produced in the p+^{209}Bi reaction, of which production cross sections is >1 mb and the half-life is >1 y. Their half-lives are as follows:

^{209}Po (102 y); ^{208}Po (2.898 y);
^{208}Bi ($3.65 * 10^5$ y); ^{207}Bi (32.2 y);
^{205}Pb ($1.52 * 10^7$ y); ^{204}Pb (>$1.4 * 10^{17}$ y);
^{202}Pb ($52.5 * 10^3$ y);

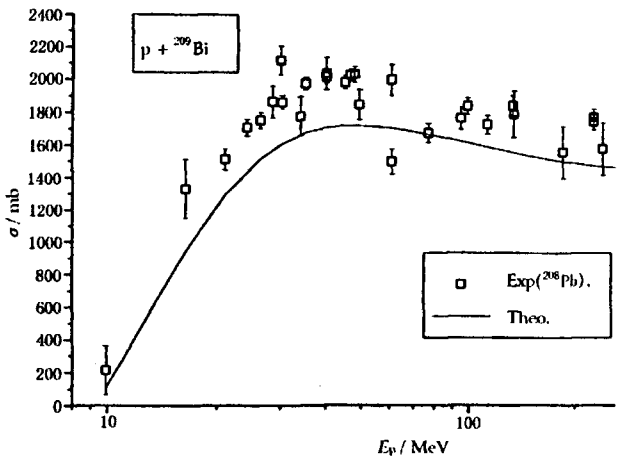

Fig. 1. Comparison of reaction cross section for the p+^{209}Bi reaction

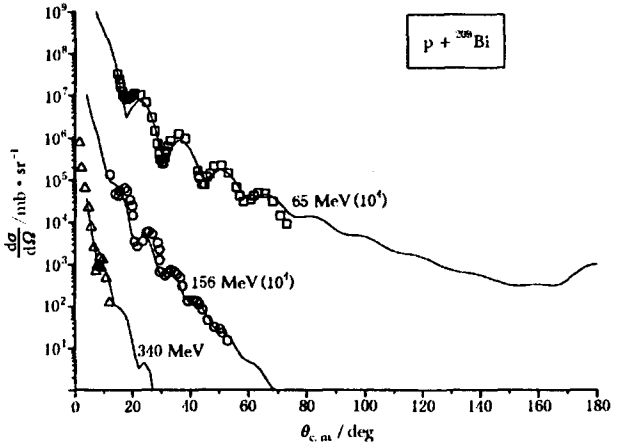

Fig. 2. Comparison of proton elastic scattering angular distributions for the p + ^{209}Bi reaction at E_p= 65 MeV[2], 156 MeV[3] and 340 MeV[4]

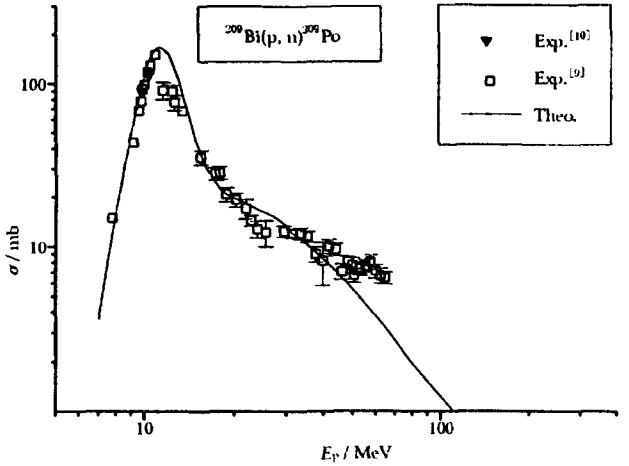

Fig. 3. Comparison of the cross section of ^{209}Bi(p, n) ^{209}Po reaction

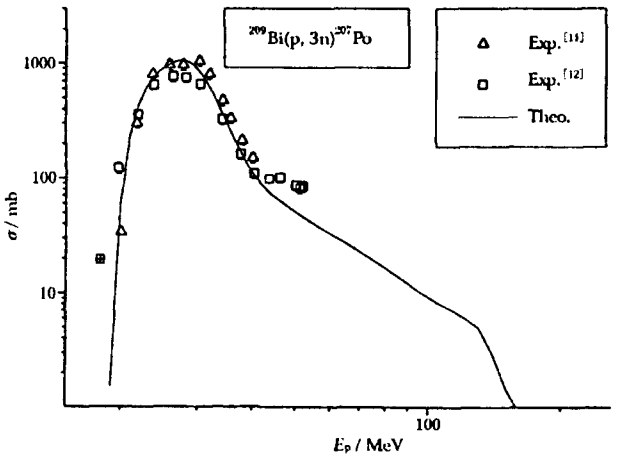

Fig. 4. Comparison of the cross section of ^{209}Bi(p, 3n) ^{207}Po reaction

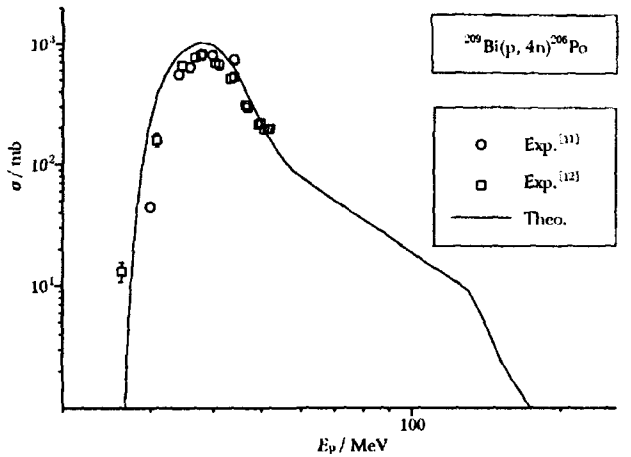

Fig. 5. Comparison of the cross section of ^{209}Bi(p, 4n) ^{206}Po reaction

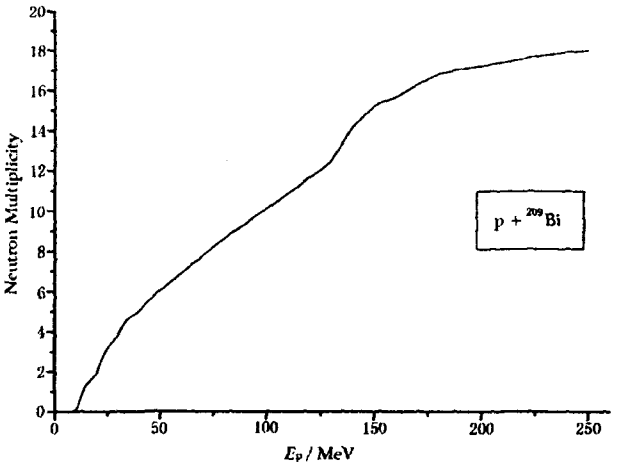

Fig. 6. Dependence of neutron multiplicity on proton energy in the p+^{209}Bi reaction

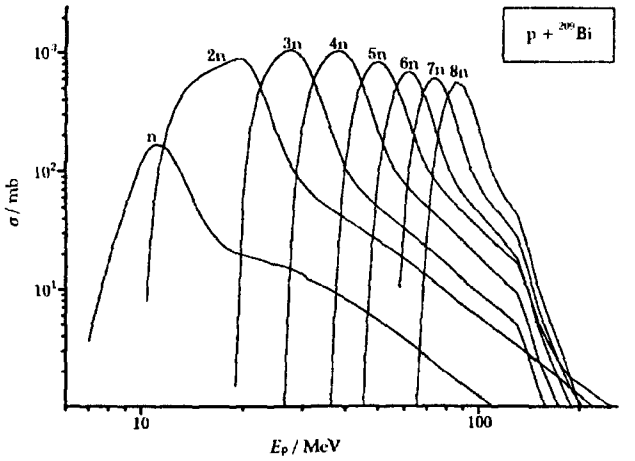

Fig. 7. The cross sections of multiple neutron emission reaction channels for p+^{209}Bi reaction

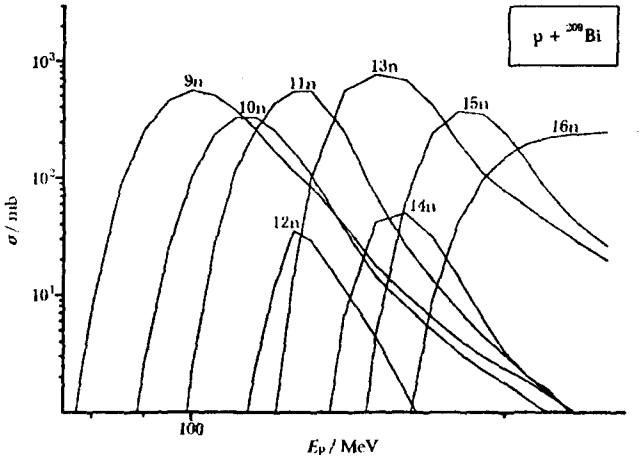

Fig. 8. The cross sections of multiple neutron emission reaction channels for p+^{209}Bi reaction

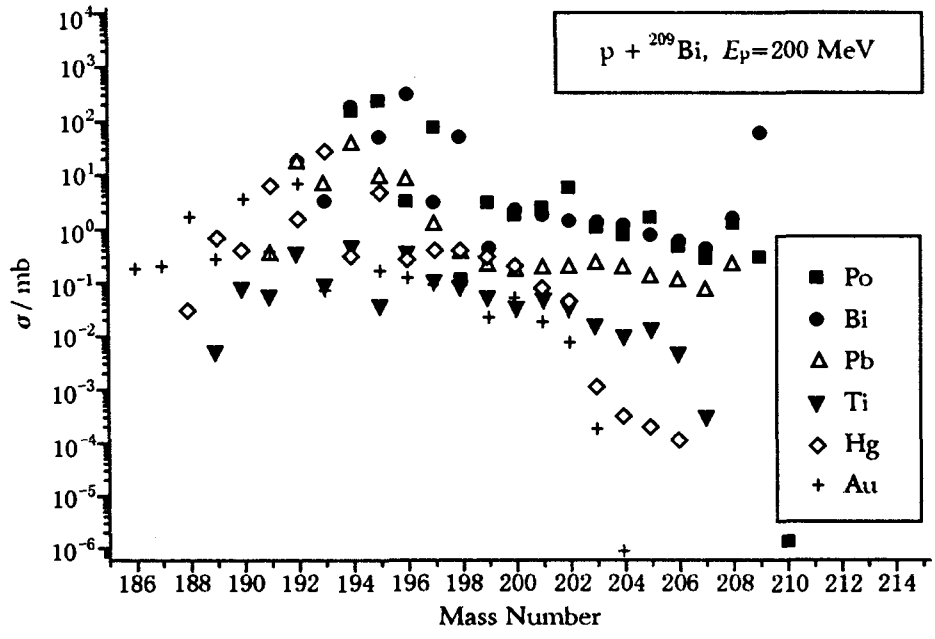

Fig. 9. The calculated value of production cross sections of the residual nuclei Po, Bi, Pb, Ti, Hg and Au for the p+^{209}Bi reaction at E_p=200 MeV

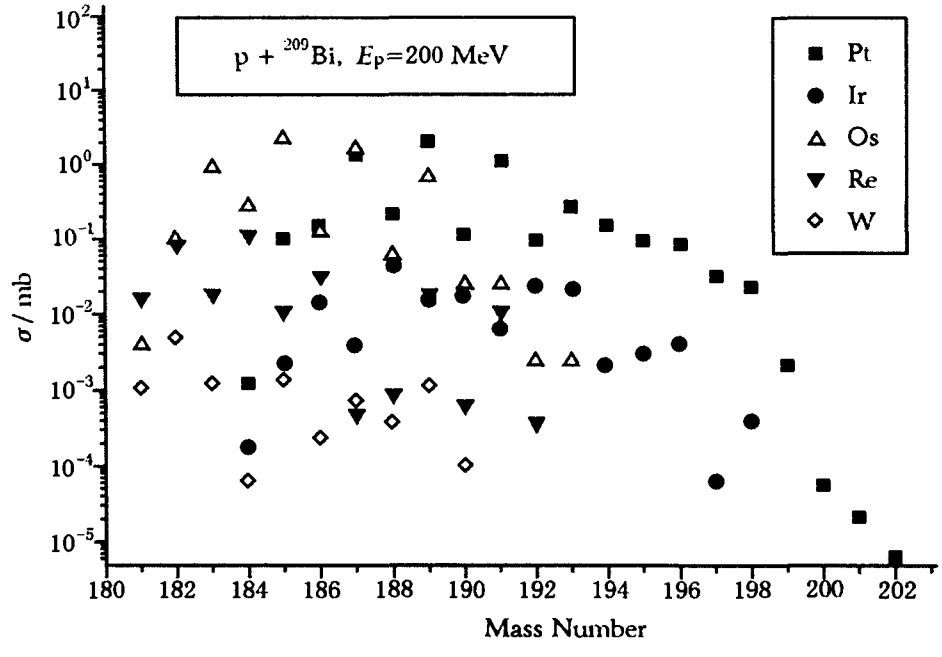

Fig. 10. The calculated value of production cross sections of the residual nuclei Pt, Ir, Os, Re and W for the p+^{209}Bi reaction at E_p=200 MeV

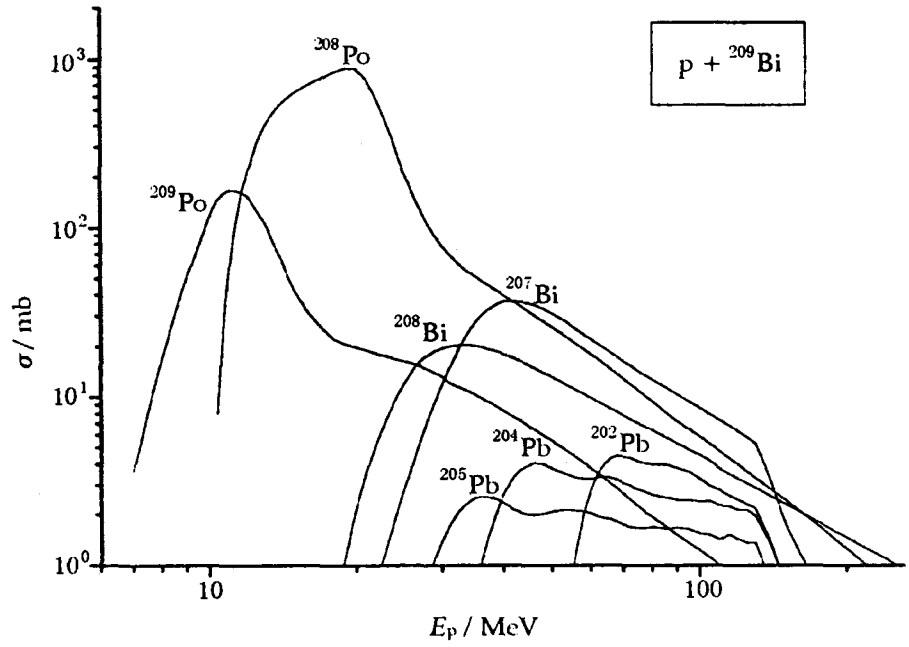

Fig. 11. Productions cross sections of long-lived radioactive nuclei in the p+^{209}Bi reaction

3 Summary

Various cross sections of p+^{209}Bi reaction are calculated in the 7 to 250 MeV energy region based on the nuclear reaction models, i. e., the optical, evaporation, and exciton models, and direct reaction theory. The comparison of the calculated results with the experimental data shows that our calculation results are reasonable. The excitation functions of some long-lived radioactive nuclei and neutron multiplicity are predicted.

References.

[1] JinFeng Zhou, QingBiao Shen and XiuQuan Sun, Nucl. Tech., 127, 113(1999)

[2] H. Sakaguchi, M. Nakamura, K. Hatanaka et al., Phys. Rev. C26, 944(1982)

[3] V. Comparat, R. Frascaria, N. Marty et al., Nucl. Phys., A221, 403(1974)

[4] R. E. Richardson, W. P. Ball, C. E. Leith et al., Phys. Rev., 86, 29(1952)

[5] Vilent P.Eismont, Anatoliy I. Obukhov, Alexander V. Prokofyev et al., Proc. of the Second International Conference on Accelerator-Driven Transmutation Technologies and Applications, Kalmar, Sweden, June 3-7, Vol 2, 592(1996)

[6] W. Bauhoff, Atomic Data and Nuclear Data Table, 35, 429(1986)

[7] P. D. Kunz, Distorted Wave CodeDWUCK4, University of Colorado, unpublished

[8] C. H. Cai and Q. B. Shen, Commun. Nucl. Data. Prog., 15, 22(1996)

[9] C. H. Cai, Q. B. Shen, Z. Q. YU, Nucl. Sci. Eng., 126, 127(1997)

[10] K. Miyano, T. Ando, H. Kudo et al., J. Phys. Sci. Jap., 35, 953(1973)

[11] J. Wing and J. R. Huizenga, Phys. Rev., 128, 280(1962)

[12] C. Birattari, E. Gadioli, A. M. Grassi Strini et al., Nucl. Phys. A 166, 605(1971)

[13] K.Miyano, T. Aneko, M.Nomoto et al., Nucl. Phys., A230, 98(1974)

III DATA EVALUATION

Comprehensive Adjustment for Complete Data of Natural Zr and its Isotopes

Liu Tingjin
(China Nuclear Data Center, CIAE)
Zhang Wei and Liu Jianfeng
(Zhengzhou University, Zhengzhou)

Introduction

The complete data of natural Zr and its isotopes ^{90,91,92,94,96}Zr were evaluated, including neutron resonance parameter, cross section, angular distribution, double differential cross section, and γ production data. The experimental data of cross section were evaluated[1], and theoretical calculations were done with theory code NUNF[2], so it is necessary to be comprehensively adjusted to make them consistence in physics for each nuclide itself and between natural element and its isotopes. This paper is devoted to describing how to make them consistence. In section 1 the data taken and energy region supplement is given. In section 2 is the adjusting at the resonance boundary. In the sections 3 and 4 is the consistence adjusting for each nuclide itself and between natural element ant its isotopes respectively. In section 5 is the check and energy balance adjusting. In section 6 is the result and comparison with existing evaluated data, and in last section is the conclusion remark.

It is a routine procedure to make consistence of a set of complete data for a nuclide itself, but it is more complicated to make the consistence between the data of natural element and its isotopes, so, so far, which is evaded in most of evaluated nuclear data libraries, either only the data of natural element or only the data of

isotopes are given. A method and a program have been developed for solving this problem[3], and the adjustment of Zr data is a typical example.

1 Data Taken and Energy Region Supplement

As a rule, the evaluated experimental data were taken as recommended ones, if there are data points enough for giving out a fitting curve in whole energy region. If there are enough experimental data only in some part of the energy region, then the experimental data were recommended in this region and theoretically calculated data were recommended in remain energy region. In this case they must be made smooth conjunction at the boundary, either the calculated data were normalized to the experimental data at the boundary, or the data were smoothed by eyes-guide in the nearby region of the boundary. The theoretically calculated data were taken for others, but they can be normalized, if there are some experimental data at some special energy points.

The experimental data, which have been evaluated and used in this evaluation, are listed in Table 1 for natural Zr and its isotopes. The symbol "√" means that there are enough energy points to give out the fit curve in the energy region from the threshold up to the energy given by the number in the parentheses. The symbol "⊗" means that there are experimental data in the given energy region, but the data points are not enough for fitting a curve. Symbol "↔" means there are experimental data in the given energy region or at some energy points.

It is impossible to spread to 10^{-5} eV either for experimental or theoretically calculated data, so the data must be supplemented to the whole energy for the reaction with no threshold. The cross section (file 3) was extended by putting in the resonance parameters (section 2). The elastic angular distribution (file 4) was spread by adding isotropic distribution. The γ production multiplicity (file 12, MT=102) was extrapolated to the 10^{-5} eV by using the data in the low energy region. The γ production spectrum for (n,γ) reaction (file 15, MT=102) was extrapolated to10^{-5} eV by using the spectrum calculated at low limit energy point, but the correction was made to the maximum energy of outgoing γ for the corresponding incident neutron energy change and, meanwhile, kept the normalization of the spectrum.

Table 1 The evaluated experimental data for natural Zr and its isotopes (cross section)

Reac.	Nucl.					
	^{90}Zr	^{91}Zr	^{92}Zr	^{94}Zr	^{96}Zr	^{0}Zr
(n,tot)	√	√	√	√		√
(n,non)						√(14.0)
(n,n)		⊗		⊗		⊗
(n,n')	√(2.4)*					
(n,2n)	√				√(15.0)	√(18.0)
(n,p)	√(18.0)	√(14.0)	√(15.0)	√(10.8~16.5)		
(n,α)			√	√	⊗	
(n, γ)				⊗	⊗	√(1.0)
(n,n_1')	√(2.5)		√(3.6)	√(3.0)		
(n,n_2')	√(2.9)		√(3.6)	√(3.0)		
(n,n_3')	√(5.0)	⊗	√(5.0)	⊗		
(n,n_4')			√(3.6)	⊗		
(n,n_5')			√(3.6)			
(n,n_7')			⊗			
DX(n)						↔ 14.1,18.0
DDX(n)						↔ 14.1,18.0
DDX(p)						↔ 14.8
DDX(α)						↔ 14.8
$\sigma_{nn}(\theta)$	↔ (1.8~11.0)	↔ (8.0,10.0)	↔ (1.8~10.0)	↔ (1.5,8.0,10.0)		↔ (0.32~14.2)

* Energy in MeV, the same below.

2 Resonance Parameters and Conjunction at the Resonance Boundary

The resonance parameters were taken from JENDL-3.2, which were evaluated latest and have a larger energy region for the resonance.

The conjunction between the cross section of the smooth region at boundary (σ_+) and the cross section (σ_-) calculated with the resonance parameters was checked. In general, they are conjoint well, but except for the total, elastic and capture cross sections of ^{90}Zr and natural Zr. The check result of ^{90}Zr is given in the Table 2. The cross section near the resonance boundary is shown in Fig.1. From the figures it can

be seen that the cross section 7.07045 b calculated with resonance parameters is not reasonable. In addition, there are experimental data in the energy region from 0.17 MeV to 0.5 MeV for natural Zr, they are from 9.0 to 9.5 b, and the cross section should increase with the energy decreasing. If the cross section of ^{90}Zr (the abundance is 51%) was taken as 7.07045 b, it is difficult to make it consistence with natural Zr. Also the cross sections in ENDF/B-6 and JENDL-3 are all about 9.6 b. So the resonance parameters should be adjusted.

Table 2 The check result of ^{90}Zr cross section at resonance boundary

σ	σ_- / b	σ_+ / b	$\Delta\sigma$ / b
σ_{tot}	7.07045	9.8770	2.80655
$\sigma_{n,\gamma}$	1.2844E-2	7.1237E-3	-5.7203E-3

The resonance boundary energy was changed. It was found that the cross section was changed considerably with changing the boundary. The results are listed in Table 3. At last, the boundary energy was taken at 171.995 keV, in this case, the cross section calculated with resonance parameters is almost the same as one in the sooth region.

Table 3 The adjusting of ^{90}Zr total cross section σ_{tb} at boundary with the resonance boundary energy E_b

E_b / keV	169	170	171	172	173	174
σ_{tb} / b	12.346	7.5918	7.07045	10.037	7.974	5.988
E_b / keV	171.8	171.9	171.95	171.980	171.985	171.995
σ_{tb} / b	7.726	8.825	9.3406	9.7322	9.8047	9.9761

Regards as capture cross section, it can be seen from the experimental data that the cross section 7.1237E-3b in the smooth region is unreasonably small. It was adjusted to1.2844E-2b, and then the cross section was made smooth change in the energy region 171.995 keV to 1.1 MeV.

The similar adjustment was made for natural Zr.

3 Consistence Adjusting for Each Nuclide Itself

This is routine procedure for any complete data evaluation, which was completed in the evaluation by using code CRECTJ5 in the following steps:

1) Total inelastic scattering CS=the sum of the CSs of inelastic scattering to continuous state and discrete levels;

2) Nonelastic CS=the sum of all partial noelastic channel CSs;

3) Elastic CS=subtracting the noelastic CS from total CS, and Total CS=elastic CS plus nonelastic CS.

The basic idea is that the whole difference in the inelastic channel is put into the total inelastic cross section, in the noelastic channel is put into the total noelastic cross section and in total channels is put into the elastic cross section.

The last step is not only for making the consistence among the total, elastic and noelastic cross sections, but also for making them satisfy the energy point rules of the ENDF/B-6 format. That is the energy point of the elastic and nonelastic cross sections must be included in the one of total cross section.

Due to the code CRECTJ5 is suitable only for the data in the ENDF/B-5 format, so the data have to be changed into ENDF/B-5 format by using code B6TOB5, and after completing the processing, the data were changed into ENDF/B-6 format by using code B5TOB-6. This is a little fussy, but must be done.

4 Consistence Adjusting Between Natural Element and its Isotopes

Natural element Zr consists of following isotopes: ^{90}Zr (51.45%), ^{91}Zr (11.22%), ^{92}Z (17.15%), ^{94}Zr(17.38%) and ^{96}Zr (2.80%). The cross section of natural Zr must be equal to the weight sum of the corresponding cross sections with the abundance as weight, but in fact, the data were measured for element and isotopes separately, they could not satisfy the consistence requirement and must be adjusted. Furthermore, when the adjusting was made, the consistence for each nuclides must be kept, which make the matter more complicated. In order to this problem, a code CABEI was developed[3] and used for adjusting.

The adjusting can be done only in the common energy region for all reaction channels of all nuclides. Due to the up resonance boundaries for different isotopes are different, the highest one was taken as the low limit of the adjustment region. For the reactions with thresholds, the lowest threshold energy of the same kind of reaction was taken as the adjustment low limit, and for the reactions with higher thresholds, the cross sections were taken as zero in the region from this energy to their corresponding thresholds. Regarding as this point, it must be paid attention to the threshold of the natural Zr, it must be equal to the lowest one of the reactions of the all isotopes, could not be lower more. This could be happen, when the Q-value of the isotope, the mass of which is smaller than natural element, is the lowest one and taken as the Q-value of the natural element, for both have the same Q-values, but have the different mass, so the different thresholds E_{th}:

$$E_{th} = Q\,(A+1)/A = (1+1/A)Q$$

By using code CABEI, the adjusting was done by following steps:

1) Total CS=elastic CS plus nonelastic CS;

2) Nonelastic CS=the sum of the CSs of all nonelastic channels;

3) Inelastic CS=the sum of the CSs inelastic scattering to continuous state and discrete levels.

The weight was chosen according to the requirement. In the step 1, the weight of the total cross section was taken as larger, so that it was less changed, for the total cross section was measured with higher precision and accuracy. Also the larger weight was also given to the natural element and ^{90}Zr, for there are more measured data for them. In the step 2, the much larger weight was given to the total noelastic cross section, so that it can be kept unchanged, otherwise, the consistence adjusted in the step 1 could be violated. Also the error itself of the data was taken into account. In the step 3, only the consistence was adjusted for each nuclide and a larger weight was given to total inelastic cross section, so that it was kept not changed in the adjusting. There are different levels for different nuclides and with the different thresholds for the inelastic continuous cross sections, it is not reasonable in physics to make them consistence between natural element and its isotopes.

The adjusting calculation was done at all energy points of all reactions of all nuclides included. The solution was exact at these energy points, but the output could not be at so many points, in general case only can be at the original mesh points. So when the output data were checked, somewhat unconsistence could be found. In this case, the adjusting can be iterated. The more the times of the iteration, the better the result.

The consistence, including both for each nuclide itself and between natural element and its isotopes, after the adjusting was checked by the code DIFF. The consistence for each nuclide itself also can be checked by ENDF utility program FIZCON. The results of both codes are the same. After several times of the iterations, now for present data the error of the consistence for each nuclide itself is less than 0.1% and between natural element and its isotopes is less than 1.0%.

If the data are in better consistence before the adjusting, then they are changed little, but if there are some difference of the natural data from the sum of all isotopes, they are changed to some extent in the adjusting, an example is given in Figs. 2 and Figs. 3. It can be seen that the (n,2n) cross section becomes lower for ^{90}Zr and becomes higher for natural Zr.

5 Check and Processing

After completing the above procedures, the directory of the data were created by using code STANEF and were checked in format and in physics by using ENDF utility programs CHEKR, FIZCON and PSYCHE. Also the code DIFF, as mentioned above, was used for checking the consistence of the data, and the code STEB was used for checking the energy balance. If the problem was found, then the data concerned were reprocessed by carrying through the corresponding procedure mentioned above.

It should be pointed out that the energy balance check result by the codes does not exactly come into existence for inelastic scattering to continuous state (MT=91) and natural element, because the Q-value in these case is not suitable for energy balance[4].

It was found that there are some problems some times for the energy balance at the energy points near the threshold, due to the reaction is just open, and there is no much energy for outgoing particles to be taken. If this is the case, the spectrum was adjusted artificially. The basic idea is that the spectrum is multiplied by a straight line $y=aE+b$, and a, b can be calculated from the difference between the energy really taken by the outgoing particles and available energy (given by the code STEB) and the normalization of the spectrum[5].

6 Results and Intercomparison

After completing all above procedure, the evaluation was completed, and the results were plotted and compared with other evaluated and experimental data. The plotting was done with codes PLOTF6, DR and ENDF/B plot code PLOTEF. Code PLOTF6 was specially developed for double differential cross section[6] and DR was developed for plotting with microcomputer.

It was shown by the intercomparison that some cross sections of present evaluation are improved considerably. Some examples are given in Fig.4 for ^{90}Zr total cross section, in Fig. 5 for ^{96}Zr(n,p), in Fig. 6 for ^{96}Zr(n,2n). The typical examples of comparisons with FENDL-2 are given in Figs.7~10 for double differential cross section at incident energies 14.1, 18.0 MeV and outgoing angles at 60, 150 degree respectively. It can be seen from these figures that, comparing with FENDL-2, some of the present double differential cross sections are improved. It should be pointed out that the present results are all calculated in physics when the parameters are adjusted based on the experimental cross sections and differential cross section.

7 Conclusion Remark

The complete data of natural Zr and its isotopes ^{90,91,92,94,96}Zr were evaluated based on experimental data available up to now and theoretical calculation with code NUNF. The data were comprehensively adjusted to make them consistence in physics for each nuclide itself and between natural element and its isotopes.

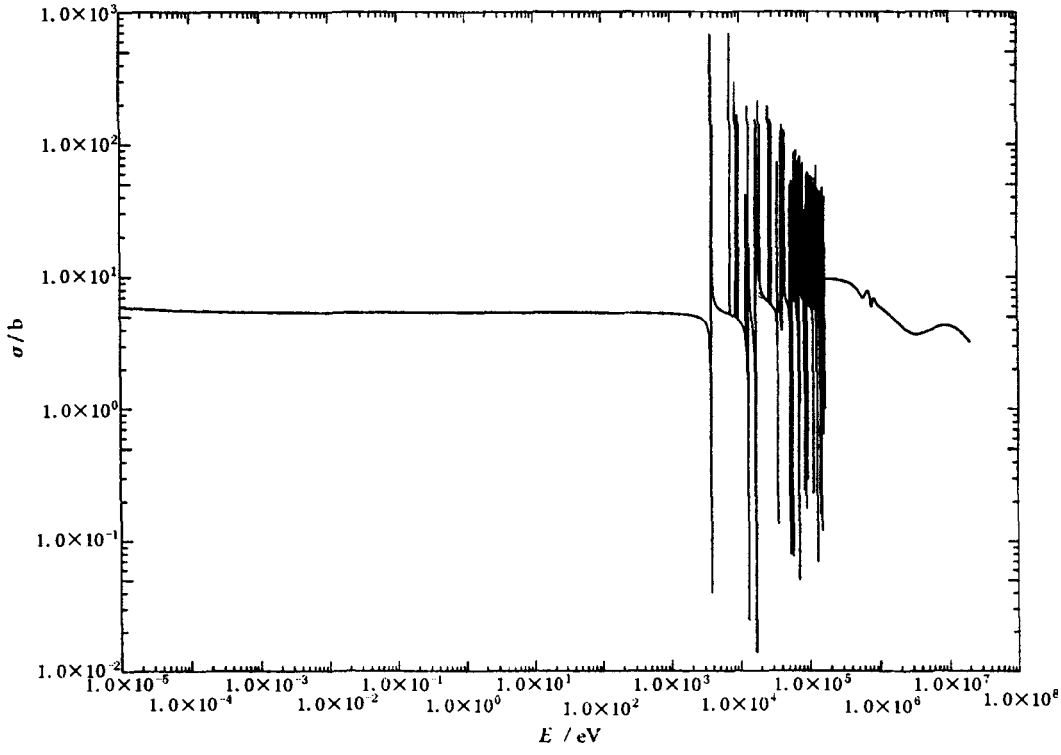

Fig. 1.1 The total cross section near the resonance boundary(1)

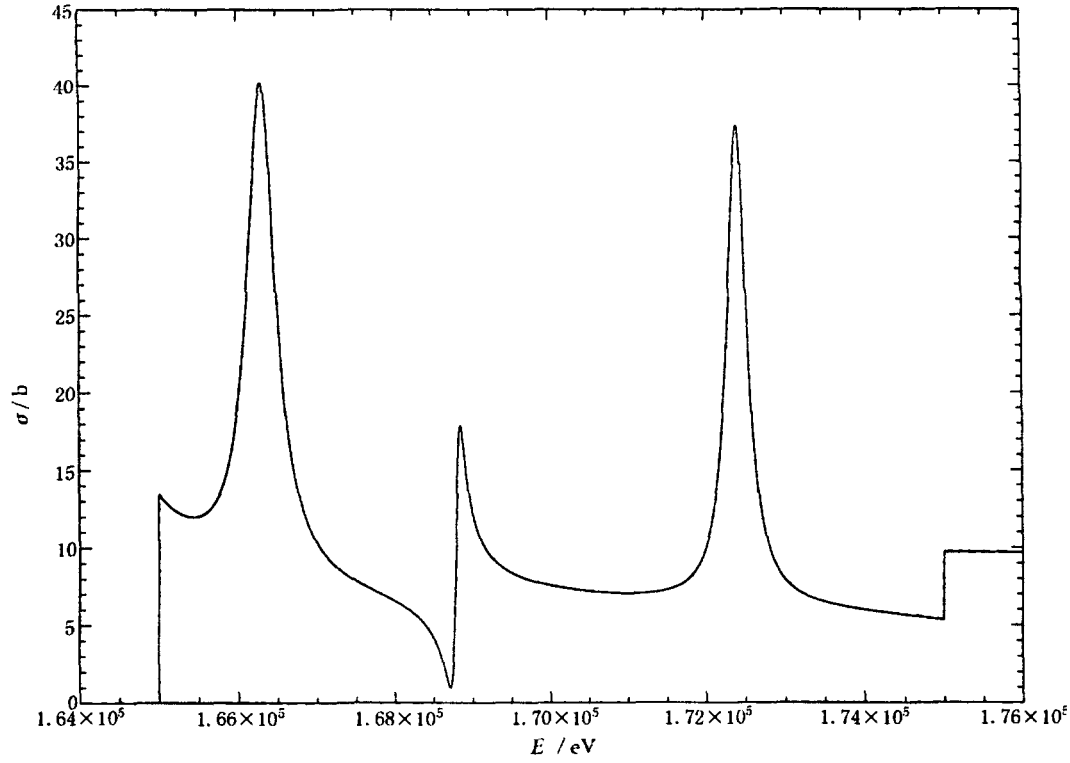

Fig. 1.2 The total cross section near the resonance boundary(2)

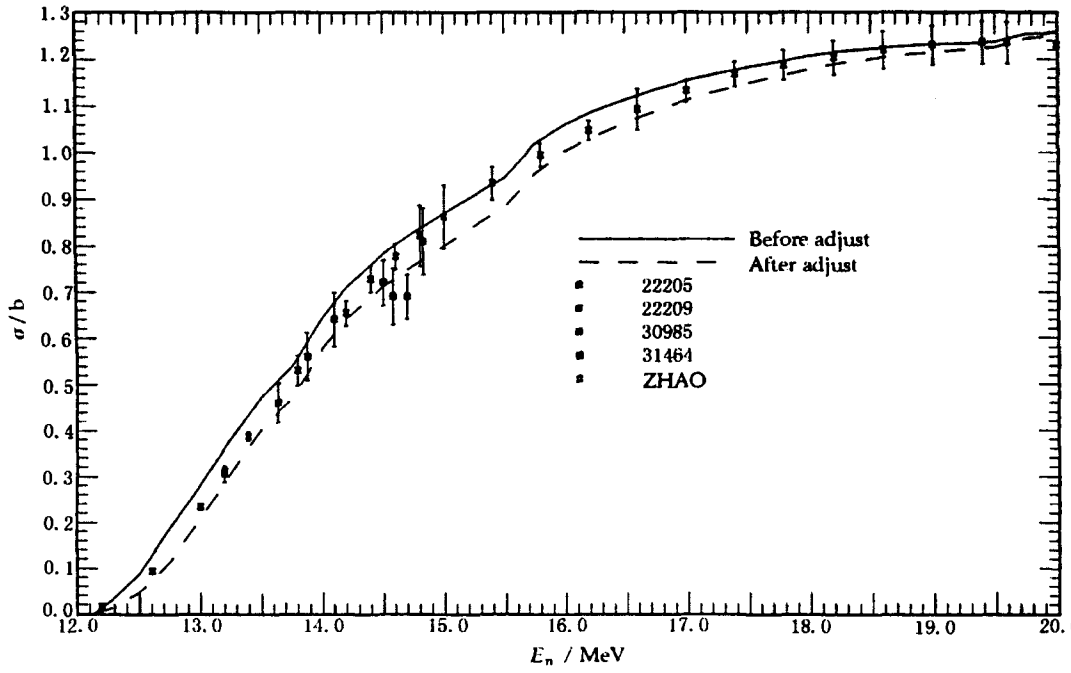

Fig. 2 The comparison of ^{90}Zr(n,2n) cross section before and after adjusting for consistence between natural element and its isotopes

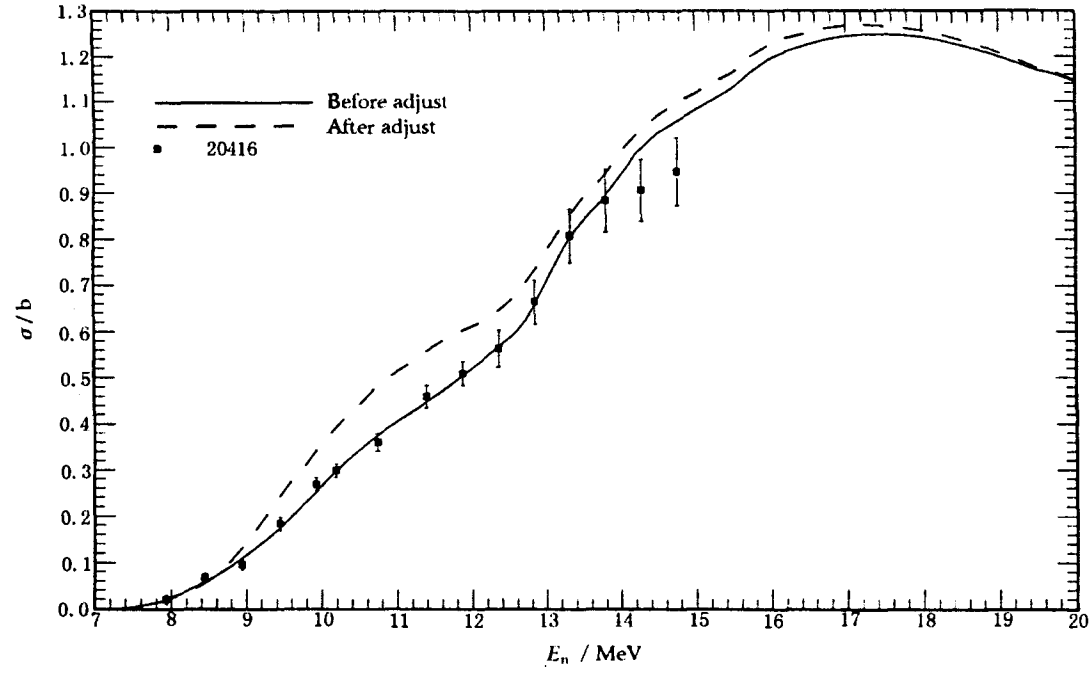

Fig. 3 The comparison of natural Zr(n,2n) cross section before and after adjusting for consistence between natural element and its isotopes

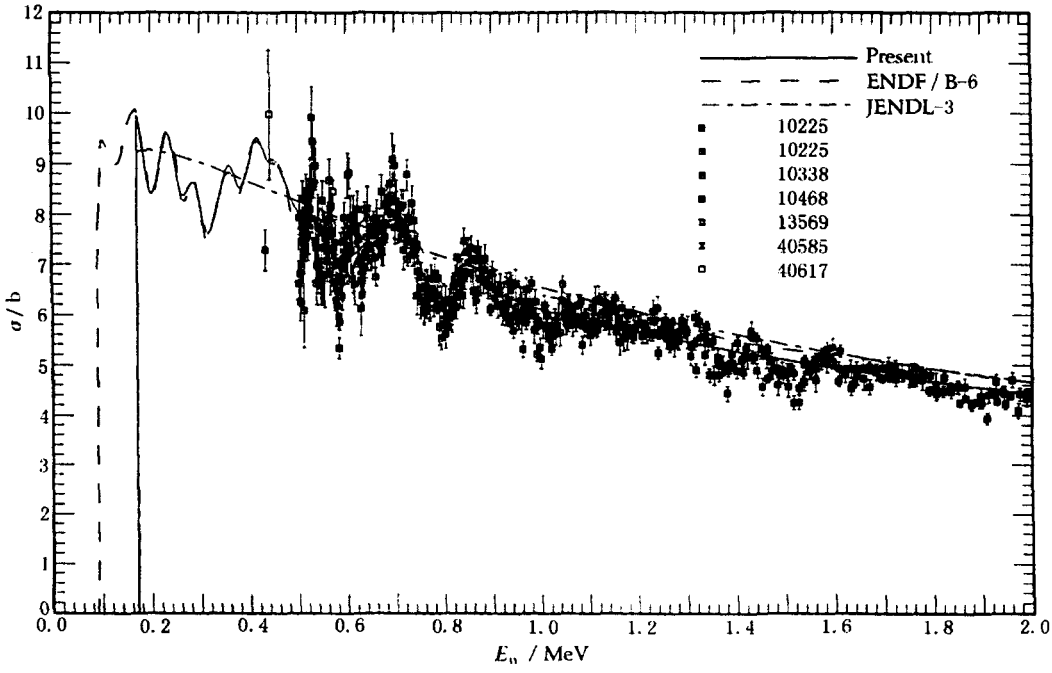

Fig. 4.1 The total cross section of ^{90}Zr(1)

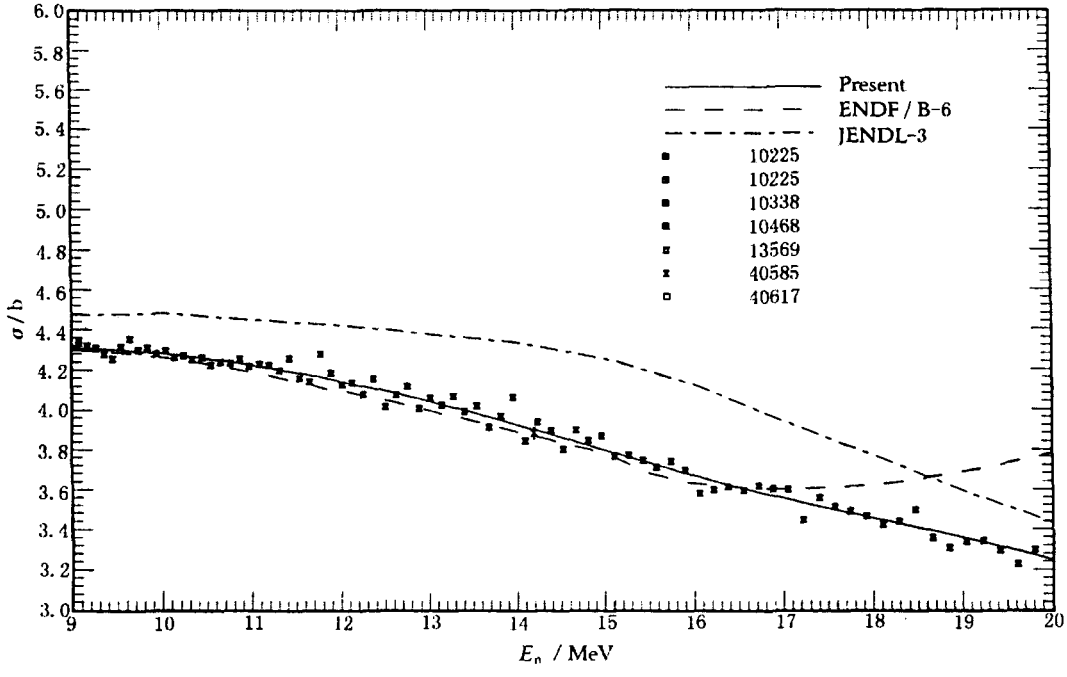

Fig. 4.2 The total cross section of ^{90}Zr(2)

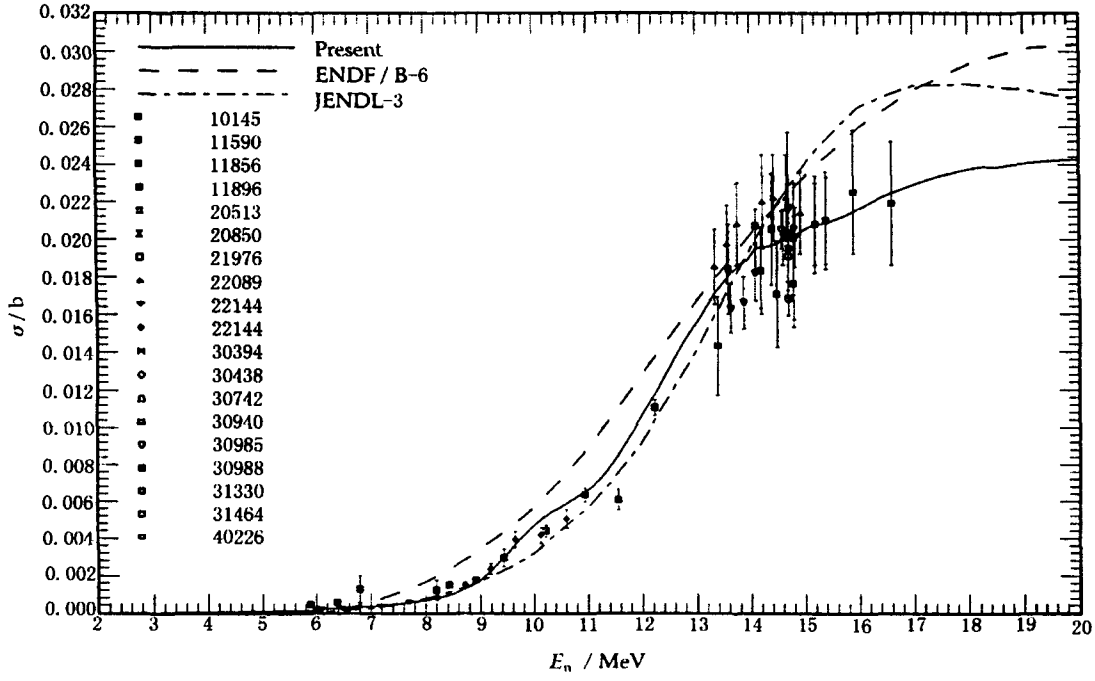

Fig. 5 The cross section of ^{92}Zr(n,p)

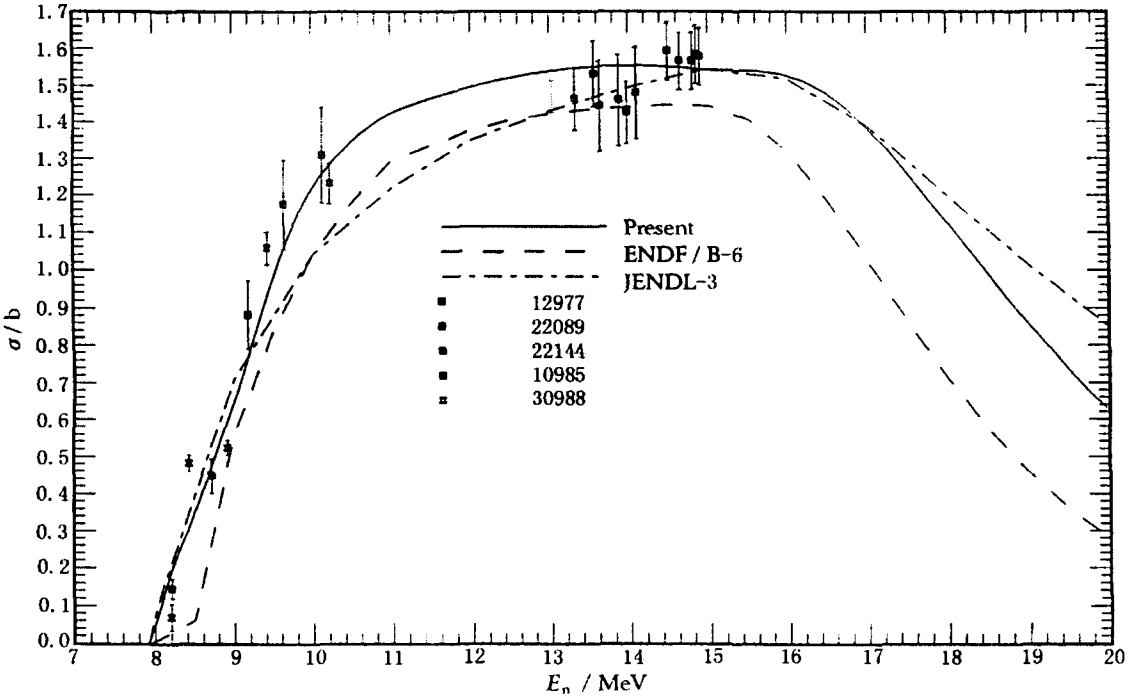

Fig. 6 The cross section of ^{96}Zr(n,2n)

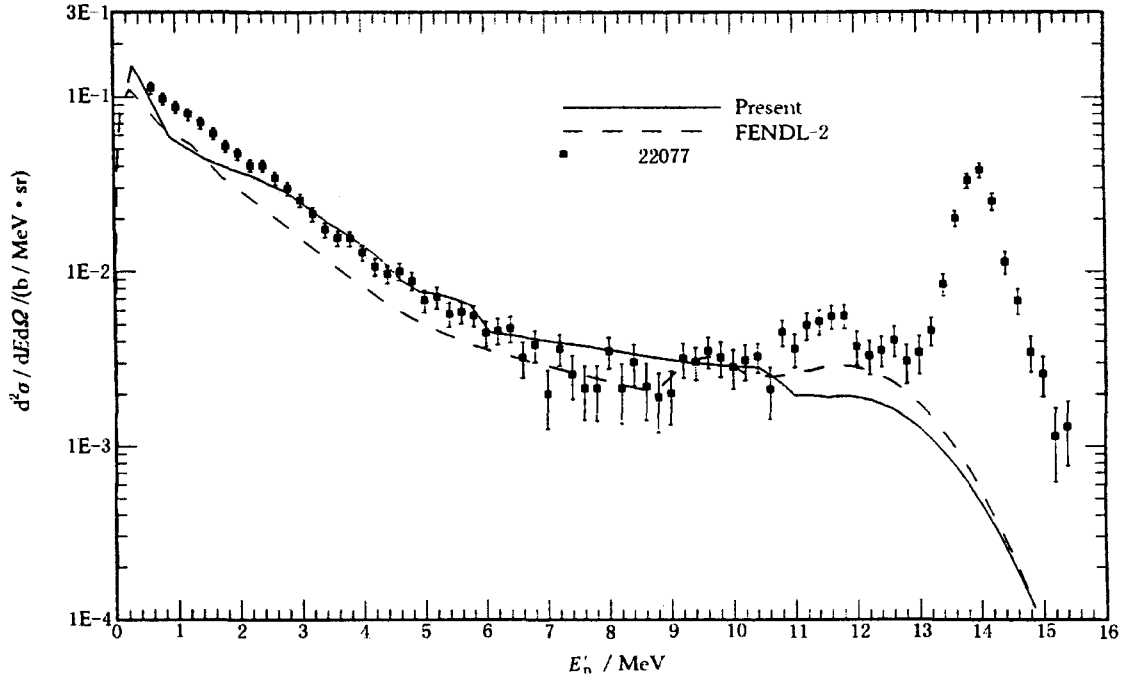

Fig. 7 The double differential cross section of natural Zr at E_n=14.1 MeV, θ=60°

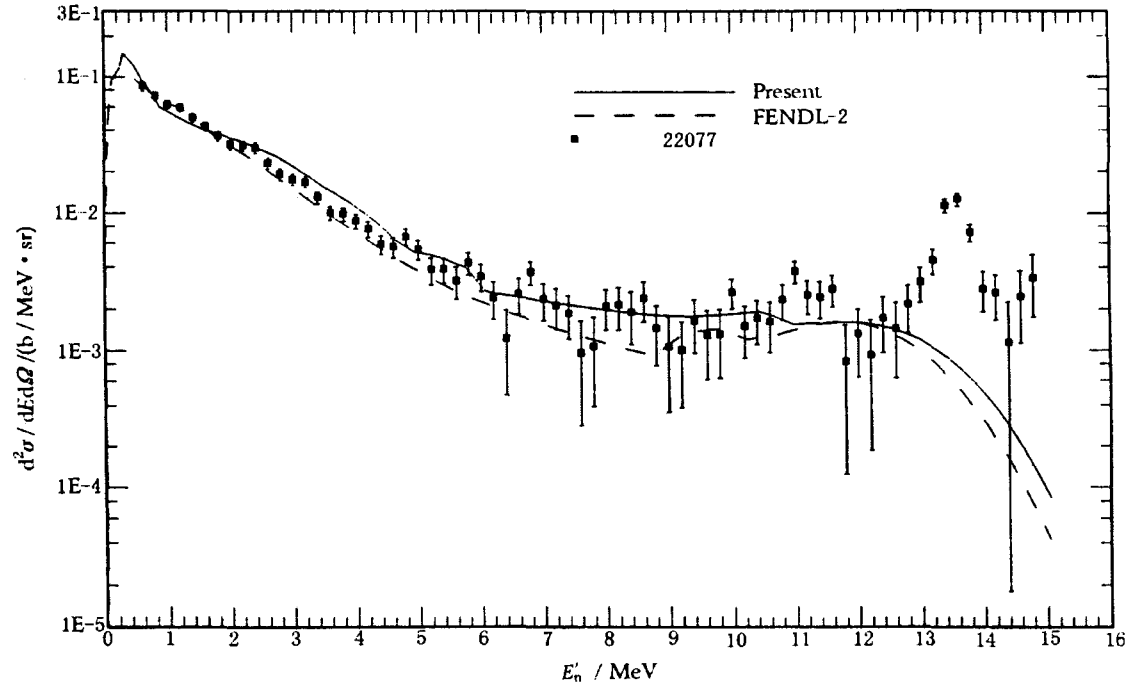

Fig. 8 The double differential cross section of natural Zr at E_n =14.1 MeV, θ=150°

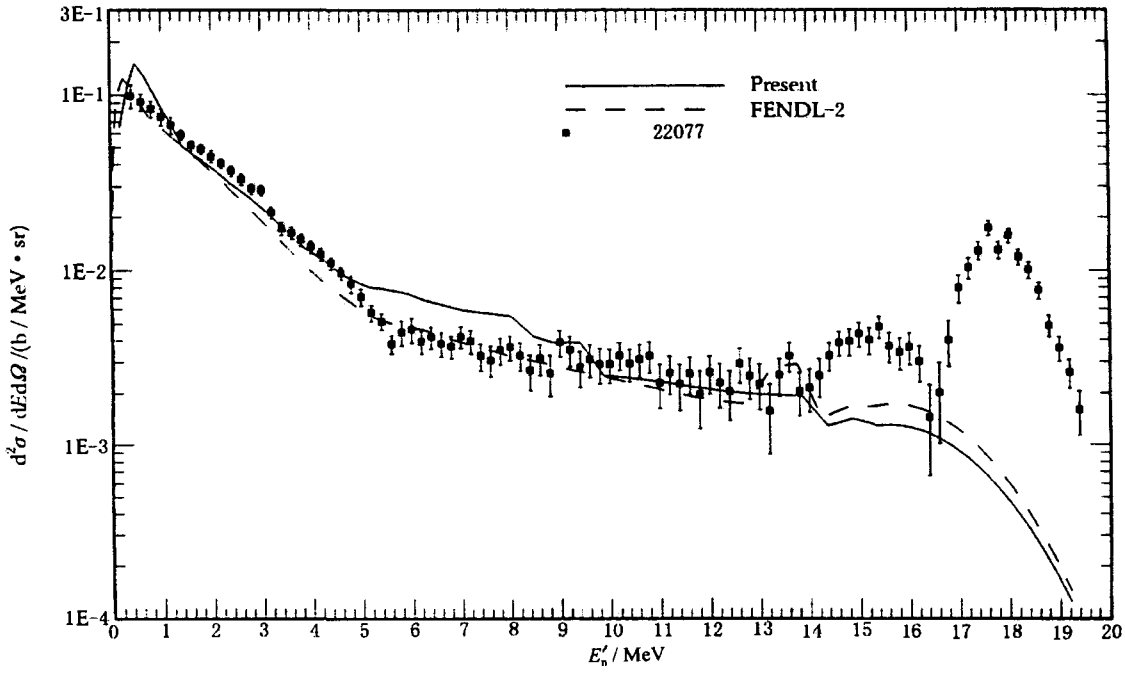

Fig. 9 The double differential cross section of natural Zr at E_n =18.0 MeV, θ=60°

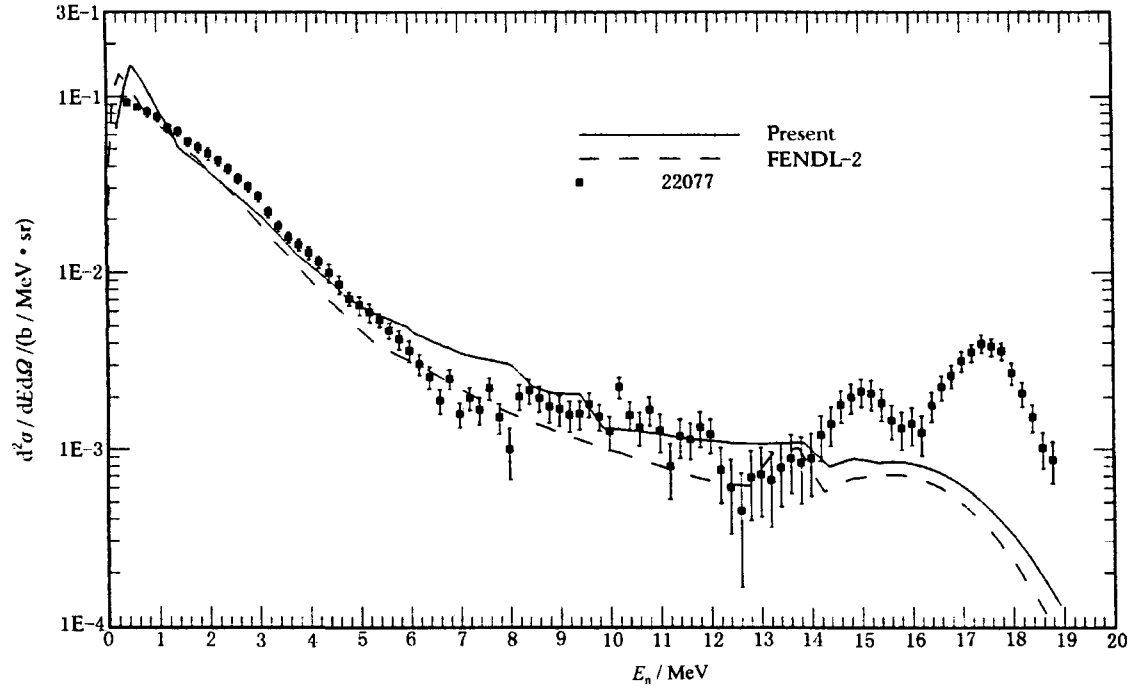

Fig. 10 The double differential cross section of natural Zr at E_n =18.0 MeV, θ=150°

Comparing the data with others from ENDF/B-6 and JENDL-3.2, the data have following features:

(1) The data are consistence in physics for each nuclide itself and between natural element and its isotopes.

(2) The energy is in good balance, which was achieved by physical calculation, not artificially adjusting, so the balance is in physics, not only in form.

(3) The double differential cross section was added. There are no such data in all other evaluated libraries, except for FENDL-2. Comparing with FENDL-2, some of them have been improved.

(4) Some cross sections were improved, such as ^{90}Zr total cross section, ^{92}Zr (n,p), ^{96}Zr(n,2n) etc.

References

[1] Zhang Wei, et al.. CNDP, 22, 107(1999)
[2] Liu Janfeng, et al.. CNDP, 22, 10(1999)
[3] Liu Tingjin, et al.. INDC(CPR)-046
[4] Liu Tingjin. CNDP, 13, 81(1994)
[5] Liu Tingjin, (to be published)
[6] Liu Tingjin, et al.. (to be published)

CN0101651

Evaluation and Calculation of Photonuclear Reaction Data for ^{209}Bi below 30 MeV

Yu Baosheng Han Yinlu Zhang Jingshang

(China Nuclear Data Center, CIAE)

Abstract

Based on available experimental data of neutron and photonuclear reaction, both neutron optical potential parameter and giant resonance parameters of gamma for ^{209}Bi were obtained. The photonuclear reaction data for ^{209}Bi were calculated, compared with experimental data and recommended below 30 MeV.

Introduction

Bismuth is a very important structure material in nuclear engineering. The photonuclear cross sections of bismuth up to 30 MeV are very important for radiation induced material damage, radiation safety, reactor dosimetry, etc.. Meanwhile, the study of the properties of photonuclear reactions is a subject of widespread interest. Therefore, the accurate photonuclear data play an important role in nuclear science and technology. In this work, the photonuclear data for ^{209}Bi were evaluated based on evaluated experimental and theoretically calculated data and compared with existing measured data.

1 Evaluation and Analysis of Experimental Data

The ^{209}Bi is existing only in natural bismuth element and its abundance is 100.0 %. At present work, the photonuclear data up to γ-ray energy of 30 MeV were evaluated as follows: the cross sections of ^{209}Bi(γ, abs), ^{209}Bi(γ,n)+(γ,n+p), ^{209}Bi(γ,2n)+(γ,2n+p), ^{209}Bi (γ,3n), (γ, n+p), (γ, n+α), (γ, p), (γ, d), (γ, t), (γ, 3He), (γ, α) ... , emission particle spectra for (γ,2n), (γ, 3n), (γ, n+p), (γ, n+α) , (γ, n'continue) and angular distributions of outgoing particles.

The various available measured data of photonuclear reaction for ^{209}Bi were collected and analyzed. They were retrieved from EXFOR master files of International Atomic Energy Agency, and supplemented with new information. There are 7 sets of measured photonuclear reaction data from 4 laboratories [1-4] in the energy region from threshold to 26.4 MeV as shows in Table 1.

The photoabsorption cross section of ^{209}Bi was measured by G.M.Gurevch[4] in the energy region from 8.5 to 30.2 MeV. The photonuclear cross sections of ^{209}Bi(γ, n)+(γ, n+p) , (γ, 2n)+(γ, 2n+p), (γ, n)+(γ,n+p) +(γ,2n)+(γ, 3n) and (γ, n)+(γ,n+p) +2(γ,2n)+2(γ, 3n) reactions were measured by R.R.Harvey[1] in gamma energy region from 8.0 to 26.4 MeV, in 1964. The photoneutron cross sections were measured by S.N.Belyaev[3] and L.M.Young[2] in energy region from 7.6 to 12.3 and 7.5 to 14.8 MeV, respectively.

Table 1 Collected Data of Photonuclear Reactions for ^{209}Bi

Year	Author	E_γ/ MeV	Sample	Detector*	Reactions
1964	R.R.Harvey	8.0 to 26.4	Natrual ^{209}Bi	PROPC	(γ, n) + (γ, n+p)
1964	R.R.Harvey	8.0 to 26.4	Natrual ^{209}Bi	PROPC	(γ, 2n) + (γ, 2n+p)
1964	R.R.Harvey	8.0 to 26.4	Natrual ^{209}Bi	PROPC	(γ, n) + (γ, n+p)+ (γ, 2n)+(γ, 3n)
1964	R.R.Harvey	8.0 to 26.4	Natrual ^{209}Bi	PROPC	(γ, n) + (γ, n+p)+ 2(γ, 2n)+ 2(γ, 3n)
1972	L.M.Young	7.5 to 14.8	Natrual ^{209}Bi	SCIN	(γ, n) + (γ, n+p)
1976	G.M.Gurevich	8.5 to 30.2	Natrual ^{209}Bi	SCIN	(γ, abs)
1985	S.N.Belyaev	7.6 to 12.3		BF_3	(γ, n)
1989	J.B.Martins	60.0 to 64.0	Natrual ^{209}Bi	TDR	(γ, abs)

* PROPC : Paraffin moderator with BF_3 counters.
SCIN : Liquid Scintillator Detector.
TRD : Makrofol Fission-Track Detector.
STANK : Gd - loaded liquid scintillator tank.

The photonuclear cross section measurements were firstly performed by R.R.Harvey[1] in gamma energy region of 8.0 to 26.4 MeV in 1964. In order to get accurate photon flux, a xenon-filled transmission ionization chamber, located between the photon collimator and sample, was used. The collimated photon beam energy were determined by using NaI γ-ray spectrometer, located after neutron detector system. The attenuation of photon flux in the sample was taken into account and the necessary corrections were made. The neutron emitted by the sample were detected using 4π paraffin moderator neutron detector consisting of 24 BF_3 proportional counters. The structures of photonuclear cross section corresponding to (γ, n)+ (γ,n+p), (γ, 2n)+ (γ, 2n+p) reactions can be observed in the measured data.

The measured results by L.M.Young[2] and S.N.Belyaev[3] for the (γ, n)+ (γ, n+p) reactions were compared with ones of R.R.harvey[1] . There is no large difference, only the giant resonance peak around 13 MeV given by L.M.Young[2] is higher slightly than R.R.Harvey[1]. Taking into account of the fact that the error given by S.N.Belyaev[3] is only the statistical one, when the systematically error was added, the data measured by S.N.Belyaev[3] be in very good agreement with the data of R.R.Harvey[1] within error bar. The comparison of cross sections for ^{209}Bi(γ,n)+ (γ,n+p) reactions is shown in Fig. 1. For ^{209}Bi(γ, 2n)+ (γ,2n+p) reactions, the data measured by R.R.Harvey[1] are shown in Fig.2.

The photoabsorption cross section was measured by G.M.Gurevich[4]. The data

were compared with R.R.Harvey[1]. The photoabsorption cross section is the sum of (γ, n), (γ, n+p), (γ, 2n), (γ, 2n+p), (γ, 3n), (γ, x) cross sections. Because the (γ, 2n+p) reaction is much smaller than the (γ,2n), the main contribution of photoabsorption cross section comes from (γ,n)+(γ,n+p)+(γ,2n)+(γ,x) as measured by Harvey[1]. The data measured by G.M.Gurevich[4] as excellent reference for photoaborption cross section below 28 MeV are shown in Fig. 3.

The measured data corresponding to sum of photonuclear (γ,n)+(γ, n+p)+(γ,2n) +(γ,3n)+(γ,x) cross sections by R.R.Harvey[1] and the (γ,abs) data by G.M.Gurevich[4] are in agreement with each other within error. The (γ, n)+(γ, n+p), (γ, 2n)+ (γ, 2n+p) cross section can be used to guide adjusting model parameters. These experimental data were shown in Fig. 4.

2 Theoretical Calculation and Recommendation

The theoretical calculation was used to fit the evaluated experimental data[1,2]. The spherical optical model, the semi-classical theory of multi-step nuclear reaction processes were used in our calculation.

In order to calculate the photonuclear data, the best neutron optical potential parameters can be searched automatically by using the code APOM[5]. Based on the fitted experimental data, including total cross section, nonelastic scattering and elastic scattering cross section and their angular distributions of n+ ^{209}Bi nuclear reactions, a set of optimum neutron potential parameters were obtained. The potential parameters for particle p, α, ^{3}He, d and t were taken from concerned references[6]. The optimum neutron optical potential parameters obtained for ^{209}Bi are as follows:

V=56.300-0.320E-24$(N-Z)/A$

W_s=max{0.0, 13.00-0.250E-12$(N-Z)/A$}

W_v=max{0.0, -1.56+0.22E}

U_{so}=6.2

R_r=1.170, r_s=1.260, r_v=1.260, r_{so}=1.170

a_r=0.750, a_s=0.580, a_v=0.580, a_{so}=0.750

Using the code DREAM, a set of discrete level, pair correction parameter, level density parameters and giant resonance parameters as well as concerned ground state mass and J^{π} used in the calculation was created from Chinese Evaluated Nuclear Parameter Library (CENPL).

The total photoneutron cross section (γ,n) was obtained by summing the cross sections excited to the ground state, excited and continuum states. The continuum state Q-value was assumed at 8.844 MeV for ^{209}Bi.

The giant resonance parameters of gamma were adjusted automatically with the code GUNF[7] by fitting the experimental cross sections of ^{209}Bi(γ,n+np), ^{209}Bi (γ,2n+(2n+p)) and ^{209}Bi (γ, n+np+2(2n+3n)) as well as ^{209}Bi (γ, abs) reactions. The giant resonance parameter obtained is given in Table 2.

Table 2 The giant resonance parameters of gamma for ^{209}Bi

σ_1^{E1} / b	0.523601	σ^{E2} / b	2.046550
Γ_1^{E1} / MeV	3.772378	Γ^{E2} / MeV	2.213692
Γ_1^{E1} / MeV	13.783440	Γ^{E2} / MeV	11.564862

The cross sections of photonuclear reactions were calculated from threshold to 30 MeV. The theoretically calculated values are in agreement with that shown in Figs. 1~4. Since the calculated data for many photonuclear reactions channels are in pretty agreement with existing experimental data, the predicted cross sections, for which there are no experimental data, are reasonable.

For ^{209}Bi(γ, x) reactions, there are no experimental data. Therefore, the cross sections of emitting charged particles (γ,p), (γ,d), (γ,t), (γ,^{3}He), (γ,α) reactions must be calculated theoretically.

The pertinent calculations were performed by using GUNF Code. The recommended cross sections for ^{209}Bi reactions from threshold to 30 MeV are given and shown in Fig. 5.

The experimental data of photonuclear emission particle spectra for ^{209}Bi are very scarce. The data were obtained from the model calculations based on the available experimental data, such as (γ,n), (γ,2n), (γ,2n+p) ...

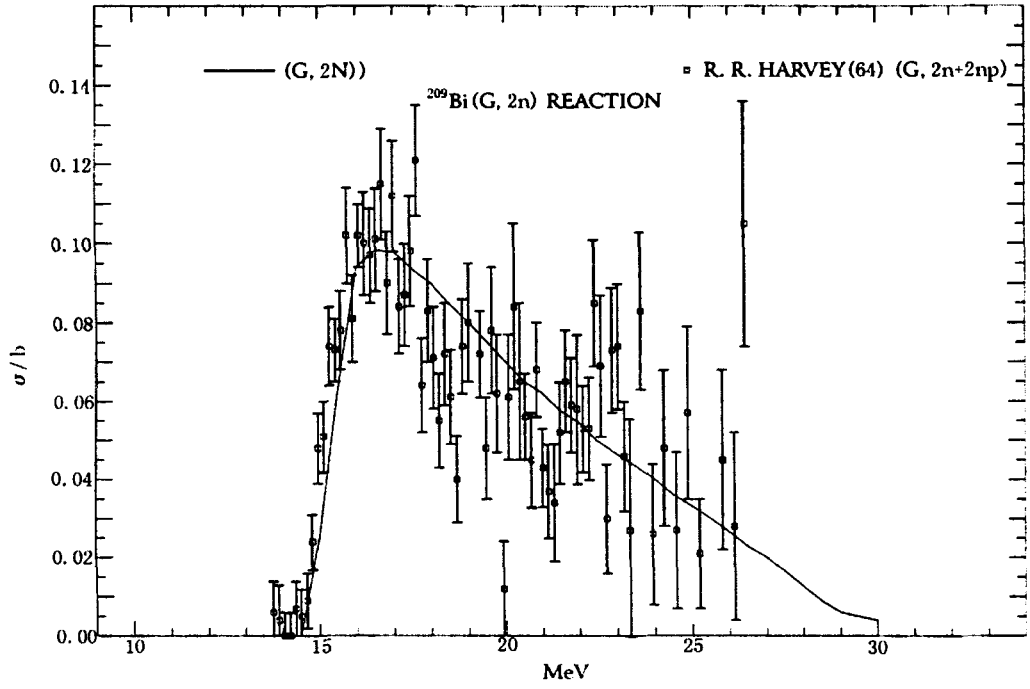

Fig. 1 comparison of evaluated and measurement for (γ,2n) reaction

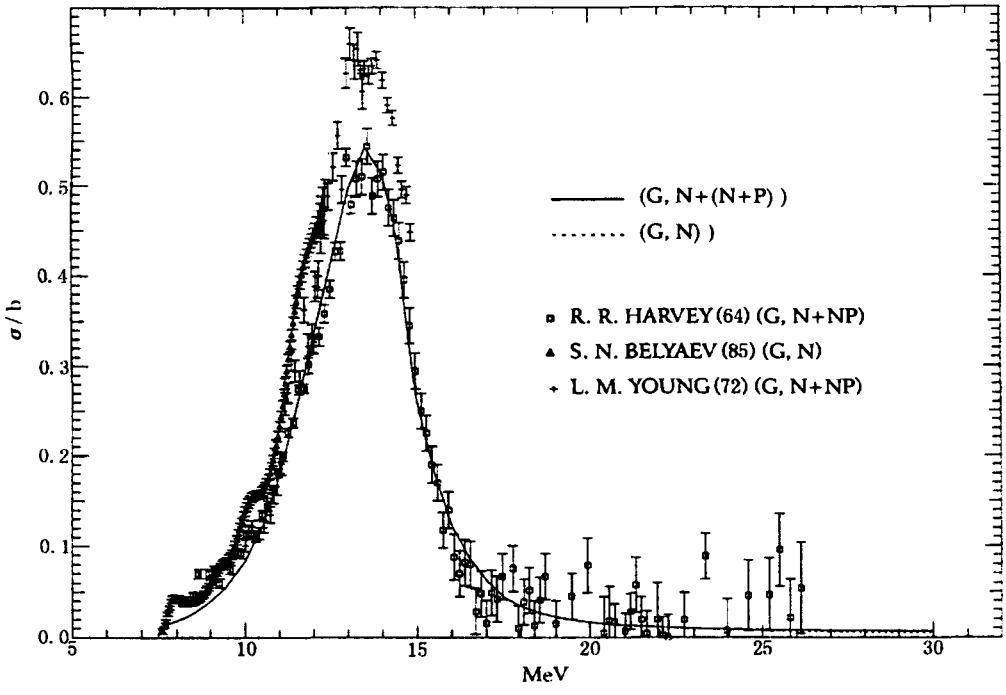

Fig. 2 comparison of evaluated and measurement for (γ,n+(n+p)) reaction

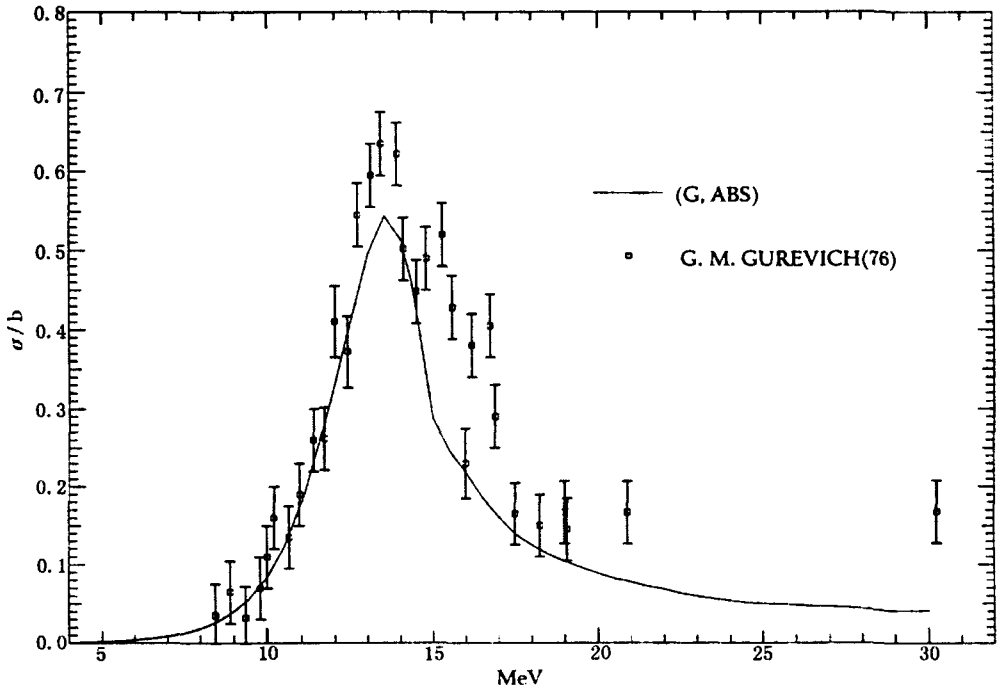

Fig. 3 comparison of evaluated and measurement for (γ,abs) reaction

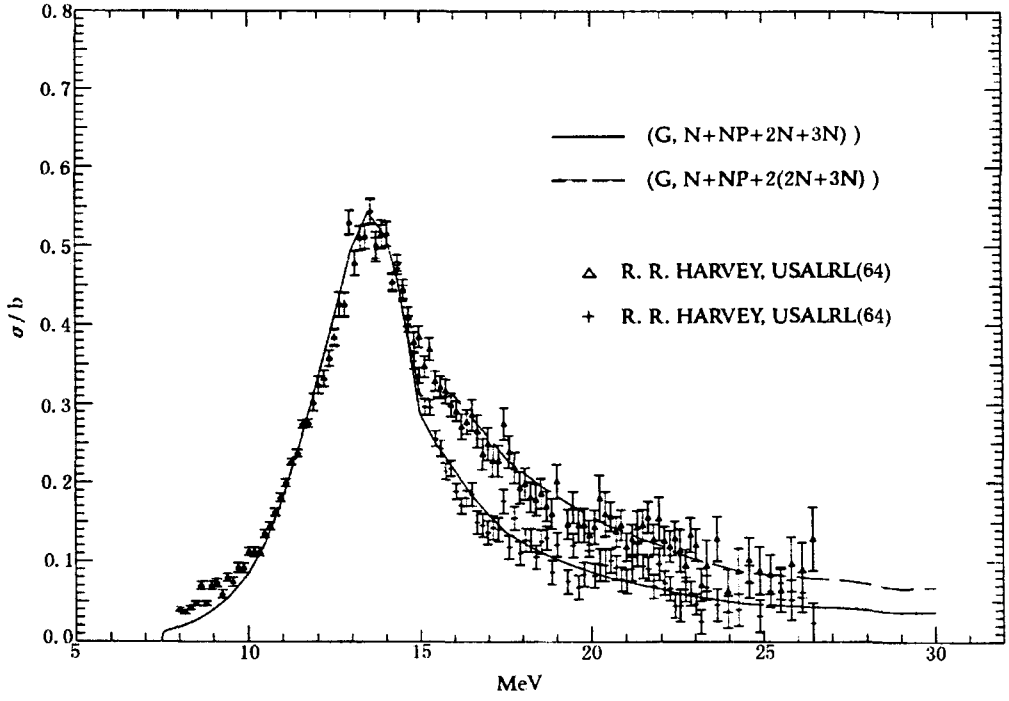

Fig. 4 comparison of evaluated and measurement for (γ,n+np+2n+3n) reaction

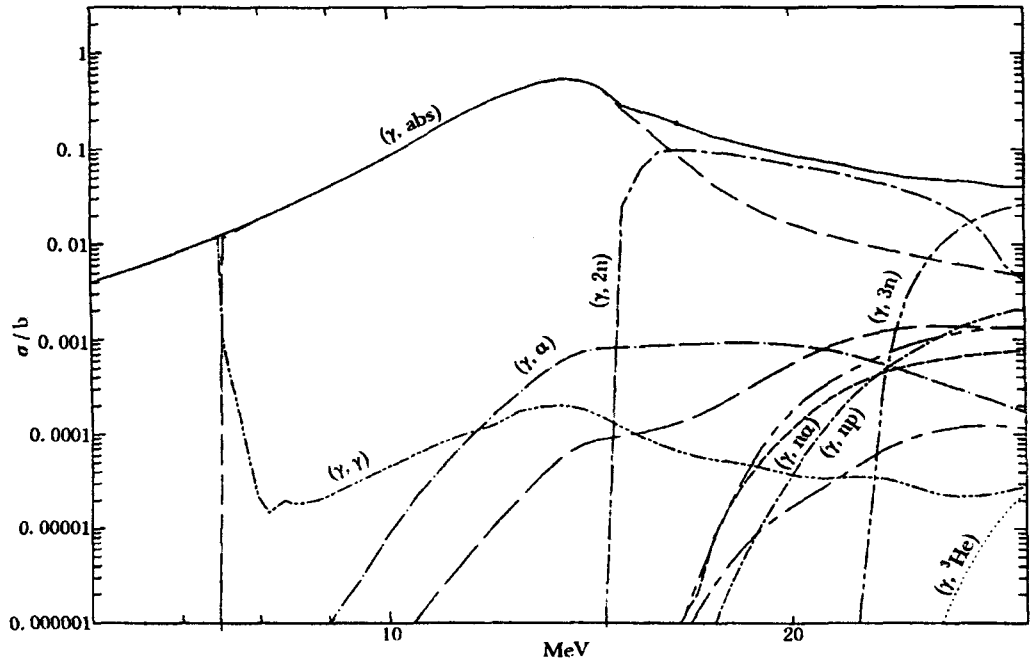

Fig. 5 Recommended data for ^{209}Bi

3 File Description for Recommended data

The photonuclear data for ^{209}Bi were recommended in ENDF/B-6 format.

The check of evaluated data was carried out by using ENDF utility codes and some codes developed at CNDC, which includes format, consistency between the total and the sum of partial cross sections, physics parameter and energy balance between incident γ and emitted particles.

The final recommended data are as follows:

MF	MT	Quantity
1	451	Compre hensive description and Dictionary
3	3	Photoabsorption cross section
3	4	Photoneutron cross section for (γ, n) reaction
3	16	Photonuclear cross section for (γ, 2n) reaction
3	17	Photonuclear cross section for (γ, 3n) reaction
3	50, 51,..., 66,...and 91	Photoneutron cross section to ground excited and continuum state.

3	102, ... ,107, 111	Photoneutron cross section for (γ,γ), (γ,p), (γ,d), (γ,t), (γ, ^{3}He), (γ,α) and (γ, 2p) reactions.
6	16,17,22,28,91	Double differential cross sections for (γ, 2n), (γ, 3n), (γ, n+α), (γ,n+p) and ($\gamma,n_{continuum}$) reactions

Summary

The data of photonuclear reactions for ^{209}Bi were evaluated. The characteristics of the data are as follows:

1) The data could reproduce experimental data very well.

2) Since the calculated results for many channels are in pretty agreement with available experimental data, the predicted photonuclear reaction data, for which there are no experimental data, are reasonable.

3) The photonuclear reaction data have been widely used in basic scientific researches on nuclear reaction mechanism etc.., so the recommended data are useful from the point of view of nuclear physics research.

Acknowledgments

The authors are indebted to IAEA (International Atomic Energy Agency), CNNC (China National Nuclear Corporation) and CIAE for their supports, and thanks to Drs. P. Oblozinsky, T.Benson and O.Schwerer for their kind help and suggestions

References

[1] R.R.Harvey et al., Phys. Rew./B,136,126(1964)

[2] L.M.Young et al., EXFOR DATA L005905 (1972)

[3] S.N.Belyaev et al., J. YF,42,1050(1985)

[4] G.M.Gurevich et al., J.ZEP,23,411(1976)

[5] Shen Qingbiao, CNDP, 7,43(1992).

[6] C.M. Perey, F.G. Perey, Atom. Data and Nucl. Data Tables, 17, 1(1976).

[7] Zhang Jingshang et al., INDC(CPR)-44/L,N0.19,p33(1998)

Evaluation of Complete Neutron Nuclear Data for ^{Nat}Cu

Ma Gonggui Luo Xiaobing
(Institute of Nuclear Science and Technology, Sichuan University, Chengdu, 610064)

Abstract

The neutron data are evaluated for ^{Nat}Cu in the energy range from 10^{-5} eV to 20.0 MeV. The evaluated neutron nuclear data include total, elastic, noelastic, total inelastic, inelastic cross sections to 29 discrete levels, inelastic continuum, (n,2n), (n,3n), (n,n'α)+(n,αn'), (n,n'p)+(n,pn'), (n,p), (n,d), (n,t), (n,^{3}He), (n,α),(n,2p) and capture cross sections. The angular distributions of secondary neutron, the double differential cross sections(DDCS), the gamma-ray production data and the resonance parameters are also included. The evaluated data are for CENDL-3 in ENDF/B-6 format.

Introduction

Copper is a very important structure material in nuclear fusion engineering. A complete neutron nuclear data were evaluated based on both experimental data measured up to 1998 and theoretical calculated data with program NUNF[1]. The evaluated data are for CENDL-3 in ENDF/B-6 format [MAT=3290] and will be utilized in the various fields of nuclear engineering.

For natural copper, the evaluated data of all reaction channels are in very good agreement with sum of the isotopic data weighted by the abundance within the error range.

The level scheme is given in Table 1, selected from Ref. [2]. The binding energy of emitted final particle are given in Table 2.

Table 1. Inelastic discrete levels and isotopes abundance

	E_1 / MeV	J^π	E_1 / MeV	J^π	E_1 / MeV	J^π	E_1 / MeV	J^π
^{63}Cu	0.0	3/2⁻	1.5470	3/2⁻	2.0926	7/2⁻	2.4972	3/2⁻
(69.17%)	0.6697	1/2⁻	1.8612	7/2⁻	2.2079	9/2⁻	2.5064	9/2⁺
	0.9621	5/2⁻	2.0112	3/2⁻	2.3366	5/2⁻	2.5120	1/2⁻
	1.3270	7/2⁻	2.0622	1/2⁻	2.3380	3/2⁻		
	1.4120	5/2⁻	2.0814	5/2⁻	2.4048	7/2⁺		
^{65}Cu	0.0	3/2-	1.6234	5/2-	2.2128	1/2-	2.5257	9/2⁺
(30.83%)	0.7706	1/2-	1.7250	3/2-	2.2785	7/2-		
	1.1156	5/2-	2.0943	7/2-	2.3290	3/2-		
	1.4818	7/2-	2.1074	5/2-	2.4066	9/2-		

Table 2. Binding energy of emitted final particle (MeV)

reaction	1)	n,γ	n,n`	n,p	n,α	n, ^{3}He	n,d	n,t
channels	2)	n,2n	n,n`p	n,n`α	n,pn`	n,2p	n,αn`	n,3n
^{63}Cu	1)	0.0	7.9161	7.1996	6.2011	17.444	11.816	16.1551
	2)	10.8542	6.1246	5.7766	6.8411	11.275	7.4915	8.89416
^{65}Cu	1)	0.0	7.0666	8.4155	7.1496	19.320	12.286	15.6887
	2)	9.90466	7.4447	6.7704	6.0959	12.313	6.6874	7.91609

1 Resonance Parameter

The resolved resonance parameters were taken from ENDF/B-6 in the energy region from 10^{-5} eV to 99.5 keV. Thermal cross sections are 12.16 b, 8.4 b and 3.75 b for (n, tot), (n, n) and (n,γ) reactions respectively.

2 Neutron Cross Section

The comparison of experimental data with evaluated ones is shown in Fig. 1~14. It can be seen that the present evaluation is in agreement with the experimental data.

2.1 Total Cross Section

Above the resolved resonance region, there are still some structures in the energy range 99.5 keV~4.0 MeV and the data become smooth in the energy range (4~20 MeV). In the energy range from 99.5 keV to 1.12 MeV, the data were mainly taken from Pandey's experimental data[3], and in the energy range from 1.12 to 4.0 MeV, the data taken from Perey's data[4]. In the smooth energy range from 4.0 to 20.0 MeV, they were obtained from Larson's experimental data[5] (see Fig. 1).

2.2 Elastic Scattering Cross Section

Above the resolved resonance region, the elastic scattering cross section was obtained by subtracting the nonelastic cross sections from the total cross section. In general, the obtained data are in agreement with the available experimental data of El-Kadi, Kinney, Smith and Holmqvist[6-9] (Fig. 2).

2.3 Nonelastic Scattering Cross Section

There are many experimental data from threshold to 20.0 MeV[10-20] measured with spherical shell and anti-spherical method. The experimental data were fitted and used as recommended data (Fig. 3).

2.4 Total Inelastic Cross Section

The recommended total inelastic scattering cross section was obtained by subtracting sum of the other nonelastic reaction cross sections from the evaluated nonelastic cross section, and are in very good agreement with ENDF/B-6 and JENDL-3. The comparison between the evaluations and measured data of Guenther, Fujita, Salnikov, Prokopec, Glazkov and Thomson[21-26] is shown in Fig. 4.

2.5 Inelastic Cross Section to the Discrete Levels and the Continuum state

The discrete inelastic scattering cross sections are given for 17 levels of ^{63}Cu and 12 levels of ^{65}Cu. There are many experimental data[7,9,21,27,28,29] for lower 4 levels (0.6697, 0.7706, 0.9621 and 1.1156 MeV) and they are in agreement with the calculated results as illustrated in Fig. 5-1 and 5-2.

The calculated results were taken as the recommended ones. In order to keep the consistence with the total inelastic scattering cross section obtained above, the discrete inelastic scattering cross sections were somewhat adjusted in the energy region below the threshold of the continuum inelastic scattering cross section.

The continuum part was obtained by subtracting the cross section of inelastic scattering to discrete levels from the total inelastic.

2.6 (n,2n) and (n,3n) Cross Sections

For (n,2n) reaction, the data were measured by Frehaut, Salnikov, Mather, Ashby[30-33] in the energy range from threshold to 14.76 MeV. Below 14.5 MeV, the evaluated data were obtained by fitting experimental data with spline function. Above 14.5 MeV, calculated data were normalized to the fitt value 660.5 mb at 14.5 MeV (see Fig. 6).

The (n,3n) cross section was taken from the model calculation due to lack of the experimental data.

2.7 (n,p) and (n,n'p)+(n,pn') Cross Sections

Only one set of data was measured by Colli[34] for these reactions. The theoretical calculated data were normalized to these measured data 46 mb and 181 mb at 14.1 MeV respectively (see Fig. 7~8), and taken as recommended ones.

2.8 (n,α) and (n,n'α+n,αn') Cross Sections

For (n,α) and (n,n'α) + (n,αn') reactions, there are no experimental data. The cross sections of ^{Nat}Cu were obtained from summing the isotopic data taken the abundance as weight (see Fig. 9~10).

2.9 (n,d) Cross Section

The experimental data by Grimes[35] at 14.8 MeV energy point was used to normalize the model calculated results (see Fig. 11).

2.10 Capture Cross Section

From the upper limit of resonance region to 3 MeV, the data were obtained by spline function fitting experimental data, measured by Voignier, Diven, Stavisskij[36~38]. Above 3.0 MeV, the calculated data were normalized to Voignier's[36] experimental datum at 3.0 MeV energy point (see Fig. 12).

3 Secondary Neutron Angular Distributions

The elastic scattering angular distributions were calculated with NUNF code, given in terms of Legendre coefficients in the c.m. system. The experimental data at 12 energy points by Galloway, Tsukada, Bucher, Gorlov[39-42], Guenther[21], Li, Anderson and Coon[43-45] were used to adjust the parameters of the optical model. The calculated results are in good agreement with these data (see Fig. 13-1 and 13-2).

The discrete inelastic angular distributions (MT=51~79) were obtained from theoretical calculation results. The angular distributions for (n,2n), (n,3n), (n,n'α), (n,n'p) and continuum inelastic ($MT=16,17,22,28,91$) were assumed to be isotropic.

4 The Double Differential Cross Section and γ-Ray Production Data

The double differential emission cross section (emission n, p, d, t, ^{3}He, α) (MF=6, MT=16, 17, 22, 28, 91, 103, 104, 105, 106, 107, 111) and γ-ray production data (MF=12, 13, 14, 15) were taken from the calculation results. An example is given in Fig. 14.

5 Theoretical Calculation

An automatically adjusting optical potential code(APOM)[46] was used for automatically searching a set of optimum neutron optical potential parameters. NUNF code was used to calculate the complete data (files 3, 4, 6, 12~15) in the energy region from 1.0 keV to 20MeV, for which the required input parameters are: optical model parameters, level density, giant dipole resonance parameters [47] and nuclear level scheme. These parameters were adjusted on the basis of experimental data.

5.1 Optical Model and Level Density Parameters

The optical potential, level density and pair correction parameters used in the calculation are given in Tables 3 and 4.

Table 3 Optical model parameters*

	Depth / MeV		Radius / fm	Diffuseness / fm
	V_0=55.563	W_0=16.076	X_r=1.1856	A_r=0.7457
	V_1=-0.4573	W_1=-0.3529	X_s=1.413	A_s=0.2569
Neutron	V_2=-0.00179	W_2=-35.467	X_v=1.413	A_v=0.2569
	V_3=-27.0387	U_0=-0.8459	X_{so}=1.1856	A_{so}=0.7457
	V_4=0.0	U_1=0.2384	X_c=1.0	
	V_{so}=3.41	U_2=0.0		

* Note: $V_r(E)=V_0+V_1E+V_2E(2)+V_3(A-2Z)/A+V_4Z/A(1/3)$;
$W_s(E)=W_0+W_1E+W_2(A-2Z)/A$;
$U_v(E)=U_0+U_1E+U_2E(2)$.

Table 4 Level density parameters and Pair correction values of 11 residual nuclei*

		n,γ	n,n'	n,p	n,α	n, ^{3}He	n,d	n,t	n,2n	n,n'α	n,2p	n,3n
^{63}Cu	*L*	7.76	7.16	7.45	7.75	8.20	7.34	7.86	6.73	7.20	8.80	6.18
	P	-0.18	1.3	2.5	-0.25	1.2	2.5	1.25	-0.15	1.22	-0.28	1.32
^{65}Cu	*L*	8.47	8.06	8.36	8.80	9.11	8.23	7.94	7.76	8.20	9.54	7.16
	P	-0.1	1.5	1.4	-0.3	1.4	2.7	1.02	-0.2	1.2	-0.2	1.3

* Note: $L=[0.00880(s(z)+s(n))+Q_b]A$; $P=p(n)+P(z)$;
Q_b=0.142 or 0.12(spherical or deformation).

5.2 Giant Dipole Resonances

The giant dipole resonance parameters used in the calculation are given in Table 5. The symbols CSG, EE and GG refer to the peak cross section, resonance energy and full width at half maximum, respectively.

Table 5 The 11 giant dipole resonance parameters(single peak)

^{63}Cu	CSG / b	0.075,0.075,0.034,0.026,0.026,0.034,0.034,0.075,0.026,0.026,0.075
	EE / MeV	16.7,16.7,16.3,16.37,16.37,16.3,16.3,16.7,16.37,16.37,16.7
	GG / MeV	6.89,6.89,2.44,2.56,2.56,2.44,2.44,6.89,2.56,2.56,6.89
^{65}Cu	CSG / b	0.075,0.075,0.034,0.026,0.026,0.034,0.034,0.075,0.026,0.026,0.075
	EE / MeV	16.7,16.7,16.3,16.37,16.37,16.3,16.3,16.7,16.37,16.37,16.7
	GG / MeV	6.89,6.89,2.44,2.56,2.56,2.44,2.44,6.89,2.56,2.56,6.89

5.3 The Coupled Channel Calculation

The Legendre Coefficients (L. C) of direct elastic scattering to ground state and direct inelastic scattering to excited states were calculated with code DWUCK at 19 energies by Han Yinlu and given in the required input format of NUNF.

6 Concluding Remarks

Due to the new experimental data are available in recent years, the evaluated data have been considerably improved, especially for cross sections of total, (n,2n), (n,p), (n,α), total inelastic reactions and inelastic scattering to some discrete levels.

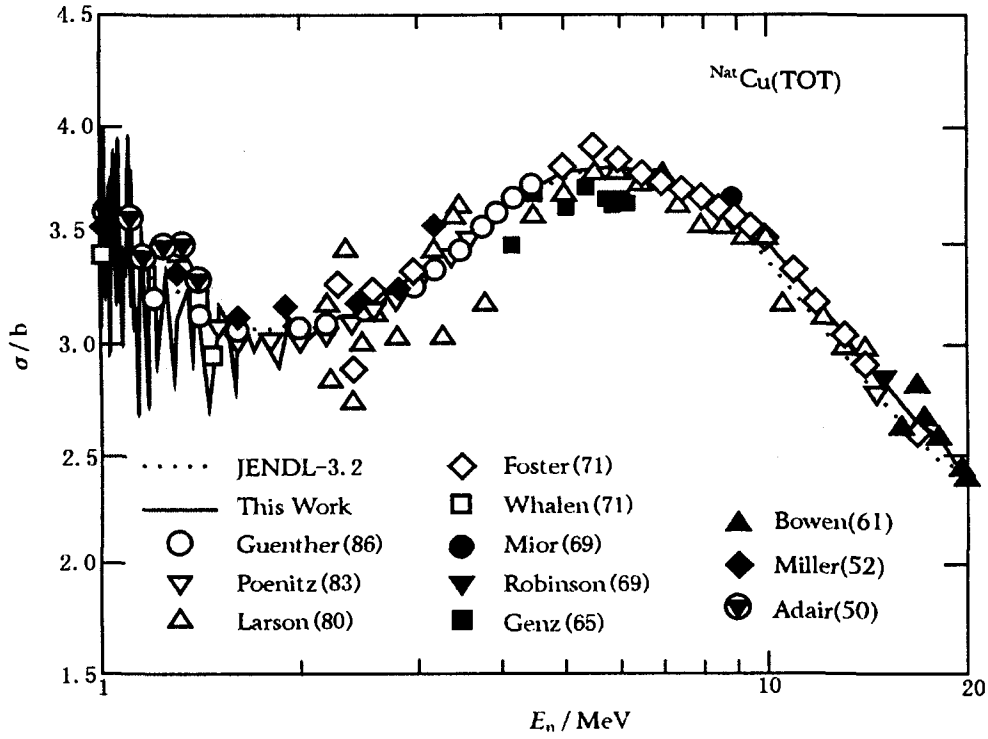

Fig. 1 Total cross section for ^{Nat}Cu

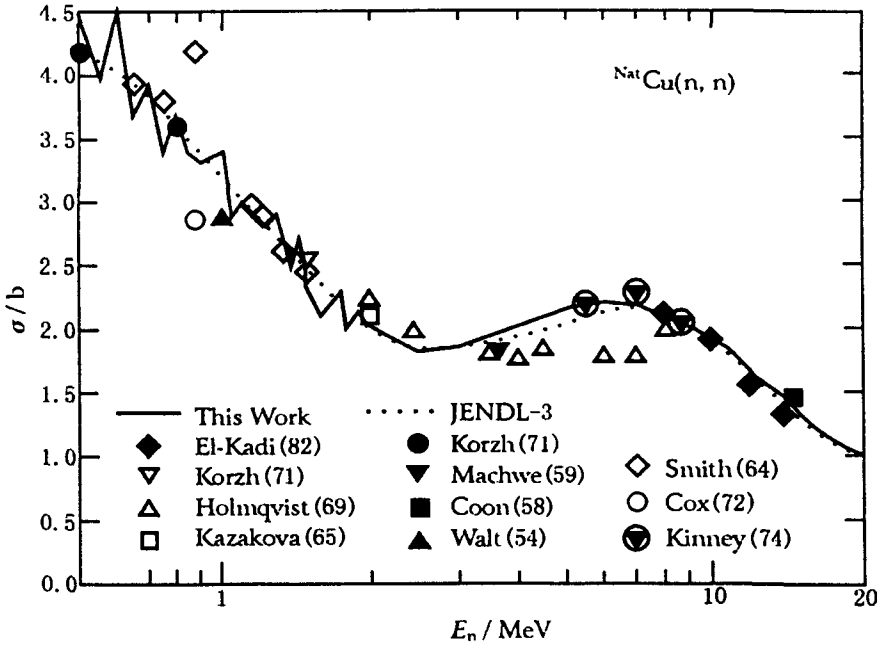

Fig. 2 Elastic cross section for ^{Nat}Cu

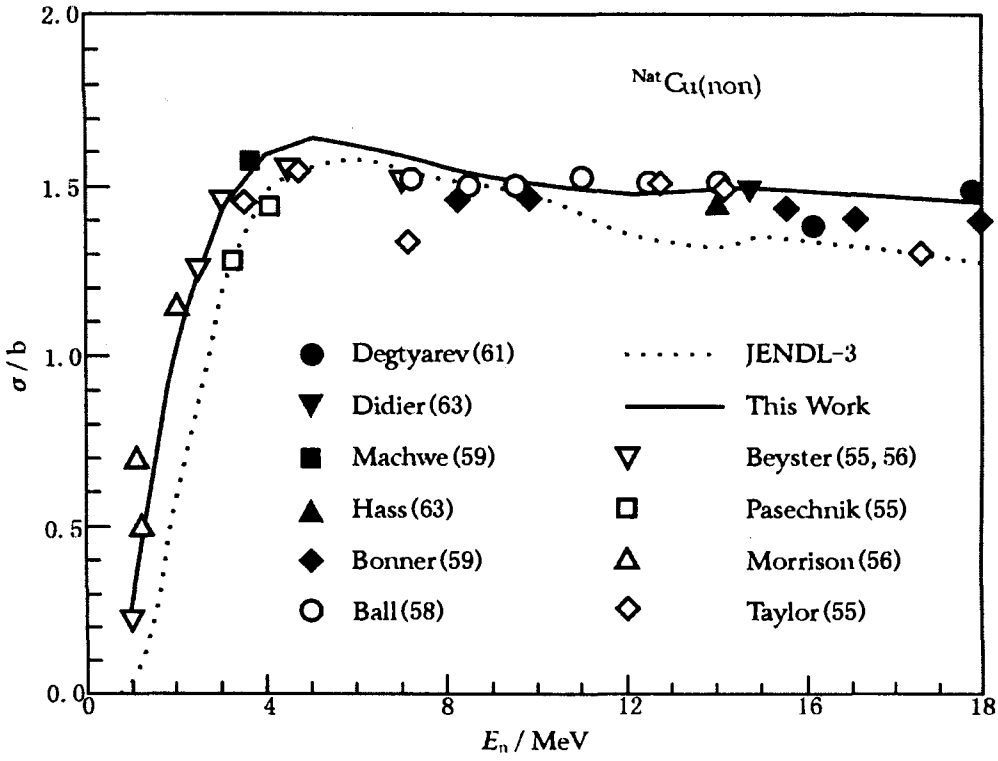

Fig. 3 Nonelastic cross section for ^{Nat}Cu

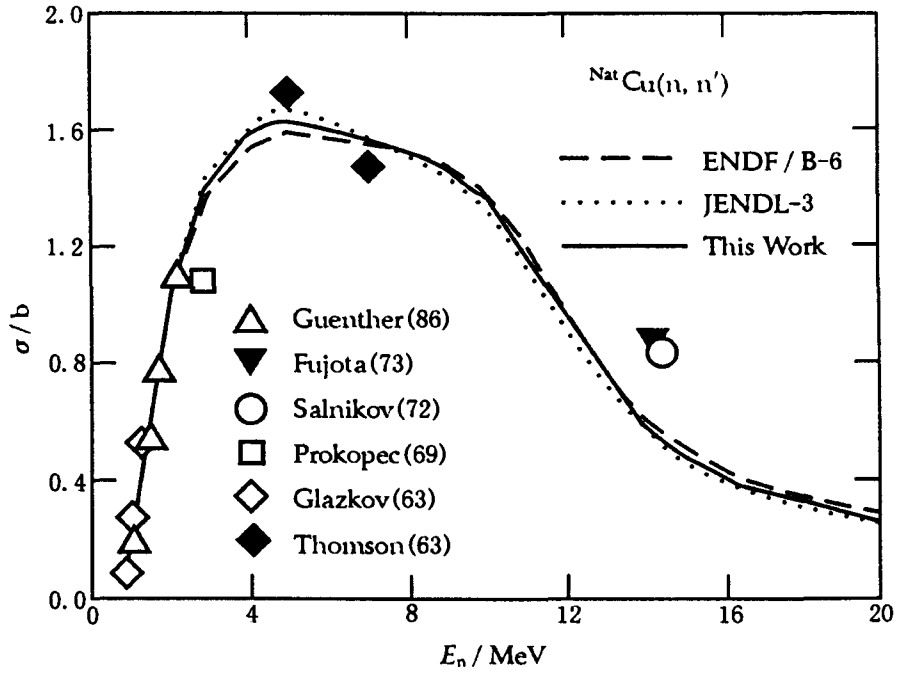

Fig. 4 Inelastic cross section for ^{Nat}Cu

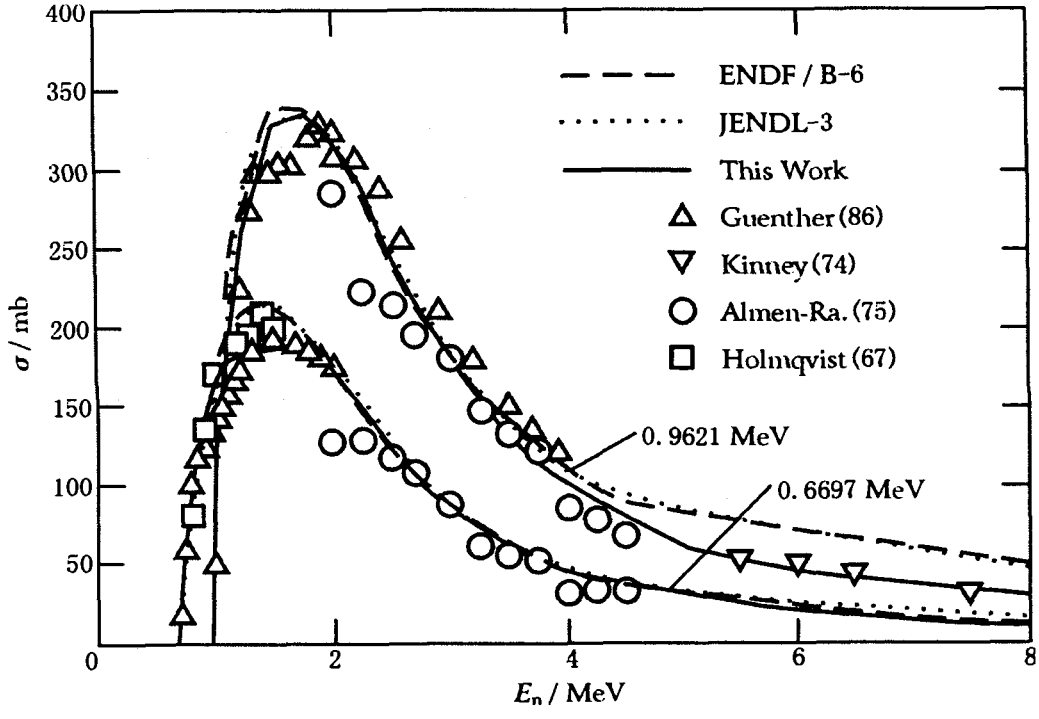

Fig. 5-1 Inelastic cross section of ^{63}Cu excited states

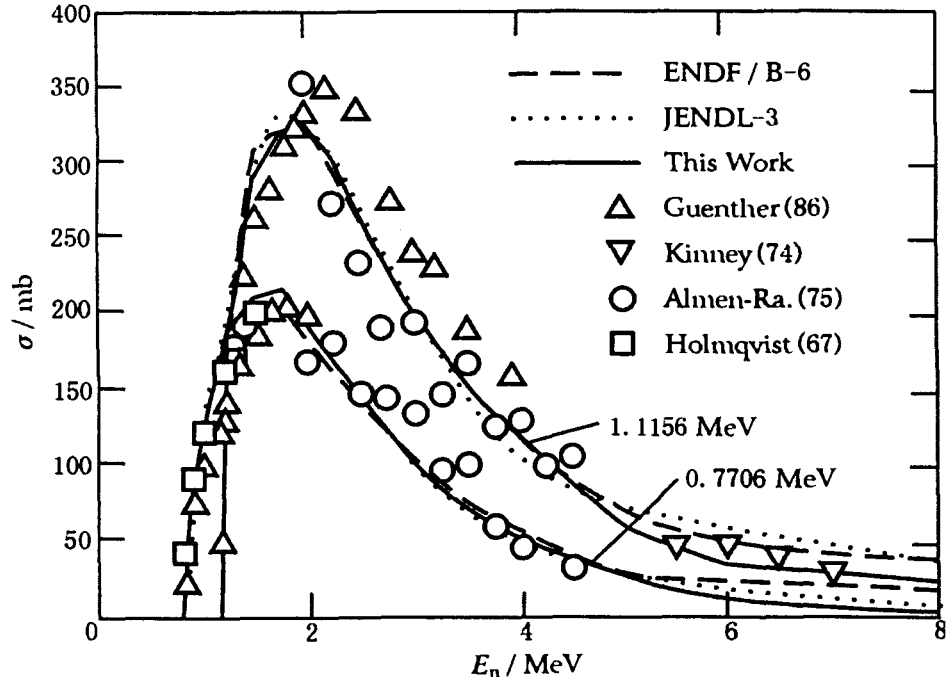

Fig. 5-2 Inelastic cross section of ^{65}Cu excited states

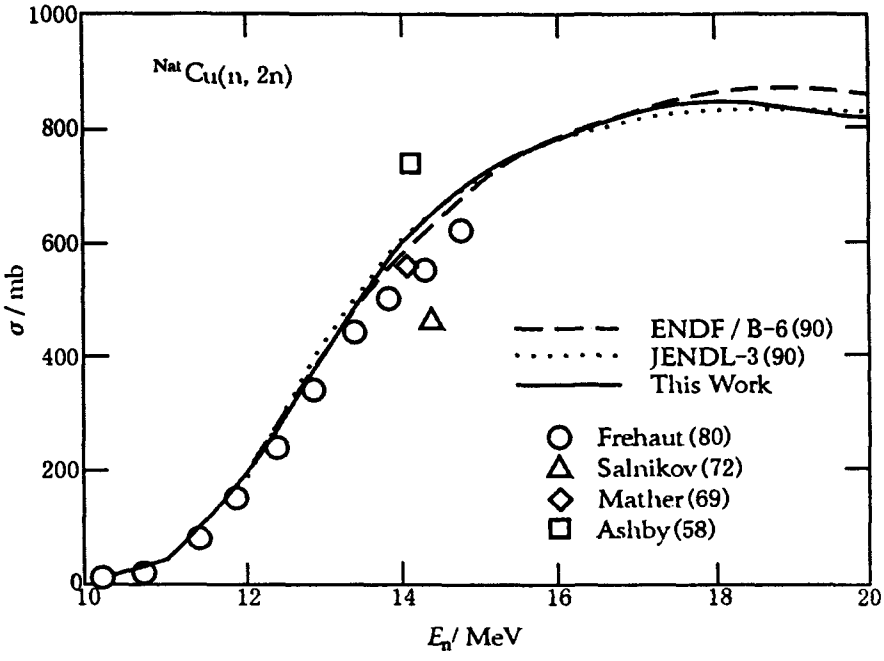

Fig. 6 (n,2n) cross section for ^{Nat}Cu

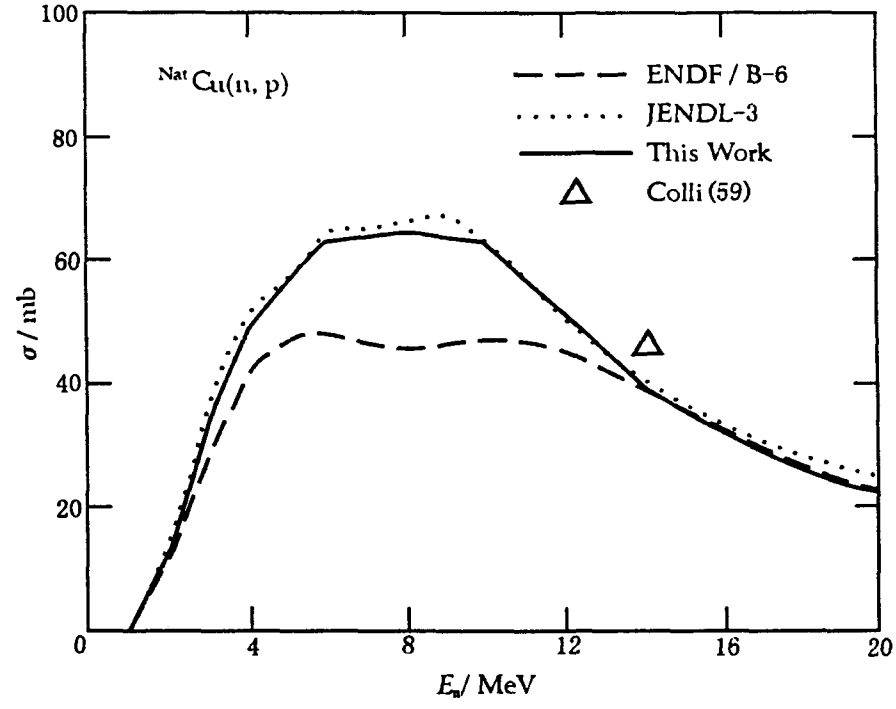

Fig. 7 (n,p) cross section for ^{Nat}Cu

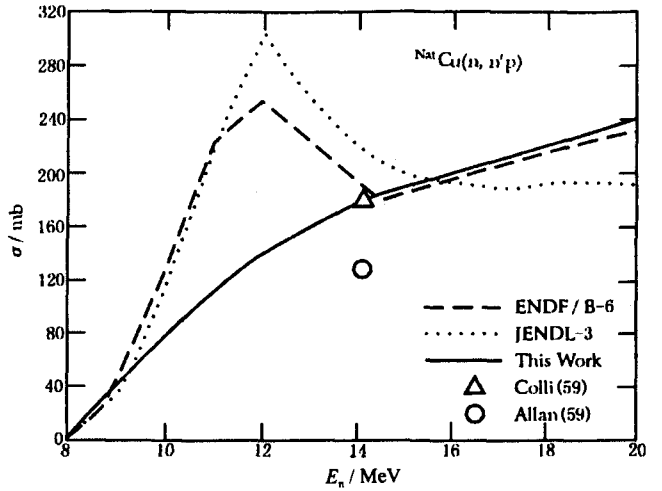

Fig. 8 (n,n'p) cross section for ^{Nat}Cu

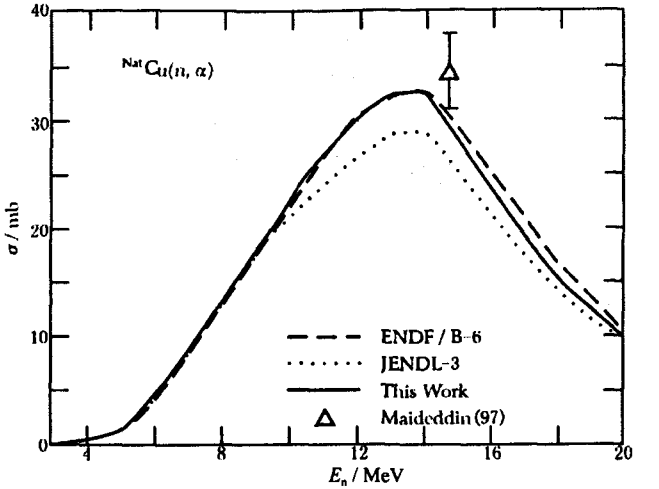

Fig. 9 (n,α) cross section for ^{Nat}Cu

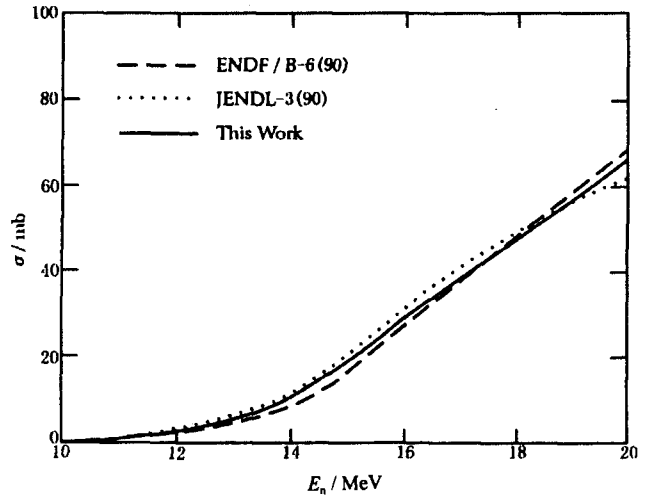

Fig. 10 (n,n'α) cross section for ^{Nat}Cu

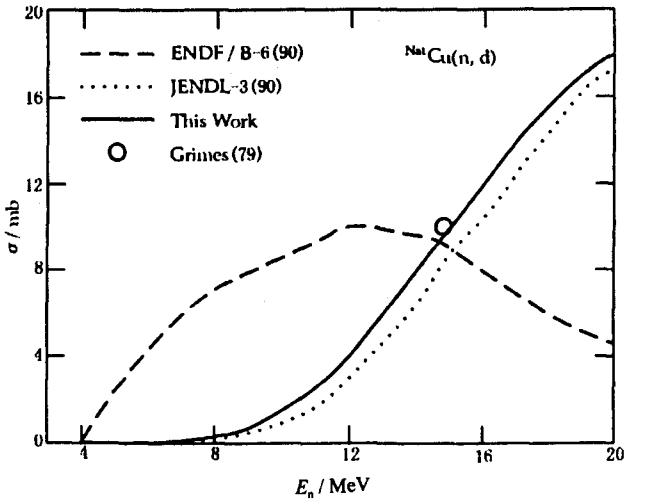

Fig. 11 (n,d) cross section for ^{Nat}Cu

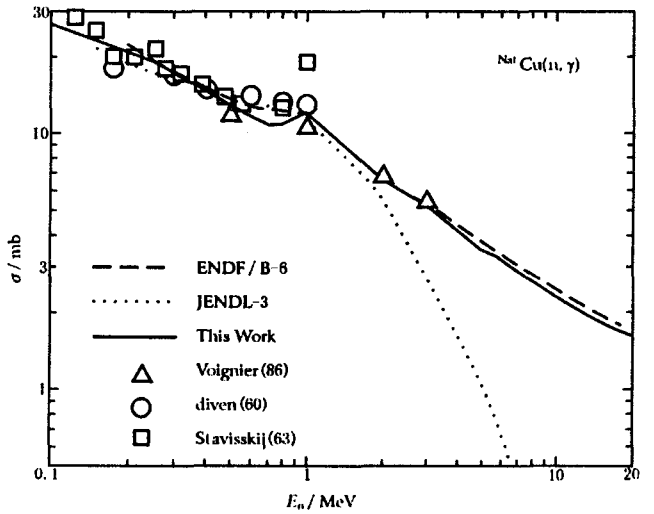

Fig. 12 (n,γ) cross section for ^{Nat}Cu

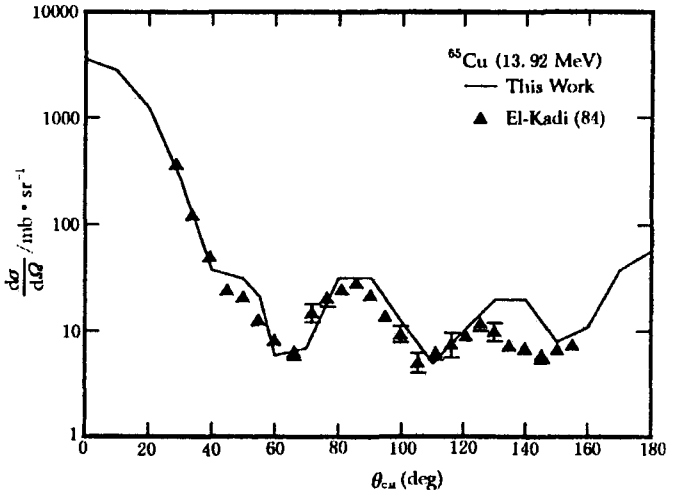

Fig. 13-2 Elastic scattering angular distribution of ^{65}Cu

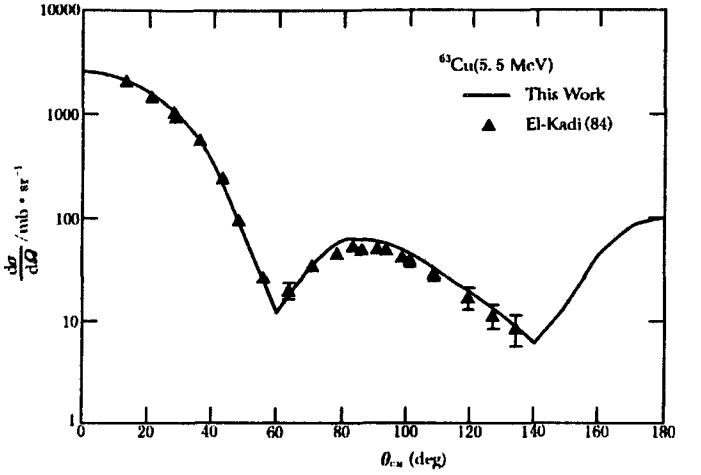

Fig. 13-1 Elastic scattering angular distribution of ^{63}Cu

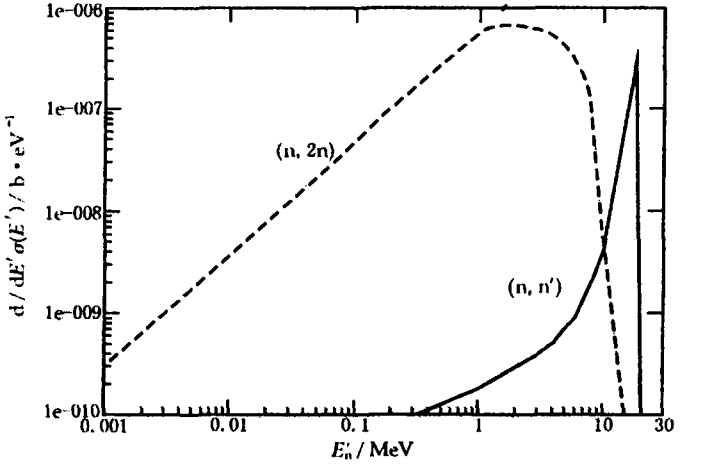

Fig. 14 (n,2n) and (n,n') continuous secondary neutron spectrum for ^{Nat}Cu at 20.0 MeV

Acknowledgments

The author wish to thank Profs. Liu Tingjin and Liang Qichang for their helps with this work, also thank Dr. Han yinlu for his help with the DWUCK code calculation.

References

[1] Zhang Jingshang. Nucl. Sci. Eng., 114; 55-63(1993)

[2] Nuclear Data Sheets, 1993,69:768; 1992,67:283; 1992,67:297; 1991,64:1991,62:626;

[3] M.S.Pandey et al., Private Communication and Phys. Rev., C15,600(1977)

[4] F.G.Perey et al., Private Communication(1977)

[5] D.C.Larson et al.,BNL-NCS-51245,1980;EXFOR-12882.011;80BNL277

[6] Ei-Kadi et al., Nucl. Phys., A390,509(1982)

[7] W.Kinney et al., ORNL-4908(1974)

[8] B.Holmqvist et al., AE-366(1969)

[9] A.B.Smith et al., Phys. Rev., B135,76(1964)

[10] H.L.Taylor et al., Phys. Rev.,100,174(1955)

[11] M.H.Mac Gregor et al., Phys. Rev.,108,726(1957);111,1155(1958)

[12] W.P.Ball et al., Phys. Rev., 110,1392(1958)

[13] Yu.G.Degtyarev et al., Atomic Energy, 11,397(1961)

[14] D.Didier et al., Phys.Rev., 24,805(1963)

[15] M.K.Machwe et al., Phys. Rev., 114,1563(1959)

[16] G.M.Haas et al., Phys.Rev., 132,1211(1963)

[17] T.W.Bonner et al., Phys. Rev., 113,1088(1959)

[18] J.R.Beyster et al., Phys. Rev.,104,1319(1956);98,1216(1955)

[19] M.V.Pasechnik et al., 55GENEVA,2,3(1955)

[20] Morrison et al., PHY,22,1135(1956)

[21] P.Guenther et al., Nucl. Phys., A448,280(1986)

[22] I.Fujita et al., J. of Nucl.Sci. and Tech., 9,301(1973)

[23] Salnikov et al., Yadernye Konstanty, 7,102(1972)

[24] Prokopec et al., UFZ,14(2),330(1969)

[25] H.Glazkov et al., Atomnaja Energija, 15,416(1963)

[26] D.Thomson et al., Phys. Rev., 129,1649(1963)

[27] A.B.Smith et al., Phys. Rev., B135,76(1964)

[28] B.Holmqvist et al., Atomnaya Energiya, 150(1964)

[29] E.Almen-Ramstrom et al., Atomnaya Energiya, 503(1975)

[30] J.Frehaut et al., 80BNL, 399(1980)

[31] Salnikov et al., Yadernye Konstanty, 7,102(1972)

[32] Mather et al., AWRE-O-47/69(1969)

[33] Ashby et al., Phys. Rev., 111,616(1958)

[34] L.Colli et al., Nuovo Cimento, 13,730(1959)

[35] S.M.Grimes et al., Phys. Rev., C19,2127(1979)

[36] J.Voignier et al., Nucl.Sci.Eng., 93,43(1986)

[37] B.C.Diven et al., Phys. Rev., 120,556(1960)

[38] Yu.Ya.Stavisskij et al., Atomnaya Energiya,15(4),323(1963)

[39] R.B.Galloway et al.,Nucl.Phys.,A318,173(1979);A212,182(1973)

[40] K.Tsukada et al.,2nd IAEA Coonf.on Nucl. Data for Reactors, Helsiki, Finland,2, 305 June(1970)

[41] W.Bucher et al., Phys.Lett., B58,277(1975)

[42] G.V.Gorlov et al., Jadernaja Fizika,8(6),1086(1968)

[43] Li Jingde et al., Chinese J.Nucl.Phys., 10,46(1988)

[44] J.D.Anderson et al., Phys. Rev., 115,1010(1959)

[45] J.H.Coon et al., Phys. Rev., 111,250(1958)

[46] Shen Qingbiao, et al., CNDP, 7,43(1993)

[47] Zhuang Youxiang, et al., Chinese Physics, 8, 721-727(1988)

The Evaluation of some Reference Fission Yield Data from ^{235}U Fission

Liu Tingjin , Liang Qichang
(China Nuclear Data Center, CIAE)

Introduction

The fission yield data used as standards in the fission yield data measurement and evaluation, or as monitor in the nuclear industry for decay heat estimation, burn-up credit study etc., are refered to the reference yield. Among them, the data of ^{235}U fission, especially at thermal energy, are most important ones.

The error of relatively measured fission yield data directly depend on the accuracy of the standard data used. The same situation is for the data calculated from measured ratio, R-value. Also the calculation credit of, like, decay heat and burn-up etc. depends on the monitor fission yield data accuracy.

At present work, the reference data for 19 product nuclides from ^{235}U fission were evaluated (there is no measured data for ^{95m}Nb of them).

1 Data Collection and Selection

The all data up to now were retrieved from EXFOR master data library by using EXFOR manage system and fission yield data evaluation system FYDES[1]. The data were also collected from the publications concerned. Altogether 157 entries (subentries) or papers were collected and are listed in Table 1.

The EXFOR BIB information and papers concerned were read carefully and analysed in physics. The data were decided to be taken or abandoned according to the measured data, conditions and discrepancy situation with others. In general, the following data were abandoned:

(1) The quantity measured is not required;

(2) Some thing is wrong in the measurements or data processing.

Table 1 The experimental data collected in the evaluation and their processing

EXFOR NO	AUTHER	LAB.	REFERENCE	DATE	ENERGY	METHOD	QUANTITY(MONITOR)	PROCESSED	COMMENTS
10828002	T.C.Chapman,	1USALRL	PR/C,17,1089	7803	-9.0+06	RC(γ), CYCLO(6.0-9.0)	FY(/^{97}Zr,^{99}Mo,^{140}Ba)		NE,S
12729002	L.E.Glendenin	1USAANL	PR/C,24,2600	8112	-8.1+06	RC,FNG, γ+RC(γ),γ+RC(β)	FY(AB,归一 200%)		NE,S
12919004	M.Lindner,	1USALRL	RCA,49,1	90	2.5-02				A(Np)
13054003	W.E.Grummitt	1CANCRC	CRC-470	51	2.5-02	RC(β),REAC(mxw)	FY(AB)	Error 5-20%, given by auther	T(earlier Period, error large)
13059005	H.B.Levy,	1USALRL	PR,124,544	61	2.5+04	CYCLO,WNS			NE,A
13059008	H.B.Levy,	1USALRL	PR,124,544	61	2.5+04	CYCLO,WNS			NE,A
13059009	H.B.Levy,	1USALRL	PR,124,544	61	2.5+04	CYCLO,WNS			NE,A
13059011	H.B.Levy,	1USALRL	PR,124,544	61	2.5+04	CYCLO,WNS			NE,A
13059012	H.B.Levy,	1USALRL	PR,124,544	61	2.5+04	CYCLO,WNS			NE,A
13065002	H.Farrar,	1CANMCM	CJP,40,1017	62	2.5-02	MA,REAC(mxw)	Ro(/^{90}Sr)	Error 2%, given by auther	T(Ro)
13065004	H.Farrar,	1CANMCM	CJP,40,1017	62	2.5-02	MA,REAC(mxw)	Ro(/^{93}Zr)	Error 1.5%, given by auther	A(not needed)
13077002	G.P.Ford,	1USALAS	PR/B,137,(4),	6502	-1.81 +07	RC,VDG,CCW,CYCLO	FY(AB)	Take 14.1,14.9, Average,En=14.5	T
13085002	N.K.Aras,	1USAORL	JIN,28,763	66	2.5-02	RC,REAC(mxw)	FY(/$^{127}_{51}$Sb,0.13)		A(too large,^{125}Sb) T(correct for standard)
13091002	H.G.Hicks,	1USALRL	PR,128,700	6210	1.4E+07	RC,CCW	Rv(/^{99}Mo,mxw)	Ro=Rv×^{99}Mo(H/mxw), Evaluated	T(Ro)
13255002	G.P.Ford,	1USALAS	LA-6129	7602	1.47+07	RC,CCW(14.7)			A(^{239}Pu)
13255004	G.P.Ford,	1USALAS	LA-6129	7602	1.47+07	RC,CCW(14.7)	Rv(/^{99}Mo,mxw)	Ro=Rv×^{99}Mo(H/mxw), Evaluated.ΔRo →4%	T(Ro)
13295002	K.Wolfsberg,	1USALAS	PR/C,3,1333	7103	2.5-02				A(^{242m}Am)
13355004	E.R.Ebersole,	1USAANL	LA-4430-MS,14	7005	5.0+05	MA,REAC(EBR-2), 0.5	REL(^{83,84,85}Kr)	Ro=REL(83/85),ΔRo =1.5%. FY=Ro×^{85}Kr,^{85}Kr evaluated 0.3197±0.016	T
13364002	M.H.Feldman,	1USAUSA	RCS,2,654(71)	51	2.5-02	RC,REAC(mxw)			A(IND)
13372002	G.W.Reed,	1USACHI	PR,92,1473	5312	2.5-02	RC,CYCLO(mxw)	FY(AB)	eΔY(1%)→10%	T
13386002	J.A.Petruska,	1CANMCM	CJP,33,693	55	2.5-02	MA,REAC(NRX,mxw)	FY(AB)	ΔY →3%	T
13387003	G.W.Reed	1USAANL	PR,98,1327	5506	2.5-02	RC, REAC(CP-5,mxw)	FY(/^{89}Sr,4.78)	Ro=FY/4.78, ΔRo →5%	T(Ro),A(too small,^{90}Sr,^{91}Y)
13389002	R.K.Wanless,	1CANMCM	CJP,33,541	55	2.5-02	MA,REAC(NRX,mxw)	FY(/^{83}Kr,0.557)	Ro=FY/0.557,ΔRo→2%	T(Ro)
13391002	A.T.Blades,	1CANMCM	CJC,34,233	5603	2.5-02	MA,REAC(mxw)	Ro(/^{86}Kr/^{134}Xe)	FY(^{86}Kr)=Ro×^{134}Xe, 7.517±0.109	T
13395002	B.Finkle,	1USAUSA	RCS,3,1368(21	51	2.5-02	RC,REAC(mxw)	FY(/^{140}Ba,6.1)	CY(6.1→ 6.206,eval.),ΔY→15%	T A(toosmall,^{111}Ag)
13395003	B.Finkle,	1USAUSA	RCS,3,1368(21	51	2.5-02	RC,REAC(mxw)	FY(/^{140}Ba,6.1)	CY(6.1→	T

Continue Table 1

EXFOR NO	AUTHER	LAB.	REFERENCE	DATE	ENERGY	METHOD	QUANTITY(MONITOR)	PROCESSED	COMMENTS
								6.206,eval.), ΔY→15%	
13396002	D.W.Engelkem e	1USAUSA	RCS,3,1372(21	51	2.5-02	RC,REAC(mxw)	FY(/^{140}Ba,6.1)	CY(6.1→ 6.206,eval.),ΔY→15%	T
13405002	T.B.Novey,	1USAUSA	CC-920,4	4309	2.5-02	RC,REAC(mxw)	FY(/^{140}Ba,6.1)	CY(6.1→ 6.206,eval.),ΔY→20%	T
13409002	G.R.Leader,	1USAUSA	RCS,2,934(133	51	2.5-02	RC,REAC(mxw)	FY(AB?)	ΔY→15%	T A(too small,^{125}Sb) Discrepant
13416002	C.W.Stanley,	1USAUSA	RCS,2,947(134	51	2.5-02	RC,REAC(mxw)	FY(/^{144}Ce,5.0)	CY(5.0→ 5.328,eval.),ΔY→15%	T
13425002	D.W.Engelkem e	1USAANL	ANL-4927	5211	2.5-02	RC(GEMUC), REAC(mxw)	FY(/^{140}Ba,6.4)	CY(6.4→ 6.206,eval.),ΔY→20%	T
13428002	L.E.Glendenin	1USAANL	GLENDENIN	55	2.5-02	MA,REAC(mxw)	FY(AB?)	ΔY→2%	T
13431002	A.P.Baerg,	1CANCRC	CJC,35,980	57	2.5-02	RC,REAC(NRX,mxw)	FY(/^{140}Ba,6.32)	CY(6.32→ 6.206,eval.),ΔY→15%	T
13432002	B.P.Bayhurst	1USALAS	TID-5787	57	2.5-02	RC,REAC(mxw)	FY(/^{99}Mo)	ΔY(~4%)→15%	T
13432003	B.P.Bayhurst	1USALAS	TID-5787	57	1.4+07	RC,CCW(14)	FY(/^{99}Mo)	ΔY(~4%)→15%	T
13432005	B.P.Bayhurst	1USALAS	TID-5787	57	1.0+06	RC,REAC(1.0)	FY(/^{99}Mo?)	ΔY(~4%)→15%	T A(^{90}Sr,too small)
13436002	R.Nasuhoglu,	1USAANL	PR,108,1522	5712	2.5-02	RC,REAC(1.0)	Rv(/^{99}Mo,mxw)	Ro=Rv×^{99}Mo(H/mxw,Eval.) ΔRo →5%	T(Ro) Discrepant
13436003	R.Nasuhoglu,	1USAANL	PR,108,1522	5712	1.1+00				A(~ev range)
13440003	W.J.Maeck,	1USAINL	ENICO-1028	8002	7.0+05	MA, REAC(EBR-2,0.7)	FY, CHN(AB,norm.100%)	CHN=CUM for all,Mass number concerned	T
13443003	G.P.Ford,	1USALAS	LA-6129	7602	-8.1+06	RC,VDG(5.0,8.1)			A(NE,S)
13444002	G.P.Ford,	1USALAS	LA-6129	7602	1.47+07	RC,CCW(14.7)	Rv(/^{99}Mo,mxw)		A(^{232}Th)
13444003	G.P.Ford,	1USALAS	LA-6129	7602	1.47+07	RC,CCW(14.7)	Rv(/^{99}Mo,mxw)	Ro=Rv×^{99}Mo(H/mxw),Eval.	T
13444007	G.P.Ford,	1USALAS	LA-6129	7602	1.4+07	RC,CCW(14.7)	Rv(/^{99}Mo,mxw)		A(^{239}Pu)
13445002	G.P.Ford,	1USALAS	LA-6129	7602	5.0+05	RC,REAC(1.0)	Rv(/^{99}Mo,mxw), Data 1	Ro=Rv×^{99}Mo(H/mxw),Eval. ΔR→4%	T
13445004	G.P.Ford,	1USALAS	LA-6129	7602	5.0+05	RC,REAC(1.0)	Rv		A(^{239}Pu)
13446002	G.P.Ford,	1USALAS	LA-6129	7602	1.0+06	RC,REAC(1.0)	Rv(/^{99}Mo,mxw)	Ro=Rv×^{99}Mo(H/mxw),Eval. ΔR→4%	T
13446003	G.P.Ford,	1USALAS	LA-6129	7602	1.0+06	RC,REAC(1.0)	Rv		A(^{238}U)
13448003	G.P.Ford,	1USALAS	LA-6129	7602	5.0+05				A(^{237}Np)
13448006	G.P.Ford,	1USALAS	LA-6129	7602	5.0+05				A(^{239}Pu)
13453002	B.P.Bayhurst	1USALAS	PR,107,325	5707	2.5-02	RC,REAC(mxw)	Ro(/^{99}Mo)	FY=Ro×^{99}Mo,eval.	A(Data unreasonable)
13453003	B.P.Bayhurst	1USALAS	PR,107,325	5707	5.0-01				A(Epithermal)

Continue Table 1

EXFOR NO	AUTHER	LAB.	REFERENCE	DATE	ENERGY	METHOD	QUANTITY(MONITOR)	PROCESSED	COMMENTS
13453004	B.P.Bayhurst	1USALAS	PR,107,325	5707	5.0-01				A(Epithermal)
13462002	A.T.Blades,	1CANMCM	ZN/A,10,838	55	2.5-02	MA,REAC(NRX,mxw)			A(Raw)
13581002	R.B.Regier,	1USAMTR	PR,113,1589	5903	2.5-02	RC(PROPC,GEMUC),REAC	Rv		A(Epithermal)
13581003	R.B.Regier,	1USAMTR	PR,113,1589	5903	2.5-02	RC(PROPC,GEMUC),REAC	Rv		A(ev range)
20768002	J.G.Cuningham	2UK HAR	AERE-R-6862	7205	1.0+06	RC(GeLi,GEMUC), REAC(1.0)	FY(AB)		T
20769002	J.G.Cuningham	2UK HAR	JIN,36,1453	7409	-1.7+06	RC(PROPC,TRD),VDG	FY(AB)		A(NE,S)
21550002	R.Brissot,	2FR GRE	NP/A,255,461	7512	2.5-02	MA(on-line), REAC(mxw)	FY(/CHN,NEDO-12154-1(74))		T
21550004	R.Brissot,	2FR GRE	NP/A,255,461	7512	2.5-02	MA(on-line), REAC(mxw)	FY(/CHN,NEDO-12154-1(74))		A(IND)
21562002	G.Siegert,	2FR ILL	PRL,34,1034	7504	2.5-02				A(IND)
21605002	G.Siegert,	2FR ILL	PR/C,14,1864	7611	2.5-02				A(IND)
21689002	W.Lang,	2FR ILL	NP/A,345,1,34	8008	2.5-02				A(IND)
21689004	W.Lang,	2FR ILL	NP/A,345,1,34	8008	2.5-02				A(IND)
21689006	W.Lang,	2FR ILL	NP/A,345,1,34	8008	2.5-02				A(IND)
21689008	W.Lang,	2FR ILL	NP/A,345,1,34	8008	2.5-02				A(IND)
21689010	W.Lang,	2FR ILL	NP/A,345,1,34	8008	2.5-02				A(IND)
21689012	W.Lang,	2FR ILL	NP/A,345,1,34	8008	2.5-02				A(IND)
21689019	W.Lang,	2FR ILL	NP/A,345,1,34	8008	2.5-02				A(IND)
21734006	J.P.Bocquet,	2FR GRE	NP/A,189,556	7207	1.4+07				A(IND)
21734012	J.P.Bocquet,	2FR GRE	NP/A,189,556	7207	1.45+07	MA,FNG(14.5)	REL(/^{90}Kr)	Ro=REL(87/88),ΔR≈1.5% FY(87)=Ro×^{88}Kr,eval., 3.3542±0.1722	T A(too large)
21743004	G.Mariolopoul	2FR GRE	NP/A,361,1,21	8105	3.0+06	γ(GeLi),REAC(HFR,mxw)			A(IND)
21743005	G.Mariolopoul	2FR GRE	NP/A,361,1,21	8105	3.0+06	γ(GeLi),REAC(HFR,mxw)			A(3MeV)
22066002	V.M.Sinclair,	2UK GRE	71CANT,,45	71	1.5+06	MA(ND),RC(others), REAC(1.5)	FY(AB)		T(^{90}Sr,two sets, delete one set)
30496003	V.K.Rao,	3INDTRM	PR/C,9,1506	7404	2.5-02				A(IND)
30575002	A.Ramaswami,	3INDTRM	JIN,42,(9),12	8009	2.5-02	γ(GeLi,TRD),REAC(mxw)	FY(AB)	CD(all corrected)	T
30666002	S.S.Hau,	3CHFTHU	PR/C,24,523	8108	2.5-02	RC(GeLi),REAC(mxw)	FY(/^{85m}Kr,1.33)	CY(1.33→1.291)	T A(^{87}Kr,too large)
30947002	R.H.Iyer,	3INDTRM	JIN,25,465	63	2.5-02				A(^{232}Th)
30953002	B.Ehrenberg,	3ISLSOR	PR/C,6,618	7208	2.5-02		FY,IND,REL,Z=36, A=87-94		A(IND)
30953004	B.Eariolopoul,	3ISLSOR	PR/C,6,618	7208	2.5-02		FY,IND,REL,Z=54, A=137-143		A(IND)
40206003	L.N.Yurova,	4CCPMIF	AE,36,(1),66	7401	1.0+06				A(^{238}U)
40489002	L.N.Yurova,	4CCPMIF	AE,47,(1),26	7907	1.3+06	γ(GeLi),REAC(BR-1,1.3)	Ro(/mxw)		T
40554004	A.N.Gudkov,	4CCPMIF	77KIEV,3,192	7704	1.3+06	γ(GeLi), REAC(BR-1,1.3)	FY(AB?)	eΔY(<4%)→4%	T(^{91}Y,too small) A(^{87}Kr,too large)

Continue Table 1

EXFOR NO	AUTHER	LAB.	REFERENCE	DATE	ENERGY	METHOD	QUANTITY(MONITOR)	PROCESSED	COMMENTS
41025002	A.N.Gudkov,	4CCPMIF	AE,65,(3),208	8809	3.0+06				A(3MeV)
10722002	R.B.Strittmat,	1USAUI	ANS,27,862	7712	2.5-02	MA,TOF,REAC(mxw)	R=IND(/CHN)		A(IND)
10722003	R.B.Strittmat,	1USAUI	ANS,27,862	7712	2.5-02	MA,TOF,REAC(mxw)	IND		A(IND)
10864008	M.Shima,	1CANMCM	CJP,56,1340	7810	2.5-02	MA,REAC(mxw)	FY,CHN(/^{101}Ru)	Ro=FY/^{101}Ru(5.04±0.05)	T(Ro)
10864010	M.Shima,	1CANMCM	CJP,56,1340	7810	5.0-01	MA,REAC(mxw)			A(EpithermalT)
10865002	W.J.Maeck,	1USAINL	ICP-1142	7809	2.5-02	MA,REAC(mxw)	FY,CHN(AB)	eΔY(<1%)→1%	T A(^{86}Kr,too large)
13055002	W.J.Arrol,	1CANMRC	CJR/B,27,757	49	2.5-02	RC,REAC(mxw)	Ro(/^{134}Xe)	FY=Ro×^{134}Xe(7.5175 evaluated) ΔY→15%	A(NE)
13059002	H.B.Levy,	1USALRL	PR,124,544	61	2.5+04	CYCLO,WNS			A(NE)
13059003	H.B.Levy,	1USALRL	PR,124,544	61	2.5+04				A(NE)
13059004	H.B.Levy,	1USALRL	PR,124,544	61	2.5+04				A(NE)
13059006	H.B.Levy,	1USALRL	PR,124,544	61	2.5+04				A(NE)
13059007	H.B.Levy,	1USALRL	PR,124,544	61	2.5+04				A(NE)
13059010	H.B.Levy,	1USALRL	PR,124,544	61	2.5+04				A(NE)
13059013	H.B.Levy,	1USALRL	PR,124,544	61	2.5+04				A(NE)
13065003	H.Farrar,	1CANMCM	CJP,40,1017	62	2.5-02	MA,REAC(mxw)	Ro(/^{89}Y)		A(^{89}Y not known)
13065005	H.Farrar,	1CANMCM	CJP,40,1017	62	2.5-02	MA,REAC(mxw)	Ro(/^{100}Mo)		T(Ro)
13066002	L.E.Glendenin	1USAANL	ANS,5,20	6206	2.5-02	RC,REAC(mxw)	Rv(/^{99}Mo,mxw)		A(NE)
13066003	L.E.Glendenin	1USAANL	ANS,5,20	6206	0.0+00	RC,REAC(mxw)	Rv(/^{99}Mo,mxw)		A(NE)
13092002	K.T.Faler,	1USAMTR	PR,131,1746	6308	0.002-0.70	RC,REAC	Rv(/^{99}Mo,mxw)		A(NE)
13092003	K.T.Faler,	1USAMTR	PR,131,1746	6308	0.002-0.70	RC,REAC	Rv(/^{99}Mo,mxw)		A(NE)
13097005	A.C.Wahl,	1USAWAS	PR,126,1112	6205	2.5-02	RC,REAC, CYCLO(mxw)	Ro,IND(/CHN)		A(IND)
13202002	J.A.Mchughj	1USALRL	UCRL-10673	6302	2.5-02	MA,REAC(mxw)	Ro(/^{85}Kr)		T(Ro)
13213003	L.R.Bunney,	1USANRD	JIN,27,273	65	2.5-02	RC,REAC(mxw)	FY,CHN(/^{99}Mo)	ΔY=Y×10%(given by Auth)	T
13221002	G.P.Ford,	1USALAS	FORD	65	2.5-02	RC,REAC(mxw)	FY,CHN(/?)		T
13233005	D.J.Gorman,	1CANMCM	CJC,46,1663	68	2.5-02				A(^{238}U)
13244002	B.R.Erdal,	1USAWAS	JIN,31,2993	6910	2.5-02	RC(β,γ),REAC(mxw)	FY(/^{89}Sr,4.73;^{143}Ce,5.71)	eΔY→7%	T
13244004	B.R.Erdal,	1USAWAS	JIN,31,2993	6910	2.5-02	RC(β,γ),REAC(mxw)	FY,CHN		T
13270003	F.L.Lisman,	1USAMTR	NSE,42,191	70	2.5-02	MA,REAC(mxw)	FY(AB?)	Delete all in error indicated ΔY(<1%)→1%	T
13270004	F.L.Lisman,	1USAMTR	NSE,42,191	70	2.5-02	RC,REAC(mxw)	FY(AB?)		T
13270006	F.L.Lisman,	1USAMTR	NSE,42,191	70	2.5-02	MA,REAC(mxw)	FY(/^{148}Nd,1.69±0.01)	CY 1.69→1.6747(eval.)	T
13270016	F.L.Lisman,	1USAMTR	NSE,42,191	70	5.0+05	MA,REAC(0.5)	FY(/^{148}Nd, 1.75±0.03)	CY 1.75±0.03→1.6747±0.0113(eval.) ΔY→2%	A(^{85}Kr,too small) T(^{86}Kr,^{90}Sr, ^{95}Mo,^{97,100}Mo,^{101}Ru, ^{102}Ru,^{104}Ru)
13270018	F.L.Lisman,	1USAMTR	NSE,42,191	70	5.0+05	RC,REAC(0.5)	FY(/^{148}Nd,1.75±0.03)	CY 1.75→1.6747(eval.)	T
13274002	N.E.Ballou,	1USABNW	ACS,,(16)	7404	1.0+06	RC,REAC(1.0)	FY(/^{85}Kr,^{88}Rb,^{138}Xe,^{138}Cs)	ΔY→5%	T

Continue Table 1

EXFOR NO	AUTHER	LAB.	REFERENCE	DATE	ENERGY	METHOD	QUANTITY(MONITOR)	PROCESSED	COMMENTS
13274003	N.E.Ballou,	1USABNW	ACS,,(16)	7404	1.5+07	RC,CCW(15)	FY(/^{88}Kr,^{88}Rb,^{138}Xe,^{138}Cs)	ΔY→7%	T
13286002	T.P.Mclaughl,	1USAUSA	MCLAUGHLIN	7109	2.5-02	RC(γ,GeLi),REAC(mxw)	FY(AB)	CD(crrectedfor used)	T
13312002	J.W.Mandler,	1USAIIT	BAP,18,768(AB	7306	1.0+06	RC,Accelerator(1-15)	Ro(CHN/CHN140)		A(NE)
13327003	W.J.Maeck	1USAINL	75WASH,1,378	7503	4.0+05	MA, REAC(EBR-II,0.4)	FY,CHN(AB, normalijed to 100%)		T
13341002	W.J.Maeck,	1USAINL	ICP-1092	76	2.5-02	MA,REAC(ETR,mxw)	Ro(/$^{143-146}$Nd)	Ro×$\sum^{143-146}$Nd,B6	T
13359002	G.Diiorio,	1USAUI	NIM/B,147,487	7712	2.5-02	MA,REAC(TRIGA,mxw)	FY,CHN(/MEEK)	ΔY(<1%)→1%	T
13372002	G.W.Reed,	1USACHI	PR,92,1473	5312	2.5-02	RC,CYCLO(mxw)	FY(AB)	eΔY(1.0%)→10%	T
13387002	G.W.Reed,	1USAANL	PR,98,1327	5506	2.5-02	RC,REAC(CP-5,mxw)	FY,IND		A(IND)
21054087	H.Wohlfarth	2GERTHD	WOHLFARTH	7612	2.5-02	SC,REAC(mxw)	FY,CHN(/^{252}Cf,IND)	ΔY(2%—30%)	A(^{83}Kr,too large) T(^{109}Ag,too small)
21155005	L.Koch	2GERKFK	RCA,29,61	81	1.0+06	RC(γ),REAC(1.0)	FY,CHN	ΔY→20%(Y<0.1)ΔY→10% (0.1<Y<1.0) ΔY →4%(Y>1.0)	T
21531002	H.Thierens,	2BLGGHT	NIM,134,299	7604	2.5-02	γ,REAC(mxw)	FY,CHN(to 200%)		T A(too large ^{91}Y,^{101}Ru) Too small,^{106}Rh
21595002	M.Rajagopalan	2SWTWUR	NSE,58,414	7512	1.8+05	γ,REAC(0.18)	FY,CHN(to 100%,Heavy)		T
21734018	J.P.Bocquet,	2FR GRE	NP/A,189,556	7207	1.4+07	MA,FNG(14.5)	FY,CHN(/Meek)		T
21834002	R.Mueller,	2GERKFK	KFK-3220	8112	5.0+05	SC,VDG(0.5MeV)	FY,PRE		A(NE)
21834003	R.Mueller,	2GERKFK	KFK-3220	8112	5.5+06	SC,VDG(5.55)	FY,PRE		A(NE)
22057003	P.D'Hondt,	2BLGMOL	BLG-586,43	8605	1.5+06	γ(GeLi),REAC(1.5)	FY(AB?)	ΔY=Y×ΔY%	T
30508006	C.K.Mathews	3INDTRM	PR/C,15,344	7701	2.5-02	RC,REAC(mxw)	FY(/^{111}Ag,0.018)	Ro(^{111}Ag)=FY/0.018	T(Ro)
40017002	P.P.Djachenko	4CCPFEI	YFI-8,7	6912	2.5-02	SC,VDG(mxw)	FY,PRE		A(PMY)
40017003	P.P.Djachenko	4CCPFEI	YFI-8,7	6912	1.2+05				A(NE)
40017004	P.P.Djachenko	4CCPFEI	YFI-8,7	6912	2.0+05				A(NE)
40017005	P.P.Djachenko	4CCPFEI	YFI-8,7	6912	3.0+05				A(NE)
40017006	P.P.Djachenko	4CCPFEI	YFI-8,7	6912	4.0+05				A(NE)
40017007	P.P.Djachenko	4CCPFEI	YFI-8,7	6912	5.0+05				A(NE)
40017008	P.P.Djachenko	4CCPFEI	YFI-8,7	6912	6.0+05				A(NE)
40200002	V.P.Zakharova	4CCPNIR	YF,16,(4),649	72	2.5-02		FY,PRE,Raw		A(Raw data)
40200006	V.P.Zakharova	4CCPNIR	YF,16,(4),649	72	2.5-02		FY,PRE		A(NE,raw data)
40234002	P.P.D'Jachenk	4CCPFEI	YF,7,(1),36	6807	1.5+07	SC,VDG(15.5)	FY,PRE		A(PMY)
40235003	P.P.D'Jachenk	4CCPFEI	YF,8,(2),286	6808	2.5-02	SC,VDG(mxw)	FY,PRE		A(PMY)
40235004	P.P.D'Jachenk	4CCPFEI	YF,8,(2),286	6808	2.8+05		FY,PRE		A(PMY)
40235005	P.P.D'Jachenk	4CCPFEI	YF,8,(2),286	6808	7.3+05		FY,PRE		A(PMY)
40235006	P.P.D'Jachenk	4CCPFEI	YF,8,(2),286	6808	1.1+06		FY,PRE		A(PMY)
40235007	P.P.D'Jachenk	4CCPFEI	YF,8,(2),286	6808	1.3+06		FY,PRE		A(PMY)
40235008	P.P.D'Jachenk	4CCPFEI	YF,8,(2),286	6808	1.7+06		FY,PRE		A(PMY)

Continue Table 1

EXFOR NO	AUTHER	LAB.	REFERENCE	DATE	ENERGY	METHOD	QUANTITY(MONITOR)	PROCESSED	COMMENTS
40235009	P.P.D'Jachenk	4CCPFEI	YF,8,(2),286	6808	2.0+06		FY,PRE		A(PMY)
40235010	P.P.D'Jachenk	4CCPFEI	YF,8,(2),286	6808	2.5+06		FY,PRE		A(PMY)
40235011	P.P.D'Jachenk	4CCPFEI	YF,8,(2),286	6808	3.1+06		FY,PRE		A(PMY)
40235012	P.P.D'Jachenk	4CCPFEI	YF,8,(2),286	6808	3.5+06		FY,PRE		A(PMY)
40235013	P.P.D'Jachenk	4CCPFEI	YF,8,(2),286	6808	5.0+06		FY,PRE		A(PMY)
40235014	P.P.D'Jachenk	4CCPFEI	YF,8,(2),286	6808	6.1+06		FY,PRE		A(PMY)
40235015	P.P.D'Jachenk	4CCPFEI	YF,8,(2),286	6808	7.0+06		FY,PRE		A(PMY)
40235016	P.P.D'Jachenk	4CCPFEI	YF,8,(2),286	6808	1.5+07		FY,PRE		A(PMY)
40527003	V.N.Andreev,	4CCPITE	YF,25,(4),732	7704	2.5-02		FY,PRE		A(PMY)

Notes for the table:

1 Abbreviation and symbol:

VDG	Van de Graaff accelerator
CYCLO	Cyclotron accelerator
REAC	Reactor
FNG	Fast neutron Generator
CCW	Cockcroft-Walton accelerator
RC	Radiochemistry method
γ	γ Spectrum method
MA	Mass Spectrometer method
mxw	Maxwell spectrum thermal neutron
AB(X)	Absolute measurement with method X
FY(/X)	Fission yield measured relatively to X
Ro(/X)	Ratio measured relatively to X
Rv(/X,MXW)	R value measured relatively to X at thermal energy point
ΔY→3%	Designed 3% error to Y
EΔY→3%	Enlarge Y error to 3%
C	Corrected
Calcu.	Calculated
Disc	Discrepant
CHN	Chain yield
CUM	Cumulative yield
IND	Independent yield
NE,S	Not needed energy range, Single energy point
NE,A	Not needed energy range, Spectrum average
PMY	Primary mass yield
SC	Semiconductor
WNS	White light neutron source

2 The abbreviations not listed above are the same as EXFOR and CINDA.

3 The unit of energy is "MeV", if not specially given, but "ENERGY" column is in eV.

(3) Large discrepancy with others and the measured method is not reliable or no information in detail;

(4) The data relatively measured, but their standards are not given. This is necessary specially for the evaluation of 'reference yield data', the 'standard data' could not be based on other standards, whose reliability are unknown.

As a result, more than half of the data were abandoned (marked by 'A' in Table 1), and 65 entries (subentries) or papers were taken (marked by 'T' in Table 1).

2 Data Corrections

The data were corrected for standard yield data, gamma intensity, and fission cross section.

As mentioned above, in general case, the data relatively measured were not directly taken, only the data, for which standards used have just been evaluated by us, were used and corrected by using the newly evaluated data

$$FY = FY_0 \times FY_{\text{snew}} / FY_{\text{sold}}$$

If the gamma intensity used is given by author, the data were corrected for it by using following new intensity data in order: evaluated decay data at CNDC[2], Table of Radioactive Isotopes, ENDSF computer library. If only one gamma line was used in the data measurement, it is simple that

$$FY_0 = FY_0 \times I_0 / I_{\text{new}}$$

If there are several gamma lines were used and there is a gamma line, whose intensity is much larger than others and the energy is in the region from 100~1000 keV, then the data were corrected as the same as above. If there are several gamma lines used with larger intensity, then the data were corrected by using following formula

$$FY = FY_0 \times \frac{1}{N} \sum_{i=1}^{N} I_i / I_{i\text{new}}$$

where N is the number of the gamma lines.

The data were corrected for fission cross section

$$FY = FY_0 \times \sigma_{f0} / \sigma_{fnew}$$

The new fission cross section were taken from ENDF/B-6.

3 Error Processing

The error given in the EXFOR data table are very different and complicated, they must be corrected or assigned for adopted data entirely. They must be 'total' and should be keep at same level for same measured method. The errors are listed in Table 2 for different methods. In general case, if the errors were given by authors in these region, they were not changed, if not they were corrected or assigned in the given region. The error could be changed in the region for same method and period, depending on the value of the yield, measured energy point, data and liboratory. If there were no error given, the error were assigned according to the measured conditions, generally upper limit. It should be pointed out that this is just 'general' case, in the special case the error could be out of the given region.

Table 2 The error(%) of measured fission yield data with different methods

Method		Fission Yield		Radio
		Before 1965	After 1965	
RC	GeLi	7~15	4~8	3~5
	NaI	8~15	6~8	3~4
	Geiger	15~25		5~6
γ Spectrum		6~10	3~6	2~3
MA		2~3	1~2	1~2

Note: 1) The error depends on fission yield value, energy point, year and laboratory measured, it can be changed in the corresponding region.

2) If the error is not given, in general case, the upper limit is taken for that.

3) The region listed in the table is just for general case, the error may be outside of the region in special case.

The error was processed as following:

(1) Standard fission yield and fission cross section correction

$$\Delta FY' = \left(\Delta FY_0'^2 + \Delta FY_{\text{snew}}'^2 - \Delta FY_{\text{sold}}'^2 \right)^{1/2}$$

or

$$\Delta FY' = \left(\Delta FY'^2 + \Delta \sigma_{\text{fsnew}}'^2 - \Delta \sigma_{\text{fsold}}'^2 \right)^{1/2}$$

where $\Delta FY'$ means relative error of data FY, $\Delta FY' = \Delta FY / FY$ (the same below).

In some cases, ΔFY_{sold}, the error of old standard, may not be included in the ΔFY , the total error of the data given by author. In this case, ΔFY_{sold} should be taken as 0.

(2) Gamma intensity correction

For gamma intensity correction, the FY error was not changed, due to the correction, in usual case, it is not large and the gamma intensity error is not given.

(3) Calculating FY from ratio R

$$\Delta FY' = \left(\Delta R'^2 + \Delta FY_s'^2 \right)^{1/2}$$

(4) Calculating ratio R from R-value

$$\Delta R' = \left(\Delta R_v'^2 + \Delta FY_E'^2 + \Delta FY_{\text{mxw}}'^2 \right)^{1/2}$$

(5) Calculating ratio R from fission yield

As mentioned above, this evaluation is for reference fission yield data, only absolute measured data and a few data measured relatively to standards, which we have just evaluated, were used. Only the ratio were used for relatively measured data, if the standards used were given (otherwise the data were abandoned). In this case

$$\Delta R' = \left(\Delta FY' - \Delta FY_s'^2 \right)^{1/2}$$

If ΔFY_s is not included in the total ΔFY, given by author, then ΔFY_s is taken as 0.

The Concrete processing of the data and their errors for each subentry (article) is given in Table 1.

4 Data Processing

The EXFOR data were processed by using fission yield data evaluation system

FYDES[1], including data table standardization, data correction, average with weight, simultaneous evaluation.

(1) Data Averaging

The data measured at same energy points for a nuclide are averaged with code AVERAG. The mean with weight and its external error were calculated. The reduced χ^2 and internal error, and their arithmetical mean and its error were also given for reference. The data, for which the average was made, are marked by 'A' and the measured data points are given by the corresponding numbers in the Table 3. It can be seen that averaging has been made for most of them.

(2) Simultaneous Evaluation

The data, for which not only absolute yields but also their ratios are measured, were simultaneously evaluated by using code ZOTT[3]. The consistent yields, ratios and their covariance matrix were calculated. The correlative measurements and treatments at present evaluation are as following:

thermal: $^{86}Kr/^{83}Kr$;

thermal: $^{102}Ru/^{101}Ru$, $^{104}Ru/^{101}Ru$, $^{106}Ru/^{101}Ru$;

thermal: $^{89}Sr/^{90}Sr$;

^{89}Sr: h/mxw;

^{91}Y: f/mxw, h/mxw;

^{95}Nb: f/mxw;

^{111}Ag: f/mxw,h/mxw.

where mxw means thermal energy point, f means fission or fast reactor spectrum, and h means around 14 MeV. It can be seen that there are two kinds of correlative measurements, one is at different energy points for the same nuclide, another is for different nuclides at same energy point. The data evaluated simultaneously are marked by 'S' in the Table 3.

5 Result, Recommendation and Discussion

The evaluated results are shown in Table 3. It can be seen that the errors are about 1% for most of product nuclides and 2%~3% for some, about 5% for $^{89}Sr(F)$,

^{91}Y(H), ^{102}Ru(F), ^{104}Ru(F), ^{125}Sb(T) and 22.6% only for ^{109}Ag(T), 10.5% for ^{125}Sb(F).The error about 1% and 2%~3% of evaluated data comes from the fact that the data measured with mass spectrometer method have the errors 1%~2% (after 1960) or 2%~3% (before 1960), and multiple sets of measurements make it reduced(in the case of the data are statistical consistent). The yields are very low, and there are only two sets measured data for both ^{109}Ag(T) and ^{125}Sb(F). For ^{125}Sb(F), two sets of data were all measured by means of radiochemistry method with large error. Although for ^{109}Ag(T), one set of data by radio-chemistry method and one by mass spectrometer method, but all with large error, in addition, there is larger discrepancy between them.

The evaluated data were compared with ENDF/B-6, JENDL-3(see Table 4). It was found that the present evaluated data are in good agreement with all others except for ^{104}Ru(F),^{111}Ag(T,F,H) and ^{125}Sb(T), for which the present data are smaller than both B-6 and J-3 or one of them by 10%~35%. In fact, the present data are smaller than both B-6 and J-3 by more 5% only for ^{111}Ag(T,F), for which the yields are quite low and there are several sets of measured data, including absolute yields and ratios. The evaluated data were obtained by averaging and simultaneous evaluation, and should be reliable to some extent.

There is only one measurement for ^{86}Kr(F), ^{89}Sr(F), and ^{102}Ru(F), the data have less reliability, although they are in good agreement with B-6 and J-3 data, so the data only taken as reference. For all others, there are more measured data and in good agreement with B-6 and J-3, although, as pointed above, not in good agreement with B-6 and/or J-3, the measured data are more reliable, the data are recommended.

It can be seen that except for the data only taken as reference, most of the data are more reliable: small error and good agreement with other's, it means high accuracy and precision.

As pointed out above that the reliability for the data of product nuclides with low yield ^{109,111}Ag, ^{125}Sb are needed to be approved further, for they have larger error or are outside of all existing evaluated data. More measurements with high accuracy are needed for them.

Table 3 Evaluated reference fission yield data from ^{235}U fission

Nucli	Energy / eV	Yield	Error	Point	Processed		Recommended
^{83}Kr	2.5000E-02	5.3937E-01	2.6115E-03	4+(2)	A	S	R
	5.5000E+05	5.8132E-01	1.4759E-02	2	A		R
^{86}Kr	2.5000E-02	1.9689E+00	7.3392E-03	6+2	A	S	R
	7.0000E+05	1.9900E+00	2.0000E-02	1			(R)
^{87}Kr	2.5000E-02	2.6445E+00	8.7407E-02	3	A		R
	1.4750E+06	2.4332E+00	7.1561E-02	2	A		R
^{89}Sr	2.5000E-02	4.7855E+00	4.3800E-02	7+1+(3)	A	S	R
	1.5000E+06	4.2200E+00	2.1000E-01	1			(R)
	1.5000E+07	4.1084E+00	1.1607E-01	1+3	A	S	R
^{90}Sr	2.5000E-02	5.8499E+00	2.8991E-02	7+(1)	A	S	R
	8.6667E+05	5.4873E+00	4.5042E-02	3	A		R
	1.4500E+07	4.6072E+00	2.7311E-01	2	A		R
^{91}Y	2.5000E-02	5.8974E+00	4.7033E-02	6+(1+1)	A	S	R
	1.8000E+05	5.8307E+00	7.7762E-02	1+1	A	S	R
	1.5000E+07	4.9312E+00	2.4815E-01	1+1	A	S	R
^{96}Zr	2.5000E-02	6.2615E+00	8.0721E-02	4	A		R
	5.5000E+05	6.1205E+00	5.3841E-02	2	A		R
^{95}Nb	2.5000E-02	6.5780E+00	3.2600E-02	5+(1)	A	S	R
	1.8000E+05	6.4531E+00	1.5442E-01	1+1	A	S	R
^{95}Mo	2.5000E-02	6.5035E+00	3.6541E-02	6	A		R
	4.2667E+05	6.3837E+00	4.2355E-02	3	A		R
^{97}Mo	2.5000E-02	5.9163E+00	3.6324E-02	6+1	A	S	R
	6.9500E+05	5.9471E+00	3.9022E-02	4	A		R
^{100}Mo	2.5000E-02	6.2135E+00	3.2212E-02	5+(1)	A	S	R
	5.5000E+05	6.2425E+00	1.4085E-01	2	A		R
^{101}Ru	2.5000E-02	5.1895E+00	3.6259E-02	5+(1+1)	A	S	R
	2.9000E+05	5.3019E+00	1.1431E-01	2	A		R
^{102}Ru	2.5000E-02	4.2954E+00	4.6497E-02	5+1	A	S	R
	4.0000E+05	4.4100E+00	2.0000E-01	1			(R)
^{104}Ru	2.5000E-02	1.8914E+00	1.4203E-02	6+1	A	S	R
	2.9000E+05	1.9905E+00	1.0950E-01	2	A		R
^{106}Rh	2.5000E-02	4.0167E-01	1.4203E-02	3+1	A	S	R
^{109}Ag	2.5000E-02	3.1000E-02	7.0000E-03	2	A		R
^{111}Ag	2.5000E-02	1.5789E-02	5.3149E-04	3+(2+3)	A	S	R
	1.5000E+06	3.1492E-02	8.9783E-04	1+2	A	S	R
	1.4500E+07	1.0272E+00	1.5797E-02	1+3	A	S	R
^{125}Sb	2.5000E-02	2.8095E-02	1.3388E-03	5	A		R
	7.5000E+05	6.5502E-02	6.8783E-03	2	A		R

NOTE:

Number	Yield data sets measured
+Number	Ratio data sets number in numerator
+(Number)	Ratio data sets number in denominator
A	Averaged with weight
S	Simultaneuos evaluation with code ZOTT
R	Recommended
(R)	Recommended but need to be improved

Table 4 Comparison of present evaluated data with JENDL-3 AND ENDF/B-6

Nuclide	E	Yield	Error	JENDL-3	ENDF/B-6	*DFJ3(%)	*DFB6(%)
$^{83}_{36}$Kr	T	5.3937E-01	2.6115E-03	5.3805E-01	5.3620E-01	0.24	0.59
	F	5.8132E-01	1.4759E-02	5.7053E-01	5.7653E-01	1.86	0.82
$^{86}_{36}$Kr	T	1.9689E+00	7.3392E-03	1.9725E+00	1.9650E+00	-0.18	0.20
	F	1.9900E+00	2.0000E-02	1.9359E+00	1.9468E+00	2.72	2.17
$^{87}_{36}$Kr	T	2.6445E+00	8.7407E-02	2.5147E+00	2.5576E+00	4.91	3.29
	F	2.4332E+00	7.1561E-02	2.4682E+00	2.5425E+00	-1.44	-4.49
$^{89}_{38}$Sr	T	4.7855E+00	4.3800E-02	4.8850E+00	4.7327E+00	-2.08	1.10
	F	4.2200E+00	2.1000E-01	4.5347E+00	4.3737E+00	-7.46	-3.64
	H	4.1084E+00	1.1607E-01	4.2150E+00	4.1226E+00	-2.59	-0.35
$^{90}_{38}$Sr	T	5.8499E+00	2.8991E-02	5.9045E+00	5.7819E+00	-0.93	1.16
	F	5.4873E+00	4.5042E-02	5.4341E+00	5.4650E+00	0.97	0.41
	H	4.6072E+00	2.7311E-01	4.6607E+00	4.5927E+00	-1.16	0.31
$^{91}_{39}$Y	T	5.8974E+00	4.7033E-02	5.9187E+00	5.8278E+00	-0.36	1.18
	F	5.8307E+00	7.7762E-02	5.6549E+00	5.7334E+00	3.02	1.67
	H	4.9312E+00	2.4815E-01	4.8924E+00	4.8227E+00	0.79	2.20
$^{96}_{40}$Zr	T	6.2615E+00	8.0721E-02	6.2641E+00	6.3392E+00	-0.04	-1.24
	F	6.1205E+00	5.3841E-02	6.0815E+00	6.2023E+00	0.64	-1.34
$^{95}_{41}$Nb	T	6.5780E+00	3.2600E-02	6.4947E+00	6.5029E+00	1.27	1.14
	F	6.4531E+00	1.5442E-01	6.3629E+00	6.4320E+00	1.40	0.33
$^{95}_{42}$Mo	T	6.5035E+00	3.6541E-02	6.4962E+00	6.5029E+00	0.11	0.01
	F	6.3837E+00	4.2355E-02	6.3643E+00	6.4320E+00	0.30	-0.76
$^{97}_{42}$Mo	T	5.9163E+00	3.6324E-02	6.0082E+00	5.9968E+00	-1.55	-1.36
	F	5.9471E+00	3.9022E-02	5.9905E+00	6.0029E+00	-0.73	-0.94
$^{100}_{42}$Mo	T	6.2135E+00	3.2212E-02	6.2323E+00	6.2923E+00	-0.30	-1.27
	F	6.2425E+00	1.4085E-01	6.3286E+00	6.2983E+00	-1.38	-0.89
$^{101}_{44}$Ru	T	5.1895E+00	3.6259E-02	5.0814E+00	5.1726E+00	2.08	0.33
	F	5.3019E+00	1.1431E-01	5.3498E+00	5.1243E+00	-0.90	3.35
$^{102}_{44}$Ru	T	4.2954E+00	4.6497E-02	4.2331E+00	4.2985E+00	1.45	-0.07
	F	4.4100E+00	2.0000E-01	4.5295E+00	4.3590E+00	-2.71	1.16
$^{104}_{44}$Ru	T	1.8914E+00	1.4203E-02	1.8397E+00	1.8807E+00	2.73	0.57
	F	1.9905E+00	1.0950E-01	2.2820E+00	2.0724E+00	-14.64	-4.11

Nuclide	E	Yield	Error	JENDL-3	ENDF/B-6	*DFJ3(%)	*DFB6(%)
$^{106}_{45}$Rh	T	4.0167E-01	1.4203E-02	4.0231E-01	4.0155E-01	-0.16	0.03
$^{109}_{47}$Ag	T	3.1000E-02	7.0000E-03	3.4482E-02	3.1221E-02	-11.23	-0.71
$^{111}_{47}$Ag	T	1.5789E-02	5.3149E-04	1.9963E-02	1.7379E-02	-26.44	-10.07
	F	3.1492E-02	8.9783E-04	4.2930E-02	4.2450E-02	-36.32	-34.80
	H	1.0272E+00	1.5797E-02	1.2006E+00	1.0761E+00	-16.88	-4.76
$^{125}_{51}$Sb	T	2.8095E-02	1.3388E-03	2.9378E-02	3.4020E-02	-4.57	-21.09
	F	6.5502E-02	6.8783E-03	7.0912E-02	6.8029E-02	-8.26	-3.86

*Note: DFJ3(%)=(PRESENT-JENDL-3)/PRESENT × 100

DFB6(%)=(PRESENT-ENDF/B-6)/PRESENT × 100

6 Conclusion

Based on available experimental data up to now and processed by using average data with weight code AVERAG and simultaneous evaluation code ZOTT, the 38 cumulative fission yield for 18 product nuclides were evaluated. Among them, 35 are recommended and only 3 taken as reference and need to be improved. The data have been updated and their errors are reduced. The recommended data can be used as standard in the evaluation and measurement or as monitor yield in the industry application. In the evaluation, only absolute yield measurements and ratios were taken, that means no standard yield (except for newly evaluated ones) were used.

References

[1] Liu Tingjin, CNDP, 19, 103(1998)

[2] Zhou Chunmei, Private Communication(1997)

[3] D. Muir, Nucl. Sci. & Eng., 101, 88(1989)

Evaluation of the Neutron Cross Section Data for $^{135\sim138}$Ba

Zhao Jingwu, Su Weining
(Department of Physics, Nanjing University, Nanjing, 210093)

Introduction

The natural Ba consists of seven stable isotopes. Its neutron cross sections are important for nuclear science and technology. However, there are some discrepancies in several evaluated nuclear data libraries. In this work, the neutron cross section data were evaluated for $^{135\sim138}$Ba in the energy range 10^{-5}eV to 20 MeV. The evaluation is based on both experimental data measured up to 1998 and calculated data with program SUNF[1]. The results are compared with the experimental and other evaluated data from ENDF/B-6 and JENDL-3.

1 Total Cross Section

Due to no experimental data for $^{135\sim138}$Ba, the experimental data of natural Ba were taken for these isotopes. There are over twenty set of experimental data. Among them, seven sets were selected in the energy range 100 keV to 14 MeV. The measured data of Foster[2], Conner[3] and Hever[4] are consistent with each other in high energy range and consistent with Coon's[5] at 14 MeV. The measured data of Miller[6] was taken for low energy range and is consistent with Wells's[7], Bennett's[8] and Foster's in energy range 1 MeV to 3 MeV. The data was fitted with the orthogonal polynomial and the fitted result was recommended as evaluated ones in the energy range 100 keV to 14 MeV. The calculated result with SUNF code was taken in the energy range 14 MeV to 20 MeV. The evaluated results are shown in Fig. 1.

2 (n, γ) Cross Section

The (n,γ) cross section was measured by Musgrove[9] in low energy for $^{135\sim137}$Ba and by Koehler[10] for ^{137}Ba in 1998, whose precision is higher than Musgrove's.

Comparing with Koehler, Musgrove's data become lower as the energy decreasing. Compared with Stroud's[11] for ^{136}Ba, the result is the same. The recommended (n, γ) cross section is increased with the energy decreasing. The calculated results with the SUNF code were recommended in energy range 200 keV to 20 MeV for $^{135\sim137}$Ba, the evaluated data for $^{135\sim137}$Ba are shown in Figs. 2~4 respectively.

There are over thirty sets of experimental data for ^{138}Ba. Eleven of them were selected in energy range 100 keV to 14 MeV. Johnsruds'[12] data were taken in low energy. The data of Hughes'[13~16] etc. are disperse, they were only taken as reference. There are five sets of experimental data by Schwerer[17~21] etc. at energy point 14 MeV. The cross section was recommended as 1 mb. The evaluated result is shown in Fig. 5.

3 (n,2n) Cross Section

The (n,2n) cross section was measured by Hulub[22] at one energy point for ^{136}Ba. The calculated data which is passed through the experimental data was recommended. The evaluated result is shown in Fig. 6. Due to no experimental data for ^{135,137,138}Ba, the calculated ones were recommended.

4 (n, α) Cross Section

There are five sets of experimental data for ^{138}Ba. Lagerwall[23] measured the cross section near the threshold energy, but the discrepancy is very large, there must be something wrong with it. The data from Staudt[24] and Lu Hanlin[25] are consistent, but the data from Lu Hanlin near 18 MeV is lower. The data from Ikeda[26] are consistent with Pepelnik[27] and Lu Hanlin's near 15 MeV. Four sets of experimental data and calculated data were fitted with the orthogonal polynomial and the result was recommended, the evaluated result is shown in Fig. 7.

Due to no experimental data for $^{135\sim137}$Ba, the calculated was adopted.

5 (n,p) Cross Section

There are two sets of experimental data for ^{136}Ba and one for ^{137}Ba. The data from Pepelnik[27] is consistent with Ikeda[26]. Because there is some dispersion for

Ikeda's data, the calculated data was recommended for ^{136}Ba. The evaluated result is shown in Fig.8. The calculated data, which pass through the experimental data of Csikai's[28], were recommended for ^{137}Ba. The evaluated result is shown in Fig. 9.

Due to no experimental data for ^{135,138}Ba, the calculated ones were recommended.

6 (n,n') Cross Section

Tuckder[29] measured the (n,n') cross section for first and second excited states in low energy region. The calculated ones were consistent with the experiment data (see Fig.10). Therefore, the calculated data were recommended for $^{135\sim138}$Ba.

7 Other

Due to no experimental data for (n,3n), (n,np), (n,nα), (n,d), (n,t) and (n,^{3}He) cross sections, the calculated data were recommended for them. The nonelastic cross section is the sum of all nonelastic reaction cross sections. The elastic scattering cross section was obtained by subtracting the nonelastic cross section from the total cross section, the cross sections of all reactions are shown in Fig. 11.

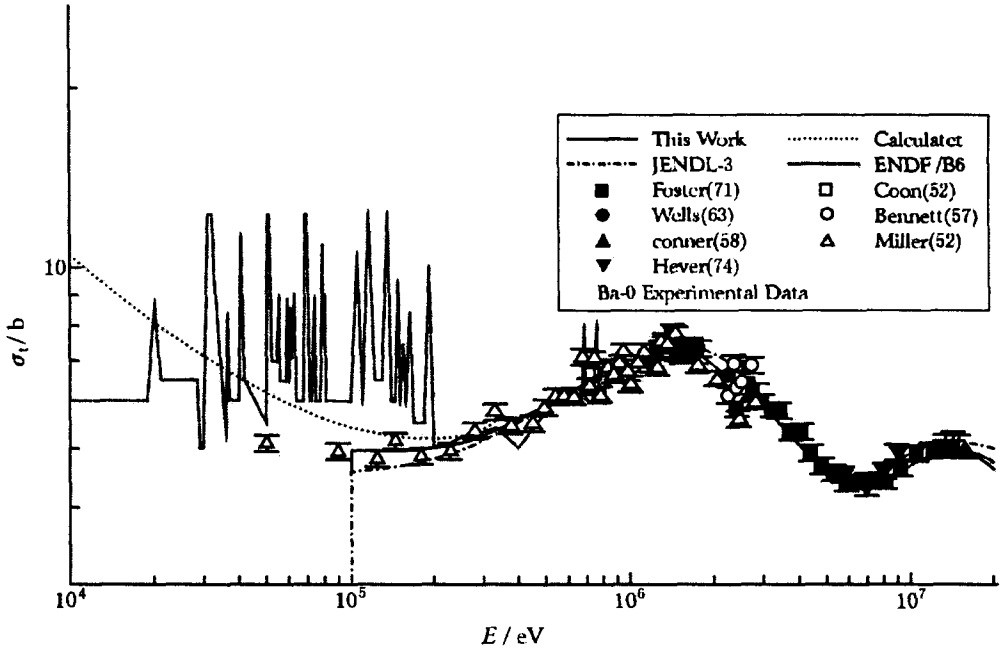

Fig. 1 ^{138}Ba total cross section

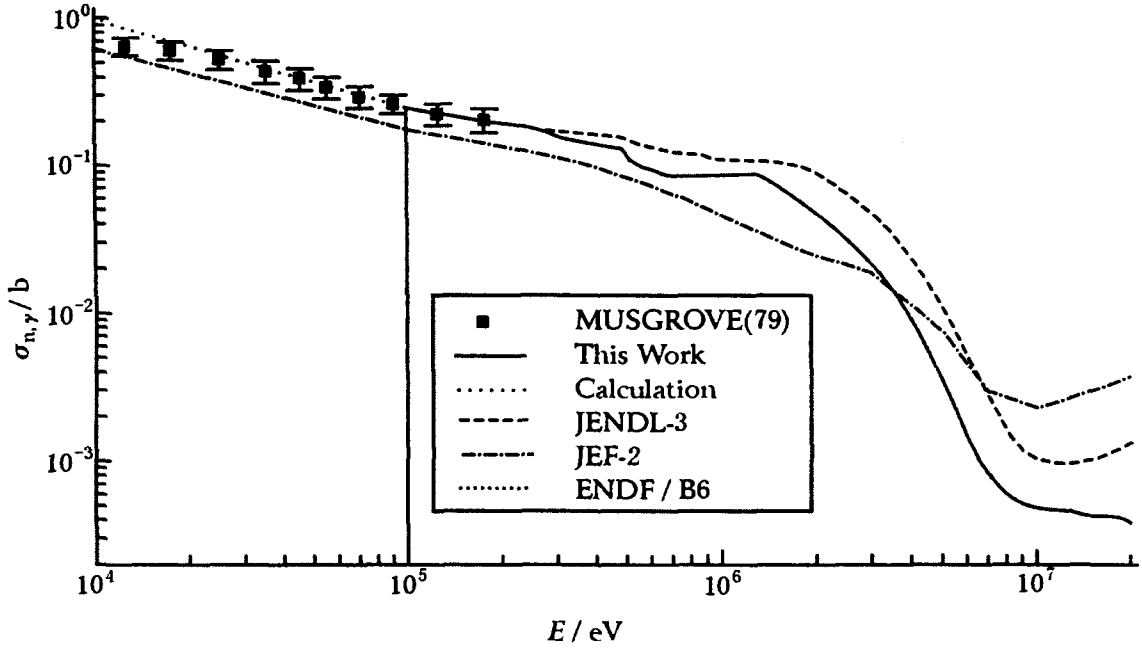

Fig. 2 ^{135}Ba (n,γ) cross section

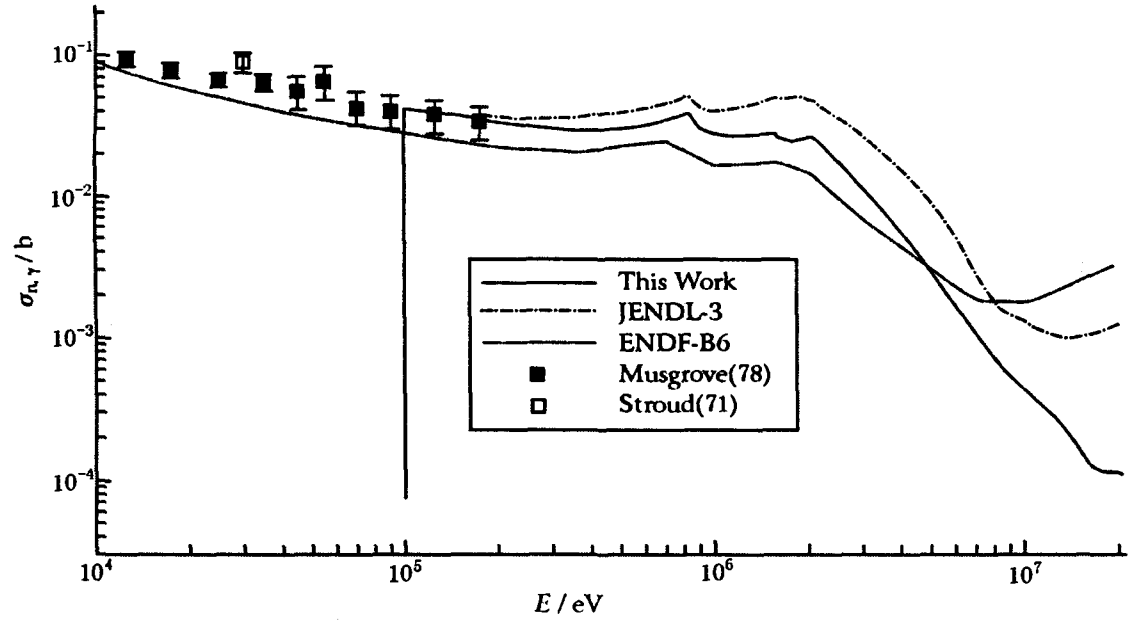

Fig. 3 ^{136}Ba (n,γ) cross section

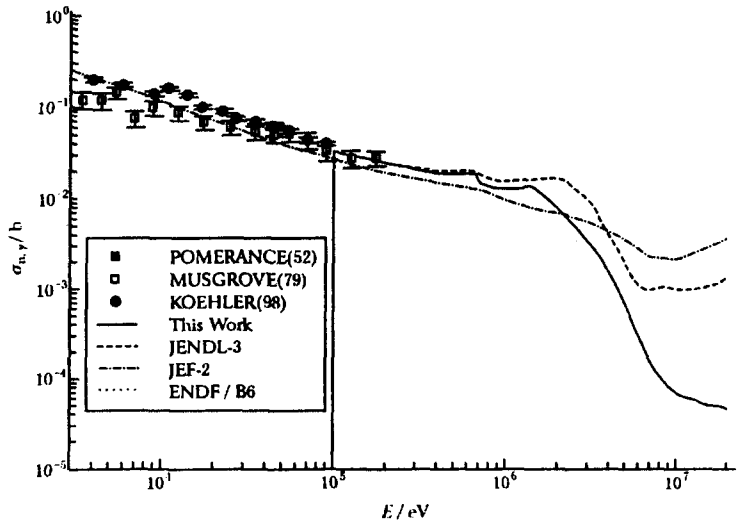

Fig. 4 ^{137}Ba (n,γ) cross section

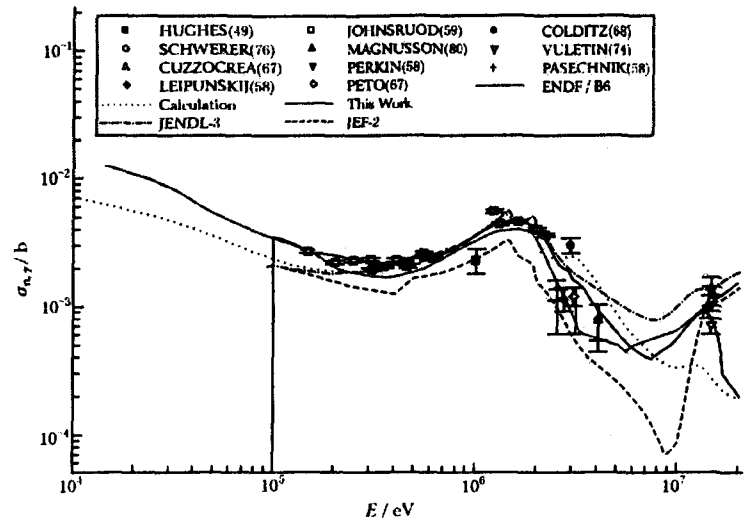

Fig. 5 ^{138}Ba (n,γ) cross section

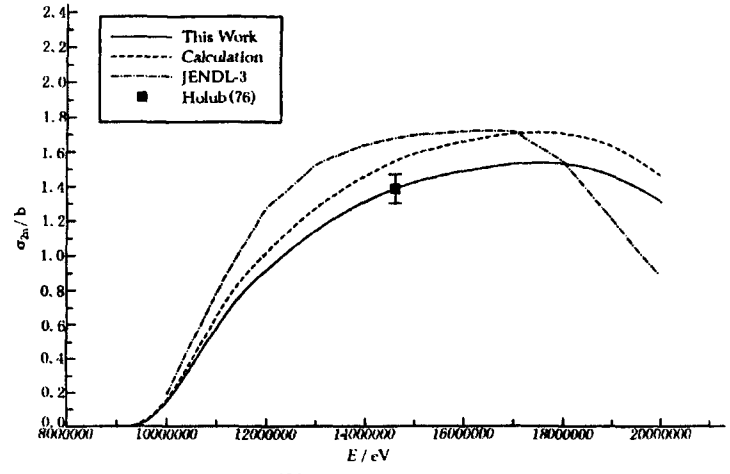

Fig. 6 ^{136}Ba (n,2n) cross section

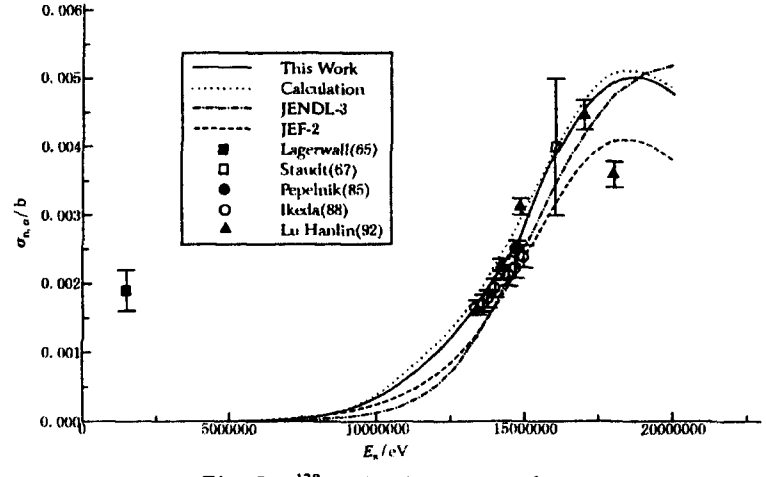

Fig. 7 ^{138}Ba (n,α) cross section

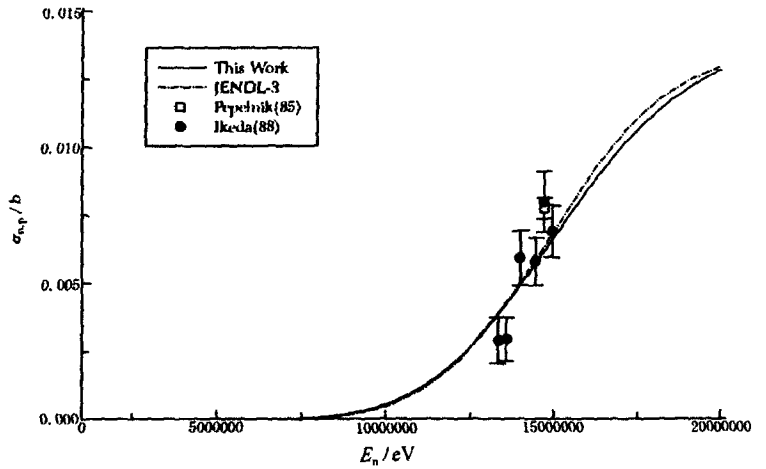

Fig. 8 ^{136}Ba (n,p) cross section

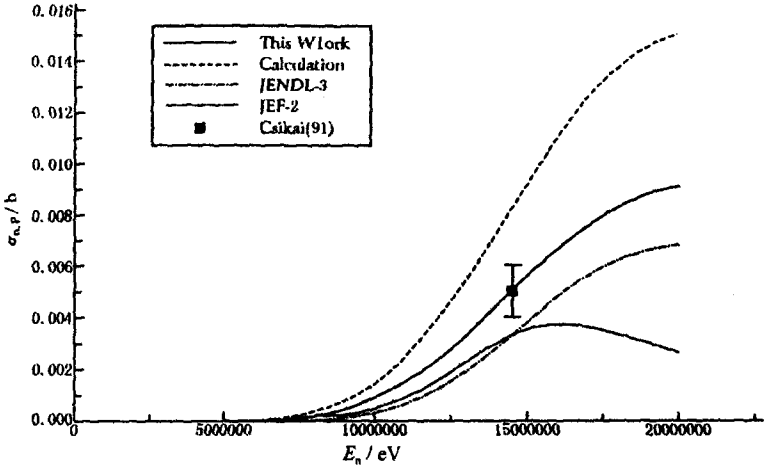

Fig. 9 ^{137}Ba (n,p) cross section

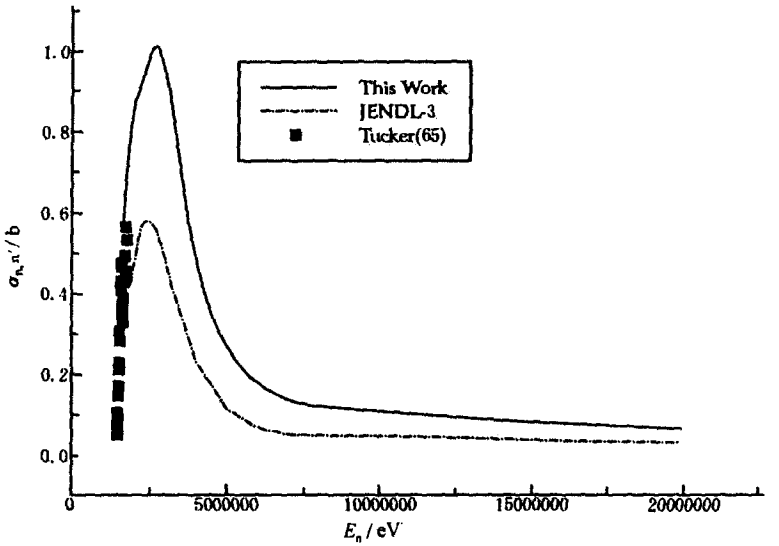

Fig. 10(a) ^{138}Ba (n,n') cross section to the first excite status

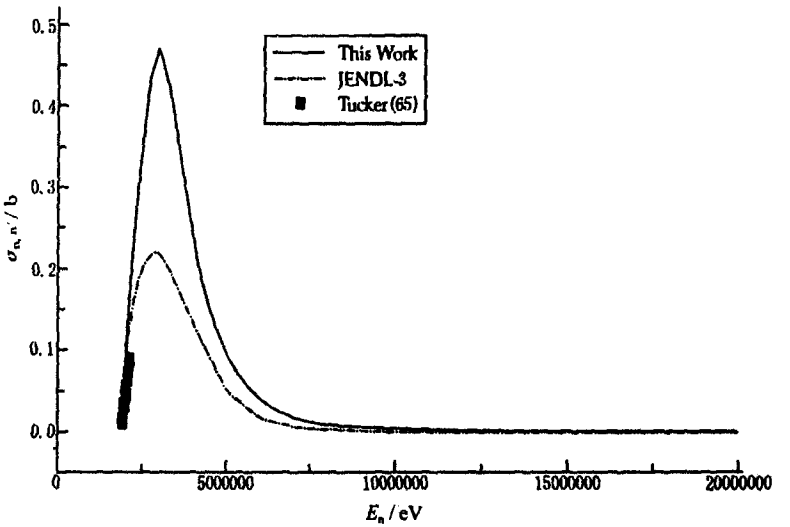

Fig. 10(b) ^{138}Ba (n,n') cross section to the second excite status

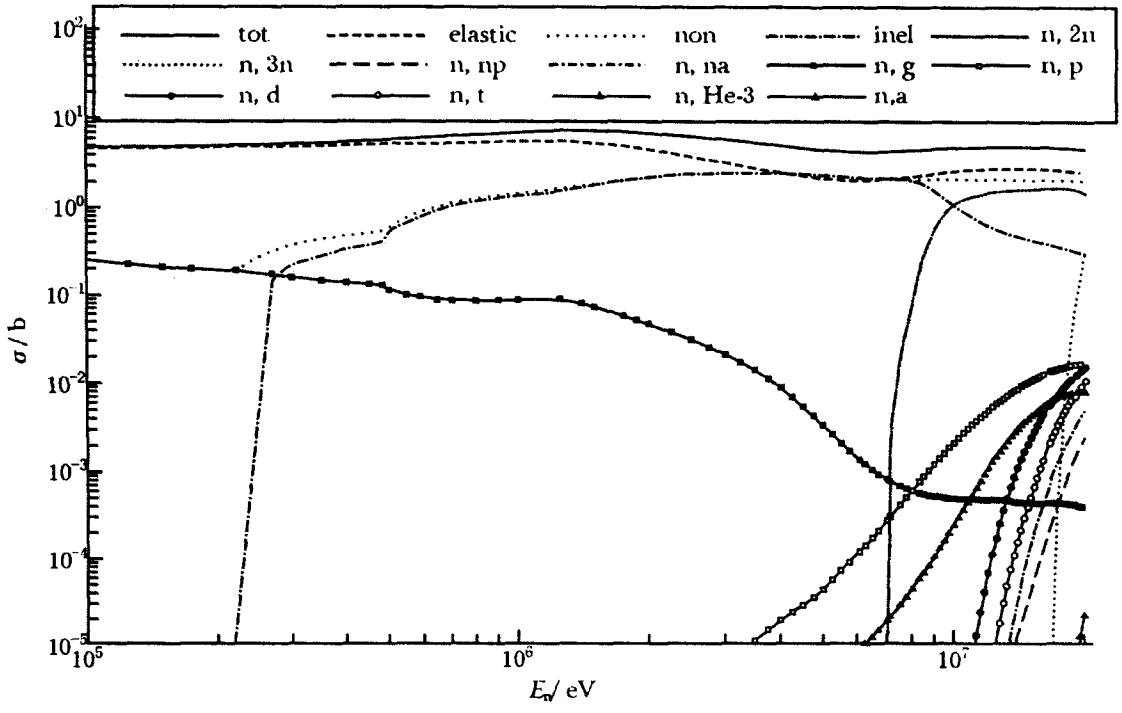

Fig. 11(a) ^{135}Ba cross section

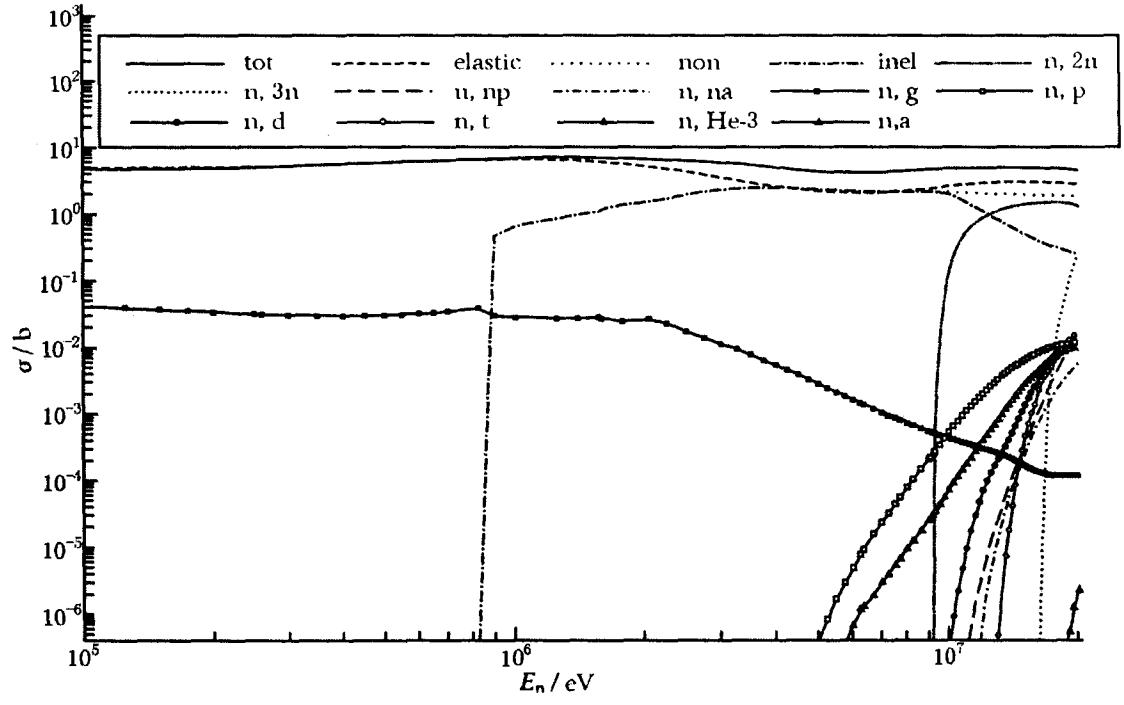

Fig. 11(b) ^{136}Ba cross section

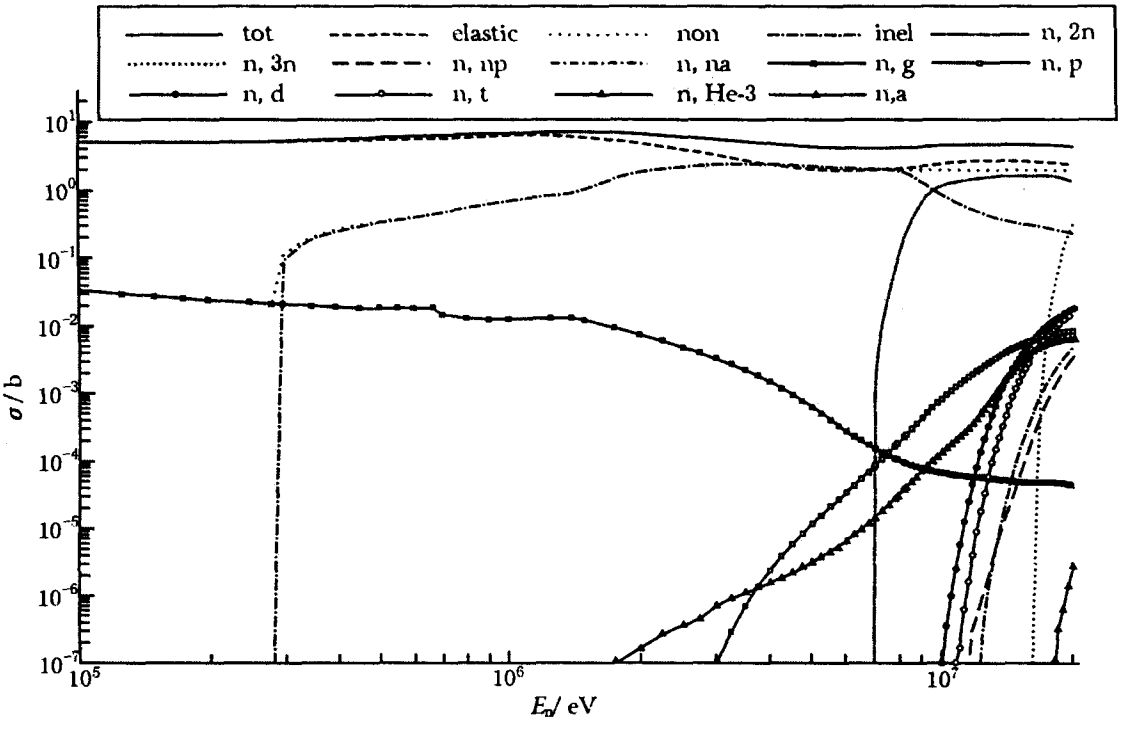

Fig. 11(c) ^{137}Ba cross section

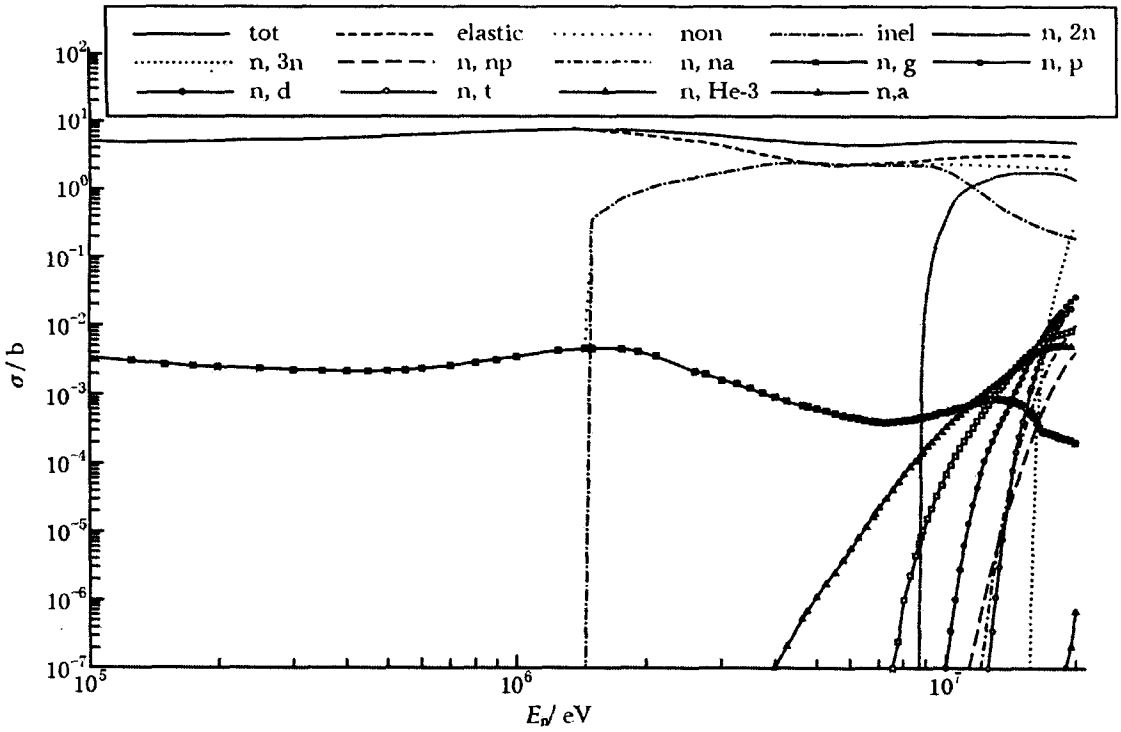

Fig. 11(d) ^{138}Ba cross section

Reference

[1] Zhang Zhengjun. Calculation with code SUNF for Ba isotopes", (to be published)

[2] D.G.Foster et al., Phys.Rev.C,3,576,1971

[3] J.P.Conner, Phys.Rev.,109,1268,1958

[4] R.D.Heuer et al.,1974

[5] J.H.Coon et al., Phys.Rev.,88,562,1952

[6] D.W.Miller et al., Phys.Rev.,88,83, 1952

[7] J.T.Wells et al., Phys.Rev.,131,1644,1963

[8] E.W.Bennett et al., Bull.Am.Phys.Soc., 2,232(X1),1957

[9] L.Musgrove et al., Nucl.Sci. and Eng.,82,(2),230,1982

[10] P.E.Koehler et al., Phys.Rev.,C,57,4,1558,1998

[11] D.B.Stroud et al., Australian AEC reports/Phys.Rev.-34P,9,1971

[12] A.E.Johnsrud et al., Phys.Rev.,116,927,1959

[13] D.J.Hughes et al., Phys.Rev.,75,1781,1949

[14] J.Colditz et al., J,OSA,105,236,1968

[15] A.I.Leipunskij et al., C,58GENEVA,15,50(2219),1958

[16] G.Peto et al., J.Nucl.Energ.,21,797,1967

[17] O.Schwerer et al., Nucl.Phys.,A,264,105,1976

[18] G.Magnusson et al., Phys.Scripta,21,(1),21,1980

[19] P.Cuzzocrea et al., Nuovo Cimento,B,52,(2),476,1967

[20] J.L.Perkin et al., J,PPS,72,505,1958

[21] J.Vuletin et al., Lettere al Nuovo Cimento,10,1,1974

[22] E.Holub et al., J.of Phys.,pt.G,2,405,1976

[23] T.Lagerwall, Zeitschrift f.Naturforschung,A,20,1583,65

[24] G.Staudt, Zeitsch f.Phys.,201,105,1967

[25] Lu Hanlin et al., Chinese J. of Nucl.Phys.,14,(3),244,1992

[26] Y.Ikeda et al., R,JAERI-1312,1988

[27] R.Pepelnik et al., C,85SANTA,1,211(JA46),1985

[28] J.Csikai et al., Annals of nucl. Sci. And Eng.,18,(1),1,1991

[29] A.B.Tucker et al., Phys.Rev.B,137,1181,1965

INTERNATIONAL ATOMIC ENERGY AGENCY

INIS Section

INFORMATION NOTE

Dear User,

We are very sorry but the first page of this article is missing in the original document.

We apologize for the inconvenience caused.

Inquiries should be mailed to:

International Atomic Energy Agency
INIS Section
P. O. Box 100
Wagramerstrasse 5
A-1400 Vienna
Austria

Fax: (+43) 1 26007 or (+43) 1 2600 29882
Phone: (+43) 1 2600 ext. 22866, 22869 or 22870
E-mail: chouse@iaea.org

In the energy range of 0.1 MeV to 1 MeV of (n, γ) reaction, the experimental data are accorded with each other. In the energy range of 1 MeV to 20 MeV, there are five laboratory's data and a great difference among them. The data are given in Table 1:

Table 1 The experimental data of (n, γ) reaction*

Laboratory	Year	Detector	Data		Monitor
			E_n/MeV	δ ± Δ δ /mb	
USAWIS**[2]	1959	Naphthaline Crystal	1.000	41.0	^{154}Sm(n, γ) relative to thermal capture=5.5b
			1.200	41.5	
			1.410	39.5	
			1.800	34.0	
			2.200	23.0	
			2.500	17.0	
			3.300	9.90	
			4.000	6.10	
			4.750	3.90	
			5.500	3.45	
			6.200	2.45	
SF JYU[3]	1976	Ge(Li)	14.7	0.9±0.3	
HUNDEB[4]	1976	Ge(Li)	3.00	19.0±5.0	^{31}P(n, γ)
INDPU[5]	1984	Ge(Li)	1.07	65.8±8.1	^{53}I(n, γ)
			1.48	62.8±5.9	
			1.89	59.8±5.7	
			2.30	36.9±4.6	
			2.85	31.4±4.3	
CCPRI[6]	1987	Ge(Li)	1.0	47±5	^{197}Au(n,γ)
			2.0	22.5±3.1	

* The activation method was used in all the experiments.

** Data were read out in large plot, so no error data given.

From the measured year, the laboratory, the detector and other factors, the SFJYU, HUNDEB, CCPRI's data are more authentic. The INDPU'data are much higher than the others, and out of their error range. The data of USAWIS were made earlier and read out from plot, but the difference among the data and SFJYU, HUNDEB, CCPRI is not large. So the USAWIS, SFJYU, HUNDEB, CCPRI's data are adopted in the fit. The comparisons among calculation data and experimental data, JENDL-3 data, ENDF/B-6 data are given in Fig.2.

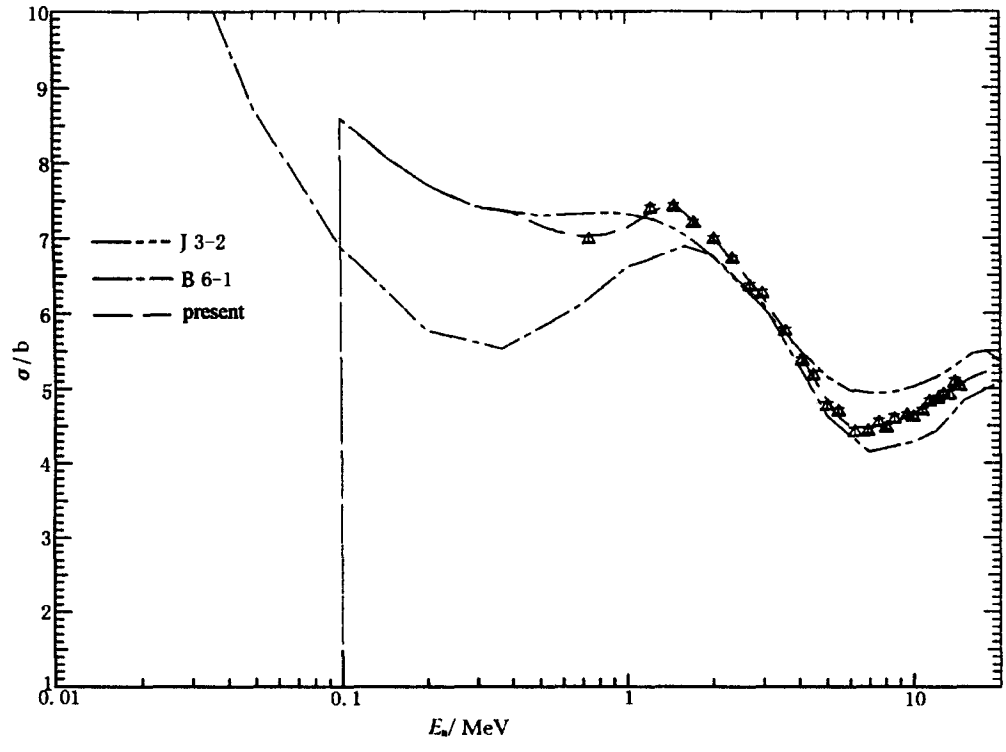

Fig. 1 Total cross section of n+^{148}Sm

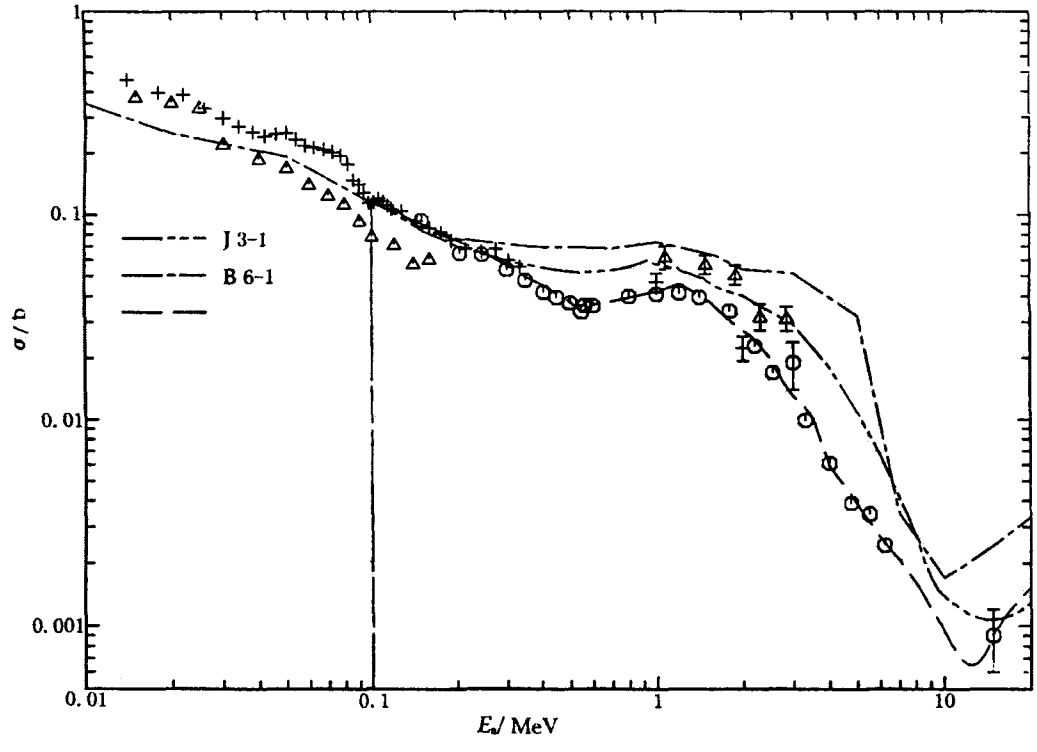

Fig. 2 ^{154}Sm (n,γ) ^{155}Sm cross section

In the end, all of the three nucleus' elastic cross section were revised to make the total section accord with the sum of other cross sections.

References

[1] Shen Qingbiao, Private Communication.

[2] A.E.Johnsrud et al., J, PR, 116, 927(1959).

[3] M.Valkonen, J, JIN, 36, 715, (1974).

[4] G.Peto et al., J, JNE, 21, 797, (1967).

[5] M.Afzal Ansari et al., J, ANE, 13,(5),287,(1986).

[6] Yu.N.Trofimov et al., J, Yk,,(4),,(1987).

Prompt Gamma-ray Absolute Intensity Calculation and Consistence Check of Thermal Neutron Capture

Zhou Chunmei

(China Nuclear Data Center)

Abstract

How to calculate the prompt gamma-ray emission probability (absolute intensity) of thermal-neutron capture is briefly introduced. The examples are given to illustrate their applications. The physical consistent checking and some discussions are also given.

Introduction

A nuclide ${}^{A}_{Z}\mathrm{X}$ (X--element symbol, A--nuclear mass number, Z--nuclear proton number) captures a thermal-neutron and forms a compound nuclide ${}^{A+1}_{Z}\mathrm{X}$ with high-excitation energy S(n) (equil to neutron binding energy); then it decays by

means of emitting gamma-rays called as prompt gamma-ray, and finally decays in to its ground state. In general, the prompt decay gamma-rays can be divided into three kinds as follows: a), primary gamma-rays from captured state, b) secondary gamma-rays from other excited states below captured state, c)gamma-rays of decaying to its ground state (sometime including primary and secondary gamma-rays).

From these prompt gamma-ray measurements, (n,γ) reaction mechanism and nuclear structure can be known, and neutron-induced prompt gamma activation analysis (PGAA) can also be done.

The availability of high-quality guided (or filtered) thermal and cold neutron beams at high and medium flux research reactors, also in developing counties, has greatly facilitated the furthering of the PGAA method.

In the experimental measurements, relative prompt gamma-ray intensities are measured. In the practical applications, prompt gamma-ray absolute intensities (emission probabilities) should be known. In general, the prompt gamma-ray emission probabilities per 100 neutron captures must be given for PGAA application.

The calculation methods of prompt gamma-ray intensities for thermal-neutron capture and their practical applications are introduced. The physical consistent checking and some discussion are also given.

1 Calculation Methods

Main and general methods of thermal-neutron capture prompt gamma-ray intensity calculation are summarized as follows:

1.1 Calculation from Gamma-ray Decaying to Ground State

When a nuclide captures a thermal-neutron, the gamma-rays decay in to its ground state, as shown in Fig. 1. If there are m gamma-rays decaying to ground state, I_k is the relative intensity for the k-th gamma-ray, α_k is its internal conversion coefficient, the equation can be written as follows,

$$N\sum_{k=1}^{m} I_k(1+\alpha_k) = 100 \tag{1}$$

were N is normalization factor for gamma-ray emission probability per 100 neutron captures,

$$N = 100 / \sum_{k=1}^{m} I_k (1 + \alpha_k) \tag{2}$$

For light nuclides, the internal conversion coefficient α_k is quite small and can be neglected, so

$$N = 100 / \sum_{k=1}^{m} I_k \tag{3}$$

From Eq. (2) or (3), normalization factor N, and then, absolute gamma-ray emission probabilities for thermal-neutron capture can be calculated.

The relative gamma-ray data[1] for ^{26}Mg(n,γ) E_n=thermal are given in Ttable 1 and its decay scheme is shown in Fig. 2. In Table 1, the gamma-ray energies, their relative intensities and levels are given, from which, using Eq. (3) formula, N(=2.584) was calculated, and the absolute gamma-ray decay intensities also can be calculated , as shown in Fig. 2.

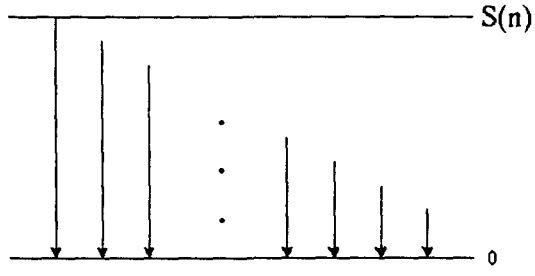

Fig. 1 Skeleton scheme of gamma-ray decaying to ground state from high excitation state

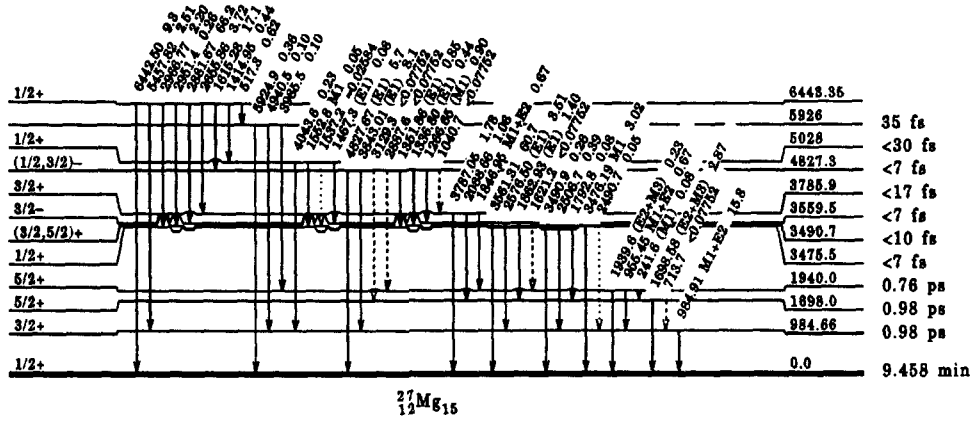

Fig. 2 Decay scheme and gamma-ray intensity from ^{26}Mg(n,γ) thermal neutron reaction

Table 1 Prompt gamma-ray data from $^{26}Mg(n,\gamma)$ thermal neutron reaction

E_γ/keV	E(level)/keV	I_γ*	Mult.**	δ**
241.6 4	1940.0 1	0.03 1	(M1)	
517.3 3	6443.35 4	0.24 3		
713.7	1698.0 1	<0.03		
955.45 8	1940.0 1	0.26 3	M1+E2	−0.08 6
984.91 3	984.66 8	6.1 3	M1+E2	+0.02 2
1040.7	4827.3 4	<0.03		
1266.65 18	4827.3 4	0.35 3	(M1)	
1336.80 20	4827.3 4	0.17 2	(E1)	
1351.86 8	4827.3 4	0.33 3	(E1)	
1414.95 18	6443.35 4	0.17 2		
1467.3 5	5028 1	0.03 1	(E1)	
(1537.2)	5028 1	≈0.01		
1552.8 7	5028 1	0.02 1	M1	
1615.28 5	6443.35 4	6.6 3		
1621.2	3559.5 1	<0.03		
1698.58 5	1698.0 1	1.11 7	(E2+M3)	≈0.0
1792.8 3	3490.7 7	0.03 1		
1846.95 18	3785.9 4	0.26 3	M1+E2	−0.0 3
1862.93 10	3559.5 1	0.54 4	(E1)	
1939.6 4	1940.0 1	0.09 2	(E2+M3)	≈0.0
2088.66 11	3785.9 4	0.41 3		
(2490.7)	3475.5 2	0.02 1		
2506.7 23	3490.7 7	0.15 2		
2576.50 6	3559.5 1	1.36 8	(E1)	
2655.86 6	6443.35 4	1.44 7		
2881.67 4	6443.35 4	25.6 8		
2887.6	4827.3 4	<0.03		
2951.4 4	6443.35 4	0.10 2		
2966.77 22	6443.35 4	0.85 6		
3129.3	4827.3 4	<0.03		
3476.19 9	3475.5 2	1.17 6	M1	
3490.9 6	3490.7 7	0.10 2		
3561.31 4	3559.5 1	23.5 7		
3787.05 15	3785.9 4	0.69 6		
3843.01 8	4827.3 4	3.14 16	(E1)	
3985.5 6	5926 2	0.04 1		
4043.6 3	5028 1	0.09 2		
4827.67 6	4827.3 4	2.20 13	(E1)	
4940.5 3	5926 2	0.04 1		
5457.82 15	6443.35 4	0.97 7		
5924.9 4	5926 2	0.14 2		
6442.50 6	6443.35 4	3.59 17		

* Relative intensity.

** Multipolarity and its mixture ratio for gamma-ray.

1.2 Calculation from Primary Gamma-ray Decaying from Capture State

When a nuclide captures a thermal-neutron, the nuclide is deexcited from its capture state by mean of decaying primary gamma-rays, as shown in Fig. 3. Suppose that there is n primary gamma-rays, j_i is the relative intensity of i-th primary gamma-ray and α_i is its internal conversion coefficient of i-th primary gamma-ray, then,

$$N\sum_{i=1}^{m} j_i(1+\alpha_i)=100 \tag{4}$$

$$N=100/\sum_{i=1}^{m} j_i(1+\alpha_i) \tag{5}$$

And for light nuclide, Eq. (5) becomes

$$N=100/\sum_{i=1}^{m} j_i \tag{6}$$

The primary gamma-ray data[2,3] for ^{28}Si(n,γ) E_n=thermal are listed in Table 2, and their decay scheme is given in the Fig. 4. From table 2, the normalization factor N(0.5917) and the gamma-ray absolute decay intensities for each gamma-ray can be calculated, as shown in Fig. 4.

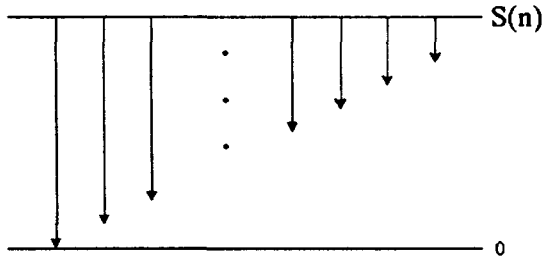

Fig. 3 Skeleton scheme of primary gamma-rays from captured state

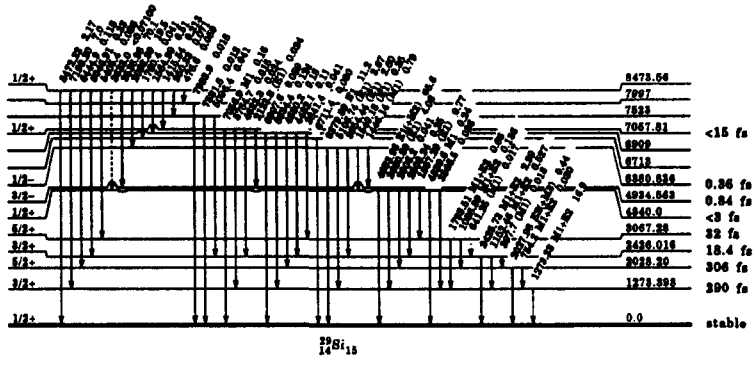

Fig. 4 Decay scheme and gamma-ray intensity from ^{28}Si(n,γ) thermal neutron reaction

Table 2 Prompt gamma-ray data from $^{28}Si(n,\gamma)$ thermal neutron reaction

E_γ/keV		E(level)/keV		I_γ*		Mult.**	δ**	
397.7	4	2426.016	15	0.03	1	(M1)		
476.6	3	8473.56	3	0.10	2			
(641.25)		3067.28	8	0.029	15	(M1)		
754.2	4	2028.20	6	0.05	2	M1+E2	−0.03	3
950.33	13	8473.56	3	0.12	2			
1038.89	10	3067.28	8	0.23	3	M1+E2	+0.04	2
x1071.0	5			0.08	2			
1152.46	6	2426.016	15	0.89	4	M1+E2	+0.09	8
1273.33	3	1273.398	11	28.5	14	M1+E2	+0.197	9
1415.54	9	8473.56	3	0.36	4			
1446.14	4	6380.836	13	1.34	5	(M1)		
1540.18	6	6380.836	13	0.59	5	(E1)		
1564.99	5	8473.56	3	0.87	6			
1760.4	5	8473.56	3	0.07	2			
1793.51	4	3067.28	8	1.12	6	M1+E2	+0.26	2
1867.29	5	4934.563	13	1.30	6	(E1)		
2027.98	9	2028.20	6	0.74	7	E2(+M3)	0.0	
2092.89	3	8473.56	3	33.0	12			
2123.8	6	7057.81	17	0.04	1	(E1)		
2425.73	4	2426.016	15	5.06	20	M1+E2	−0.32	7
2508.24	13	4934.563	13	0.42	5			
2906.2	5	4934.563	13	0.07	2			
3538.98	4	8473.56	3	118.5	36			
3566.5	5	4840.0	4	0.06	2			
3633.0		8473.56	3	<0.12				
3660.80	6	4934.563	13	6.9	3	(E1)		
3841.4	6	6909		0.07	2			
3954.44	5	6380.836	13	4.4	3	(E1)		
4482.1	4	6909		0.18	5			
4632.3	7	7057.81	17	0.04	2			
4839.6	4	4840.0	4	0.40	5	M1		
4880.2	5	6909		0.30	5			
4933.98	3	4934.563	13	110.8	34	E1(+M2)	−0.05	10
5096.4	7	7523		0.07	2			
5106.74	6	6380.836	13	6.2	3	(E1)		
5405.4	9	8473.56	3	0.06	2			
5634.4	4	6909		0.21	3			
5784.7	7	7057.81	17	0.03	1			
6046.91	16	8473.56	3	0.55	6			
6379.80	4	6380.836	13	19.0	10	E1		
6444.9	5	8473.56	3	0.20	4			
6711.4	9	6713		0.05	2			
6907.6	7	6909		0.10	3			
7056.9	4	7057.81	17	0.27	5	M1		
7199.20	5	8473.56	3	11.9	5			
7521.8	9	7523		0.02	1			
7993.9	9	7997		0.03	1			
8472.22	7	8473.56	3	3.66	20			

* Relative intensity. ** Multipolarity and its mixture ratio for gamma-ray.

x Unplaced in level scheme

2 Physical Consistent Check

The most important is the physical consistent check of intensity balance check for each levels.

For decay gamma-ray to ground state, the Eq. (1) becomes

$$\sum_{k=1}^{m} I_k(1+\alpha_k) = 100/N \tag{7}$$

For primary gamma-ray from captured state, the Eq. (4) becomes as follows,

$$\sum_{i=1}^{n} J_i(1+\alpha_i) = 100/N \tag{8}$$

from Eq. (7) and (8), Eq.(9) can be got as,

$$\sum_{i=1}^{n} J_i(1+\alpha_i) \approx \sum_{k=1}^{m} I_k(1+\alpha_k) \tag{9}$$

The Eq. (9) is correct within their uncertainty range. For other levels, in addition to captured state and ground state, the intensities coming into and going out the level j are the same within thier uncertainty range, as shown in Fig. 5.

$$\sum_{j=1}^{m} I_{jin}(1+\alpha_{jin}) - \sum_{j=1}^{n} I_{jou}(1+\alpha_{jou}) \approx 0 \tag{10}$$

In formula (10), I_{jin}, α_{jin}, I_{jou}, and α_{jou} are gamma-ray relative intensities and their internal conversion coefficients for coming into and going out level J respectively.

In Table 3, the calculation and checking results of intensity balance for each levels from ^{28}Si(n,γ) reaction are given. From Table 3 it can be seen that the intensities are consistent within their uncertainties.

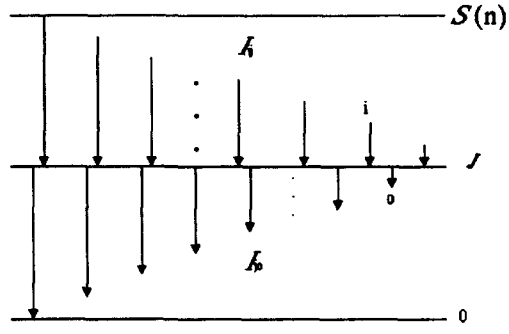

Fig. 5 Skeleton scheme of intensity balance calculation for excitation level

Table 3 Calculation and checking results of intensity balance from ^{28}Si(n,γ) reaction at E_n=thermal

	RI[@]						TI[#]						NET FEEDING[*]	
LEVEL	(OUT)		(IN)		(NET)		(OUT)		(IN)		(NET)		(CALC)	
0	0.000		169	4	−169	4	0.000		169	4	−169	4	0.2 23	
1273.398 11	28.5	14	27.4	7	1.1	16	28.5	14	27.4	7	1.1 16		0.7 10	
2028.20 6	0.79	8	0.83	8	−0.04	11	0.79	8	0.83	8	−0.04	11	−0.02	7
2426.016 15	5.98	21	5.7	4	0.3	4	5.98	21	5.7	4	0.3	4	0.17 23	
3067.28 8	1.38	7	1.43	7	−0.05	10	1.38	7	1.43	7	−0.05	10	−0.03	6
4840.0 4	0.46	6	0.59	5	−0.13	8	0.46	6	0.59	5	−0.13	8	−0.08	5
4934.563 13	119	4	120	4	0	5	119	4	120	4	0	5	0 3	
6380.836 13	31.5	11	33.0	12	−1.5	17	31.5	11	33.0	12	−1.5	17	−0.9	10
6713	0.050	20	0.070	20	−0.02	3	0.050	20	0.070	20	−0.02	3	−0.012	17
6909	0.86	9	0.87	6	−0.01	11	0.86	9	0.87	6	−0.01	11	−0.01	7
7057.81 17	0.38	6	0.36	4	0.02	7	0.38	6	0.36	4	0.02	7	0.01	4
7523	0.090	23	0.120	20	−0.03	3	0.090	23	0.120	20	−0.03	3	−0.018	18
7997	0.030	10	0.100	20	−0.070	23	0.030	10	0.100	20	−0.070	23	−0.041	14
8473.56 3	169	4	0.000		169	4	169	4	0.000		169	4	100.3	23

[@], relative intensity. [#], relative intensity including internal conversion. [*], absolute intensity balance.

3 Discussion

In general, neutron binding energy is high, and captured state is a high excitation state and its decay scheme is quite complex. A lot of weak-intensity gamma-ray are unable to be measured experimentally. Besides, measured uncertainties from background deducting and gamma-spectra analysis lead to gamma-ray intensity uncertainties. Strictly speaking, intensities of coming into and going out a level are unable to be exactly same, only can be consistent within their uncertainties. The normalization factors from primary gamma-rays from captured state and decay gamma-rays to ground state are different since above reasons. In the data evaluation, normalization factor in thermal-neutron capture reaction is usually calculated from the gamma-rays of decay to ground state.

References

[1] S.Raman, et al., Phys.Rev. C46, 972 (1992)

[2] N.A.Islam, et al., Phys.Rev. C41, 1272 (1990)

[3] T.A.Walkiewiez, et al., Phys.Rev. C45, 1597 (1992)

CN0101657

Prompt Gamma-ray Data Evaluation of Thermal Neutron Capture for A=20~35

Zhou Chunmei
(China Nuclear Data Center)

The prompt gamma-ray data and their decay schemes of thermal-neutron capture for stable nuclei with mass number A=20~35 (^{20}Ne, ^{21}Ne, ^{22}Ne, ^{23}Na, ^{24}Mg, ^{25}Mg, ^{26}Mg, ^{27}Al, ^{28}Si, ^{29}Si, ^{30}Si, ^{31}P, ^{32}S, ^{33}S, ^{34}S, ^{35}Cl) have been evaluated with the method and programs as before[1]. The evaluated data have been changed into ENSDF format and checked in Physics and ENSDF format.

Reference

[1] Zhou Chunmei, CNDP, 22, 76 (1999)

CN0101658

Nuclear Data Sheets for A = 62 and 63

Huo Junde
(Department of Physics, Jilin University, Changchun 130023)

The 1989 evaluation of A=62 (90Ki08)[1] and 1991 evaluation of A=63 (91Ki10)[2] have been revised using available experimental decay and reaction data since the last evaluations.

In this A=62 updated evaluation there are some new data and reactions, such as $T_{1/2}$ for ^{62}Cr, ^{208}Pb(^{64}Ni, Xγ) for ^{62}Fe, ^{60}Ni(α, ^{2}He) and ^{60}Ni(^{12}C, ^{10}C) for ^{62}Ni, ^{50}Cr(^{16}O,

3pnγ) for ^{62}Cu, ^{60}Ni (^{12}C, ^{10}Be) and ^{40}Ca (^{28}Si, α2pγ) for ^{62}Zn, and ^{40}Ca (HI, Xγ) for ^{62}Ga, specifically.

In this A=63 reevaluation there are some new data and reactions, such as $T_{1/2}$ for ^{63}Cr and ^{63}Mn, ^{18}O (^{48}Ca, p2nγ) and ^{64}Ni (d, ^{3}Heγ) for ^{63}Co, ^{40}Ca (^{28}Si, 5pγ) and ^{64}Zn (d, ^{3}Heγ) for ^{63}Cu, ^{40}Ca (^{28}Si, 4pnγ) and ^{50}Cr (^{16}O, 2pnγ) for ^{63}Zn, and ^{40}Ca (^{28}Si, αpγ), ^{40}Ca (^{32}S, 2αpγ) for ^{63}Ga, specifically.

The detailed level schemes and decay schemes, and experimental reaction and decay data for A=62 and 63 are summarized and presented.

Updated evaluations of nuclear data sheets for A=62 and 63 have been sent to National Nuclear Data Center, USA, and will be published in 《Nuclear Data Sheets》.

Reference

[1] M. M. King, Nuclear Data Sheets, 60, 337 (1990)

[2] M. M. King, Nuclear Data Sheets, 64, 815 (1991)

IV SYSTEMATICS RESEARCH

Investigation on the Systematic Behavior of Isomeric Cross Section Ratios of Neutron-Induced Reactions around 14MeV

Huang Xiaolong
(China Nuclear Data Center, CIAE)

Introduction

In a nuclear reaction where the residual nucleus leaves at an excited level with a measurable half-life, we call this level as isomer state. And generally the extent, to which each isomer is populated in the reaction, can be characterized by the isomeric cross section ratios. Experimental and theoretical studies on the isomeric cross section ratios can provide some useful information on the spin-cutoff parameter as well as on the level structure of the product nucleus. Besides the significance in fundamental studies, the isomeric cross section ratios are also of some practical importance. For example, the data are primarily needed in reactor technology.

Since isomers differ in their spin, it is possible to calculate these cross section ratios theoretically using the spin density relation based on the statistical theory. But in cases where experimental measurements are extremely tedious or scarce, the systematics, if used with caution, could provide useful information for the isomeric cross section ratios. At present, systematics is ideally suited for study in isomeric cross section ratios, because the experimental data especially as a function of projectile energy are not enough available. There are also deficiencies in nuclear model calculations. For example variations in input model parameters and input level structure of the residual nucleus may cause appreciable changes in the calculated data.

In this paper, the isomeric cross section ratios ($R=\sigma^m/(\sigma^m+\sigma^g)$) for neutron-induced reactions around 14 MeV are systematic ally analyzed briefly. It's expected that such analysis could provide some helpful information in the systematic studies.

1 Systematic Analysis

The possible nuclear reactions induced by 14 MeV neutrons include (n,γ), (n,n'), (n,2n), (n,3n), (n,p), (n,d), (n,t), (n, ^{3}He), (n,α), (n,2p), (n,np) and in the heavy target mass nucleus, (n,f) processes. In most cases, (n,p), (n,α) and (n,2n) reactions are the strongest; the (n,^{3}He) and (n,2p) reactions are weak. In present work we restrict our discussion to these reactions, where the isomeric state has a half-life larger than 1 second. At the same time their experimental cross sections (σ^t,σ^m and σ^g) must be measured by the same laboratory or authors. In Table 1 are listed all isomeric states collected by us with such conditions and their relevant properties, and also gives the calculated or directly measured isomeric cross section ratios.

Table 1 Isomeric cross section ratio R for neutron-induced reactions at E_n ~14MeV

Reactions	Target			J_m	J_g	R	Ref.(EXFOR Acc. No.)	
	A	$(N-Z)/A$	J_t				a)	b)
^{153}Eu(n,2n)^{152m1}Eu	153	0.1765	5/2+	0–	3–	0.2115	20541.027	20541.029
^{159}Tb(n,2n)^{158}Tb	159	0.1824	3/2+	0–	3–	0.2504	20541.036	20541.038
^{151}Eu(n,2n)^{150}Eu	151	0.1656	5/2+	0–	5–	0.27	20541.023	20541.024
^{80}Se(n,α)^{77}Ge	80	0.15	0+	1/2–	7/2+	0.3056	31496.013	31496.012
^{105}Pd(n,p)^{105}Rh	105	0.1238	5/2+	1/2–	7/2+	0.3151	30336.030	30336.029
^{165}Ho(n,p)^{165}Dy	165	0.1879	7/2–	1/2–	7/2+	0.0244	20289.009	20289.008
^{168}Er(n,α)^{165}Dy	168	0.1905	0+	1/2–	7/2+	0.6667	12033.045	12033.044
^{180}W(n,2n)^{179}W	180	0.1778	0+	1/2–	7/2–	0.2626	20668.003	20668.002
^{86}Sr(n,2n)^{85}Sr	86	0.1163	0+	1/2–	9/2+	0.2854	30348.005	30348.003
^{90}Zr(n,2n)^{89}Zr	90	0.1111	0+	1/2–	9/2+	0.2948	10088.018	10088.017
^{92}Mo(n,α)^{89}Zr	92	0.087	0+	1/2–	9/2+	0.2795	41240.043	41240.042
^{92}Mo(n,2n)^{91}Mo	92	0.087	0+	1/2–	9/2+	0.2	30014.008	30014.007
^{95}Mo(n,p)^{95}Nb	95	0.1158	5/2+	1/2–	9/2+	0.2693	22125.005	22125.006
^{96}Mo(n,x)^{95}Nb	96	0.125	0+	1/2–	9/2+	0.27	21935.008	21935.007
^{96}Ru(n,x)^{95}Tc	96	0.0833	0+	1/2–	9/2+	0.2754	10214.024	10214.025
^{97}Mo(n,p)^{97}Nb	97	0.134	5/2+	1/2–	9/2+	0.2562	22089.079	22089.078
^{98}Mo(n,x)^{97}Nb	98	0.1429	0+	1/2–	9/2+	0.3481	22089.083	22089.082
^{117}Sn(n,p)^{117}In	117	0.1453	1/2+	1/2–	9/2+	0.3243	30136.009	30136.007
^{119}Sn(n,p)^{119}In	119	0.16	1/2+	1/2–	9/2+	0.4619	22280.016	22280.017
^{184}Os(n,2n)^{183}Os	184	0.1739	0+	1/2–	9/2+	0.3351	30290.003	30290.004
^{46}Ti(n,p)^{46}Sc	46	0.0435	0+	1–	4+	0.29		20721.089
^{170}Er(n,p)^{170}Ho	170	0.2	0+	1+	6+	0.8433	20860.009	20860.010

Continue Table 1

Reactions	Target			J_m	J_g	R	Ref.(EXFOR Acc. No.)	
	A	$(N-Z)/A$	J_t				a)	b)
^{237}Np(n,2n)^{236}Np	237	0.2152	5/2+	1	6–	0.7407		10408.002
^{74}Se(n,2n)^{73}Se	74	0.0811	0+	3/2–	9/2+	0.5353	20614.004	20614.005
^{192}Os(n,2n)^{191}Os	192	0.2083	0+	3/2–	9/2–	0.5354	Q	Q
^{60}Ni(n,p)^{60}Co	60	0.0667	0+	2+	5+	0.52	20390.007	20390.008
^{63}Cu(n,α)^{60}Co	63	0.0794	3/2–	2+	5+	0.68	20390.010	20390.009
^{93}Nb(n,2n)^{92}Nb	93	0.1183	9/2+	2+	7+	0.3099	30348.011	30348.009
^{112}Sn(n,t)^{110}In	112	0.1071	0+	2+	7+	0.541	10806.004	10806.004
^{35}Cl(n,2n)^{34}Cl	35	0.0286	3/2+	3+	0+	0.8172	Q	Q
^{75}As(n, p)^{75}Ge	75	0.12	3/2–	7/2+	1/2–	0.91	20303.008	20303.009
^{76}Ge(n,2n)^{75}Ge	76	0.1579	0+	7/2+	1/2–	0.84	30286.004	30286.003
^{78}Se(n,2n)^{77}Se	78	0.1282	0+	7/2+	1/2–	0.7		30154.009
^{81}Br(n,p)^{81}Se	81	0.1358	3/2–	7/2+	1/2–	0.6905	40009.029	40009.028
^{82}Se(n,2n)^{81}Se	82	0.1707	0+	7/2+	1/2–	0.7989	11722.014	11722.013
^{80}Kr(n,2n)^{79}Kr	80	0.1	0+	7/2+	1/2–	0.5123	11884.005	11884.003
^{112}Sn(n,p)^{112}In	112	0.1071	0+	4+	1+	0.8753	41032.007	41032.008
^{113}In(n,2n)^{112}In	113	0.1327	9/2+	4+	1+	0.8288	10214.010	10214.011
^{72}Ge(n, α)^{69}Zn	72	0.1111	0+	9/2+	1/2–	0.5655	40009.017	40009.012
^{69}Ga(n, p)^{69}Zn	69	0.1015	3/2–	9/2+	1/2–	0.5526	21291.007	21291.005
^{70}Zn(n, 2n)^{69}Zn	70	0.1429	0+	9/2+	1/2–	0.5608	Q	Q
^{71}Ga(n, p)^{71}Zn	71	0.1268	3/2–	9/2+	1/2–	0.6098	20721.062	20721.061
^{74}Ge(n,α)^{71}Zn	74	0.1351	0+	9/2+	1/2–	0.541	40009.019	40009.018
^{91}Zr(n,p)^{91}Y	91	0.1209	5/2+	9/2+	1/2–	0.5521	11896.009	11896.007
^{92}Zr(n,x)^{91}Y	92	0.1304	0+	9/2+	1/2–	0.5333	21784.008	21784.007
^{126}Xe(n,2n)^{125}Xe	126	0.1429	0+	9/2–	1/2+	0.5166	11884.013	11884.012
^{128}Xe(n,2n)^{127}Xe	128	0.1563	0+	9/2–	1/2+	0.549	11884.014	11884.015
^{70}Zn(n,p)^{70}Cu	70	0.1429	0+	5–	1+	0.5857	21976.023	21976.022
^{81}Br(n,2n)^{80}Br	81	0.1358	3/2–	5–	1+	0.6209	20106.012	20106.013
^{98}Mo(n,p)^{98}Nb	98	0.1429	0+	5+	1+	0.8571	31281.002	31281.003
^{114}Sn(n,p)^{114}In	114	0.1404	0+	5+	1+	0.6866	41032.010	41032.011
^{115}In(n,2n)^{114}In	115	0.1478	9/2+	5+	1+	0.7285	30285.002	30285.003
^{116}Sn(n,p)^{116}In	116	0.1379	0+	5+	1+	0.5652		12003.002
^{59}Co(n,2n)^{58}Co	59	0.0847	7/2–	5+	2+	0.6078		11755.002
^{58}Ni(n,p)^{58}Co	58	0.0345	0+	5+	2+	0.5455	30604.003	30604.004
^{62}Ni(n,p)^{62}Co	62	0.0968	0+	5+	2+	0.5294	30644.012	30644.011
^{65}Cu(n,α)^{62}Co	65	0.1077	3/2–	5+	2+	0.5413	31432.005	31432.003
^{116}Cd(n,p)^{116}Ag	116	0.1724	0+	5+	2–	0.368	21976.039	21976.038
^{128}Te(n,p)^{128}Sb	128	0.1875	0+	5+	8–	0.5	20540.021	20540.022
^{130}Te(n,p)^{130}Sb	130	0.2	0+	5+	8–	0.5207	20540.024	20540.025
^{115}In(n,p)^{115}Cd	115	0.1478	9/2+	11/2–	1/2+	0.543	40999.002	40999.003
^{118}Sn(n,α)^{115}Cd	118	0.1525	0+	11/2–	1/2+	0.5968		10357.003
^{116}Cd(n,2n)^{115}Cd	116	0.1724	0+	11/2–	1/2+	0.4945	11645.019	11645.017
^{120}Sn(n,α)^{117}Cd	120	0.1667	0+	11/2–	1/2+	0.5013	22089.096	22089.095
^{120}Te(n,2n)^{119}Te	120	0.1333	0+	11/2–	1/2+	0.4978	21300.021	21300.020
^{122}Te(n,2n)^{121}Te	122	0.1475	0+	11/2–	1/2+	0.5511	10497.028	10497.027
^{134}Ba(n,2n)^{133}Ba	134	0.1642	0+	11/2–	1/2+	0.5052	Q	Q
^{127}I(n,p)^{127}Te	127	0.1654	5/2+	11/2–	3/2+	0.4734	31080.003	31080.007
^{128}Te(n,2n)^{127}Te	128	0.1875	0+	11/2–	3/2+	0.4532	11999.014	11999.015
^{130}Te(n,2n)^{129}Te	130	0.2	0+	11/2–	3/2+	0.5405	30135.005	30135.003

Continue Table 1

Reactions	Target			J_m	J_g	R	Ref.(EXFOR Acc. No.)	
	A	$(N-Z)/A$	J_t				a)	b)
^{134}Xe(n,2n)^{133}Xe	134	0.1940	0+	11/2−	3/2+	0.4524	Q	Q
^{138}Ba(n,α)^{135}Xe	138	0.1884	0+	11/2−	3/2+	0.5	20289.007	20289.006
^{136}Xe(n,2n)^{135}Xe	136	0.2059	0+	11/2−	3/2+	0.4928		30698.010
^{138}Ce(n,2n)^{137}Ce	138	0.1594	0+	11/2−	3/2+	0.5084	20541.003	20541.005
^{142}Nd(n,α)^{139}Ce	142	0.1549	0+	11/2−	3/2+	0.8333	12033.020	12033.019
^{140}Ce(n,2n)^{139}Ce	140	0.1714	0+	11/2−	3/2+	0.5	20541.007	20541.009
^{142}Nd(n,2n)^{141}Nd	142	0.1549	0+	11/2−	3/2+	0.35	20541.012	20541.014
^{144}Sm(n,2n)^{143}Sm	144	0.1389	0+	11/2−	3/2+	0.4118		30763.003
^{186}W(n,2n)^{185}W	186	0.2043	0+	11/2+	3/2−	0.2825	Q	Q
^{109}Ag(n, p)^{109}Pd	109	0.1376	1/2−	11/2−	5/2+	0.324	21426.011	21426.013
^{110}Pd(n,2n)^{109}Pd	110	0.1636	0+	11/2−	5/2+	0.2908		30763.005
^{114}Cd(n, α)^{111}Pd	114	0.1579	0+	11/2−	5/2+	0.2857	11583.013	11583.014
^{68}Zn(n,p)^{68}Cu	68	0.1176	0+	6−	1+	0.4091	30394.006	30394.005
^{102}Pd(n,p)^{102}Rh	102	0.098	0+	6+	1−	0.3291	21609.008	21609.007
^{103}Rh(n,2n)^{102}Rh	103	0.1262	1/2−	6+	1−	0.4124	20393.006	20393.004
^{106}Pd(n,p)^{106}Rh	106	0.1321	0+	6+	1+	0.3333	10145.014	10145.013
^{106}Cd(n, p)^{106}Ag	106	0.0943	0+	6+	1+	0.3268	10484.006	10484.005
^{107}Ag(n,2n)^{106}Ag	107	0.1215	1/2−	6+	1+	0.4288	20891.021	20891.019
^{148}Sm(n,p)^{148}Pm	148	0.1622	0+	6−	1−	0.4118	21609.018	21609.017
^{165}Ho(n,2n)^{164}Ho	165	0.1879	7/2−	6−	1+	0.5592	20802.008	20802.007
^{175}Lu(n,2n)^{174}Lu	175	0.1886	7/2+	6−	1−	0.3376	20802.012	20802.013
^{45}Sc(n,2n)^{44}Sc	45	0.0667	7/2−	6+	2+	0.4254	11645.003	11645.002
^{46}Ti(n,t)^{44}Sc	46	0.0435	0+	6+	2+	0.1482	20669.002	20669.003
^{87}Rb(n, α)^{84}Br	87	0.1494	3/2−	6−	2−	0.475	40223.015	40223.016
^{84}Sr(n,p)^{84}Rb	84	0.0952	0+	6−	2−	0.4896	20721.074	20721.073
^{85}Rb(n,2n)^{84}Rb	85	0.1294	5/2−	6−	2−	0.4075	30350.003	30350.002
^{89}Y(n,α)^{86}Rb	89	0.1236	1/2−	6−	2−	0.2514	41240.028	41240.027
^{87}Rb(n,2n)^{86}Rb	87	0.1494	3/2−	6−	2−	0.3963	30350.008	30350.007
^{190}Os(n,p)^{190}Re	190	0.2	0+	6−	2−	0.04	30290.012	30290.013
^{138}Ba(n,p)^{138}Cs	138	0.1884	0+	6−	3−	0.3824	21976.044	21976.043
^{198}Pt(n,2n)^{197}Pt	198	0.2121	0+	13/2+	1/2−	0.46	30718.004	30718.002
^{196}Hg(n,2n)^{195}Hg	196	0.1837	0+	13/2+	1/2−	0.5	12219.003	12219.002
^{198}Hg(n,2n)^{197}Hg	198	0.1919	0+	13/2+	1/2−	0.47	20536.032	20536.034
^{204}Pb(n,2n)^{203m1}Pb	204	0.1961	0+	13/2+	5/2−	0.4951	Q	Q
^{90}Zr(n,p)^{90}Y	90	0.1111	0+	7+	2−	0.2093	40226.017	40226.018
^{93}Nb(n,α)^{90}Y	93	0.1183	9/2+	7+	2−	0.4069	11590.057	11590.056
^{91}Zr(n,n+p)^{90}Y	91	0.1209	5/2+	7+	2−	0.0943	20513.014	20513.015
^{121}Sb(n,2n)^{120}Sb	121	0.157	5/2+	8−	1+	0.2644	10497.025	10497.024
^{187}Re(n,2n)^{186}Re	187	0.1979	5/2+	8+	1−	0.217	32600.002	32600.003
^{123}Sb(n,2n)^{122}Sb	123	0.1707	7/2+	8−	2−	0.2958		30154.010
^{153}Eu(n,2n)^{152m2}Eu	153	0.1765	5/2+	8−	3−	0.1225	30051.009	30051.008
^{185}Re(n,2n)^{184}Re	185	0.1892	5/2+	8+	3−	0.1818	40083.005	40083.004
^{54}Fe(n,2n)^{53}Fe	54	0.037	0+	19/2−	7/2−	0.105	20536.005	20536.004
^{182}W(n,p)^{182}Ta	182	0.1868	0+	10−	3−	0.0199	20668.007	20668.006
^{197}Au(n,x)^{194}Ir	197	0.198	3/2+	11	1−	0.0746	21916.016	21916.017
^{191}Ir(n,2n)^{190m2}Ir	191	0.1937	3/2+	11−	4+	0.0867	31411.005	31411.004
^{197}Au(n,2n)^{196m2}Au	197	0.198	3/2+	12−	2−	0.066	21709.011	21709.010

a): total or ground state. b): isomeric state. Q): S.M.Qaim[1].

Looking for the systematics, the total (energy-integrated) cross sections for neutron-induced reactions around 14 MeV are generally considered as a function of mass A, charge Z, neutron number N, neutron excess(N-Z) or relative neutron excess (N-Z)/A of the target nucleus. As all empirical formulae for total cross section use one parameter, namely (N-Z)/A, to fit the experimental data, the isomeric cross section ratio R was also only investigated as a function of (N-Z)/A.

The plotting of R vs (N-Z)/A of the target nucleus is shown in Fig.1. It can be seen that R was not strongly dependent on (N-Z)/A. If the (N-Z)/A was replaced by $(J_m+J_g)/A^{1/3}$ where J_m and J_g represent the spin of isomeric and ground states respectively, one can find that R may be a function of $(J_m+J_g)/A^{1/3}$. So there exist systematic features on R vs $(J_m+J_g)/A^{1/3}$ (see Fig.2 in details) but not (N-Z)/A.

Some systematics of isomeric cross section ratios on isomer spin J_m were proposed in Refs.[2] and[3]. These systematics gave a parabolic type of dependence on J_m with a peak at J_m 3~5. They also gave a conclusion that the influence of the ground state spin J_g on the isomeric cross section ratio is similar to that for the isomer state spin J_m. The effects of J_m and J_g on isomeric cross section ratios were demonstrated in Figs. 3. Fig. 3 shows that the isomeric cross section ratios were found to be relatively independent of the J_g. It was mainly affected by J_m. J_m strongly influences the isomeric cross section ratio R. Fig. 3 is also given the effect of target spin J_t on the isomeric cross section ratio, which indicated that the effect of J_t on R is not obvious.

Ref.[4] gives a formula, which describe the isomeric cross section ratio at 14.5 MeV. The authors said that the formula ensure a better description of the experimental data. As the formula is a function of (J_m-J_g), the plotting of R vs (J_m-J_g) is performed and shown in Fig. 4. No conclusive evidences about the systematic features on R vs (J_m-J_g) can be found.

2 Conclusion

In present work the effect of (N-Z)/A, $(J_m+J_g)/A^{1/3}$, J_m, J_g, (J_m-J_g) and J_t on isomeric cross section ratios R are systematically investigated. The isomeric cross section ratios are primarily governed by the spins of the isomeric state concerned but not by the spin of the ground state or other parameters. They are strongly dependent on J_m or $(J_m+J_g)/A^{1/3}$. No conclusive evidences were found regarding the effect of (N-Z)/A, (J_m-J_g) or J_t on isomeric cross section ratios, which are not existed or obvious.

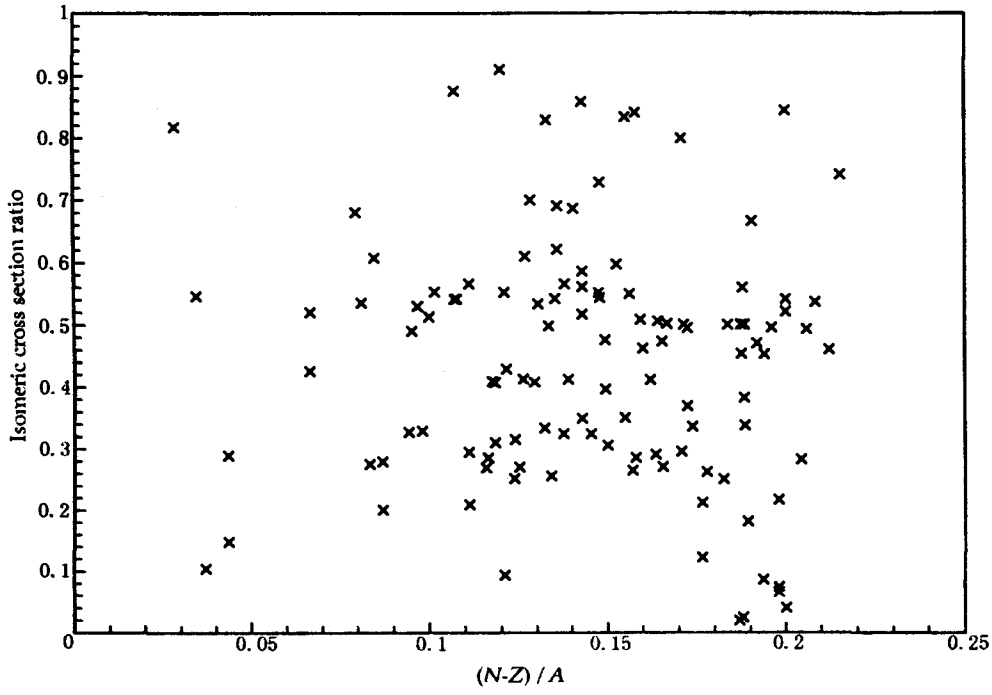

Fig. 1 Isomeric cross section ratio as a function of $(N\text{-}Z)/A$

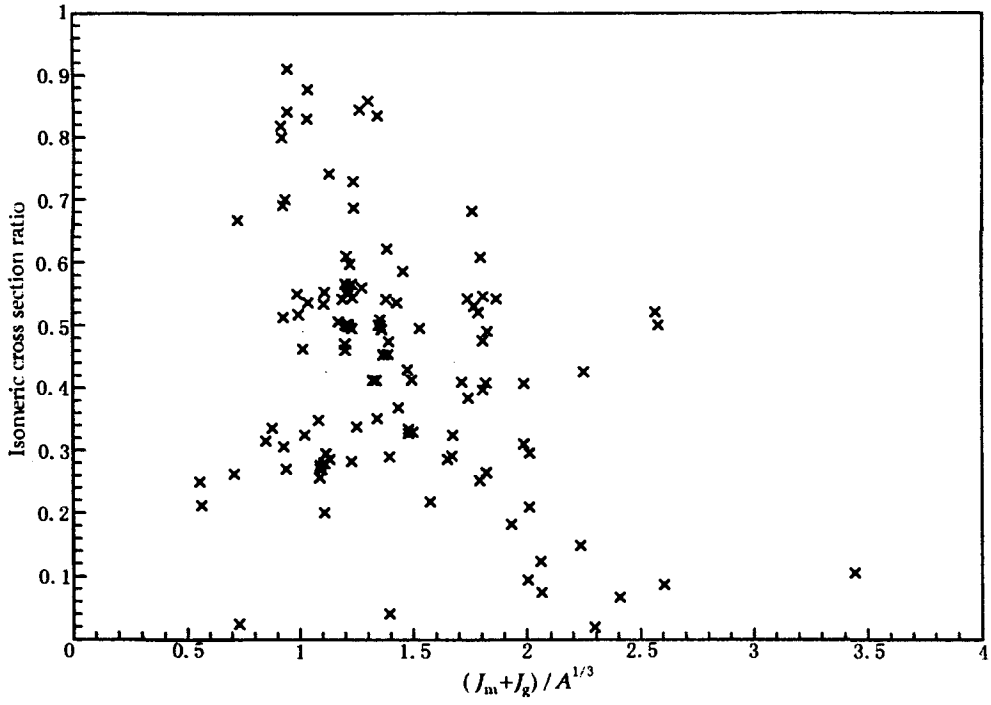

Fig. 2 Isomeric cross section ratio as a function of $(J_m+J_g)/A^{1/3}$

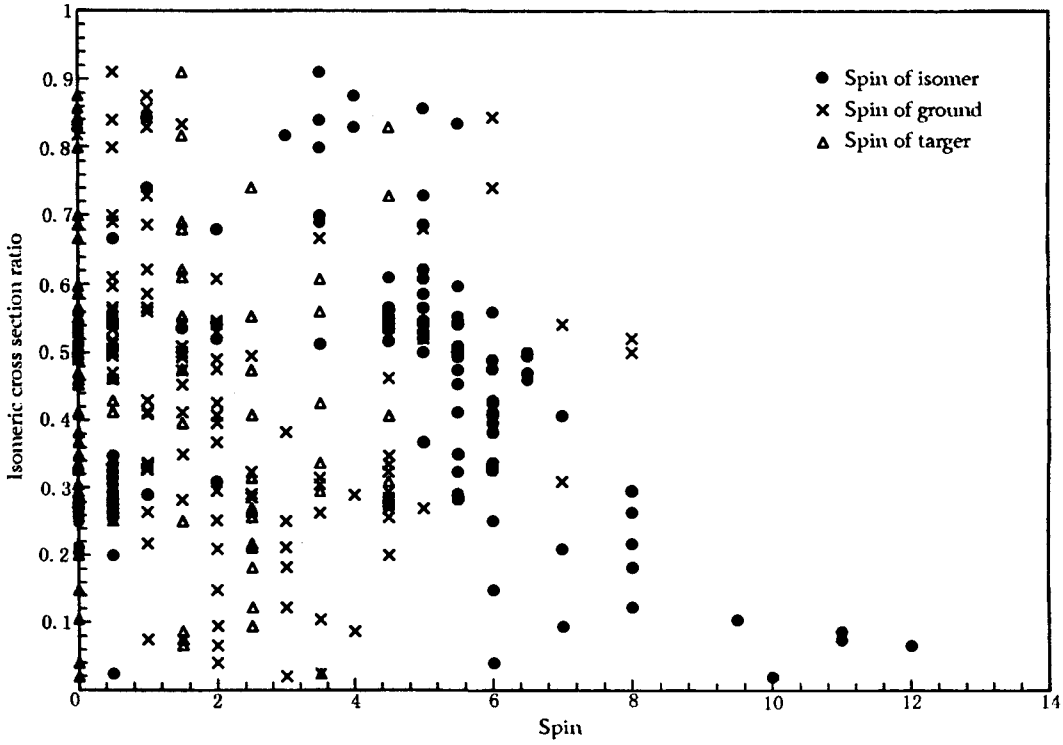

Fig. 3 Isomeric cross section ratio as a function of different spin

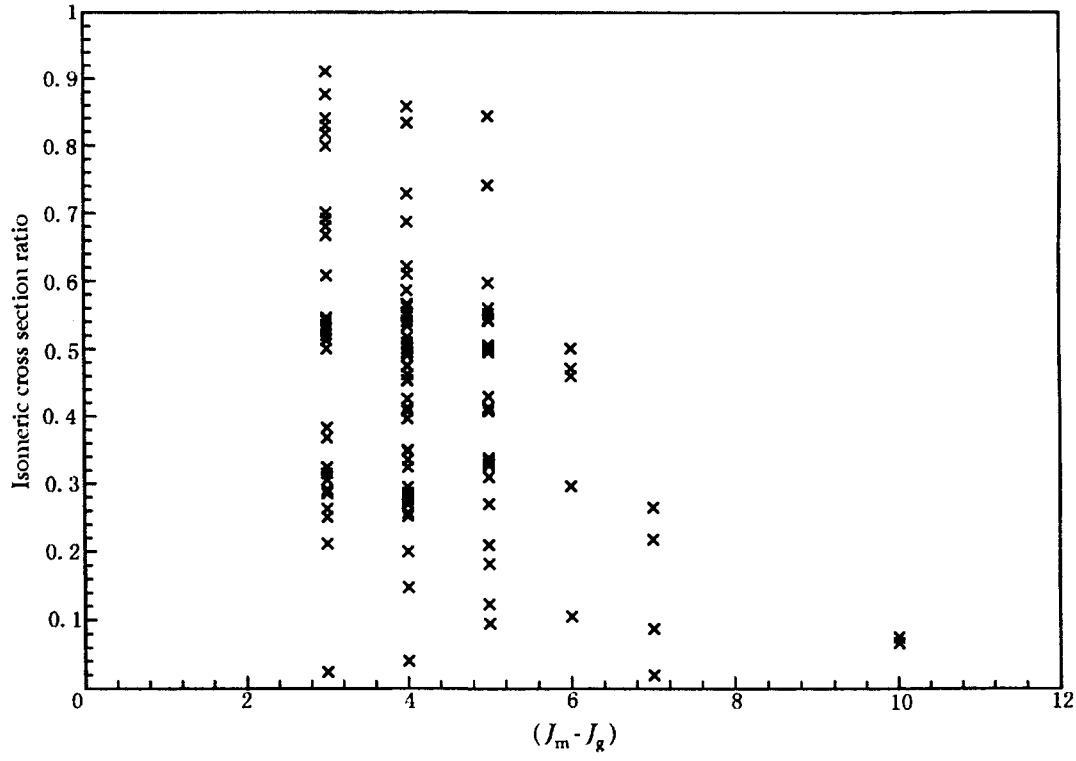

Fig. 4 Isomeric cross section ratio as a function of $(J_m - J_g)$

As there is lack of quantitative experimental data and deficiencies in nuclear model calculations, systematics seems to be an ideal method of study in isomeric cross section ratios. From the mechanistic and practical point of view, systematics on isomeric cross section ratios appears to be meaningful.

References

[1] S.M.Qaim, Handbook of Spectroscopy, Vol. III, 141(1981).

[2] Huang Xiaolong, Cai Dunjiu, Nucl. Sci. Eng. 125, 371(1997).

[3] J. Kopecky et al., Report ECN-200 (1987).

[4] S.A.Badikov et al., Proc. Int. Conf. on Nucl. Data for Sci. & Tec., Mito, Japan, 930(1988).

V BENCHMARK TEST

Brief Report on the Testing Calculation of the Fission Rate for the ^{238}U

Rong Jian
(China Nuclear Data Center, CIAE)

The fission rate, P_f, for the ^{238}U produced by a 14 MeV neutron source at the center of a uranium mental is a very important factor of the fission system. Several experiments were to measure the factor. In 1960's, a famous experiment was made by J.W. Weale[1] in the Atomic Weapons Research Establishment of British. The total neutron leakage and the reaction rate distributions were measured for the $^{235}U(n,f)$, $^{238}U(n,f)$, $^{238}U(n, \gamma)$ and $^{239}Pu(n,f)$ in natural uranium piles with density 16.3 g/cm^3 and total weight up to 20 tons with 14 MeV neutrons.

Another experiment was made by Dr. Wang Dalun[2] in the 1980's in China with a uranium-barren sphere of 51 cm in radius and a 14 MeV D-T neutron source at the center .

The calculations for the Weale experiment were done by Haight[3], in which a simplifying assumption was used. Several calculations[4,5] for these experiments were also done in China, based on CENDL-2 and ENDF/B-6. The simplifying model was used in these works too. But there are some differences in the conclusions between the two experiments, and the calculation results are also not agreed with each other. So it is necessary to do the further calculation.

In our calculation, Monte-Carlo method was applied and the newly released data, CENDl-2.1 and ENDF/B-6.5, were used. The comparison between the calculated results and experimental ones were made. The experiment facilities are given in Table 1.

The formula to calculate the reaction rate is:

$$P_x=N_x/A \tag{1}$$

Where the N_x is the total number of the x type reaction in the experiment facility, and the A is the intensity of the neutron source.

In these experiments, the N_x can not be measured directly. Instead, the distribution of the reaction rate $f_x(r)$ was measured at first, and then the N_x can be calculated as follows:

$$N_x = 2\pi\rho \int_0^{\pi} \int_0^{R} r^2 f_x(r) \sin\theta \, d\theta \, dr \tag{2}$$

where ρ is the density of the experiment material, R is the equivalent radius of the experiment facility.

The code NJOY[6] was used to generate the ACE file from the ENDF file, which was used in the Monte Carlo code for our calculations. The calculated results are given in the Table 2.

Table 1 The experiment facilities:

Experiment	Radius / cm	Compositions / %	Desinity / g/cm^3)
Weale	58.077	^{234}U(0.0055) ^{235}U(0.7200) ^{238}U(99.2745)	16.3
WANG Dalun (China)	51.0	^{234}U(0.0034) ^{235}U(0.4154) ^{236}U(0.003087) ^{238}U(99.579)	18.8

Table 2 The comparison between the calculations and the experiments

Experiment	Reaction ratios	Experiments	ENDF/B-VI	CENDL-2.1
Weale	^{235}U(n,f)	0.281±0.017	0.2570	0.2454
british	^{235}U(n,γ)	-	0.05763	0.05654
	^{238}U(n,2n)	0.277±0.008	0.3792	0.3811
	^{238}U(n,f)	1.18±0.06	1.0656	1.0266
	^{238}U(n,γ)	4.08±0.24	4.2727	4.1778
	Leakage	0.41±0.02	0.3256	0.2898
WANG Dalun	^{235}U(n,f)	0.115±0.052	0.1407	0.1346
(China)	^{235}U(n,γ)	-	0.03173	0.03113
	^{238}U(n,2n)	-	0.3782	0.3800
	^{238}U(n,f)	0.897±0.036	1.0217	0.9867
	^{238}U(n,γ)	-	4.1160	4.0289
	Leakage	-	0.2639	0.2366

From Table 2, it can be seen that the calculated P_x^U by using the two nuclear data libraries are very close, but they are all not well agreed with the experimental results. The they are all smaller than Weale's results and all larger than the Wang's results. We think that the two nuclear data libraries are all reliable, because they all have been tested with lots of benchmarks and engineering calculations. The calculated method and results are also reliable, because the two codes used in our calculation are used very popular in the world. In general, there could be no such large different values between the calculations and experiments. The measured results of two experiments are very different. It is possible that the leakage from the system was overestimated in the Weale's experiment, so the results are higher. And in the Wang's experiment, the leakage of the system was neglected, so the results are lower. Maybe a new experiment should be done to clarify the discrepance.

References

[1] J.W. Weale et al.. Measurements of the Reaction Rate Distribution Produced by a Source of 14MeV Neutrons at the Center of a Uranium Metal Pile. Reactor Science and Technology, Vol14, 91(1961)

[2] D.L. Wang, China Nuclear Science Reports (in Chinese) CNIC-00506 SINPC-0001 (1991)

[3] R.C. Haight, et al.. Reaction Rates in a Uranium Pile Sorrounding a 14-MeV Neutron Source: Calculations of the Weale Experiment. Nuclear Science and Energy, Vol61, 53(1976)

[4] R.B Lu, private communication (1993)

[5] Z.J Na W.L Sun , private communication (1995)

[6] R.E. MacFarlane, et al.. The NJOY Nuclear Data Processing System Version91. Los Alamos National Laboratory, La-12740-M (1994)

The Sensitivity Profile of the Fast Reactor k_{eff}

Rong Jian

(China Nuclear Data Center, Beijing)

The nuclear design calculations have always been limited in their accuracy by both computational methods and uncertainties in cross-section data. After a period of extensive refinements in calculation methods, like the node method and Monte-Carlo method, and the rapidly development in the computer, more emphasis has been directed toward improving cross-section data. For this purpose, we should know the uncertainty that brought by the inherent errors of the cross section data[1]. The sensitivity profile should be known to calculate the uncertainty.

1 General Sensitivity Profile

The sensitivity profile is the rate of change in the response per rate of change in some specific cross-section. Consider a reactor integral parameter, R, of the homogeneous bilinear ratio form[2]:

$$R=\frac{\int \Phi^*(\xi)\hat{H}_n(q(\xi))\Phi(\xi)\mathrm{d}\xi}{\int \Phi^*(\xi)\hat{H}_d(q(\xi))\Phi(\xi)\mathrm{d}\xi} \tag{1}$$

where $\hat{H}_n$ and $\hat{H}_d$ are suitable operators which depend on the various cross sections, $\Phi(\xi)$ and $\Phi^*(\xi)$ are the forward and adjoint fluxes respectively, ξ is the position vector in phase space.

Using variational perturbation theory, Oblow[3] has demonstrated the sensitivity profile function.

$$P_{Rq}(\rho)=\frac{\mathrm{d}R}{R}\Big/\frac{\mathrm{d}q(\rho)}{q(\rho)}=I_1+I_2+I_3+I_4 \tag{2}$$

where

$$I_1=q(\rho)\frac{\int \Phi^*(\xi)\dfrac{\mathrm{d}H_n(q(\xi))}{\mathrm{d}q(\rho)}\Phi(\xi)\mathrm{d}\xi}{\int \Phi^*(\xi)H_n(q(\xi))\Phi(\xi)\mathrm{d}\xi} \tag{3}$$

$$I_2 = -q(\rho)\frac{\int \Phi^*(\xi)\frac{\mathrm{d}H_\mathrm{d}(q(\xi))}{\mathrm{d}q(\rho)}\Phi(\xi)\mathrm{d}\xi}{\int \Phi^*(\xi)H_\mathrm{d}(q(\xi))\Phi(\xi)\mathrm{d}\xi} \tag{4}$$

$$I_3 = \frac{q(\rho)}{R}\int \frac{\partial R}{\partial \Phi(\xi)}\frac{\mathrm{d}\Phi(\xi)}{\mathrm{d}q(\rho)}\mathrm{d}\xi \tag{5}$$

$$I_4 = \frac{q(\rho)}{R}\int \frac{\partial R}{\partial \Phi^*(\xi)}\frac{\mathrm{d}\Phi^*(\xi)}{\mathrm{d}q(\rho)}\mathrm{d}\xi \tag{6}$$

Each of the derivatives above are functional derivatives characterizing the rate of change of some variable with respect to another per unit volume in phase space.

We can develop the expression of the $\mathrm{d}\Phi(\xi)/\mathrm{d}q(\rho)$ by differentiating the Boltzmann equation. The Boltzmann equation in operator form is:

$$\mathrm{L}[q(\xi)]\Phi(\xi) = [A(q(\xi)) - \lambda B(q(\xi))]\Phi(\xi) = 0 \tag{7}$$

where $\mathrm{L}[q(\xi)]$ is the Boltzmann operator, $B(q(\xi))$ is the fission operator and all the other operators are included in the $A(q(\xi))$ operator.

Assuming λ ($=1/k_{\mathrm{eff}}$) is a constant, differentiating Eq. (7),

$$\mathrm{L}[q(\xi)]\frac{\mathrm{d}\Phi(\xi)}{\mathrm{d}q(\rho)} = -\frac{\mathrm{dL}[q(\xi)]}{\mathrm{d}q(\rho)}\Phi(\xi) \tag{8}$$

So we can define the symbol

$$\Psi(\xi,\rho) = \frac{\mathrm{d}\Phi(\xi)}{\mathrm{d}q(\rho)} \tag{9}$$

The definition of the adjoint operator is:

$$\int \Gamma^*(\xi)\mathrm{L}[q(\xi)]\Psi(\xi,\rho)\mathrm{d}\xi = \int \Psi(\xi,\rho)\mathrm{L}^*[q(\xi)]\Gamma^*(\xi)\mathrm{d}\xi \tag{10}$$

Using the same method we can get:

$$\mathrm{L}[q(\xi)]\Gamma(\xi) = \frac{\partial R}{\partial \Phi^*(\xi)} \tag{11}$$

We can introduce[4] the final form of the sensitivity profile is:

$$P_{Rq}(\rho)=\frac{\mathrm{d}R}{R}\Big/\frac{\mathrm{d}q(\rho)}{q(\rho)}$$

$$=[\frac{q(\rho)\int\Phi^{*}(\xi)\frac{\mathrm{d}H_{n}[q(\xi)]}{\mathrm{d}q(\rho)}\Phi(\xi)\mathrm{d}\xi}{\int\Phi^{*}(\xi)H_{n}[q(\xi)]\Phi(\xi)\mathrm{d}\xi}-\frac{q(\rho)\int\Phi^{*}(\xi)\frac{\mathrm{d}H_{d}[q(\xi)]}{\mathrm{d}q(\rho)}\Phi(\xi)\mathrm{d}\xi}{\int\Phi^{*}(\xi)H_{d}[q(\xi)]\Phi(\xi)\mathrm{d}\xi}] \tag{12}$$

$$-\frac{q(\rho)}{R}[\int\Gamma^{*}(\xi)\frac{dL[q(\xi)]}{\mathrm{d}q(\rho)}\Phi(\xi)\mathrm{d}\xi+\int\Gamma(\xi)\frac{\mathrm{dL}^{*}[q(\xi)]}{\mathrm{d}q(\rho)}\Phi^{*}(\xi)\mathrm{d}\xi]$$

Once Φ, Φ^{*}, Γ, Γ^{*} have been determined, sensitivity functions for any and all elements of the cross section data field for a given problem can be calculated from Eq. (12).

2 Sensitivity Profile of the k_{eff}

The k_{eff} can be considered as a reaction rate ratio of the neutron production and neutron absorption. From Eq. (7), the k_{eff} can be viewed as

$$k_{\mathrm{eff}}=\frac{\int\Phi^{*}(\xi)B[\Sigma(\xi)]\Phi(\xi)\mathrm{d}\xi}{\int\Phi^{*}(\xi)A[\Sigma(\xi)]\Phi(\xi)\mathrm{d}\xi} \tag{13}$$

Through the Eq. (12) we can get the sensitivity function a

$$p_{\Sigma(\rho)}^{k_{\mathrm{eff}}}=\frac{\mathrm{d}k_{\mathrm{eff}}/k_{\mathrm{eff}}}{\mathrm{d}\Sigma(\rho)/\Sigma(\rho)}=-\frac{\Sigma(\rho)}{k_{\mathrm{eff}}}\frac{\langle\Phi^{*}(\xi),(\frac{\mathrm{d}A[\Sigma(\xi)]}{\mathrm{d}\Sigma(\rho)}-\frac{1}{k_{\mathrm{eff}}}\frac{\mathrm{d}B[\Sigma(\xi)]}{\mathrm{d}\Sigma(\rho)})\Phi(\xi)\rangle}{\langle\Phi^{*}(\xi),\frac{1}{k_{\mathrm{eff}}}B[\Sigma(\rho)]\Phi(\xi)\rangle} \tag{14}$$

The blankets imply integration over the ξ phase space.

And the integrated sensitivity is

$$S_{\Sigma(\rho)}^{k_{\mathrm{eff}}}=\sum P_{\Sigma(\rho)}^{k_{\mathrm{eff}}} \qquad \text{(Summed up the } P_{\Sigma(\rho)}^{k_{\mathrm{eff}}} \text{ in all energy)} \tag{15}$$

3 Sensitivity Analysis Results of the k_{eff} for the Fast Reactor

One-dimensional analyses are presented below for GODIVA[5] and ZPR-6/7[6]. ZPR-6/7 is a large (3100 liters), plutonium oxide fueled fast critical assembly

composed with stainless steel drawers of fuel and diluent. GODIVA is a bare sphere of enriched uranium metal and the radius of core is 8.741 cm. The neutron fluxes of the two assemblies are showed in Fig. 1 and Fig. 2, respectively. The atom densities of the ZPR-6/7 and GODIVA are given in Table 1~2.

Table 1 Atom Densities for GODIVA (Atoms/barn-cm)

Isotope	Atom Densities
^{234}U	0.04500
^{235}U	0.002498
^{238}U	0.000492

Table 2 Atom Densities for ZPR-6/7 (Atoms/barn-cm)

Isotope	Core Radius - 88.16cm	Blanket Thickness - 33.81cm
^{239}Pu	0.00088672	-
^{240}Pu	0.00011944	-
^{241}Pu	0.0000133	-
^{235}U	0.0000126	0.0000856
^{238}U	0.00578036	0.0396179
Mo	0.0002357	0.0000038
Na	0.0092904	-
O	0.01390	0.000024
Fe	0.013431	0.004637
Cr	0.002842	0.001295
Ni	0.001291	0.0005635
Mn	0.000221	0.0000998

Using the Eq. (14) and (15), we calculated the k_{eff} sensitivity profile of the $\bar{\nu}$, $\sigma_{n,f}$ and $\sigma_{n,\gamma}$ for the two fast critical assemblies. The NJOY[7] was used to generate the 126 group constant files. The evaluated date of the CENDL-2 are used in our work and the structure of the group constant is same as it which given in the Ref. [4]. The forward and adjoint fluxes were calculated by using the SCALE[8]. NSLINK was used as the interface between the NJOY and SCALE. The integrated sensitivity results are listed in the Table 3~4, and some of the sensitivity profiles are showed in the following figures.

Table 3 Integrated Sensitivity of GODIVA

Reaction	Results given by this work(%) (k_{eff}: Cal. 0.994457) (k_{eff}: Exp. 1.000±0.001)	Results given by Ref.[4](%) (k_{eff}: Cal. 1.0033)
^{235}U $\bar{\nu}$	+1.007	+0.982
^{235}U (n,f)	+0.596	+0.659
^{235}U (n,γ)	-0.038	-0.037
^{238}U $\bar{\nu}$	+0.0092	+0.0098
^{238}U (n,f)	+0.0073	+0.007
^{238}U (n,γ)	-0.001	-0.001
^{234}U $\bar{\nu}$	+0.01	+0.0083
^{234}U (n,f)	+0.0056	+0.006
^{234}U (n,γ)	-0.0008	-

Table 4 Integrated Sensitivity of ZPR-6/7

Reaction	Results given by this work(%) (k_{eff}: Cal. 0.987993) (k_{eff}: Exp. 1.000)	Results given by Ref.[4] (k_{eff}: Cal. 0.9885)
^{239}Pu(n,f)	0.5936	0.591
^{240}Pu(n,f)	0.01619	0.016
^{241}Pu(n,f)	0.01329	0.013
^{235}U(n,f)	0.01023	0.009
^{238}U(n,f)	0.08006	0.079
^{239}Pu $\bar{\nu}$	0.8234	0.819
^{240}Pu $\bar{\nu}$	0.02216	0.023
^{241}Pu $\bar{\nu}$	0.01783	0.018
^{235}U $\bar{\nu}$	0.01251	-
^{238}U $\bar{\nu}$	0.1719	0.166
^{239}Pu(n,γ)	-0.06745	-0.067
^{240}Pu(n,γ)	-0.00908	-0.009
^{241}Pu(n,γ)	-0.00063	-0.001
^{235}U(n,γ)	-0.00075	-0.001
^{238}U(n,γ)	-0.2845	-0.239
Na(n,γ)	-0.00318	-0.003
Fe(n,γ)	-0.01702	-0.020
Ni(n,γ)	-0.00439	-0.004
Cr(n,γ)	-0.00698	-0.007

The results given by Ref. [4] in Table 3~4 and in Fig. 3~5 were calculated by the FORSS code system. The FORSS is a code system used to study relationships

between nuclear reaction cross sections, integral experiments, reactor performance parameter predictions, and associated uncertainties. Through the comparison between our results and the results given by Ref. [4], it can be seen that there aren't any large differences between the two calculations. The differences were come from the nuclear data that used in the two calculations. The data of the ENDF/B-6 were used in the Ref. [4], and the data of the CENDL-2 were used in our calculation. It is the largest reason for the differences between the two results. It means that our methods are available.

From the Eq. (12) and (14), it can be seen that the sensitivity profiles are determined with the cross section, the forward flux and the adjoint flux. The fission of the ^{238}U is a threshold reaction. So the sensitivities of $\bar{\nu}$ and $\sigma_{n,f}$ are only appeared in the high energy. The ratio of the (n,γ) cross section in low energy and the cross section in high energy is higher then the ratio for the $\sigma_{n,f}$. So the ratio of sensitivity of the $\sigma_{n,\gamma}$ in the low energy is larger than the ratio of $\sigma_{n,f}$ in the low energy.

4 Uncertainty Analysis Method

The uncertainty analysis is based on the sensitivity profile and the values of the covariance matrix elements. Covariance matrices may be found on the evaluated files. The sensitivity profile can be got from above, and the response parameter R should be defined firstly. Using the methods described in part A, the sensitivity profile, $P^g_{\Sigma^g_i}$, can be calculated, which the g is the label of energy group. With the covariance matrix the relation between the sensitivity and the resulting relative uncertainty $\Delta R/R$ can be derived[9] as

$$(\frac{\Delta R}{R})^2 = \sum_i \sum_j \sum_g \sum_{g'} P^g_{\Sigma^g_i} P^{g'}_{\Sigma^{g'}_j} \frac{Cov(\Sigma^g_i, \Sigma^{g'}_j)}{\Sigma^g_i \Sigma^{g'}_j} \tag{16}$$

This method is also used in ECN to calculate the uncertainty of the fusion reactor blanket[10]. Based on the above work we plan to do the uncertainty analysis for the nuclear data in the future.

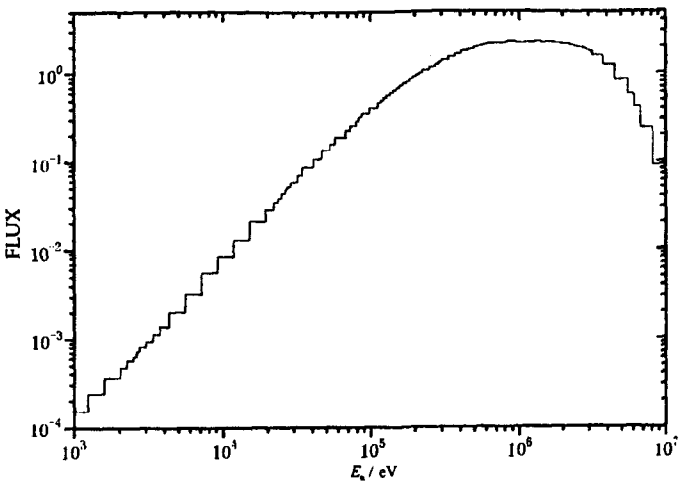

Fig. 1 Neutron flux in the center of GODIVA

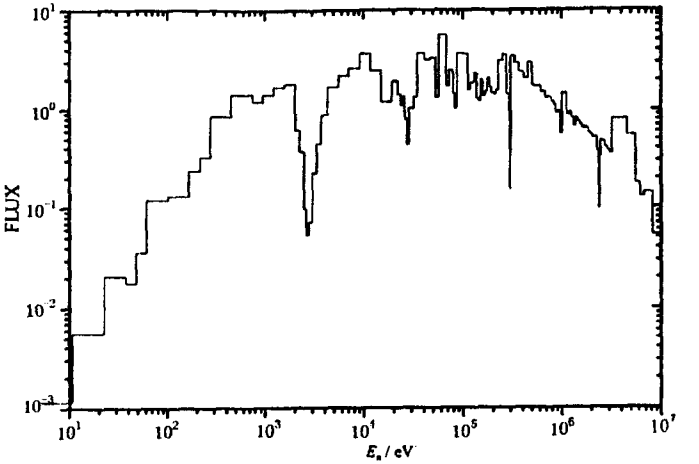

Fig. 2 Neutron flux in the center of ZPR-6/7

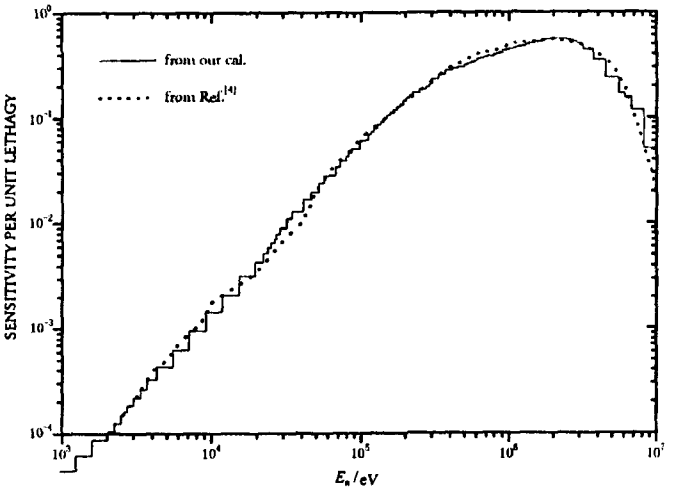

Fig. 3 Sensitivity of k_{eff} in GODIVA to the ^{235}U neutron yield per fission

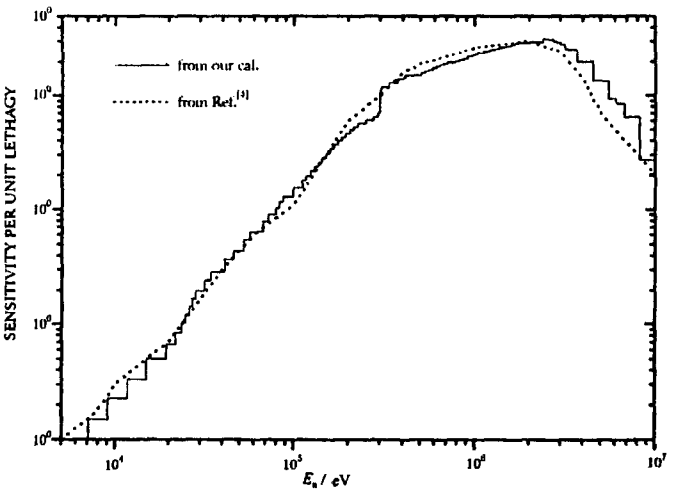

Fig. 4 Sensitivity of k_{eff} in GODIVA with respect to the ^{235}U (n,f)

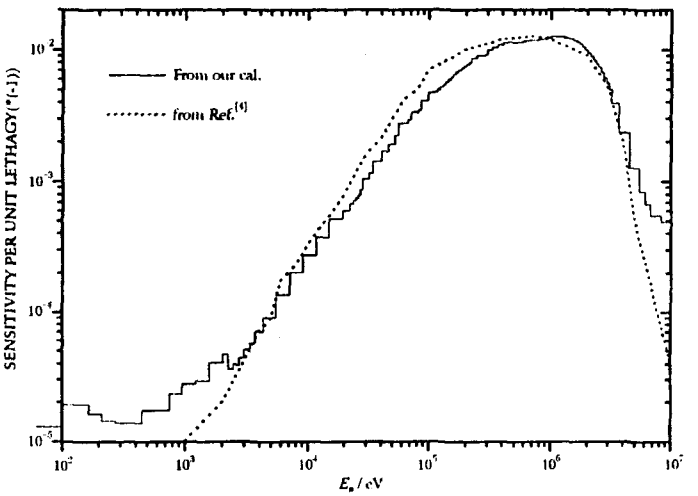

Fig. 5 Sensitivity of k_{eff} in GODIVA to the ^{235}U capture cross section

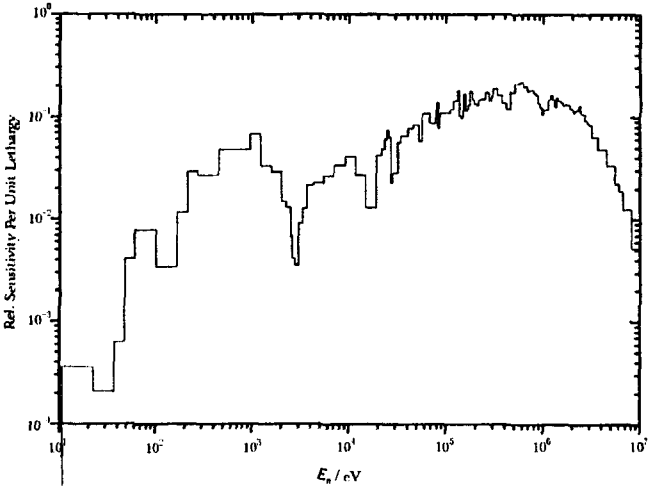

Fig. 6 Sensitivity of keff in ZPR-6/7 to the ^{239}Pu neutron yield per fission

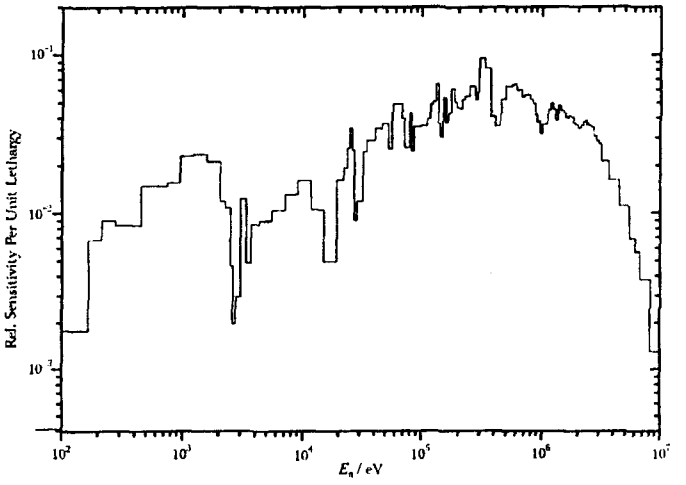

Fig. 7 Sensitivity of k_{eff} in ZPR-6/7 to the ^{239}Pu fission cross section

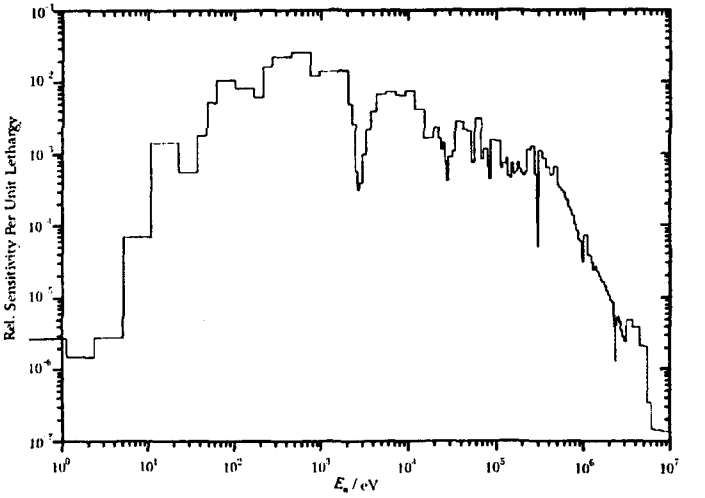

Fig. 8 Sensitivity of k_{eff} in ZPR-6/7 to the ^{239}Pu capture cross section

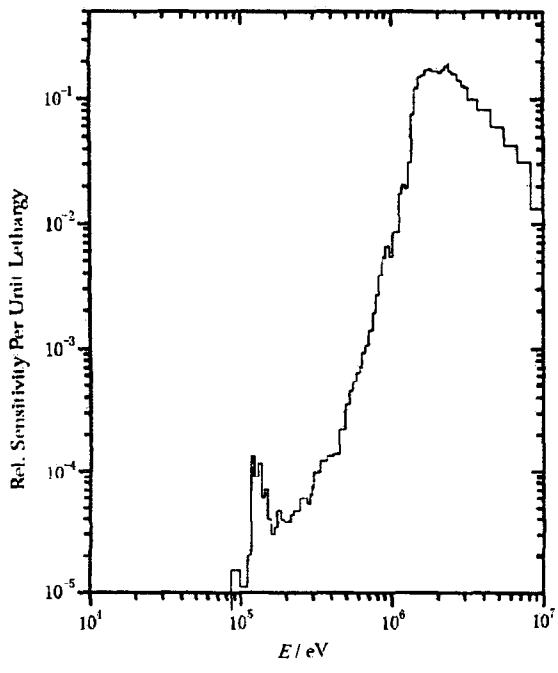

Fig. 9 Sensitivity of k_{eff} in ZPR-6/7 to the ^{238}U neutron yield per fission

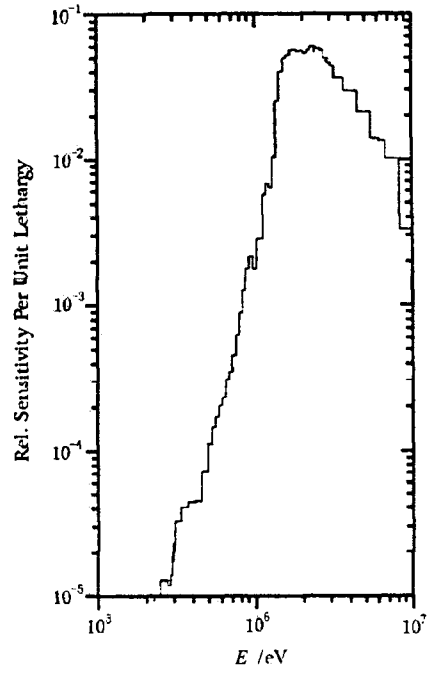

Fig. 10 Sensitivity of k_{eff} in ZPR-6/7 to the ^{238}Pu fission cross section

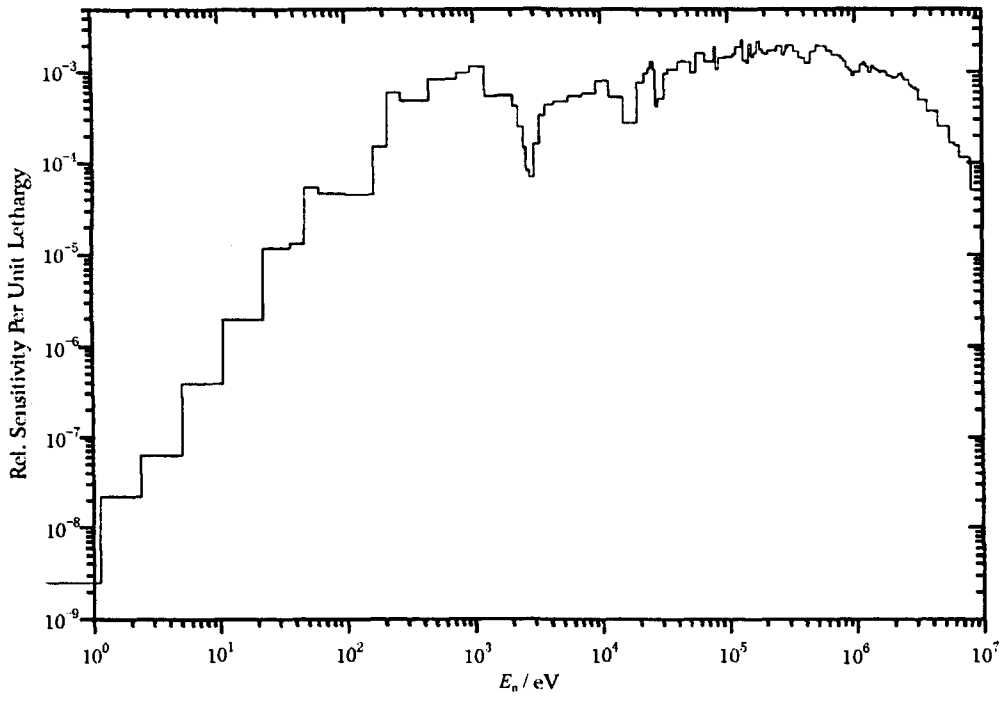

Fig. 11 Sensitivity of k_{eff} in ZPR-6/7 to the ^{235}U neutron yield per neutron

Reference

[1] S. A.W. Gerstl, et al.. Cross Section Sensitivity and Uncertainty Analysis with Application to a Fusion Reactor. Nuclear Science and Engineering, 62, 137(1977)

[2] E. Greenspan. SENSITIVITY FUNCTION FOR UNCERTAINTY ANALYSIS. P193, Advances in Nuclear Science and Technology Vol. 14 , Plenum Press , New York 1982

[3] E.M. Oblow. Sensitivity Theory from a Differential Viewpoint. Nuclear Science and Engineering, Vol. 59, 187-189, 1976

[4] C.R. Weisbin. et al.. Application of FORSS Sensitivity and Uncertainty Methodology to Fast Reactor Benchmark Analysis. ORNL/TM-5563, 1976

[5] International Handbook of Evaluated Criticality Safety Benchmark Experiments. NEA/NSC/DOC(95) , Sep. 1997 Edition

[6] Sensitivity Coefficiant Compilation for CSEWG Data Testing Benchmarks. ENDF-265, Aug. 1978

[7] NJOY94.35 Code System for Producing Pointwise and Multigroup Neutron and Photon Cross Sections for ENDF/B Data. Los Alamos National Laboratory, August 1996

[8] SCALE Modular Code System for Performing Criticality Safety Analyses for Licensing Evaluation , Version 4.1. Oak Ridge National Laboratory, Dec. 1993

[9] A. Hogenbirk Sensitivity and Uncertainty Analysis of the Nuclear Heating in the Coils of a Fusion Reactor. ECN-C-90-034, Aug. 1990

[10] A. Hogenbirk. Calculation of Design Uncertainties for the Development of Fusion Reactor Blankets, Taking into Account Uncertainties in Nuclear Data. ECN-Rx-94-058, July 1994

VI NUCLEAR DATA ACTIVITIES

Activities and Cooperation in Nuclear Data Field in China During 1999

Zhuang Youxiang
(China Nuclear Data Center, CIAE)

1 Meetings Held in China in 1999

1) Nuclear Data Evaluation working Group Meeting. Jan.15, Beijing.
2) The Meeting on "Communication of Nuclear Data Progress" (CNDP), June 11~13, Yantai.
3) The Standing Committee Meeting of China Nuclear Data Committee, Aug. 24, Beijing.
4) The Symposium of Nuclear Data Measurement Working Group, Sep. 13~18, Wulumuqi.
5) The Joint Symposium of Nuclear Data Evaluation Working Group and Nuclear Theory Working Group, Nov. 24~28, Haikou.
6) The Meeting on Evaluation and Calculation of Neutron Data for Actinoides, Dec. 25, Beijing.

2 The International Meetings and Workshops in Nuclear Data Field Attended By Staffs of CNDC in 1999.

1) The 1st Research Co-ordination Meeting on WIMS-D Library Project, Feb. 15Ma, Liu Ping, Vienna, Austria.
2) The Meeting of NEA Working Party on International Evaluation Cooperation, Apr. 18~23, Liu Tingjin, ORNL, USA.
3) The 22nd Meeting of International Nuclear Data Committee, May 10~16,

Liu Tingjin, Vienna, Austria.

4) The Consnltants' Meeting on Technical Aspects of Co-operation of the Nuclear Reaction Data Centers, May 18~20, Zhuang Youxiang, Vienna, Austria.
5) The 2nd RCM on "Fission Product Yield Required for Transmutation of Minor Actinide Nuclear Waste", Oct. 12~16, Liu Tingin, Vienna, Austria.
6) The 3rd Research-co-ordination Meeting on "Compilation and Evaluation of Photonuclear Data for Appliation", Oct. 25~29, Yu Baosheng and Zhang Jingshang, JAERI, Japan.
7) Development of a Database for Prompt Gamma-ray Neutron Activation Analysis, Nov. 2~4, Zhou Chunmei, Vienna, Austria.
8) 1999 Symposium on Nuclear Data, Nov. 18~19, Zhuang Youxiang, JAERI, Japan.
9) Workshop on Advanced Nuclear Data Online Services, Nov. 29~Dec. 3, Sun Zhengjun, Vienna, Austria.
10) Workshop on Installation and Use of LINUX for Nuclear and Atomic Data Computation on Personal Computer, Dec.13~17, Sun Zhengjun and Ge Zhigang, Vienna, Austria.

3 The Foreign Scientists in Nuclear Data Field Visited CNDC/CIAE in 1999.

Dr. Y.Ikeda, JAERI, Japan, Mar. 21~24.
Dr. Robert C.Block, Rensselaer Polytechnic Institure, U.S.A. Sep. 30.
Dr. T.Nakagawa, NDC/JAERI, Japan, Oct. 10~13.
Dr. P.Oblozinsky, NDS/IAEA, Austia, Oct. 30~Nov. 6.

4 Staff of CNDC Worked or Working in Foreign Country.

Huang Xiaolong, NDC/JAERI, Japan, Sep. 5, 1998~Sep. 4, 1999.
Shu Nengchuan, ORNL/USA, MAR. 26 scheduled one year.
Wang Shunuan, Shiraz Univ. Iran, Dec. 9, 1999~Mar. 2, 2000.

CINDA INDEX

Nuclide	Quantity	Energy/ eV		Lab	Type	Documentation				Author, Comments
		Min	Max			Ref	Vol	Page	Date	
^{9}Be	N Emission	5.9+6	6.4+6	BJG	Expt	Jour CNDP	23	1	Jun 2000	Chen Jinxiang +, DA/DE, TBL
^{Nat}Cu	Evaluation	1.0-5	2.0+7	SIU	Eval	Jour CNDP	23	91	Jun 2000	Ma Gonggui +, SIG, DA, DA/DE, CRV
^{90}Zr	Evaluation	1.0-5	2.0+7	AEP	Eval	Jour CNDP	23	68	Jun 2000	Liu Tingjin +, SIG, DA, DA/DE
^{91}Zr	Evaluation	1.0-5	2.0+7	AEP	Eval	Jour CNDP	23	68	Jun 2000	Liu Tingjin +, SIG, DA, DA/DE
^{92}Zr	Evaluation	1.0-5	2.0+7	AEP	Eval	Jour CNDP	23	68	Jun 2000	Liu Tingjin +, SIG, DA, DA/DE
^{94}Zr	Evaluation	1.0-5	2.0+7	AEP	Eval	Jour CNDP	23	68	Jun 2000	Liu Tingjin +, SIG, DA, DA/DE
^{96}Zr	Evaluation	1.0-5	2.0+7	AEP	Eval	Jour CNDP	23	68	Jun 2000	Liu Tingjin +, SIG, DA, DA/DE
^{Nat}Zr	Evaluation	1.0-5	2.0+7	AEP	Eval	Jour CNDP	23	68	Jun 2000	Liu Tingjin +, SIG, DA, DA/DE
^{135}Ba	Evaluation	1.0-5	2.0+7	NAN	Eval	Jour CNDP	23	120	Jun 2000	Zhao Jingwu +, SIG, CRV
^{136}Ba	Evaluation	1.0-5	2.0+7	NAN	Eval	Jour CNDP	23	120	Jun 2000	Zhao Jingwu +, SIG, CRV
^{137}Ba	Evaluation	1.0-5	2.0+7	NAN	Eval	Jour CNDP	23	120	Jun 2000	Zhao Jingwu +, SIG, CRV
^{138}Ba	Evaluation	1.0-5	2.0+7	NAN	Eval	Jour CNDP	23	120	Jun 2000	Zhao Jingwu +, SIG, CRV
^{141}Pr	Calculation	1.0+3	2.0+7	AEP	Theo	Jour CNDP	23	52	Jun 2000	Shen Qingbiao +, SIG, DA, DE, CRV
^{186}W	(n,γ)	5.0+5	1.5+6	BJG	Expt	Jour CNDP	23	8	Jun 2000	Zhang Guohui +, ACTIV, CS, TBL
^{209}Bi	γ-reaction	Thrsh	3.0+7	AEP	Eval	Jour CNDP	23	82	Jun 2000	Yu Baosheng +, SIG, DA, DE
	p-reaction	7.0+6	2.5+7	UNW	Theo	Jour CNDP	23	59	Jun 2000	Gao Bo +, SIG, DA, DE
^{235}U	Fission Yield	2.5-2	1.5+7	AEP	Eval	Jour CNDP	23	105	Jun 2000	Liu Tingjin +, Reference Fission Product Yield
^{239}Pu	Calculation	1.0+3	2.0+7	AEP	Theo	Jour CNDP	23	35	Jun 2000	Shen Qingbiao +, MDL, SIG, DA, DA/DE
^{240}Pu	Calculation	1.0+3	2.0+7	AEP	Theo	Jour CNDP	23	42	Jun 2000	Shen Qingbiao +, MDL, SIG, DA, DA/DE

图书在版编目（CIP）数据

中国核科技报告 CNIC-01475, CNDC-0027：核数据进展通讯. No.23：英文/刘挺进等著. —北京：原子能出版社，2000. 6

ISBN 7-5022-2202-2

I. 中… II. 刘… III. 核技术-研究报告-中国-英文 IV. TL-2

中国版本图书馆 CIP 数据核字 (2000) 第 36148 号

原子能出版社出版发行

责任编辑：李曼莉

社址：北京市海淀区阜成路 43 号 邮政编码：100037

中国核科技报告编辑部排版

核科学技术情报研究所印刷

开本 787×1092 mm 1/16 印张 10 字数 165 千字

2000 年 6 月北京第一版 2000 年 6 月北京第一次印刷

印数：1—600

定价：10.00 元